Effects on coated paper quality of uncoated and coated sheet drying strategy

by

Françoise Forel

A thesis submitted to the Faculty of Graduate Studies and Research in partial
fulfillment of the requirements for the degree of
Doctor of Philosophy

Department of Chemical Engineering
McGill University
Montréal, Canada

March, 1st 2004

Library and
Archives Canada

Published Heritage
Branch

395 Wellington Street
Ottawa ON K1A 0N4
Canada

Bibliothèque et
Archives Canada

Direction du
Patrimoine de l'édition

395, rue Wellington
Ottawa ON K1A 0N4
Canada

Your file Votre référence
ISBN: 0-612-98254-8
Our file Notre référence
ISBN: 0-612-98254-8

NOTICE:
The author has granted a non-exclusive license allowing Library and Archives Canada to reproduce, publish, archive, preserve, conserve, communicate to the public by telecommunication or on the Internet, loan, distribute and sell theses worldwide, for commercial or non-commercial purposes, in microform, paper, electronic and/or any other formats.

The author retains copyright ownership and moral rights in this thesis. Neither the thesis nor substantial extracts from it may be printed or otherwise reproduced without the author's permission.

AVIS:
L'auteur a accordé une licence non exclusive permettant à la Bibliothèque et Archives Canada de reproduire, publier, archiver, sauvegarder, conserver, transmettre au public par télécommunication ou par l'Internet, prêter, distribuer et vendre des thèses partout dans le monde, à des fins commerciales ou autres, sur support microforme, papier, électronique et/ou autres formats.

L'auteur conserve la propriété du droit d'auteur et des droits moraux qui protège cette thèse. Ni la thèse ni des extraits substantiels de celle-ci ne doivent être imprimés ou autrement reproduits sans son autorisation.

In compliance with the Canadian Privacy Act some supporting forms may have been removed from this thesis.

While these forms may be included in the document page count, their removal does not represent any loss of content from the thesis.

Conformément à la loi canadienne sur la protection de la vie privée, quelques formulaires secondaires ont été enlevés de cette thèse.

Bien que ces formulaires aient inclus dans la pagination, il n'y aura aucun contenu manquant.

Canada

ABSTRACT

Drying occurs twice during coated paper production: first, when drying the base paper, then when drying the sheet freshly coated with an aqueous suspension of pigment particles. The effects on coated paper quality from the impingement drying conditions used at both base paper and coated paper drying stages were studied for the light weight coated (LWC) paper. A central feature of the study was the development of the capability to dry coated paper by impingement in superheated steam. The variables investigated were the drying fluid, air or superheated steam, drying fluid temperature, drying time and temperature, and coating-to-drying delay time. The effects of drying on the uncoated paper physical properties and the coated paper physical and printing properties were determined.

The drying of the base paper with superheated steam gave higher strength and hydrophobicity but lower optical properties and smoothness than drying in air. When steam-dried base paper was coated and dried in air or steam it gave a rougher, less glossy, less bright coated paper than air-dried base paper. Print mottle remained high when air drying was used subsequently for the coated sheet.

The biggest effect on LWC coated paper quality derived from the choice of drying medium, air or superheated steam. Coating-to-drying delay time had no effect. Most of the properties of steam-dried coated paper were fixed by 0.6 s drying time. Properties the most affected were surface properties: print quality, gloss and roughness, while bulk properties were less sensitive. Drying with superheated steam gave lower gloss and smoothness than drying in air. Print mottle was significantly improved with steam drying of the coated sheet.

Superheated steam drying of coated paper has advantages only if used for the coated sheet not the base sheet.

RÉSUMÉ

La fabrication industrielle du papier couché comprend deux périodes de séchage: le séchage du papier support, et le séchage du papier après enduction d'une suspension de pigments. Les effets sur la qualité du papier couché provenant des conditions d'opération lors du séchage du papier support et du papier couché ont été étudiés dans le cas du papier couché à faible poids de couche (LWC). Une caractéristique centrale de cette étude a été le développement d'une unité de séchage du papier couché avec la vapeur surchauffée. Ainsi les variables examinées lors du séchage par contact direct ont été le fluide de séchage, l'air ou la vapeur surchauffée, la température du fluide de séchage, ainsi que le temps d'attente entre le couchage et le séchage. Les effets du séchage ont été déterminés quant aux propriétés physiques du papier support et aux propriétés physiques et d'imprimabilité du papier couché.

Le séchage du papier LWC avec la vapeur surchauffée a donné un papier plus résistant et plus hydrophobe avec des propriétés optiques et de rugosité inférieures comparé au papier séché dans l'air. Le papier couché sur le papier support séché à la vapeur a une rugosité plus élevée, un brillant et une blancheur plus faibles. Le moutonnement d'impression est resté plus élevé après séchage de ce papier couché dans l'air.

Après enduction l'effet le plus important sur la qualité du papier LWC s'est avéré provenir du choix du fluide de séchage, air ou vapeur surchauffée. Lors du séchage dans la vapeur surchauffée la plupart des propriétés ont été fixées au temps de séchage le plus court étudié, 0.6 s. Les conditions de séchage ont eu un large effet sur les propriétés de surface : la qualité d'imprimabilité, le brillant et la rugosité, un effet plus limité sur les propriétés du volume. Le moutonnement d'impression a été amélioré de façon significative lors du séchage dans la vapeur surchauffée.

L'utilisation de la vapeur surchauffée pour le séchage du papier couché présente des avantages lors du séchage après enduction mais n'est pas recommandé pour le séchage du papier support.

ACKNOWLEDGEMENTS

I am grateful to the many persons who helped me during this study. I would like first to thank W.J.M. Douglas and M.E. Weber for their guidance and energy along the research and deep involvement in the production of this document. A special word of thanks to Manoj Dixit for introducing me to the coating-drying project and for the close partnership he offered in this project, and to the students who assisted me in parts of the work.

I would like to express also my sincere gratitude to McGill workshop personnel, especially Walter Greenland and Alain Gagnon, as well as Paprican staff, especially Sylvie St-Amour, Sylvie Sauriol, Grazyna Stepien, and Tony Manfred for their time, advises and generous help. May I thank also my kind colleagues in the group, Jean-Philippe Bernié, S.J. Hashemi, Mohsen Sadeghi and in the Pulp & Paper Research Center for sustaining a very friendly and lively environment.

Financial assistance from FCAR (now Fonds Nature et Technologies) and the Mechanical Wood-Pulp Network Center of Excellence is acknowledged.

Finally, I wish to express my heartfelt thanks to my wonderful friend and companion for his patience, understanding and support: Vincent, merci!

TABLE OF CONTENTS

Chapter 4 Effects of superheated steam drying on base paper properties 82

Chapter 5 Development of coated paper properties during drying: Commercial base paper 100

LIST OF FIGURES

LIST OF TABLES

Chapter 1 Introduction

1. Industry significance

Printed products represent eighty percent of the communication market in western countries. The traditional role of paper as an information carrier has lost its pre-eminent position since the availability of electronic communications. On the other hand, a promising perspective for future end-uses of paper is provided by the increasing demand for attractive, colourful and well presented documents for commercial promotion and magazines, for which paper is used as the means of persuasion. Coated papers provide the necessary base for these applications requiring quality approaching the photographic image. Thus, coated paper consumption continues to grow at about five percent per year, faster than most other paper grades.

The challenge for the coated paper industry is to remain competitive among other paper grades and electronic media by adapting its products to meet the increasingly demanding requirements of consumers in the field of colour reproduction. The coated paper grade is therefore a natural target for continuing research toward quality and cost-effectiveness improvement. The drying stage is the most critical stage during coated paper production both in terms of energy consumption and development of the final product quality. Investigation of a novel drying technique which has the potential of energy savings and beneficial effect on coated paper properties is therefore of great relevance.

The pulp and paper industry is a major contributor to Canada's trade balance. With an annual production of 23 MT, Canada is the world's third largest producer of paper and board. Newsprint has for a long time been the largest paper grade production in Canada, but is now a mature market. Therefore there is an incentive to convert to coated paper, especially light coated grades for magazines production. Also most paper is produced out of mechanical pulp in Canada because it is cheaper and cleaner than chemical pulp. The light coated mechanical grade was therefore the natural choice for this study.

2. Objectives

The objective of this study was to evaluate the effects on coated paper properties from using superheated steam for drying the base sheet, the paper after coating, or both stages in the production of the Light Weight Coated (LWC) paper grade. This objective included identifying the mechanisms by which superheated steam drying affected the final coated paper quality.

A preliminary objective of the present study was to develop further the coating-drying experimental facility that was built in our laboratory, the procedures and the know-how, which would enable comparative studies of paper coating and drying alternately in air and in superheated steam with good control of the basic parameters of both the coating and the drying.

3. Conventional coated paper drying

Coated paper consists in two layers: the base paper and the coating layer. The coating layer is applied to the dry base paper as an aqueous suspension usually on both sides. Drying therefore occurs twice during coated paper production: when drying the base paper and when drying the freshly applied coating suspension.

3.1 Base paper drying

Uncoated paper is conventionally dried by contact with rotating steam-heated cylinders, Figure 1.1. The drying stage removes only a small fraction of the total amount of water removed during the whole papermaking process yet it is the most energy consuming stage as this moisture fraction is much harder to displace. This is aggravated by the low energy efficiency of heat-conduction process used in the drying section: over 30 cylinders are necessary to dry LWC base paper to its final moisture content, usually 3 to 5 % wet basis moisture content. Also the moisture evaporated from paper is not used to its full potential as it is mixed with air surrounding the cylinders. Another major shortcoming is the many draws in between cylinders where the web is not always supported which increases the number of web breaks and represents direct production losses. Even though very important paper properties such as tensile strength develop during drying there is not much possibility in conventional paper drying section to change paper properties by adjusting operating parameters except for curl and final moisture content. However as will be seen in section 4.3 from this chapter there is some potential to change paper properties during drying with using superheated steam instead of air as the drying medium.

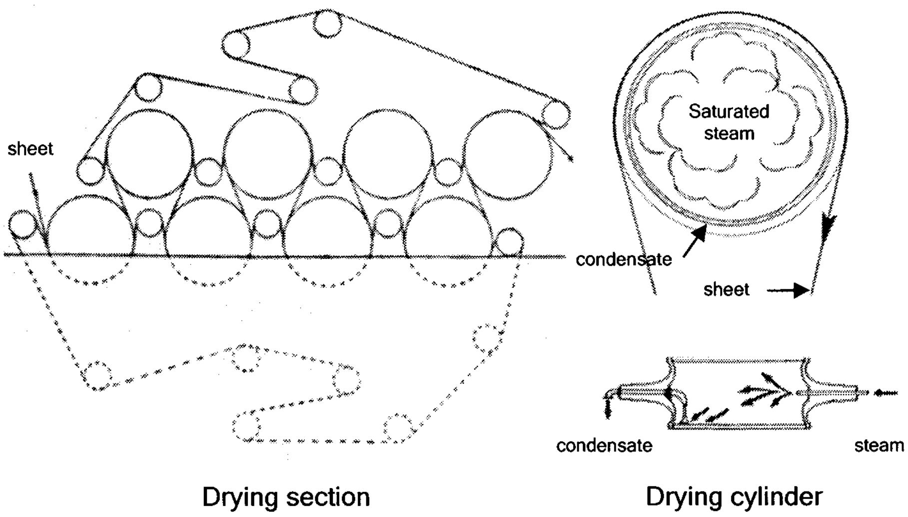

Figure 1.1 Conventional uncoated paper drying

3.2 Coated paper drying

Coated paper drying is usually performed with a combination of different drying techniques: infrared dryer, air flotation dryer and conventional cylinder dryer. Figure 1.2 presents a typical coated paper drying section layout. A non contact drying technique is required immediately after coating to avoid damaging the freshly coated surface. Infrared dryers provide energy to the web in the form of electromagnetic radiation. Both gas fired and electric units are available. Air floatation dryers provide non-contact two-sided convective drying of coated web. The advantages of the air dryers are the infrared dryers' drawbacks: no fire hazard, high energy efficiency. The infrared dryer are mainly useful for rapid heating of the coated web immediately after the coating unit. They also provide more flexibility to the drying rate profile control. Major part of the drying occurs in the air floatation dryer which needs to become more efficient to suit new production requirements. They are arranged in rows to provide drying intensity profile control in the machine direction of sheet travel. Cylinder dryers are used only marginally for web tension control at the end of drying, as this contact drying process cannot be used until the coating is sufficiently dry that its structure cannot be harmed by contact with drying cylinders.

The drying section, along with the aspects of coating formulation and base paper properties, is a very critical element for developing coated paper properties. The coating consolidation process controlling final product quality occurs during drying. Thus, a poor drying strategy may spoil a potentially good coating. Coating-to-drying time delay, drying intensity and temperature profiles are believed to be the main parameters controlling coated sheet quality.

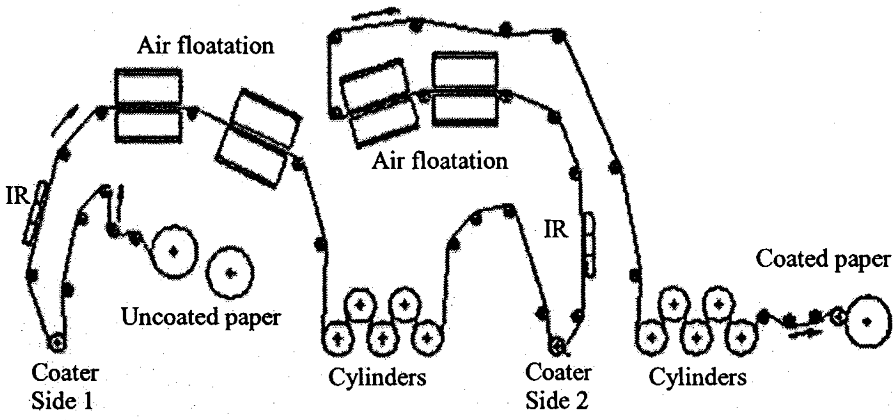

Figure 1.2 Coated paper drying

4. Superheated steam drying

4.1 History

Superheated steam as the drying medium to dry bulk solids such as pulp, food and coal is currently used in industry. Although a patent with no supporting data was recorded in 1952 to dry paper with superheated steam as the drying medium, there has been no known industrial application yet. In the early 1980's, Douglas and Mujumdar at McGill University renewed the interest for the concept of drying paper in superheated steam. Researchers from their laboratory have been investigating the superheated steam drying of paper intensively since that time, documenting drying rates and effects on paper quality, summarized by Douglas (1994). Based on the McGill results the Pulp and Paper Research Institute of Canada, Paprican, modified its air impingement drying pilot plant unit to operate also with superheated steam as the drying fluid. This unit has operated with superheated steam, but the results have not been published. Besides the Canadian publications, the Technical Research Center of Finland, VTT, has recently reported pilot plant scale work on superheated steam drying of paper (1995, 1998, 1999).

4.2 Advantages

The experiments carried out at McGill University on the concept of drying paper in superheated steam showed that superheated steam offers three types of advantages over air as a drying medium. First, above a certain temperature called the inversion temperature, the evaporation rate is greater in steam than in air at equal mass impinging jet flow, Bond (1991). These higher drying rates are of great interest since the drying section often represents the bottle neck for speed-up of the paper machine because of the much lower drying rates obtained by conduction from conventional steam heated cylinders. Second, exhaust steam can be reused directly after recompression and cleaning, as the process acts as a steam generator at the rate that water is removed from the paper. Elimination of the discharge to the air of the warm, humid air from conventional paper dryers leads to higher energy efficiency. Finally, and of major interest for the present paper property focussed study, drying in superheated steam gives higher strength for paper made from mechanical and thermomechanical pulp. Preliminary experimental work by Cui et al. (1985, 1986) and David (1987), and extensive studies by Poirier et al. (1994, 1995), McCall and Douglas (1994, 1995, 2001 and 2004) have demonstrated the thermally induced effects of superheated steam drying on standard paper properties. For drying in superheated steam, the sheet temperature reached while the moisture content is still high is higher than for drying in air. Softening and "micro-flow" of some of the amorphous wood polymers, mainly lignin, is thereby made possible. Lignin "micro-flow" allows for more development of fibre bonded area and therefore increases sheet strength but decrease sheet optical property. The work of Li (1993) in the same laboratory further documented the effect of superheated steam drying on paper surface properties, which provided key findings leading to the present study. Fines present at the surface of paper improves its smoothness by filling the pores between the long fibres. With steam drying lignin micro-spreading at surfaces of fibre increases surface strength and hydrophobicity but decreases smoothness.

4.3 Effects on coated paper properties

For papers containing a large fraction of mechanical pulp so a large fraction of lignin-rich fibres, superheated steam drying brings interesting changes in the processes involved in the coating process, potentially affecting thereby the properties of the coated sheet. An understanding of the mechanisms responsible for these changes provides the basis for anticipating the kind of differences in the coated layer properties resulting from drying coated paper in a steam environment.

4.3.1 Stronger base sheet

Web breaks occur frequently at the coater from the rewetting of a web that is already weak because of the large fraction of mechanical pulp. This runnability problem is usually addressed by the addition to the furnish of chemical pulp to obtain a stronger fibre network. Using superheated steam as the drying medium for base sheet drying increases its strength, which might allow papermakers to reduce the amount of expensive chemical pulp used.

4.3.2 Hydrophobic base sheet

The higher base sheet hydrophobicity developed in superheated steam drying should decrease the rate of transport of water into it from the wet coating layer. This effect should result in better runnability at the coater, a stronger coated sheet that would perform better in the printing press, and reduced coating components transport into the base sheet which means reduced loss of particles from the base sheet-coating interface and better coating components distribution within the coated layer.

4.3.3 Coated layer structure

With superheated steam drying the submission of the freshly applied coating layer almost instantaneously to a considerably higher temperature than for drying in air, can be expected to cause some major changes in development of the porous structure of the coating. Two temperature sensitive parameters are latex film forming and the viscosity of the coating suspension. The effect of higher temperature cannot be assessed before carrying out the experiments because the coating consolidation process is still quite incompletely understood.

5. Summary

In the present thesis base sheet and coated sheet were dried alternatively in an experimental drying fluid, superheated steam, and the conventional drying medium, air. Surface, structure and printing properties were evaluated to document the effects of superheated steam on coated paper quality. The development of some coated paper properties during drying and printing properties with printing conditions were also documented to develop explanations for coated paper properties behaviour.

The results are divided into four chapters. Chapter 4 presents the effects of superheated steam drying on uncoated base paper properties. Chapter 5 deals with the development of properties during drying, studied with laboratory paper coated on commercial base paper. Chapter 6 and 7 relate to the effects of drying conditions on coated paper quality and printability, respectively, for paper coated on laboratory base paper.

Chapter 2 Prior knowledge

1. Light Weight Coated paper

1.1 Materials

Coated paper is a layered composite product consisting of a base sheet and one or several layers of coating material usually present on both sides. For the grade used in the present study, LWC – Light Weight Coated paper, Figure 2.1 presents a SEM view of a cross-section of a typical sheet.

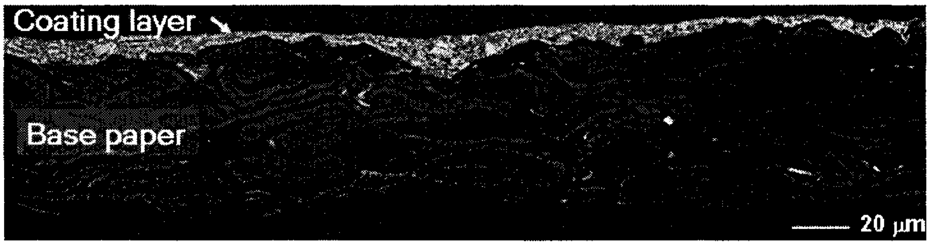

Figure 2.1 SEM cross section of LWC paper

The furnish from which LWC base paper is made usually contains mostly mechanical pulps (> 50%), to which chemical pulp (up to 35%) and fillers (up to 15%) are added in order to render the sheet, respectively, stronger and brighter. The base paper grammage typically ranges from 35 to 50 g/m^2, and the coat weight from 8 to 13 g/m^2 per side.

The dominant component of the coating materials is the pigment, typically either various grades of clay (english clay, kaolin clay, delaminated clay) or calcium carbonate (ground or precipitated). Binder material, usually starch or synthetic polymer latex, is required to obtain cohesion between pigment particles and adhesion to the base paper surface. The coating is applied to dry paper (95 to 98% wet basis solids content) as an aqueous suspension of solids content ranging from 55 to 65% in order to obtain a uniform layer. Additives such as dispersant, rheology modifiers or defoamers are used for suspension properties control. Table 2.1 summarizes the materials for coated paper.

The materials for coated paper are selected to produce the least expensive sheet combining the opposing objectives of low basis weight, high opacity and gloss while maintaining good runnability in both the paper machine and the printing press. Table 2.2 provides details of the materials for typical LWC paper as used in this study, for which the pigment chosen was clay, the binder was a styrene-butadiene synthetic polymer latex.

Table 2.3 gives the dimensions of the coated paper layers as used in this study with a base paper grammage of 40 g/m^2 and a coat weight of 10 g/m^2.

1.2 Industrial process

The dry base paper is produced as for uncoated grades, then the coating is applied and the sheet re-dried.

Base paper production involves wood pulping by a mechanical or chemical process, pulp dilution, sheet forming, pressing, drying and calendering. The process most frequently used for coating the LWC grade is blade coating, in which an excess of the aqueous coating suspension, commonly called the coating colour, is applied to the dry base sheet. The coating blade pressed against the paper reduces and levels the wet coating layer to reach a final coat weight of 8 to 13 g/m^2 for each side. The wet coating layer formed under the blade tip undergoes very fast consolidation by movement of water into the base sheet, followed quickly by removal of water from the base sheet and the coating in the coated paper dryer. Coating is generally done one side at a time, with the one-side coated sheet being completely dried before the second side is coated. In an alternate technique, film coating, paper is coated on both sides simultaneously while passing between two rolls which carry pre-metered amounts of the coating suspension.

Coated paper drying is usually performed with a combination of drying techniques. A non-contact drying technique is required immediately after coating to avoid damaging the wet freshly coated surface. Non-contact processes used are infrared drying and/or air flotation drying. Drying is often completed using conventional cylinder dryers. Infrared dryers, either gas fired or electric, provide energy as electromagnetic radiation to the web. Air flotation dryers provide non-contact two-sided convective drying of the coated web as it passes suspended between opposing air impingement flows on the two sides of the sheet. The advantages of impingement air drying are the drawbacks of infrared drying: no fire hazard, high energy efficiency and good mass transfer characteristics. As an infrared dryer is an effective technique for the heat transfer aspect but not for the mass transfer required in drying it serves mainly for rapid heating of the coated web and drying of just the surface of the coated layer immediately after the coating unit. IR dryers also provide good flexibility for drying rate profile control.

Table 2.1 LWC coated paper composition (dry basis)

	Material	**Role**	**Composition**
Base paper	Mechanical pulp	Cheap fibre supply	> 50%
	Chemical pulp	Strength	15 to 33%
	Fillers	Opacity	Up to 15%
	Water	*Residual moisture*	*3 to 5%*
Coating	Pigment	Surface finish	80 to 90%
	Binder	Cohesion and adhesion	10 to 15%
	Co-binder	Flow + water retention aid	1 to 2%
	Additives	Suspension property control	< 1%
	Water	*Suspension vehicle*	*54 to 82%*

Table 2.2 Coated paper material dimensions

Constituent	**Characteristics**	**Density, g/cm^3**
Fibre (softwood)	Length 2 - 6 mm	Fibre wall 1.5
	Diameter 20 - 60 μm	
	Wall thickness 2 - 10 μm	
Fines (fibre debris)	< 80 μm	1.5
#2 clay plus delaminated clay in 1:1 ratio	Particle size 0.05–5 μm	2.56
	Distribution^{g} 78 to 84% < 2 μm	2.56
	Aspect ratio 4-8 (#2)/ 8-16 (delaminated)	
Binder	Polymer latex 0.1-0.2 μm	1

Table 2.3 Coated paper layer dimensions

Constituent layers	**Thickness**	**Density, g/cm^3**
Base paper, uncoated^{m}	78 μm	0.5
Coated paper, uncalendered^{m}	82 μm	0.6
Coated paper, calendered^{m}	55 μm	0.9
Coating layer, wet^{c}	10.5 μm	1.52
Coating layer uncalendered^{m}	7.5 μm	1.33
Coating layer, calendered^{m}	6 μm	1.67
Base paper pore size	1 to 10 μm	
Coating pore size	0.01 to 0.1 μm	

Notation for properties: m - measured in the present study, c - calculated, g - given by manufacturer, otherwise from literature.

The major part of the drying typically occurs in the air flotation dryer, with manufacturers attempting to make them more efficient and compact. The air impingement nozzles of flotation dryers are arranged in arrays to provide drying intensity profile control in the machine direction of sheet travel. After the coating is sufficiently dry that its structure cannot be harmed by contact, cylinder dryers are sometimes used for web tension control.

The dry coated sheet is then calendered, i.e. passed between rolls where temperature and compression are used to develop the surface finish of paper, especially gloss and smoothness.

1.3 The coated paper product

Coated paper quality relates primarily to its coating layer properties: the degree of coverage of the fibres by the coating material and the coating layer structure. Coating coverage is very important for low coat weight grades. The large physical and chemical difference between coating materials and uncoated paper is the source of significant differences in properties. With full coverage, many coating properties relate to the coating porous structure which develops through the successive stages of production. The pore diameter and porosity ranges from 0.01 to 0.1 μm and from 20 to 30% for the coating, from 1 to 10 μm and around 30% for LWC base paper after coating and calendering. The nature of the micro-porous structure of the coating influences strongly the optical, mechanical and absorption properties of coated paper. The surface finish is also of great importance as it affects paper gloss, a key end-use property of coated paper. Applying fine, platelet shaped pigment materials followed by calendering sharply reduces paper roughness. Paper gloss is the degree to which the paper surface reflects light in the specular reflection direction. Paper gloss is related to surface micro-roughness, i.e. the number and arrangement of facets of the surface. Table 2.4 provides a range of values for key coated paper properties typical of LWC coated paper grade.

The bulk and surface properties of coated paper are influenced by the coating suspension composition, the base sheet properties, as well as the drying and calendering process parameters. The complex interaction between the numerous components of the coating process seriously limits the extent to which the action of the individual basic parameters can be determined. The effects on coated paper properties of drying strategy, long recognized as a major determinant, especially for print quality, are the focus of the present study.

Table 2.4 Typical values for key LWC coated paper properties

Property	**Range of values**
Thickness	50 to 70 μm
Brightness	60° to 70°
Opacity	85° to 90°
Roughness	0.5 to 1.5 μm
Gloss	45° to 65°

2. Coating layer consolidation

This section focuses on the dewatering and drying mechanisms during coating consolidation.

2.1 Coating consolidation process

2.1.1 Consolidation on impervious substrates

Because of the complexity of the development of coating structure on paper, this process has been studied with impervious substrates. Watanabe and Lepoutre (1982) observed the time evolution of the coated surface gloss and opacity (reflectance over black background), illustrated in Figure 2.2, and showed that coating consolidation proceeds in three stages.

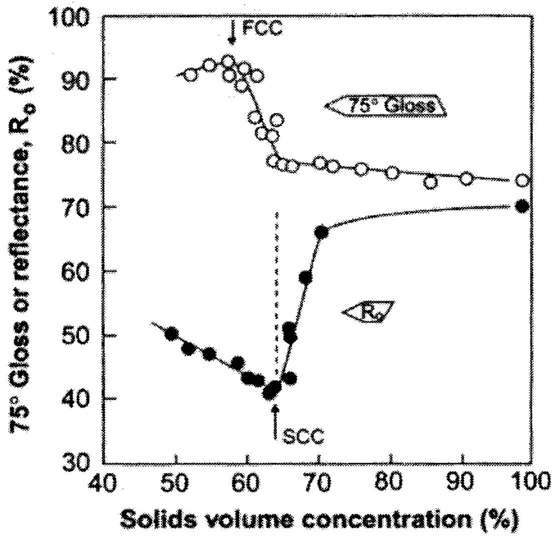

Figure 2.2 Coating consolidation process taken from Watanabe and Lepoutre (1982)

Their study was done with latex binder, as in the present investigation. In the first stage, water evaporation brings the pigment particles closer together until a coherent but still deformable network is built. The first stage ends at a condition named the First Critical Concentration (FCC), at which the gloss drops suddenly because of the formation of menisci breaking the wet (shiny) surface. During the second stage of consolidation the pigment network shrinks under capillary forces while film formation by the binder further enhances shrinkage. When complete packing of the pigment particles of the coating layer is approached, the replacement of water in the larger pores by air induces a sharp increase in opacity: this is the Second Critical Concentration (SCC). Subsequently during the third stage of consolidation water is removed from the finer coating capillaries until complete dryness.

This three-stage consolidation behaviour is universal but the critical concentration values and final coating structures vary depending on the pigment shape, latex binder type and amount used as well as the drying condition. Stanislawska and Lepoutre (1996) found that the FCC and SCC of a 10 g/m^2 of a clay-latex coating on polyester film were reached after 50 and 75 s for drying at room temperature under natural convection.

Particularly significant differences in consolidation derive from the range of synthetic polymer latices used as the binder. Specifically, for the common butadiene-styrene polymer latices, the variable proportions of the monomers give quite different characteristics, especially for the glass transition temperature, T_g, at which the polymer structure changes from hard to soft. A change in the ratio styrene:butadiene from low to high changes the T_g value of the polymer from low to high. Under conditions used for drying coated paper, a latex binder of low T_g deforms into a film around the pigment particles, but a high T_g binder generally does not undergo film forming. For a non-filming latex (high T_g), little shrinkage occurs regardless of the amount of latex used. For a filming latex (low T_g), two consolidation regimes are observed depending on the proportion of latex, Stanislawska and Lepoutre (1996). In the case of low latex content (< 15% of dry pigment mass), consolidation is dominated by the packing property of the pigment. By contrast, for high latex content (> 20% of dry pigment mass) the pigment particles become completely surrounded by a film of latex binder. Drying stress can be transmitted through this continuous latex matrix, enhancing the degree of shrinkage and leading to less glossy and rougher coated substrate. These experiments from Stanislawska and Lepoutre (1996) with clay-latex coating quantified the effects of latex content and drying intensity on coating consolidation on polyester film. Increasing the latex content from 5 to 8% did not change the coating shrinkage much but decreased gloss by 5 points. Increasing the latex content from 8 to 16% increased shrinkage from 18 to 50% and decreased gloss by 5 points. For low latex content drying in the oven instead of a room temperature increased shrinkage from 10 to 18% but did not affect gloss much.

2.1.2 Consolidation on porous paper

The consolidation process is different on an absorbent substrate such as paper because water transport occurs by evaporation but also by water movement towards and into the substrate. Such transport starts from the moment the coating suspension contacts the base paper and continues until sufficient evaporation occurs in the dryer that menisci form at the coating free surface, thereby providing the driving force which reverses the direction of water transport. On a porous substrate therefore coating immobilisation occurs much faster, within a few tenths of a second to several seconds, as elaborated in section 2.2.3, depending on the coating process, the coating composition and the base paper. Rapid consolidation is experienced when a low coat weight is applied and/or very absorbent base paper is coated, which is the case for the LWC grade being investigated here. Although the consolidation process occurs through the same three phases as with an impervious substrate, the dewatering rate now plays a key role in controlling both the structure and the composition of the coating. Immediately after the coating application and until the FCC immobilisation point is reached, about 75% solids content for a clay/latex system such as in this study, Lepoutre (1989), the base paper extracts water from the wet coating layer. As water moves from the coating layer to the base paper a cake of pigment particles builds up at the coating/paper interface and grows until the entire coating suspension layer is immobilised and menisci form at the surface. At that point, the FCC, evaporation becomes dominant over drainage into the base sheet and capillary forces cause the pigment network to shrink and the latex film forms. The SCC, solids content at which coating compaction is complete, is then typically reached between 80% and 90% solids content (Hagen, 1993).

With transport of water from pigmented suspensions into a porous network, three filtration processes may occur as reviewed by Lee and Whalen-Shaw (1993): medium filtration, depth filtration and cake filtration. Pigment particles larger than the filter pores are naturally retained, which is termed medium filtration. Pigment particles smaller than the support pores may still be retained by impact with the pore walls and by bridging, which constitutes depth filtration. Cake filtration occurs through the pigment bed build-up by loss of water. Lee and Whalen-Shaw (1993) propose that both medium and depth penetration processes occur in the very short time after application until a cake builds up and filtration continues through this cake. With clay as the pigment and about 80% of the clay particles being smaller than 2 μm, some of the solids in the coating suspension could penetrate into the larger paper pores which may be of up to 10 μm diameter. However observations of coated paper cross-sections by Lepoutre and de Silveira (1991) show limited coating penetration, which confirms the effectiveness of depth filtration in preventing significant pigment penetration. Later Huang and Lepoutre (1998) reviewed this observation stating there is no extensive coating penetration but locally coating may penetrate as much as 20 μm deep on very open sheets. Thus the conclusion is that mostly water, charged with soluble binder and co-binder and very fine coating material, is transported into the base paper.

The presence of a filter cake has been demonstrated by Salminen et al. (1995) and Lezelter (1995) using the scrape-off method. This method is used in experiments with pilot coater (a replicate of an industrial installation except for the much narrower width), i.e. under dynamic conditions with industrial coating and paper. After the coating application unit the freshly coated sheet heads to the drying unit. A blade is manually pressed against the moving web with as constant an angle and pressure as possible. The coating material thereby removed from the web is assumed to be the liquid coating suspension standing above the growing filter cake. The scrape-off coating weight is measured and used to calculate the filter cake weight by difference from the known total coat weight applied. The results from these experiments are detailed in the next section.

2.2 Process of dewatering of the coating

2.2.1 Dewatering mechanisms

For coating on a porous material such as dry base paper a central characteristic is the transport of water and fine particulate material from the coating suspension into the base paper. The mechanisms for water transport into dry paper proposed by Nissan (1976) are the following: (1) diffusional transport of water vapour in the pores; (2) capillary transport of liquid in the pores; (3) surface diffusion in the pores; (4) water transport through the fibres (inside the fibre wall). In the case of coating application there is another driving force: the hydrodynamic (external) pressure force in the coating application and metering zones. Figure 2.3 presents the location of the dewatering mechanisms during industrial coating application: from the time of application, capillary and diffusion water transport may occur. At the time of application and levelling by the blade, external pressure is another driving force for water transport inside the base paper.

The extent of dewatering from external pressure depends on the intensity and duration of the pressure pulse. Figure 2.3 suggests that even though the pressure during blade application of the coating suspension to the base paper is much higher than that corresponding to the paper sorption potential (capillary pressure and diffusion), the latter is the dominant dewatering driving force because of the very short duration of the coating levelling. Based on experiments of water penetration into paper at short time scale, Eklund and Salminen (1986) expect negligible dewatering to occur under the blade tip. Subsequently the measurements of Salminen et al. (1995) indicated that very little water penetration occurred under the blade pressure of their experiments on a pilot coater. Fujiwara et al. (1993) proposed dewatering by penetration during paper decompression after the blade. This is again dewatering under external pressure, not by applied pressure but reduced pressure after coating blade compression of the base sheet.

2.2.2 Dewatering rate modeling

The prediction of water sorption rates with mathematical models is a great challenge because water transport inside paper is not fully understood and it is difficult to define the parameters accounting for paper and coating suspension properties. The highly nonuniform conditions of the coating suspension material and the difficulty of making accurate measurements during the very short time scale of dewatering prevent reliable validation of the models.

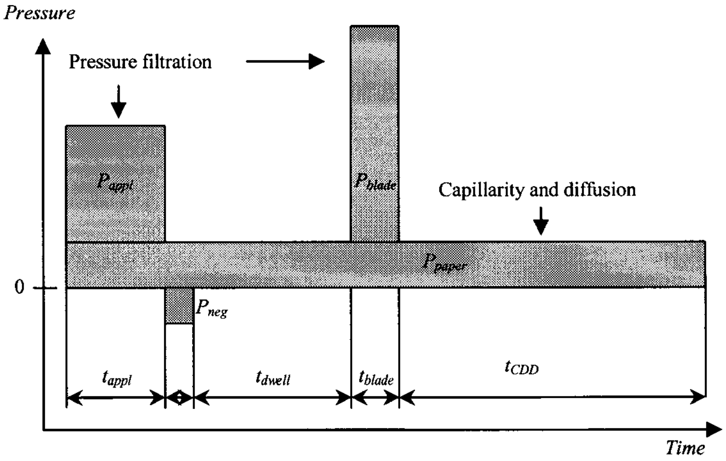

	Application	**Dwell time**	**Blade tip**	**Delay time (CDD)**
Pressure (10^5 Pa)	2.5/0.3	0.1-0.4	12	0.1-0.4
Time (ms)	2/1.8	1-60/1.8	0.03	0.1-0.5

Figure 2.3 Intensity and duration of pressure pulses in blade coating process, modified from Lezelter and Eklund (1993)

The dewatering rate is determined by a force balance between paper sorption potential, a sum of capillary pressure and diffusion, plus external pressure and resistance to flow. The sorption potential of paper depends on its fibre surface chemistry and its porous structure. Two quite different approaches have been explored in describing the dewatering mechanism for capillary movement under external pressure when a coating suspension is applied to the dry base paper. The first approach considers penetration into the base paper, with flow resistance originating from the paper structure, while the second mechanism is based on filtration through the pigment filter cake (rapidly built up), with flow resistance originating from the pigment cake. These models do not apply for sized (hydrophobic) paper, for which water transport by capillary force is suppressed, leaving molecular diffusion as the dominant driving force for the consequently much slower dewatering, Engström and Rigdhal (1986). The present study concerns the light weight coated paper grade, for which sized base paper is usually not used.

a. Penetration into the base paper

The first approach models the penetration of a wetting liquid into a porous medium. Two approximations may be taken for the structure of the porous network. With the simplest approximation, the medium is idealized as an array of cylindrical capillaries, each of radius R making an angle Φ with the surface of the sheet as in Figure 2.4. The pressure difference driving the penetration, ΔP, is the sum of the capillary pressure originating from the meniscus in the pore and any pressure imposed externally.

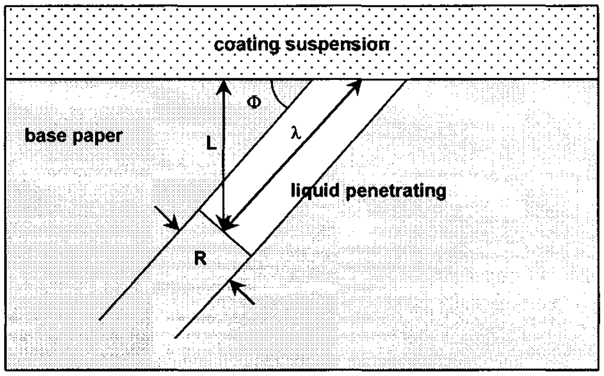

Figure 2.4 Dewatering from the coating suspension into the base paper: Schematic

Assuming fully developed creeping flow of a Newtonian fluid over the length of a capillary, λ, filled with fluid, the average velocity along the axis of the pore is:

$$v = \frac{d\lambda}{dt} = \frac{R^2(\Delta P)}{8\mu\lambda} \tag{2.1}$$

with μ the viscosity of the wetting fluid. Since the depth of penetration normal to the surface is L, and $L = \lambda \sin\Phi$, then

$$\frac{dL}{dt} = \sin^2\Phi \frac{R^2(\Delta P)}{8\mu L} \tag{2.2}$$

Integrating from $t = 0$, where $L = 0$, and defining the tortuosity $\tau = \lambda/L = 1/\sin\Phi$, gives the Lucas-Washburn equation:

$$L = \frac{1}{2\tau}\sqrt{\frac{R^2(\Delta P)t}{\mu}} \tag{2.3}$$

The velocity of penetration $U = dL/dt$, hence:

$$U = \frac{1}{4\tau}\sqrt{\frac{R^2(\Delta P)}{\mu t}} \tag{2.4}$$

It is well known that the Lucas-Washburn treatment does not apply for short penetration times because it predicts infinite acceleration. At very short times the inertia force of the liquid is larger than friction of the capillary wall. Assuming the inertial regime, Bosanquet (1923) derived an expression for the penetrating velocity at short time along the axis of the capillary, the Bosanquet velocity:

$$v\big|_{t\to o} = \frac{d\lambda}{dt} = \sqrt{\frac{\Delta P}{\rho}} \tag{2.5}$$

with ρ the fluid density. The velocity of penetration perpendicular to the sheet is:

$$U\big|_{t\to o} = \frac{1}{\tau}\sqrt{\frac{\Delta P}{\rho}} \tag{2.6}$$

Thus penetration is assumed to occur in three stages: first, a rapid acceleration from rest to the Bosanquet velocity; second, an inertial regime with penetration at the Bosanquet velocity; and third, a viscous flow regime starting when the distance from the Lucas-Washburn equation falls to the Bosanquet distance value. The first stage is believed to be very short while the second stage period lasts until the distance predicted from Bosanquet velocity equals that from the Lucas-Washburn. The switch time from Bosanquet to Lucas-Washburn regime is given by:

$$t^* = \frac{\rho R^2}{4\mu} \tag{2.7}$$

Using $R = 1\ \mu\text{m}$, $\rho = 1000\ \text{kg/m}^3$ and $\mu = 10^{-3}$ or 10^{-1} kg/ms, this switch time is very short, about 300 or 3 ns. Therefore this treatment does not change the estimation of liquid penetration time much compared to using only the Lucas-Washburn treatment.

This approach suffers from 3 main limitations as noted by Salminen (1988): (1) the dynamic character of the capillary pressure (contact angle changes because the penetration velocity is not constant and there is interaction between water and fibre); (2) the expansion of the fibre network (fibre swells by contact with water because fibre wall bonds and inter-fibre bonds are broken) which affects the cross section of the penetrating front and the velocity by changing the radius-dependent capillary pressure; (3) the neglecting of liquid transport through the vapour phase (in the pores, at the surface of fibres on inside the fibre wall). From experiments of penetration of water into paper at a very short time scale (1.5 ms), Salminen showed that the Lucas-Washburn treatment applies when the pressure is applied (penetrated volume increases as a function of square root of time) but no longer applies when paper sorption ability is the only driving force (penetration a linear function of time). Since the penetrated volume was very sensitive to temperature, he concluded that spontaneous penetration into paper is controlled by vapour flow ahead of the liquid front.

For paper the one dimensional form of Darcy's law is also often used to model water penetration. Darcy's law asserts that for one-dimensional flow in a porous medium the superficial velocity normal to the surface, u, is proportional to the pressure gradient divided by the liquid viscosity. The proportionality constant is the permeability of the porous medium, K. The superficial velocity is the volume of fluid entering unit area of sheet per unit time, hence:

$$u = \frac{Q}{A} = \frac{K(\Delta P)}{\mu L} \tag{2.8}$$

with Q the volumetric flow rate, A the sheet area. From conservation of mass, the velocity of penetration perpendicular to the sheet is:

$$U = \frac{dL}{dt} = \frac{u}{\varepsilon} \tag{2.9}$$

with ε the porosity of the material. Combining (2.8) and (2.9) gives:

$$\frac{dL}{dt} = \frac{K(\Delta P)}{\varepsilon \mu L} \tag{2.10}$$

Integrating from $t = 0$, $L = 0$ gives the Darcy's law form of the Lucas-Washburn equation:

$$L = 2\sqrt{\frac{K(\Delta P)t}{\varepsilon \mu}} \tag{2.11}$$

Comparing eq. (2.11) and (2.3), the following relationship is obtained between radius of a cylindrical pore and permeability of the array of cylindrical pores:

$$R = 4\tau\sqrt{\frac{K}{\varepsilon}} \tag{2.12}$$

For a complex porous network as for paper, the permeability is often described by the Kozeny-Carman equation, Kozeny (1927), Carman (1937):

$$K = \frac{\varepsilon^3}{k_0 \tau^2 (1-\varepsilon)^2 S_p^2} \tag{2.13}$$

with k_0 a shape factor, S_p the surface area per unit volume of particles forming the porous medium.

b. Pigment cake filtration

The second approach considers penetration by filtration through a filter cake of coating materials at the base paper/coating layer interface, a filter cake which forms very shortly after coating application. Liquid transport through the immobilised filter cake may be modelled with eq. (2.3) or (2.11) derived above, using the filter cake porous network characteristics instead of those of the base paper. Letzelter and Eklund (1993) used the permeability approach with the Kozeny-Carman equation for modeling the permeability of the filter cake. Assuming the filter cake to be incompressible they derived the following expression for the mass of water transported through the porous material, m, at time t:

$$\frac{m}{f} = \sqrt{C \cdot A \cdot \Delta P \cdot t} \tag{2.14}$$

with f the filtration area, C a structure parameter, A a coating suspension parameter (accounting for viscosity). Lohmander et al. (1999) also used the Darcy's law approach with the Kozeny-Carman equation, assuming a compressible filter cake and the permeability to be a function of the filter cake solids content, which lead to an equation similar to (2.11) (applied to the filter cake characteristics) but with an additional compressibility term:

$$L = \sqrt{2\alpha \frac{\hat{\phi} - \phi_0}{\phi_0} \frac{K(\phi)(\Delta P)t}{\mu}} \tag{2.14}$$

with α a constant between 0 and 1, ϕ, ϕ_0, and $\hat{\phi}$ the filter cake solids content at t, at $t = 0$ and its average value (constant). The parameter α is related to the concentration gradient occurring in the cake, determined by their experiments. This model cannot yet be used to predict filtration process because simulated values were fitted to measurements obtained with static experimental conditions and model materials, as well as because the relationship between solids compressible pressure and solids content is unknown. Eriksson and Rigdahl (1994) showed that the idealized filtration mechanism is unrealistic, there being in fact three regions during dewatering: filter cake (high solids), liquid coating (low solids), and in between a transition region with a solids content gradient. Additionally Lohmander et al. (1999) found a solids content gradient in the filter cake for dewatering from a model coating through a non hygroscopic filter.

2.2.3 Discussion

Although the modelling of coating dewatering is not yet satisfactorily completed, considerable understanding has been achieved as summarized by Lezelter (1995) and Salminen et al. (1995). As soon as the coating suspension contacts paper, rapid dewatering into the base paper starts. Consequently a consolidated coating layer at the paper/coating interface, the filter cake, rapidly forms at the base sheet. Dewatering then occurs by filtration of the upper region of the coating layer, not yet consolidated, through the immobilised part of the coating layer which is growing from the base sheet interface. A solids content gradient in the upper liquid region, as proposed by Eriksson and Rigdahl (1994), has been shown by the measurements of Lezelter (1995) on a pilot coater. Thus an acceptable picture of the coating solids content profile is as given in Figure 2.5.

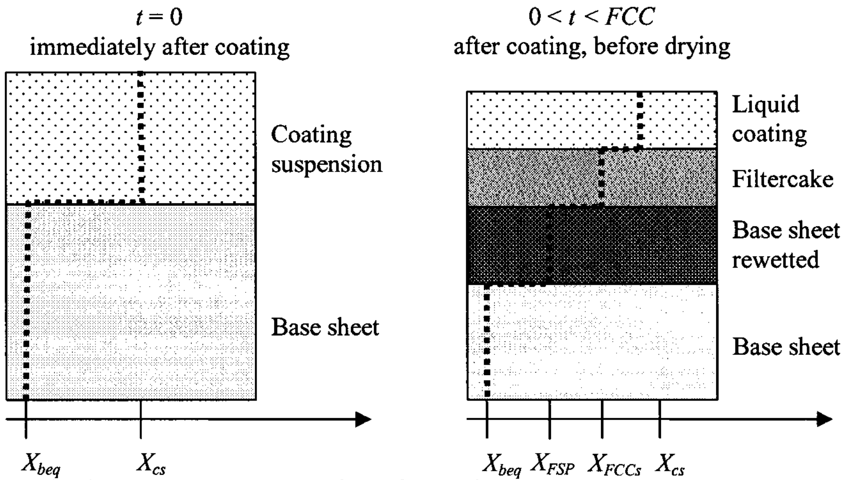

X: local moisture content per unit volume of material
$X_{beq,}$ base sheet equilibrium moisture content; X_{FSP} base sheetfibre saturation moisture content
X_{cs} coating suspension initial moisture content; X_{FCC} coating immobilization moisture content;
X_{ceq} coating equilibrium moisture content
For simplicity the moisture content changes at boundaries were represented as step changes

Figure 2.5 Coated paper moisture distribution after coating, before drying

An important observation from these experiments is that dewatering rate also greatly depends on the type of base paper, sized or unsized, i.e. hydrophobic or hydrophilic, not only the filter cake characteristics. As a conclusion, paper sorption is the mechanism controlling water transport in early dewatering followed by resistance to flow of the filter cake when it is thick enough to do so.

Coating dewatering determines the extent of consolidation of the coating layer prior to drying and is important in this study. Therefore the calculation of the timescale for penetration of water is now examined. By the time a 10 g/m^2 (dry) coating layer reaches its first immobilisation solids content, FCC, 75%, 2.5 g/m^2 of water will be transported to the base paper if the initial solids content was 63%. Paper porosity being about 50%, 2.5 g/m^2 is equivalent to a penetration depth of 5 μm when the whole coating layer reaches its FCC solids content. Using the simple model of cylindrical pores and the permeability form of the Lucas-Washburn, the penetration time may be derived from eq. (2.11) with capillary pressure $\Delta P = 2\sigma\cos\theta / R$ as the only driving force:

$$t = \frac{L^2 \mu \tau}{2\sigma\cos\theta}\sqrt{\frac{\varepsilon}{K}} \qquad (2.14)$$

with σ the surface tension, θ the contact angle. With K values typically in the 10^{-15} m^2 (Asensio 2000 and Chapter 4 section 2.2), $\tau = 3$, $\sigma = 0.07$ N/m, $\theta = 0$, application of eq. (2.14) for $L = 5$ μm gives $t = 6$ or 600 μs for $\mu = 10^{-3}$ or 10^{-1} kg/ms. This calculated time appears unrealistically short. The limitations of this approach were discussed in the previous section. Longer absorption times may be expected from expansion of the fibre network for example, or because the flow is vapour flow driven rather than capillary, or because of the resistance to flow from a growing filter cake. In order to get a better approximation of the time for the coating layer to reach its FCC solids content, the time required for 2.5 g/m^2 of water to penetrate, calculated from various experiments reported in the literature is given in Table 2.5. These experiments span a wide range of dewatering conditions (variable dwell times during pressurized and non pressurized penetration) and materials. The calculations show that the coating layer reaches the FCC solids content, i.e. reaches immobilisation, within several tenths of a second to 1 second.

2.3 Process of drying of the coating

2.3.1 Drying mechanisms

a. Before the Second Critical Concentration (SCC): liquid water flow

For industrial installation, the delay time from coating application to onset of drying is usually 0.1 to 0.5 s. The coating layer may not have reached its FCC yet. If the coated paper reaches the dryer before the FCC, water continues to drain into the base paper, while evaporation starts on the wet external surface of the coating which accelerates the process of coating immobilization.

Table 2.5 Experimental dewatering timescale from literature

Reference	**System**	**Method**	**Time to FCC**
Lepoutre, 1978	Coating (Clay, latex, CMC, 60%, 14 g/m^2) Publication grade paper Laboratory coater	Gloss	1.0
Engström, 1986	Coating (clay, CMC, latex, 59%) Paper (mechanical pulp) Pilot coater (fountain applicator + blade)	Scrape-off	1.6 s
Eklund and Salminen, 1986	Water Paper Rotating wheel (no external pressure)	Volume uptake	0.25 s
Fujiwara, 1991	Coating (Clay-CaCO3, latex-starch, 65%, 10 g/m^2) Paper (chemical pulp unsized) Pilot Coater (roll applicator + blade)	Scrape-off	0.6 s
Salminen, 1995	Coating (clay, latex, CMC, 63%, 15 g/m^2) Paper (LWC) Pilot coater (roll applicator + blade)	Scrape-off	0.3 s
Lezelter, 1995	Coating (Clay-CaCO3, latex, CMC, 62%, 20 g/m^2) Paper (chemical pulp unsized) Pilot coater (roll applicator + blade)	Scrape-off	0.5 s

If the coated paper reaches the dryer after the FCC, water transport into the base sheet has already stopped and only water transport towards the coating surface exists. With the combination of water depletion into the base sheet by dewatering and/or in the opposite direction by evaporation, menisci form at the coating surface, that is the coating immobilizes as a coherent yet still loose matrix (FCC), Watanabe and Lepoutre (1982). Such menisci provide the driving force to start capillary flow from the interior of the coating layer to the coating surface. After their initial increase during the warm-up period, drying temperature and rate remain constant fixed by the dryer operating conditions, water being continuously supplied to the coating surface. Surface tension forces draw water to the exterior surface, thereby causing further packing of pigment particles. Coating shrinkage reflects volume lost through water evaporation. The interfacial forces between latex polymer and water cause latex particle deformation and film forming. Latex film forming is enhanced when the difference between the sheet temperature and the latex film forming temperature increases. Watanabe and Lepoutre (1982) showed that for drying coating on impermeable substrate at room temperature latex coalescence occurs mostly between the FCC and SCC that is when capillary forces apply and liquid water is still present in the coating. They believe sufficiently high capillary forces should apply to trigger latex coalescence. Stanislwaska and Lepoutre (1996) later showed that coalescence may continue beyond the SCC for higher latex content (20 pph or 17% of coating dry mass) for coating on impermeable substrate. They also showed the presence of two regimes of shrinkage depending on the latex content. Shrinkage is controlled by the pigment packing below a critical latex content, but by the latex filming properties above this critical latex content. Above a critical latex content there is a continuous latex binder matrix allowing stresses occurring during latex film forming to be transmitted.

b. After the Second Critical Concentration (SCC): water vapor flow

When the rate of capillary transport of water to the external surface of the coating can no longer match the rate of evaporation of water, the evaporation front recedes from that surface into the coating matrix, the SCC. The sheet temperature increases and the drying rate drops. Water transport to the external surface may then occur in the vapor phase by bulk flow and diffusion of water vapor. Watanabe and Lepoutre (1982) experiments show that the coating structure is fixed at the SCC and no further change occurs. These experiments were done for drying coating on impermeable substrate at room temperature.

2.3.2 Coated sheet drying modeling

Modeling the drying of the wet coating layer deposited on dry porous paper is an enormously difficult, unachieved challenge. It is necessary to account for water transport initially in one direction and then reversal of the direction of water transport, through a structure of the coating layer which is undergoing great changes very rapidly. Moreover it is very difficult to obtain the measurements required for validation of such models. For the drying of coated paper, currently simple macroscopic models treating the overall heat and mass balances are used to predict drying rates. Such models do not account for the great complexity of the actual processes of dewatering and drying which determine product properties and quality. Only a few attempts have been made to achieve micro-scale models involving description of liquid water and water vapor transport in the thickness dimension of the base sheet and the coating layer. These attempts have used such limiting and unrealistic assumptions as no change in coating layer thickness, no dewatering, and no thickness direction temperature gradients. It is not within the scope here to address the complex modeling issues. Table 2.6 presents the characteristics of 5 models. These models were reviewed by Noboa and Seyed-Yagoobi (1999) and Hashemi et al. (2000), who concluded that none of them describe satisfactorily the drying process including the dewatering stage.

Table 2.6 Coated paper drying models

	Mechanisms	**Limitations**
Farkas et al. (1991)	Liquid flow by capillarity Vapor flow by diffusion Latex binder transport by both capillarity with liquid and diffusion	No coating dewatering No coating shrinkage Latex diffusion
Heikkila (1993)	Coating dewatering 3-stage: before / after coating consolidation drying external control / after coating consolidation drying internal control	No binder transport
Rajala and Karlsson 1995	Liquid flow by Darcy's law Vapor flow by diffusion	No coating dewatering No binder transport
Pan et al. (1995)	Liquid flow by Stokes flow Vapor flow by diffusion Binder transport by diffusion Rigid coating porous network	No coating dewatering No shrinkage Only after coating consolidation
Bernada and Bruneau (1996)	Liquid and vapor by diffusion Starch binder transport by diffusion Coating shrinkage Coating dewatering 2-stage: before (liquid-solid) / after coating consolidation ((liquid-solid-gas)	Dewatering simulation insufficient Low intensity drying simulated only Isothermal coating

3. Factors affecting coated paper quality

3.1 Effect of coating composition

The coating composition plays a role in how the various coating ingredients behave during consolidation. The final coating layer structure, especially its porosity and pore size distribution, is affected by the nature of the pigments, including shape, size distribution and the level of interaction with binders and co-binders. The packing characteristics of the pigment-binder system are believed to influence greatly the rate and extent of dewatering during the stage of filter cake build-up.

In addition to the effect of the binder on thickness-direction strength of the coating, the nature and amount of the binding material also affects coating structure and surface properties. Well-known effects include: the higher the binder content the greater the extent of coating shrinkage, hence both a lower porosity coating structure and a rougher surface; for latex binders, the higher the glass transition temperature the more open the coating structure, Lepoutre, (1989).

Another issue is certainly the extent of binder migration. Water transport during coating and drying, first into the base sheet, subsequently toward the coating external surface, may carry binder material and redistribute it across the thickness dimension of the coating layer and the base sheet. Water soluble binders such as starch may migrate towards both the base sheet and the coating external surface. Insoluble binders such as a synthetic polymer latex have more limited transport, probably mainly towards the base sheet. In this connection Groves et al. (2001) found no effect of varying drying rates on the surface latex binder content of the coating, but this was for coating on plastic sheets, not paper. A variable binder content at the coating external surface which depends on the extent of binder transport during consolidation, may affect surface porosity and wettability, and thereby affect print quality. The prevailing opinion is that because of the greater ease of migration of starch binder, such coatings tend to have more uneven binder surface content, and thereby more print mottle (see section 3.4).

The presence of co-binders, viscosity modifiers, is of importance through directly affecting the coating flow and the water retention ability of the coating suspension and thereby the extent of dewatering and the associated latex binder particle loss into the base sheet.

Finally, the water content of the applied coating suspension is an important parameter affecting the extent of dewatering into the base sheet, the coating layer formation under the tip of the coating blade, and the runnability of the coating process at the coating unit (too dry a coating may create streaks). The optimum initial water content provides a balance between reducing that unwanted dewatering into the base sheet without creating poor runnability at the coater.

3.2 Effect of the base paper

Base paper properties and the local variability in these properties influence coated paper quality by affecting the development and early consolidation of the coating layer. As base paper properties are reflected in coated paper properties, coating may not be used to hide a poor base sheet. Papermaking parameters such as furnish, freeness, sheet forming, pressing, drying as well as calendering design and operating parameters affect three main properties of the base sheet involved for the coating: absorbency, surface properties and formation of the base paper.

3.2.1 Base paper absorbency

The dewatering phenomenon controlled by base paper absorbency brings complex interactions between the base sheet and the coating suspension, which affect the development of coated paper properties in addition to those deriving from the coating and drying process parameters. In general, dewatering into the base sheet is prejudicial to coated paper quality as it may result in binder loss and poor consolidation. However some dewatering is considered beneficial, as discussed below.

Paper absorbency is governed by the fibre surface chemistry and the fibre network structure, not only its void fraction or porosity but also its pore size distribution. Higher drainage rates from the wet coating are obtained with paper for which water sorption occurs more through capillary flow than from external pressure during the coating application. For the mechanical pulp base papers important for the LWC grade of coated paper, the determining mechanism for dewatering is capillary transport. Paper absorbency affects coating solids pick-up and coat weight distribution as well as coating structure and composition.

- Coat weight: It is believed that at the same blade pressure the coat weight hold on paper is higher for a more absorbent base sheet because the resulting higher dewatering rate leaves more consolidated solids as the paper passes under the coating application blade tip. As the blade levels only the available non consolidated coating, more coating should therefore remain on a more absorbent paper.
- Coat weight distribution: The local nonuniformity of coating weight, which has a major negative impact on coating properties, may be better or worse with increasing paper absorbency depending on how absorbency is changed. When paper absorbency is increased by increasing sheet porosity, a greater nonuniformity of coat weight distribution is obtained because the larger water drainage is accompanied by a greater loss of latex binder particles and smaller pigment particles into the base sheet, Huang and Lepoutre (1998). This locally nonuniform transport into the base sheet in turn creates, at a given coat weight, more poorly covered areas at the coated surface. Increased dewatering from greater base sheet absorbency also promotes fibre swelling and thereby, greater roughening of the base sheet surface. This mechanism might lead to rougher, less glossy coated paper and/or to more local nonuniformity of coat weight. On the other hand reducing paper absorbency by sizing (making it more hydrophobic) does not always lead to better paper quality, Engström (1994). His approach to formation and consolidation of the coating layer for blade coating attempted to explain this seemingly contradictory effect of paper absorbency. Engström theorized that because sized base sheets drain less water from the coating suspension, which would reduce the detrimental mechanism described above, this reduced dewatering would also be accompanied by lower compressibility under the blade tip, which is a mechanism leading to poorer coat weight distribution. The fibre plasticizing resulting from water transport from the coating layer to the base sheet fibres is thought to be the source of the advantageously increased paper compressibility while it passes under the coating blade tip.
- Coating structure: The void fraction of the coating layer depends on the base paper regardless of the machine speed, Engström and Rigdahl (1986). The time for pigment ordering and packing directly depends on the dewatering rate.
- Coating composition: With higher base sheet absorbency and thereby more dewatering, fewer latex binder and fine pigment particles are left at the coating external

surface because of small particle entrainment in the water drainage towards the base sheet. Although water transport subsequently reverses towards the coating external surface after drying starts, particle transport away from the exterior surface is probably irreversible for the binder particles.

3.2.2 Base paper surface properties

Paper surface properties, specifically roughness and compressibility, may act during the blade metering stage of the coating process to affect the final coating layer quality. Rougher base paper picks up more coating because of its higher surface area available for anchoring the coating. Rougher paper generally gives rougher and less glossy coated paper. Another effect of base sheet roughness is the coat weight distribution, which depends on the nature of the roughness. There are divergent views about the formation of the coating layer under the blade tip. The conventional opinion has been that the blade runs on the peaks of the base sheet and fills its valleys with coating, with very little compression of the base paper under the blade tip. In this picture a rougher paper will lead to a more locally uneven coat weight. However according to Engström and Morin (1996) the blade pressure compresses and thereby smoothes the base paper, leading to formation of the coating layer by fluid flow of coating between the blade tip and compressed base paper. Accordingly, a significant compression of the base paper occurs, determined jointly by the blade pressure and paper compressibility. As noted in the previous section, compressibility can be increased through plasticization of fibres by water drainage from the coating suspension. Engström and Lafaye (1992) found that the paper which was rougher from being uncalendered gave a more even coat weight distribution because of being more compressible.

3.2.3 Base paper local grammage nonuniformity

Paper local grammage nonuniformity, i.e. paper formation, is expected to influence coated paper quality first by affecting the local nonuniformity of the other properties already discussed, such as porosity and compressibility, and second by affecting the coat weight distribution through a "compensating effect". Several publications, Tomimasu et al. (1990) and Matsubayashi et al. (1992), report finding of higher coating mass at locations in the base paper of lower fibre mass, i.e. lower local grammage. However the results reported from laboratory research relating formation to coated paper quality have usually been inconclusive, Huang and Lepoutre (1995), Hua et al. (1996). Three major limitations are responsible for this uncertainty. First this work was done with handsheets and formation cannot be varied with laboratory sheet forming in the way formation of machine –formed paper varies. Moreover when the formation of machine-formed paper is varied other paper properties are also varied, thus obscuring the effect of formation. Second, the paper formation measurement techniques which have been available, giving some single-number index of formation, are blind to the two-dimensional reality of fibre mass distribution and for this reason cannot realistically characterize formation. Finally, such studies should include comprehensive investigation of the influence of other properties of the base sheet which affect coated paper quality. The study by Hashemi et al. (2000) avoided the first two of the three problems noted above concerning laboratory investigations of the effect of base sheet formation. This study used commercial base paper of different formation and determined formation more realistically through use of a method which characterizes formation nonuniformity as a function of scale of formation. They found that base paper formation affects coating mass distribution as measured by burnout test.

For low coat weight, the effect of formation is expected to play a larger role, as is supported in the Drage et al. (1999) study on a pilot coating machine concerning the effect of paper formation on coated paper quality. With improvement in base sheet formation she found first, improvements in base sheet strength, brightness and lower porosity and second, for blade coated paper, a significant corresponding improvement in gloss, print gloss, print density and print mottle with both mechanical and chemical base sheets.

3.3 Effect of drying parameters

3.3.1 Mechanisms of the effects of drying

During coating-drying the water transport from the coating into the base sheet and through the coating to the surface brings particles closer together, thereby changing the coating structure from a wet suspension into a dry porous structure. Like dewatering above discussed, the drying conditions prevailing during consolidation are therefore expected to affect the coating structure and hence the coated paper properties. First, the drying occurring while the coating layer is not yet immobilised influences the structure of the dry coating layer, e.g. the characteristics of its pore and surface through its effect on water transport and latex film forming. Second, water transport also affects the distribution of binder content in both the thickness direction and in the plane of the sheet at the exterior surface.

Drying influences the porous structure first because it affects the dewatering rate by changing the temperature of the coating layer and the base sheet, which changes the liquid phase viscosity and hence the dewatering rate. Drying conditions also affect the coating shrinkage through affecting the sheet moisture and temperature history. There is then the possibility that the presence and extent of bulk flow of vapour in specific drying conditions may affect the porosity by disturbing the pigment packing, Xiang and Bousfield (2000).

Drying affects as well the surface roughness through its effect on the coating setting-rate, as explained earlier, and on the extent of coating shrinkage. If the setting is too rapid then the particles do not have time to align and achieve an orderly arrangement, leading to rough paper. Because of the large distribution in pigment particle size, shrinkage is by nature nonuniform and affects directly the surface disruption, Groves et al. (1991). Under conditions of high drying rate the increased shrinkage disrupts the particle alignment at the surface. The gloss, a measure of surface microroughness, decreases in response to the shrinkage, Stanilawska and Lepoutre (1996).

Uneven binder content and distribution in the thickness dimension and at the coating external surface may result from the competitive mechanisms of drainage into the nonuniform base sheet and evaporation from the free surface. During the first phase of the consolidation process, latex binder particles and fine pigment particles may be drained towards the base paper. When the immobilisation solids content is reached, menisci form at the coating surface, reversing the capillary transport of water, thereby stopping the drainage. Further consolidation of the coating occurs as water is removed from the pigment network by evaporation. Insoluble binder particles move in both directions by viscous drag of the water transport, towards and into the base sheet and towards the coated surface. This transport of a particulate binder is restrained or stopped by entrapment in the fibre or pigment network. By contrast, soluble binders move without restraint with the water as it is transported in each direction. Earlier consolidation of the coated surface in some local areas may prevent further accumulation of insoluble binders at the coating free surface in those regions. Entrapment of particulate binders in the coating network hinders such binder movement. As consolidation proceeds, more binder particles are entrapped. As Groves et al. (2001) stated the movement of latex binder towards the free surface may therefore be not very significant. Thus binder particle movement towards and into the base sheet tends to be irreversible, and therefore should be minimised.

3.3.2 Drying strategy

There is often mention in the literature of a critical moisture content range within which drying intensity should be low to ensure good paper print quality, Hagen (1986), Engström (1994). This drying strategy is based on the concept that uneven binder migration is the cause of the recurrent major print defect, print mottle, and discussed in section 3.4. With respect to binder migration, different drying strategies should be applied when the binder is starch or water insoluble latex because they do not migrate in the same manner as discussed in the previous section. With starch as the binder, the drying intensity near both the entrance and exit of the drying section may be maintained high without degrading coated paper quality but should be decreased between the first and second critical moisture concentrations (FCC and SCC) in order to control the soluble binder migration towards the coating surface, Engström (1994). Starch binder is transported with water and eventually deposits at the location of water evaporation. At first the evaporation front remains at the surface but later if the evaporation rate is too high, it will recede inside the coating preventing starch migration to the surface. By contrast, when a polymer latex binder is used, the objective should be to minimise water drainage and the accompanying loss of binder into the base sheet by minimising the time delay between application of the coating suspension and the onset of drying. In industrial practice, reducing this time of coating-to-drying delay time, referred as *CDD* in the present work, is accomplished by bringing the drying section as close as possible to the coating station.

Whether print mottle is related to binder migration or to other phenomena, which is discussed in the next section, drying strategy when the coating layer is near its immobilisation point is expected to affect print mottle. Eklund et al. (1995) and Kim et al. (1998) also identified a critical moisture content range where drying intensity should be kept low for good print quality. However they did not observe differences in binder content or binder content distribution at the surface between papers dried under low or high drying intensity in the critical moisture content range. The existence of this drying strategy within a critical solids content range may derive from the fact that the effect of drying conditions on coating structure varies with solids content. Development of the coating structure is believed to proceed in the three stages described in section 2.1. Before any coherent pigment matrix exists high drying rate may not be harmful. However after the FCC, when a deformable matrix of pigments is formed and water is removed from within the pores of this matrix, drying rate is expected to be critical. Too high a drying rate may be harmful because the flow of water may disrupt the fresh coating as proposed by Xiang and Bousfield (2000). After complete immobilization (SCC) a higher drying rate is expected to have less effect since the matrix is completely set. Xiang and Bousfield (2000) also suggest that after the SCC the temperature may affect the coating structure by causing latex sintering. Finally this drying strategy probably exists because of the local nonuniformity in moisture content. Local variation in coat weight leads to local variation in moisture content during drying. Coating layer immobilization occurs much more quickly in areas where the local coat weight is lower than the sheet average value. The drying rate or temperature around the immobilization point will therefore affect the coating structure differently in areas of locally low and high coat weight. Consequently maintaining low drying rate and low coating layer temperature around the immobilization point is believed to minimize the development of local variability in coating structure.

3.4 Coating-drying parameters and print quality

Although the most important unwanted property of coated paper is print local nonuniformity, it is still not fully understood how to control print mottle. The mechanisms proposed for the development of this characteristic are now reviewed. This review focuses on print mottle for coated paper in the offset lithography printing process.

3.4.1 Types of print mottle

Print mottle is the local nonuniformity in print density. The two most frequently reported types have been described by Plowman (1994), Engström (1994) and Morin (1996):

- Back trap mottle: this type of mottle occurs with multiple printing units. The ink layer applied to paper in a previous unit transfer back to the blanket of succeeding printing units. This backtrapping process is normal behaviour. But if this backtrapping process occurs unevenly, a serious print defect, back trap mottle, is obtained. In the common technique of printing four colors successively, the back-trap mottle is believed to come from uneven setting of the ink at the paper surface because of uneven paper surface properties. For fast setting ink, i.e. for which setting time is within the timescale of printing, the effect of paper local nonuniformity on ink setting rate becomes more important. The rate of ink setting depends on both the ink characteristics, the capacity of the ink vehicle to move out from the ink, and the substrate porous structure, the capacity to take ink vehicle. For a slow setting ink, the ink setting rate is controlled by the ink characteristics as the limiting factor is the slow motion of ink vehicle. By contrast, for a fast setting ink, the porous structure of the printed substrate becomes the limiting factor for the process of ink setting as it may not be able to take ink as rapidly as it comes. Therefore local nonunifomity in porous structure will become apparent in the form of mottle. The intensity of back-trap mottle varies with the color and the order in which the color is applied. Back-trap mottle occurs mostly with cyan ink but is also seen with magenta. Black, the slowest setting color, and the first to be applied, is not susceptible to the back trap mottle. Yellow is not subject to back trap mottle as it is the last color applied. Back trap mottle is also said to be favoured by the combination of an ink which is fast setting and a paper which encourages fast setting.
- Wet mottle or water interference mottle: this type of mottle is related to using water fountain solution with multiple printing units. Lithography is a planar printing process based on the principle that water and an oil-based ink do not mix. The blanket areas where there is to be no image, i.e. no ink printed, receive water fountain solution to prevent ink transfer to these areas. If water transferred to paper in the non-image areas of the previous unit does not penetrate sufficiently quickly, then ink intended to be printed

on those areas in the next printing unit will not transfer. If this effect occurs nonuniformly due to paper surface absorption nonuniformity, a wet mottle or water interference mottle print is obtained.

3.4.2 Paper properties controlling print mottle

Most printing professionals agree that back trap mottle is related to ink setting. Oil-based inks consist of pigments and resin dispersed in solvent, with oil used as an application vehicle. When such ink is applied to paper its solvent and oil content, i.e. the liquid phase of the ink (the liquid vehicle) is transported to the paper. This transfer occurs mostly to the entire structure of the coating layer by capillarity, marginally by diffusion into the latex binder (Rousu et al., 2002), and to the air through evaporation. With solvent removal by combination of these mechanisms the ink film viscosity increases and the resin molecules start to crosslink, making the ink film tacky, Schoelkopf et al. (2000). Thus ink setting occurs as the liquid phase leaves the ink film. When completely set, the ink becomes resistant to rub-off and back trapping.

Typically two paper surface properties are considered important for either back-trap or wet mottle: surface porosity and surface chemical composition - more specifically surface binder content. For these paper properties the local nonuniformity, not the absolute value, are important in the development of either back-trap or wet mottle as it is the locally nonuniform absorption of ink or fountain solution which causes nonuniform print density (Engström, 1994).

- Nonuniform binder distribution: this has long been the most common explanation for mottle. The chemical composition nonuniformity creates mottle not by a chemistry related mechanism (surface energy or wettability) but through its effect on porosity. This mechanism remains a controversial issue mostly because techniques used to measure binder content may give misleading results. Also the techniques used to measure latex binder content do not distinguish between binder, surfactant or dispersant all of which are present in the coating suspension applied, Groves et al. (1991, 2001). Different treatments appear necessary depending on the type of binder, starch or polymer latex. However as starch is often used in combination with latex, inconsistent results are reported. With starch, more widely used in the past than now, a number of studies relate starch migration and print mottle to nonuniform starch content at the coating surface. In this soluble polymer case, binder migration occurs easily as starch is transported integrally with the movement of water. Ink density is believed to depend sensitively on starch content, so mottle may be caused by surface starch content nonuniformity. With latex the potential for migration to the printing surface is much less than with starch because the transport of these 0.2 μm particles which with water by viscous drag is greatly retarded with increasing packing of the consolidating coating layer, as discussed in section 4.3.1. Increasingly studies are reporting no effect on print mottle from binder content uniformity at the surface coated paper (Eklund et al. 1995 [starch, latex 1:1], Kim-Habermehl et al. 1998b [latex only], Xiang et al. 2000b [starch, latex 1:7]).

- Nonuniform porosity distribution: the porous structure controls the absorption rate of the ink liquid phase, thereby controlling the ink setting rate. Porosity, mean pore size and pore size distribution near the coating layer exterior surface are important parameters determining the transport rate of ink liquid phase by capillarity. Several experimental studies, Eklund et al. (1995), Kim-Habermehl et al. (1998b), Xiang et al. (2000b), showed that the intensity of print mottle was affected by the local nonuniformity of porosity not of binder content. These investigations measured the chemical composition in regions where different porous structures were identified, and found negligible difference in binder content. Porosity is determined during the drying and calendering stages. Local nonuniformity in porosity may be created during drying by nonuniform water vapour transport rates or nonuniform coating shrinkage, and during calendering by compression of nonuniform roughness or grammage. Local nonuniformity in coat weight and binder content may also contribute to coating porosity nonuniformity.

Coat weight local variability is often identified as the cause of mottle (Matsubayashi et al. 1992, Engström et al. 1993, Eklund et al. 1995) but acting indirectly through affecting local nonuniformity of either binder content or porosity, as noted above. Matsubayashi found a strong correlation between local ink density and local coat weight through meticulous work in measuring local values of each property at precisely the same location. Engström and Morin (1993) [latex only] studied the local nonuniformity of both the solid print and the coating layer after removal of the base sheet by the procedure, commonly referred to as the burnout technique, which enables isolating the coating layer. They used frequency analysis to relate the scale of the local nonuniformity in coat weight to that in print density. For local nonuniformity in the range 4-8 mm they found a positive correlation between variance in coat weight and print density. As noted by Yamasaki et al. (1993) and Xiang et al. (2000b), the extent of latex film forming is another property that may affect print mottle but these works do not have the quantitative measurements.

While these studies provide evidence that local nonuniformity in the porous structure with which the ink fluid phase interacts plays an important role in determining print mottle, this interaction may occur only over a certain pore size range. When the binder is a polymer latex, nonuniform binder migration appears to be an unlikely source of print mottle. First, early in the coating consolidation process the migration of such solid particles is constrained by the high level of packing of pigment particles. Then later during coating consolidation, these binder particles undergo deformation and film forming, ending any possibility of binder migration, Groves et al. (2001). Other components present in the coating such as surfactants with latex binders, or dispersants may also travel with the water and change the surface chemical composition, thereby affecting the uniformity of printed coated paper.

3.4.3 Papermaking parameters affecting mottle

Any parameter in the coating-drying process that affects the local nonuniformity of porosity or binder content, especially those controlling dewatering and drying rates, will in turn affect print mottle.

- The base paper, its furnish, whether it was precalendered or sized are parameters affecting water absorption, water induced roughening and compression during coating application (Lepoutre et al. 1986, Engström et al. 1993). All these processes have an effect on the local nonuniformity of coat weight, binder and porosity.
- The coating suspension composition, including pigment and binder type, may lead by different mechanisms to print mottle. The type of water retention aid used will also affect the amount of dewatering as addressed below. For clay based coating Matsubayashi et al. (1992) found that there was little relation between print mottle and surface latex content, but that this correlation increased with pigments of increasing proportion of $CaCO_3$, becoming very significant for a pure $CaCO_3$ pigment coating. The same observation was made by Piette et al. (1999) who found no effect of latex content

on ink immobilization speed (ink setting rate) for a 100% clay coating but a significant effect when the pigment was 80% $CaCO_3$. Between binders starch is recognized to lead to more print mottle than latex (Engström et al. 1991, Yamasaki et al. 1993) because of its high tendency to migrate, as discussed above.

- The coating application technique affects the forming and consolidation of the coating especially its coat weight variation. Blade coating is generally considered to be is a void-filling technique while coating with a metering size press (MSP) is more of a contour-like technique. However based on inspection of SEM cross sections, Lepoutre (1991) concluded that these are over simplified descriptions. Undoubtedly the arrangement of the coating solids depends on the application technique. Engström et al. (1993) found that with both coating application techniques, print mottle relates to coat weight nonuniformity, but indirectly through affecting another coating property. He concluded that for the MSP application technique, porosity variation was the property controlling print mottle, while with blade application the cause appeared to be binder content variation.

- The rate of dewatering to the base paper may affect print quality. Dewatering affects coat weight distribution by fibre roughening (roughness increase due to fibre swelling and debonding after water sorption) and may carry some important components of the coating such as binder. Dewatering in turn depends on the coating water retention property (controlled by the co-binder), on base paper sorption potential and the time delay from coating to drying (Fujiwara et al. 1989, Engström et al. 1993).

- The drying strategy is generally considered an important determinant of print mottle. The coating-to-drying time delay (CDD), the profile of drying rate and temperature experienced by the coated sheet as it goes from wet to dry are variables directly affecting mottle. The type of dryer (IR or air impingement drying) does not seem to be critical at the same drying intensity level. Norrdahl et al. (1991) and Kim-Habermehl et al. (1998a) have found that there is a solids content range where evaporation rate and temperature should be kept below a critical value. This solids content range appears to be around the First Critical Concentration, FCC, defined by Watanabe and Lepoutre (1982) and discussed in section 2.1.2. On-line drying profiles are used as print quality control tools Moreau-Tabiche et al. (1996), Fisera et al. (1999). A solids content history that optimizes print quality is first identified experimentally, and then applied during production to ensure good quality paper.

- During calendering, coated paper is compressed to a locally nonuniform extent depending on the nonuniformity of grammage, roughness and formation of the base sheet. Areas which are locally thicker than sheet average value will be compressed more, leading to lower coating porosity regions, Engström et al. (1993).

4. Superheated steam drying of uncoated and coated paper

Preliminary experimental work by Cui (1985, 1986) and David (1987), followed by extensive studies by Poirier et al. (1994a, 1994b), McCall and Douglas (1994,1995, 2001, 2004) in this laboratory has demonstrated the effects of superheated steam drying on paper properties and suggested the mechanisms for these effects. The work of Li (1993) in this same laboratory further documented the effect of superheated steam drying on paper surface properties, providing key findings leading to the present study. Tables 2.7 and 2.8 summarize the results from these studies in order to compare them with that obtained in the present study presented in Chapter 4.

4.1 Drying paper in superheated steam: Mechanisms

4.1.1 Drying rate periods

Paper drying is characterised by successive stages of increasing drying rate, constant drying rate, and falling drying rate periods. For convective drying by contact with a drying fluid, the temperature history experienced by the sheet during these three steps is fundamentally different whether the sheet is in contact with air and or superheated steam as the drying fluid. During the initial period for drying in contact with hot air the sheet temperature and hence the drying rate rise slowly as the sheet temperature increases to approach the wet-bulb temperature of the air-water vapour gas phase, typically about 50°C, Bond (1991). By contrast, in contact at atmospheric pressure with a single component gas phase, superheated steam, the temperature of wet sheet jumps essentially instantaneously to 100°C, as required by thermodynamic equilibrium between water and steam, Bond (1991), and Poirier (1991). During the constant drying rate period, free water evaporates at a constant rate while the sheet remains at a constant temperature, either the wet bulb temperature or 100°C depending on whether in contact with humid air or steam. When there is no longer free water at the evaporating surface of the sheet, the sheet temperature starts to rise and therefore the drying rate starts to fall, signalling the start of the falling rate drying period. If convective drying were continued until all water was removed, which is of course not done in practice, then as complete dryness is approached the drying rate would approach zero and the sheet temperature would approach that of the drying fluid.

4.1.2 Fibre constituent plasticization

Many amorphous polymers undergo a glass transition for temperatures above the glass transition temperature, T_g, of that polymer. For polymers like hemicellulose and lignin, this glass transition temperature is a very sensitive function of moisture content, being lower at higher moisture content because of water acting as a plasticizer. Such polymers go from rigid at temperatures below its T_g, to soft at temperatures above its T_g. For the sheet temperature and moisture content conditions of drying paper it is the condition of the lignin which may be either rigid or softened. Although the glass transition temperature of lignin is above 100°C at low moisture contents of the dry material, at the high and moderate moisture contents of paper at the onset of drying the glass transition temperature of lignin is in the 50°-100°C range (Salmén, 1984).

The combination of high sheet temperature (100°C) at the high moisture content occurring when a moist sheet is dried in superheated steam produces the softening and possibly micro-flow of the amorphous components of the fibre wall: hemicellulose and lignin. For the high moisture content at the start of drying paper, the sheet temperature with any drying process is always above the T_g of hemicellulose. By contrast the T_g of wet lignin is above the wet bulb temperature of about 50°C of a wet sheet being dried in air, but is below the 100°C temperature of a wet sheet being dried in superheated steam. Therefore drying a lignin-containing paper in superheated steam transforms lignin from its hard to soft structural form, thereby producing its softening and micro-flow. McCall et al. (1995, 2001, and 2004) show that this structural change allows more development of fibre bonded area and significant changes in paper properties. The fines content of mechanical pulp, richer in lignin and hemicellulose than whole fibres, is particularly affected by this thermal softening, Poirier (1991). A micro-spreading of the softened polymers that are thereby characteristic of drying lignin-containing sheet in superheated steam results in increased bonded area or increased bond strength at fibre-fibre crossings.

4.2 Drying uncoated paper in superheated steam: Influence on paper properties

The extent of the effects of superheated steam drying on the properties of uncoated paper therefore depends primarily on the lignin content of the fibres used to make paper. The lignin content depends on the pulping process, either mechanical or chemical. For paper made of mechanical or thermomechanical pulp, containing a large fraction of lignin (25-45%), drying in superheated steam produces large effects on paper properties related to fibre bonding, mainly higher strength and lower light scattering, Poirier et al. (1994), McCall and Douglas (1994, 2001, 2004). Tensile strength, elastic modulus or burst strength are reported to be 20 to 30% higher when such paper is dried in superheated steam rather than in air, while tear resistance or zero-span tensile strength are unchanged. The increased bonded area however also causes a corresponding reduction in optical properties, in light scattering and thereby about a five point loss in brightness.

Studies on the effect of steam drying for paper made of virgin kraft pulp further support this view. For paper made of low yield chemical pulp, containing a small fraction of lignin (5-15%), smaller and in few cases opposite effects were observed (Poirier et al., 1995). Kraft pulp is usually subjected to a mechanical treatment, refining, to develop the bonding potential of fibres. As paper made from such mechanically refined kraft pulp is stronger, the benefit from the lignin softening obtained from superheated steam drying is therefore reduced. Kraft pulp fibres, highly flexible from having a low lignin content and having already developed their full bonding potential, are therefore subject to little enhancement of strength properties when dried in superheated steam. In the case of kraft (chemical) pulp the higher temperature reached in superheated steam leads to stress relaxation during drying which has the opposite effects on paper properties as an increase in bonded area.

The above summarizes the effects of superheated steam for two extreme cases: paper made from high yield mechanical pulp and low yield kraft pulp. In reality mechanical and chemical pulps may be produced at various lignin contents, and paper may be made not from a single pulp but a blend of various pulps. It is therefore notable that the benefits on strength properties from drying in superheated steam were also found for the case of linerboard made not from virgin high yield kraft pulp but from recycled pulp with significant lignin content, McCall and Douglas (2001, 2004).

As for effects on surface properties, paper dried in superheated steam exhibits roughness higher by about 0.5 μm, Li (1993). This effect was attributed to a greater extent of stress relaxation at the surface of the paper because of the higher temperature of the wet sheet that is characteristic of drying in superheated steam. This effect could be detrimental to the quality of uncoated printed papers. However this should not be so for use as the base sheet for coated paper since some roughness is indeed required to hold the coating layer to the paper and to achieve a uniform coat weight distribution. Surface strength is evaluated by printing the paper with tacky ink applied by a rotating inked disc at an accelerating speed. The extent to which fine material or loosely bonded fibres are transferred from the paper surface to the inked disc reveals the paper surface strength. The increased bonded area reported for superheated steam drying is considered the source of the higher surface strength found. The micro-flow of lignin, a hydrophobic polymer, present in greater amount in the fines at higher surface of fibres also results in a higher contact angle and slower water penetration Li (1993). The porosity of paper dried in steam is not much different from that dried in air and remains constant over the drying. However the volume of the smaller pores (0.2 to 0.6 μm) which control light scattering, decreases as drying proceeds. As complete dryness is approached, the volume of micropores is less for paper dried in steam than in air. This difference is consistent with the earlier observation that for drying in superheated steam it is primarily the fines material which deforms, not the long stiff fibres, and it is the network of long fibres which is responsible for the overall porosity.

4.3 Drying coated paper in superheated steam

In the absence of this subject from the literature there is no prior knowledge to report, this area being the topic of the present investigation.

Table 2.7 Summary of effects of superheated steam on paper properties from previous studies: Chemical and mechanical pulps

	Chemical pulps		**Mechanical pulps**		
Pulp type	KP*	KP	TMP	CTMP	BCTMP
Reference	Poirier et al., 1995	McCall and Douglas, 2001, 2004	Poirier et al., 1994	McCall and Douglas, 1994	McCall and Douglas, 2001
Paper grade	Fine paper	Linerboard	Newsprint	Newsprint	Tissue
Basis weight	60 g/m^2	200 g/m^2	60 g/m^2	60 g/m^2	60 g/m^2
Drying temp.	160°C	150-200°C	160°C	150°C	200°C
Specific volume	+ 2-10%	n/a	no change	+ 2%	up to 25%
Tensile strength	- 5-20%	+ 1-18%	+ 20%	+ 30%	no change
Tensile energy	- 10 %	n/a	+ 20%	+ 29%	n/a
Stretch	n/a	n/a	no change	n/a	n/a
Elastic modulus	n/a	n/a	+ 20%	n/a	n/a
Wet tensile	n/a	n/a	no change	n/a	n/a
Burst strength	n/a	n/a	+ 25%	+ 20%	n/a
Tear strength	n/a	n/a	no change	- 8%	n/a
STFI comp. str.	n/a	+ 9-25%	n/a	n/a	n/a
Internal bond str.	n/a	n/a	+ 10%	+ 27%	n/a
Fold	n/a	n/a	no change	n/a	n/a
Zero-span str.	n/a	n/a	no change	+ 6%	n/a
Air resistance	n/a	+ 3-42%	n/a	n/a	n/a
Roughness	n/a	n/a	+ 7%	n/a	n/a
Water abs. time	n/a	n/a	+ 100%*	n/a	n/a
Brightness	- 0-10%	no change	- 9%	- 12%	n/a
Opacity	no change	no change	no change	no change	n/a
Light absorption	no change	n/a	no change	+ 14%	n/a
Light scattering	+ 10%	no change	- 17%	- 17%	n/a

$$\%\ change = \frac{SHSvalue - AIRvalue}{AIRvalue} 100$$

KP: kraft pulp; TMP: thermomechanical pulp; CTMP: chemithermomechanical pulp

BCTMP: bleached CTMP; OCC: old corrugated containers; DIP: de-inked pulp

KP: several chemical pulps were studied: kraft, semibleached kraft, fully bleached kraft, and beaten kraft*

Table 2.8 Summary of effects of superheated steam on paper properties from previous studies: Pulp blends

	Pulp blends				
Pulp type	OCC	TMP + 3.4% DIP	TMP + 3.4% DIP	TMP + 8.5% Filler	TMP + kraft
Reference	McCall and Douglas, 2001	McCall and Douglas, 1994	McCall and Douglas, 2001	McCall and Douglas, 2001	Li, 1993
Paper grade	Linerboard	Newsprint	Newsprint	Fine paper	Newsprint
Basis weight	200 g/m^2	60 g/m^2	140 g/m^2	60 g/m^2	60 g/m^2
Drying temperature	250°C	200°C	200°C	200°C	160°C
Specific volume	+ 4%	+ 6%	no change	+ 5%	n/a
Tensile	+ 13%	+ 15%	+ 23%	+ 22%	n/a
Tensile energy	+ 7%	no change	+ 27%	+ 29%	n/a
Stretch	- 4%	- 13%	+ 5%	+ 6%	n/a
Elastic modulus	+ 19%	n/a	+ 7%	+ 19%	n/a
Burst	+ 2%	+ 5%	+ 5%	+ 26%	n/a
Tear	n/a	n/a	n/a	n/a	n/a
STFI comp. str.	+ 7%	n/a	+ 37%	n/a	n/a
Scott	-10%	n/a	n/a	n/a	n/a
Internal bond str.	n/a	n/a	n/a	n/a	n/a
Fold	n/a	n/a	n/a	n/a	n/a
Zero span	+ 21%	n/a	n/a	n/a	n/a
Air resistance	+ 41%	n/a	n/a	n/a	n/a
Roughness	n/a	n/a	n/a	n/a	+ 5%
Oil absorption time	n/a	n/a	n/a	n/a	+ 40%
Contact angle	n/a	n/a	n/a	n/a	+ 10%
Linting	n/a	n/a	n/a	n/a	- 60%
Brightness	no change	- 12%	- 8%	-5%	n/a
Opacity	no change	no change	no change	no change	n/a
Light abs. coeff.	n/a	+ 29%	n/a	n/a	n/a
Light scat. coeff.	n/a	- 14%	n/a	n/a	n/a

$$\% \, change = \frac{SHSvalue - AIRvalue}{AIRvalue} 100$$

KP: kraft pulp; TMP: thermomechanical pulp; CTMP: chemithermomechanical pulp

BCTMP: bleached CTMP; OCC: old corrugated containers; DIP: deinked pulp

Chapter 3 Experimental

1. Introduction

This chapter describes the equipment and operating procedures used for the production of laboratory coated paper. Figure 3.1 gives the sequence of steps for production of coated paper in the case of laboratory formed base paper (Chapters 4, 6 and 7) and for commercial base paper (Chapter 5). Careful attention is required for the coating-drying steps, performed on a custom facility built at McGill University for close integration of the coating with the impingement drying of the freshly coated paper in either of two drying fluids air or superheated steam. Several changes were made to the original design of this facility, mainly for reducing the coating-to-drying time delay, increasing coat weight range and improving productivity. As particular attention was given to the production of coated paper of quality comparable to commercial paper, section 6 reports several tests made for validating the satisfactory operation of the critical production steps. Section 7 gives the details of paper property testing while section 8 lists the drying condition combinations tested and presents the statistical treatment of data.

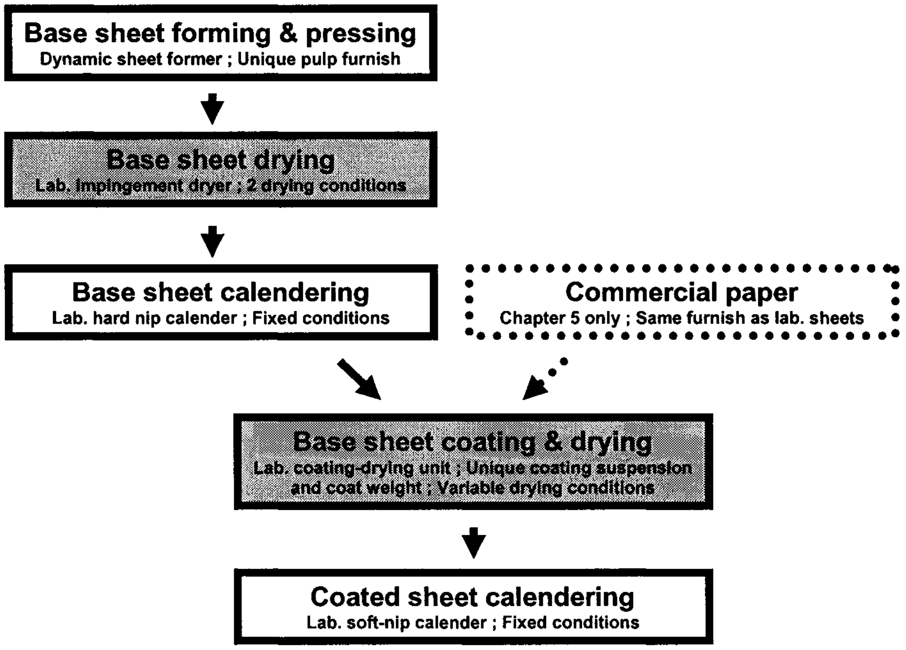

Figure 3.1 Coated sheets production steps

2. Base paper

2.1 Base paper supply

For the experiments with commercial base paper reported in Chapter 5, a choice of the source of paper was required. Thus commercial LWC base paper from three companies was used to produce coated paper in the experimental coating-drying facility. Of these, the base paper having the best formation and which gave the best coating coverage in the laboratory coating unit was selected for the present study.

One objective of this study was to investigate the difference in quality of coated paper between the use of base paper dried in air or dried in superheated steam. As no commercial LWC base sheet is dried in superheated steam, this objective requires the production of base paper in our laboratory where handsheets may be dried in either air or superheated steam. For this purpose handsheets were prepared from the LWC base sheet furnish of the same mill from which commercial base paper was obtained, as noted above. The furnish composition is given in Table 3.1. These never-dried, laborato ry produced base sheets were dried in either air or superheated steam in the drying unit of the laboratory coating-drying facility.

Table 3.1 Furnish composition

Furnish	**Composition %**	**Species**	**Composition %**
Mechanical Pulp	67	Fir	60
		Black Spruce	40
Kraft Pulp	33	Balsam Fir	55
		Spruce	45

2.2 Base sheet forming

The several methods available to produce wet handsheets and their main features are listed in Appendix A section 1. The Dynamic Sheet Former technique was chosen because of its capability to produce an anisotropic sheet analogous to that from a paper machine, of its high reproducibility in terms of formation and grammage, the large size of rectangular sheet produced and the availability nearby of a unit at Paprican, Pointe Claire. The Dynamic Sheet Former is a laboratory batch former producing sheets of structure intermediate between machine formed sheets and standard handsheets. Similar to forming in a paper machine, the Dynamic Sheet Former provides the ability to control and vary the fibre orientation and to achieve nonuniform distribution of fines and fillers in the sheet thickness direction. This forming system usually gives sheets with better formation, i.e. of lower local nonuniformity of grammage, than machine-formed paper. A description of the Dynamic Sheet Former and the base sheet making operating parameters are recorded in Appendix A section 1.

2.3 Base sheet drying

2.3.1 Development of general procedure for base sheet drying

a. Sheet insertion

While developing procedures to dry uncoated handsheets, some problems appeared, whether air or superheated steam was used for drying. First, the tight clearance at the entrance of the dryer for insertion-retraction of the sheet support tray would not allow passage of the handsheets because of these being considerably thicker than the coated commercial base sheets for which it had been designed. This difference in thickness derived from two sources: this was a wet sheet, over 50% moisture content, and handsheets made on the Dynamic Sheet Former were of higher bulk (lower density), hence thicker than paper machine formed base sheets. A new recessed base plate was thus required for the handsheet drying application. In the case of base sheet drying, plate flatness was not a concern therefore inexpensive aluminium, 1/8-inch (0.318 mm) thick, half the thickness of the original stainless steel plate, was selected.

b. Sheet restraint

For mounting a wet sheet, another problem was that regular adhesive tape was ineffective on wet surfaces. Rubber magnets to replace the tape were found unsuccessful. Making metallic rectangular clips to hold the sheet presented difficulties. Once an additional sheet support plate was adopted for superheated steam drying, as described in section 2.3.1c, another technique could be considered. This alternate technique for securing the wet sheet to the base plate consisted in wrapping a larger base sheet around the new thinner base plate and taping it from the back side (not under impingement drying). With teeth machined on the four edges of the new thin base plate and the magnetic attraction of this new thin plate to the thick main base plate, the required full restraint was provided to the wet sheet during drying. This achievement of full restraint in both dimensions during drying was confirmed by drawing geometric curves, circles or rectangles, before and after drying: the superposition of such curves was perfect. Further demonstration that drying was carried out under full restraint in both directions came from the documentation of the tensile strength variation along the width (CD) of the sheet. As is demonstrated on Figure 3.2, the breaking length varies little within the width for a sheet dried with this technique for restraint mounting. By contrast, a sheet simply taped on to the plate with the regular method showed a significant trend of higher strength near the edges, a clear indication of drying with insufficient restraint. The absolute values have no meaning on Figure 3.2 because these sheets were generated with drying conditions different than those used in the subsequent experimental program.

c. Local nonuniformity of drying

The next problem came from limitations of the batch impingement dryer. As is described in section 4.3, the convection dryer is equipped with a diffuser for the drying fluid and a rapidly oscillating nozzle plate with a nozzle pattern optimised to decrease the local heat transfer nonuniformity under the flow field of multiple round jets. The staggered pattern of nozzles acts to minimise local nonuniformity in one dimension while oscillation of the nozzle plate minimises nonuniformity in the other dimension.

These design precautions reduce but do not eliminate the local heat transfer nonuniformity. Thus, this nozzle pattern is reproduced on the sheet because paper shrinks unevenly under uneven heat transfer. With the nozzle plate oscillation system, there will always be some local nonuniformity. Where the plate stops to reverse direction, the areas of the paper directly under the nozzles experience higher intensity drying conditions. This source of nonuniformity was accentuated in the original version of this facility by the oscillation amplitude (total plate travel length) being equal to the distance between two adjacent nozzles: 28 mm. Thus for each cycle the areas of the sheet which were directly under nozzles when the plate reversed motion in one direction were directly under another set of nozzles when the plate reversed motion in the other direction. This undesirable feature was eliminated by redesigning the system with a changed amplitude of oscillation. A series of amplitudes (twice the slider-crank mechanism eccentricity) 16, 20, 23, 24 and 25 mm were tried. The design leading to the least visible imprinting nozzle pattern was selected: 23 mm.

Another type of heat transfer nonuniformity, occurring almost exclusively on the sheets dried in superheated steam was visible as a circular zone in the center. It was found that overdrying rather than underdrying was the cause of this 'cockling' in the center region. Also, the pattern of drying rates higher in the centre and lower at the periphery reflected the effect of cross flow on drying rates under nozzles traversed by the spent air coming from adjacent nozzles. As spent drying fluid exhausts at the periphery, toward the centre such cross flow was a minimum and drying rate greater. Thus the impingement plate rather than the diffuser was presumed responsible for the problem. Minimizing this effect by slightly underdrying the sheet and completing the drying in the ambient was successful in eliminating most of the pattern. This two-step base sheet drying procedure applied likewise to air drying, described in section 2.3.4 of this chapter. Further base sheet calendering completed the pattern removal. Figure 3.3 presents images of the surface of the base sheet with the successive drying conditions tested for minimizing imprinting of the local drying nonuniformity.

2.3.2 Development of procedures for base sheet drying in superheated steam

A major challenge when drying in superheated steam is to avoid condensation, which requires preheating the sheet prior to insertion inside into drying chamber. As the sheet is preheated by being mounted on a preheated support plate, the sheet must in addition be protected from losing moisture before entering the drying chamber. The use of the recessed plate to enable base sheet insertion into the drying chamber, as noted earlier, provided the opportunity to investigate a new technique to overcome steam condensation. In the earlier design the sheet to be dried was placed on a ¼ inch thick steel plate. External preheating of this thick plate created a problem for base sheet taping and also of moisture loss prior to sheet insertion into the drying chamber. The revised strategy derives from the fact that the time for condensation is very short for the very thin, cool base sheet but very large for the heavy steel base plate which is therefore the predominant source of condensation. Therefore the base plate must be preheated to above 100°C and the sheet protected from large heat sink in the heavy steel plate. The new strategy was to use another thin base plate, on which the wet sheet was mounted carefully outside the dryer. Then, when the main base plate had been preheated in the dryer and then retracted, this new thin base plate carrying the already mounted never-dried sheet was placed quickly on the preheated main base plate. This additional plate must be sufficiently thin to be quickly heated by contact with the thick base plate, yet sufficiently thick to provide a stiff support to the sheet. After some trials, a 0.04 mm-thick plate made of magnetic spring steel was chosen. Being magnetic enabled securing this very thin plate to the main base plate by inserting several magnetic plugs into the aluminium base plate. During the short time required for the thin plate to be sufficiently heated by the preheated base plate, the sheet remains covered with a plastic pad, to minimize loss of moisture and heat transfer to the sheet is minimised by means of a silicon rubber insulating sheet placed beneath it. Many test experiments were necessary to determine the time for preheating the base plate in the drying chamber and the time subsequently for the thin secondary base plate to be heated by the thick primary base plate. The moisture content loss before the sheet enters the drying chamber was determined to be only a decrease from 1.3 to 1.2 kg water/kg dry fibre. This rather complex combination of techniques was proven to be successful in avoiding both significant moisture loss from the sheet before it enters the drying chamber and avoiding steam condensation on the never-dried sheet upon its entry into the superheated steam environment in the drying chamber. Figure 3.4 shows a schematic drawing of the wet base sheet support assembly.

2.3.3 Base sheet drying time selection

The drying time required to achieve a target final moisture content must be determined by trial. For drying the base sheet from an initial moisture content of $X = 1.22$ kg/kg dry, Figure 3.5 presents the drying time - final moisture content relations for 40 m/s jet velocity and 140°C jet temperature for both air and superheated steam as the drying fluid. As noted in section 2.3.1c, it was necessary to use a two-step drying procedure: first impingement drying, followed by room temperature natural convection drying. The evidence from earlier studies in this laboratory (Poirier, 1992), is that a steam environment affects paper properties during an intermediate stage of drying, that is, when the dry basis moisture content is within the range 1.2 and 0.3 kg/kg. For the $X = 0.5$ kg/kg - $V_j = 40$ m/s – $T_j = 140$°C conditions of Figure 3.5 the selected drying times 8 s for air and 13 s for SHS allowed meeting these two requirements. At the 140°C jet temperature the drying rate is higher in air than in steam, as reported by previous researchers in this group.

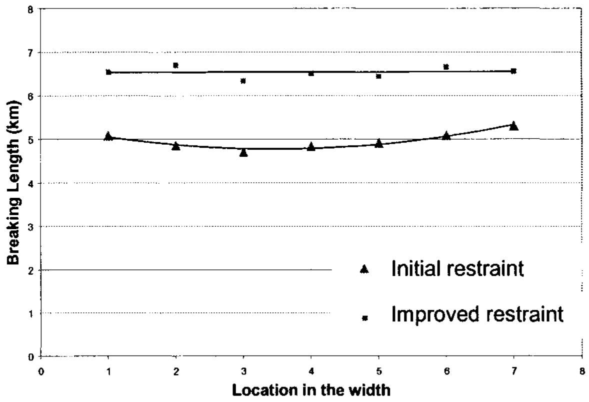

Figure 3.2 Tensile strength variation in cross machine direction

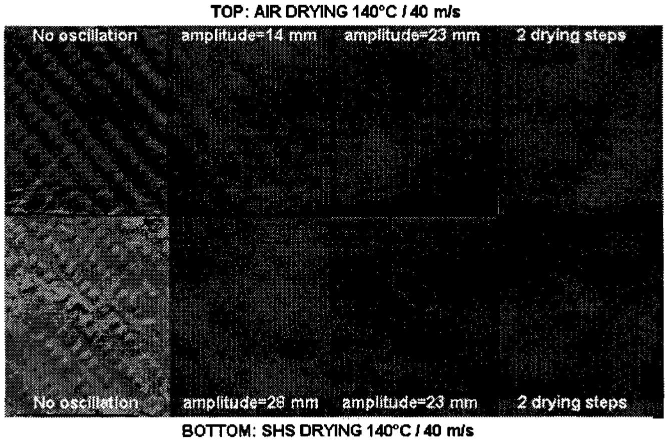

Figure 3.3 Minimizing local drying nonuniformity imprinting in base sheet

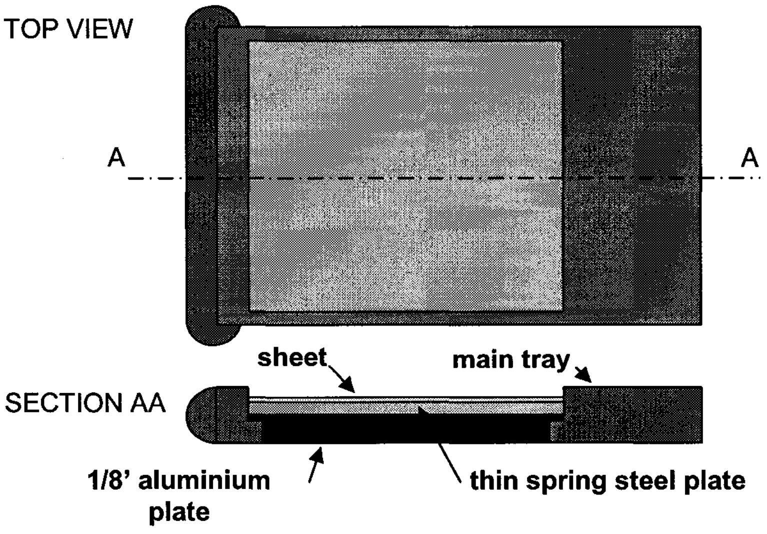

Figure 3.4 Sheet support plate assembly for base sheet drying

This difference occurs because the initial sheet temperature is 100°C in steam at atmospheric pressure but is the wet bulb temperature in air drying, ca. 40-50°C. For superheated steam there is thus a lower temperature difference for heat transfer to the moist sheet from the impingements. Also, at the same jet velocity and jet temperature the steam mass flow rate is lower because of lower fluid density. At equal mass flows and in a given dryer geometry, the drying rate in superheated steam is lower below what is called the "inversion temperature" but is higher above this temperature. The inversion temperature results from the two competitive factors responsible for heat transfer: the temperature difference between the drying fluid and the wet sheet (ΔT) and the heat transfer coefficient. The difference in physical properties between air and steam gives for these conditions a higher heat transfer coefficient for steam.

2.3.4 Base sheet drying procedure

The base sheet drying procedure is recorded in Appendix A section 2.

2.4 Base sheet calendering

In commercial production of the LWC grade of coated paper a light calendering of the base paper is usually performed before coating. Therefore laboratory sheets here were similarly calendered, which provided better flat lay and smoothness. Paprican laboratory hard nip calendar was used at room temperature and with the minimum calendering load possible (5 kN/m).

3. Coating suspension

3.1 Coating formulation

The components of the coating suspension obtained from industrial suppliers were chosen to match current industrial practice for LWC papers in North America. The coating suspension was composed of pigments, viscosity modifier, and binder to build a cohesive porous network of pigment in a coating layer well bonded to the base sheet. Other additives used in smaller quantity in the industrial continuous process (biocides, defoamers...) were not required in this laboratory study. The coating formulation is recorded below, Table 3.2 . Of the two common pigments, clay and calcium carbonate, the more commonly used pigment, clay, was selected here. #2 clay (cheapest, low brightness) and delaminated clay (more expensive, for better surface finish) were used in 1:1 ratio as is often the case for LWC coated paper grade. Of the two common binders, styrene-butadiene latex and starch, of T_g = 12°C, latex was chosen as the current trend favours this binder. As for viscosity modifier, a thickener in this case, carboxymethylcellulose (CMC), one of the most popular, was used. The coating suspension solids content was adjusted to 63% with distilled water.

Table 3.2 Coating suspension composition

Component	**Composition***	**Mass fraction**	**Volume fraction**
Clay #2 and delaminated clay, 50:50	100 pph	0.55	0.32
Styrene-butadiene Latex	13 pph	0.07	0.11
CMC	0.7 pph	0.004	0.01
Water (solids content 63%)	-	0.37	0.56

**Expressed following conventional practice in pph, "parts per hundred", mass of each component per 100 g of pigment (%)*

3.2 Coating preparation

From the dry clay as received, a stabilised clay suspension is first prepared before adding the other components. Both #2 and delaminated clay grades are added gradually in equal parts to distilled water mixed with a dispersant (sodium polyacrylate) at 0.03% by weight of dry clay. This suspension is prepared at 74% solids content. The pH is adjusted to 8 using sodium hydroxide and the suspension is stored in a refrigerator at least overnight to stabilise. Both pH and solids content are measured and adjusted again on the day the coating suspension is prepared.

The coating suspension is prepared using standardised shear conditions using a high shear mixer and mixing sequence to achieve good reproducibility of rheological characteristics. The clay suspension and CMC, both stored in a refrigerator, are first brought to room temperature. The clay suspension is mixed again and the solids content and pH are carefully adjusted. Then the mixing sequence proceeds as follows: (1) CMC is first added gradually to the clay suspension at high shear; (2) then latex is added at low shear; (3) finally some additional distilled water is added to reduce the solids content to the target 63%; (4) pH is adjusted to 8; (5) the coating suspension is degassed in a dessicator connected to a vacuum chamber in order to remove air bubbles entrapped while mixing the ingredients, as bubbles may cause coating defects by bursting under the blade; (6) finally, the suspension is filtered and the solids content measured and given a final adjustment to 63% (degassing induces a slight solids content increase)

3.3 Coating suspension testing

As the coating suspension was a fixed parameter throughout the present study, good reproducibility in coating preparation was ensured by carrying out two basic tests for each batch, the measurement of viscosity and "water retention value". The coating suspension viscosity was evaluated once per coating batch on a rotational viscometer (HAAKE Rotovisco). The "water retention value" was evaluated the AA-GWR (Abo Akademi Gravimetric Water Retention) allowing the gravimetric measurement of dewatering under pressure through a filter. The description of these tests is recorded in Appendix A section 3. Figure 3.6 presents the viscosity of the coating suspension as a function of shear. The water retention value evaluated three times for each coating batch was 46 g/m^2 with a variation of +/-2 g/m^2 from batch to batch.

4. Coating-drying facility

4.1 General

The experimental facility was a laboratory coating unit designed, built and integrated with an impingement dryer to enable investigation of the drying of coated paper in air under conditions comparable to those used industrially, as well as for the investigation of a new drying fluid for coated paper, superheated steam. Two important coated paper production parameters, coating contact time with the base sheet and the delay time between coating and drying reproduce industrial conditions. Coating paper involves a complex interaction between the drainage of water from the coating suspension into the base sheet and transport of water in the opposite direction for evaporation from the coated surface. This interaction strongly influences the final coating structure and composition. Commercially available laboratory coating units do not represent the reality of industrial coated paper machines, typically having too long a coating-to-drying delay time, and permit only the use of air, the standard drying fluid. Thus commercial laboratory coating units do not have the versatility required for the research objectives of this study, including investigation of an experimental drying fluid, superheated steam. The main features of this new facility are therefore (1), very rapid coating application;

(2), very short and variable coating-to-drying delay time, accurately controlled, independent from the coating speed and within the industrial range; (3), variable drying intensity; (4), operation with either air or superheated steam as the drying fluid, both for the production of the base sheet to be used for coating and for the coated sheet.

4.2 Blade coater

4.2.1 Laboratory blade coating and industrial practice

Blade coating was chosen because this process is the coating technique most used in industry. In this process an excess of pigmented suspension is applied to the dry running web and is metered subsequently by means of a stationary blade pressed against a rubber-covered roll. The blade coater of this laboratory was designed to replicate the industrial process as closely as possible. Compared to commercial lab coaters the coating speed is high, with dwell-times of industrial relevance, and the coating-to-drying delay time is much lower, being comparable to that in industrial practice. The main differences from industrial practice are that this laboratory coater is a batch process where the blade travels over a stationary sheet, with the coating suspension being applied and metered at the same time. The blade is a short section of an actual industrial blade, the coating surface of which makes a 45° angle to the paper, spreading the coating pool over a rectangular sheet taped to a smooth steel base plate mounted in a sheet holder tray. The sheet dimensions are 170 mm MD x 140 mm CD where CD (cross direction) is the coating blade length direction and MD (machine direction) is the direction of coating blade motion over the sheet, in both cases as in industrial coating. The sheet is mounted so that MD-CD dimensions of coating are the MD-CD dimensions of forming the base sheet. The sheet holder tray for paper insertion into and retraction from the impingement dryer moves very rapidly back and forth in what is the CD dimension for the coating. The various elements of this facility are now detailed: the coating blade, the blade loading arrangement, the blade coater carriage system. A schematic diagram of the facility is shown in Figure 3.7, with a close-up view in Figure 3.8.

4.2.2 Blade coater carriage system

Figure 3.9 shows the blade coater assembly the main elements of which are described below.

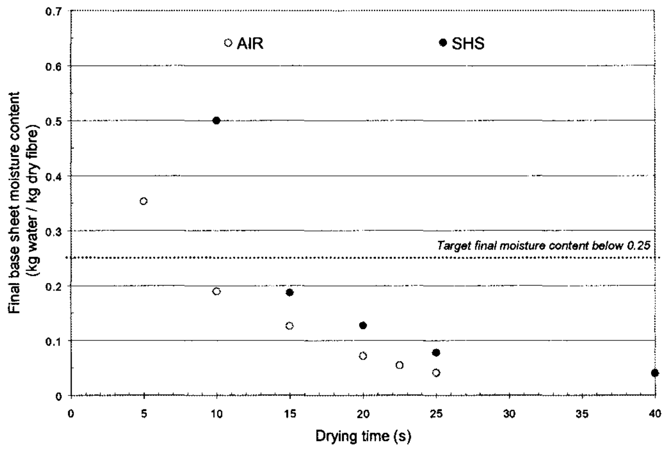

Figure 3.5 Base sheet drying time for X_i=1.22 kg/kg, V_j=40 m/s, T_j=140°C

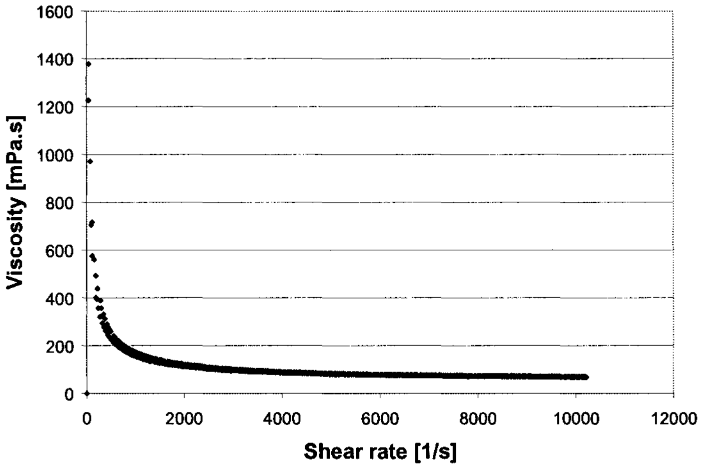

Figure 3.6 Coating suspension viscosity

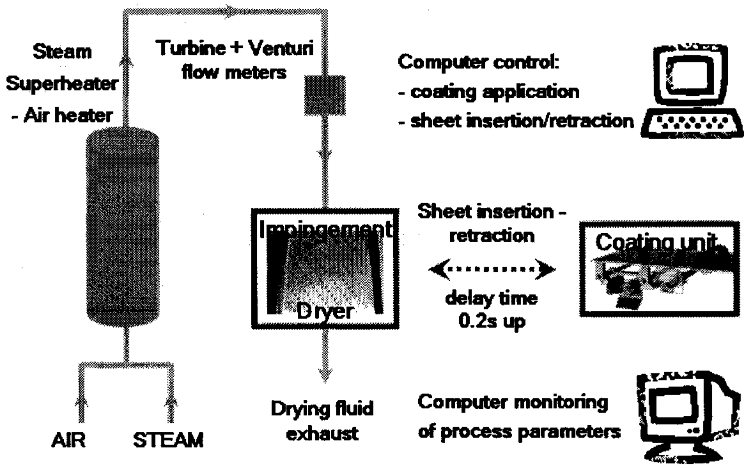

Figure 3.7 Coating-drying unit flow diagram

The entire blade coater and drive unit assembly are held rigidly from above by a supporting plate which is bolted to the impingement dryer on one side and to the main equipment support structure at two points on the other side. This arrangement gives strong stability to the coating operation and maintains constant the alignment of the coater to the sheet holder tray. The entire blade holding system is suspended from the main carriage plate that moves on a dual shaft assembly connected to the drive system. The latter runs on the ball screw having a 6.35 mm diameter pin. Great attention was directed to the blade motion system design in order to apply a very uniform coating layer with good reproducibility. For this reason a stepper motor has been preferred over a pneumatic or hydraulic mechanism. The weight of the blade holding unit was reduced to a minimum and the stepper motor operating parameters were tuned to optimise the blade motion profile. Specifically, the blade speed-blade MD position profile is trapezoidal. A minimum distance for acceleration, from rest to the constant coating speed, about 90 mm in 0.12 is used. The blade motion profile then provides a sufficient length, 170 mm, coated at a steady high coating speed of 1.5 m/s. The blade motion ends with a rapid deceleration to rest over 75 mm, as shown in Figure 3.10. The blade travels the first 45 mm of a total of 90 mm of the acceleration stage without contacting coated paper. The next 45 mm of the acceleration stage the blade contacts paper. The 45 mm length of coated paper, coated while the blade is still accelerating, is not used for the subsequent paper property tests. During the last 75 mm of the deceleration phase the blade is also lifted in order to clear the space required for the sheet holder tray insertion which starts before completion of blade travel.

4.2.3 Blade

The blade is bevelled to have characteristics designed to optimise coated sheet quality. A compound bevel plastic, "soft-tip", blade was preferred over a simple steel or ceramic blade because of better wear resistance, better coverage and higher coating weight achieved. In the printing press any fibres of the base sheet that remain uncovered or poorly covered will interact with the ink differently than pigmented areas, therefore causing printing non-uniformity. Blade wear is not only a cost problem but also affects the coat weight control effectiveness. As the blade wears, its bevel geometry is changed, thereby changing the coat weight control characteristics. Thus the greater durability of a soft-tip blade helps maintain a constant coat weight over time. The soft-tip blade was preferred to a ceramic tipped blade previously used in this laboratory facility to achieve higher coat weight. Figure 3.11 and Table 3.3 document the blade geometry and dimensions.

Table 3.3 Blade dimensions

Dimension	**Reference in** Figure 3.11	**Specification**
Blade length	*a*	120 mm
Blade width	*b*	63.5 mm
Blade extension	*c*	86.5 mm
Blade thickness	*d*	0.457 mm
Blade "adjacent" length	*e*	0.5 mm
Blade main level angle	α	45°
Blade second bevel angle	β	35°

4.2.4 Blade loading system

The blade loading system is critical to maintaining a uniform load in the CD dimension throughout the MD coating length in order to get a uniform coat weight. The blade is clamped at 45° in the blade holder plate by means of three screws along its cross direction width. This plate is mounted tightly on two sliding pins.

The vertical position of the entire blade holding plate is adjusted by means of two fine screws which allow adjustment of the height of the blade tip. These two screws control the distance between the blade tip and the paper, thereby determining the film thickness allowed to pass and hence the coat weight. The fine control of this distance is provided by measuring the strain applied on two die springs using two load cells mounted at each end of the blade. The die springs are compressed to a variable extent by making this screw positioning up or down of the blade holding system. With this configuration the higher the blade load, i.e. the higher the force on the springs, the higher the gap in between the paper and the blade, so the heavier the coat weight achieved. Figure 3.12 presents the blade load – coat weight curves for the 3 types of base paper. The blade loads selected were 27 N/m for laboratory-made sheets, both air and SHS dried, and 29.5 N/m for commercial sheets.

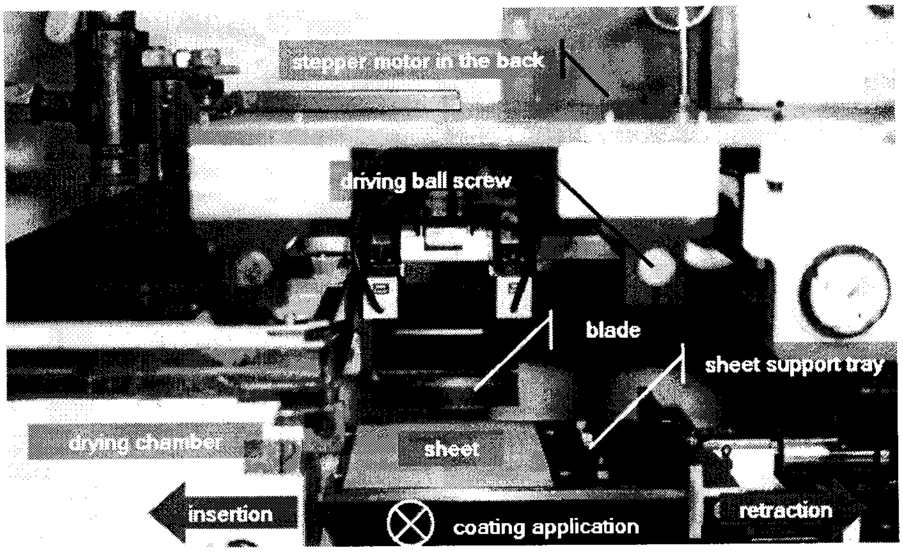

Figure 3.8 Close up view of coating-drying facility

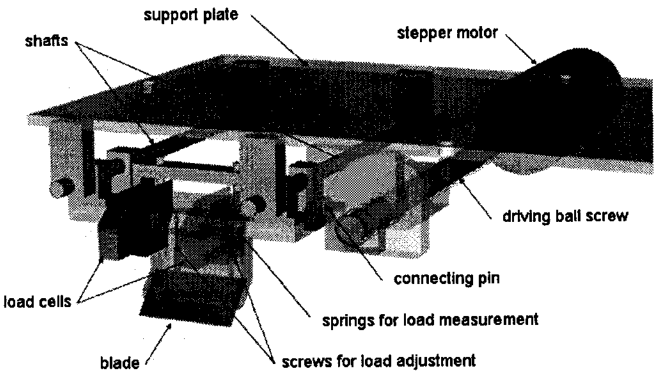

Figure 3.9 Blade coater assembly

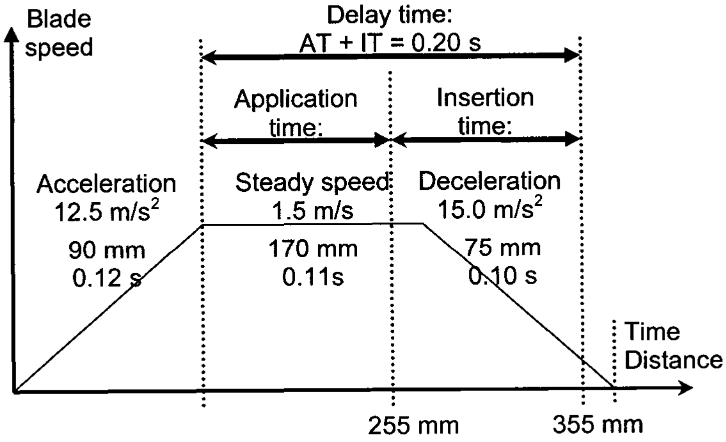

Figure 3.10 Coating blade motion profile

4.3 Impingement dryer

Analogous to the industrial practice of drying coated paper under air impingement in air flotation dryer, drying of uncoated or coated paper is achieved in this laboratory facility under multiple impinging jets from a perforated nozzle plate. A key difference from industrial practice is that here the drying medium can be either air, as in industry, or the experimental drying fluid, superheated steam. The drying fluid, along with moisture evaporated from the sheet, exhausts to a condenser through the open areas in the sheet holder that match openings in the four corners of the drying chamber. In order to obtain a uniform jet velocity over the nozzle plate an air diffuser plate was placed a few millimetres above this plate. The nozzle hole pattern is staggered in one dimension, as in industrial practice in air impingement dryers, and the nozzle plate oscillates in the other dimension (the coater cross direction) at 7 Hz frequency and 23 mm amplitude. The combination of these two design features acts to minimise the two-dimensional local nonuniformity of the impingement flow field and hence of local drying rate. The oscillation is provided by a slider–crank mechanism driven by a single gear motor. The parameters of this design were carefully optimised towards the objective of minimizing local nonuniformity of drying through minimizing the local nonuniformity of exposure of each small element of the wet sheet to the drying fluid over the range from one nozzle to the next. The drying chamber is insulated to reduce the time required for preheating and to obtain uniform temperature within the drying chamber during use. Description of the multiple round impinging jet flow field for the sheet being dried may be expressed using three nondimensional groups for similarity analysis, including two geometric ratios.

- Reynolds number: $Re = \frac{\rho \cdot Vj \cdot D}{\mu}$
- Nozzle-sheet spacing to nozzle diameter ratio: $\frac{H}{D}$
- Nozzle-to-nozzle spacing to nozzle diameter ratio: $\frac{L}{D}$
- Open area ratio: nozzle area / nozzle plate area
- Exhaust area ratio: exhaust openings area / nozzle area

Another potential nondimensional ratio is, V_j/V_p, the ratio of nozzle exit velocity to the speed of transit of the wet sheet under the impingement flow field. With the experimental facility here, this ratio is complicated by the wet sheet transit speed being for an oscillating motion. Values of these parameters are recorded in Table 3.4.

The wet sheet is fully restrained in both directions to standardise properties of the dried sheet and to avoid tearing while passing in and out of the drying chamber at high speed through a slot of minimal clearance. For drying the base paper, for which substantial shrinkage may occur, the wet sheet is wrapped around the thin base plate, taped on the back of the plate, and secured further by teeth indented on each side of the thin base plate. For drying the coated paper, for which shrinkage is limited, the sheet is taped on each side on top of the thin base plate.

Table 3.4 Drying chamber characteristics

Fluid Characteristics	
Jet temperature	Air 20°C - 450°C / Steam 100°C - 500°C
Jet velocity	0 – 120 m/s
Jet Reynolds number	2,000 – 12,000
Drying Chamber Dimensions	
Nozzle geometry	Straight cut, round
Nozzle diameter – D	3 mm
Nozzle-to-nozzle spacing – L	28 mm in CD* / 8 mm in MD* ($L/D = 9.3$)
Nozzle exit-to-sheet spacing - H	26 mm ($H/D = 8.7$)
Nozzle open area	10.22 cm^2 (Open area ratio= 3.33%)
Exhaust area	29 cm^2 (Exhaust area ratio= 2.8)
Nozzle plate oscillation	7 Hz at 11.5 mm amplitude

**CD – cross machine direction and MD – machine direction of the coating application direction*

4.4 Sheet insertion and retraction from dryer

4.4.1 Sheet holder tray

In order to avoid tearing of the sheet during sheet insertion into the dryer the sheet support assembly was modified from the previous design: the sheet level was recessed relative to the drying chamber entrance slot. Different sheet support assemblies were used for drying the base sheet and for drying the coated sheet. In both cases the sheet support assembly consists in a sheet holder tray and a thin base plate on which the sheet is mounted. The sheet holder tray is supported outside the dryer by a strong pin connection to the pneumatic cylinder shaft and inside the dryer on a pair of parallel guides. The sliding frame comprises a central slot where the base plate supporting the sheet rests and a pair of openings, equal in size and symmetrically positioned on each side of the slot. When the sheet holder tray is inside the drying chamber these four openings match the four corresponding openings in the dryer for the exhaust drying fluid to exit to the condenser. In both extreme positions of the sheet holder tray, i.e. fully inserted or fully retracted, the drying chamber is completely sealed. When drying the base sheet the insertion time is not critical so the ¼-inch (0.635 mm) stainless steel tray from previous design was used. An aluminium plate was fitted into the central slot of the tray and the sheet was taped to a thin magnetic spring steel plate as already shown in Figure 3.4. When drying the coated sheet a specially made titanium tray with a central recess to allow thin base plate sliding was preferred because titanium is lighter, thereby allowing shorter insertion time. Figure 3.13 shows a schematic drawing of the coated sheet assembly. The front plate, bolted on the drying chamber, has a narrow opening through which the sheet holder tray enters and leaves. The design details ensure full sealing of the drying chamber except during the short period during very rapid insertion and retraction each 0.1 s. When the tray is fully inserted, the seal is achieved by means of an aluminium plate mounted at its end with a round gasket located in a groove machined into this rectangular plate. When the tray is fully retracted, the sealed is assured by a round titanium bar welded to other side of the sliding frame, with silicone on the ends where it conforms softly to the metal front plate. This system of double seals provides total sealing for air drying. For drying with superheated steam, the small leak which persists prior to tray insertion is removed from the environment of the wet sheet by exhausting to a vacuum cleaner. Even with a perfect seal and the drying chamber well insulated, some heat would be conducted from the dryer to the sheet holder tray and potentially to the sheet while it is being coated. This undesired effect is countered by directing an air shower to cool the end of the tray adjacent to the dryer.

4.4.2 Control of coating-to-drying delay time

A fast acting 305 mm-stroke pneumatic cylinder was installed to achieve very high speed insertion and retraction of the sheet holder tray into and out of the drying chamber. Through use of high activating air pressure 90 psig, 621 kPag, the insertion is sufficiently fast as would damage the tray after extended use. Therefore both ends of the cylinder have adjustable cushions (air release from the chamber is restricted) and a stiff spring is installed on the piston for cushioning on retraction since the piston does not travel the full stroke length.

An optical sensor with a digital display gives the time required, with a resolution of 0.1 ms, for complete insertion and retraction of the sheet as the delay from time of coating to the onset of drying is of primary importance in the drying of coated paper. This IR sensor comprises a transmitter and a receiver. The time recorded is while the signal is not reflected by metal plates which are mounted 200 mm apart on the tray, the distance required for full insertion of the freshly coated sheet. Because the direction of coating of the sheet is at 90° to the sheet insertion-retraction direction, the coating-to-drying delay time varies over the sheet. Only the maximum delay time is directly known from the addition of the insertion time recorded, 0.09 s, and the total time of coating application at steady speed, 0.11 s, i.e. a total of 0.20 s. Assuming that the sheet insertion is at steady speed, and thereby equal to the ratio 200 mm over the recorded insertion time, the delay time distribution over the sheet may be determined as illustrated in Figure 3.14 The "sheet" considered in Figure 3.14 is just the dimensions of the final coated sheet as used for testing, 120 mm (MD) x 100 mm (CD).

4.4.3 Development of procedure for drying coated paper in superheated steam

Drying the freshly coated sheet under air impinging jets can be done without much difficulty provided the sample is well secured on the base plate. Drying the coated sheet under superheated steam impinging jets is much more challenging than for air drying because of the necessity, at every step of the procedure, to avoid any condensation on the sheet being dried. Inserting into the dryer a room temperature tray supporting the sheet is acceptable in air drying but cannot be done for drying in superheated steam as this would cause condensation on the sheet. Steam condensation is unacceptable for drying a freshly coated sheet as the coating layer would thereby be diluted, subjected to mass redistribution and would have the integrity of the coating layer destroyed. The only solution is to preheat the sheet support plate sufficiently before insertion into the drying chamber. However, by preheating the base plate, mounting the sheet is rendered much more difficult and results in an increase in base paper temperature that affects coating application. As detailed in section 2.3.2 for the case of drying the base paper, a new strategy was developed for drying paper in superheated steam. This strategy consists of having two support plates for the wet sheet. The heavy, primary support plate, which is preheated, carries a very thin, secondary support plate which is not preheated and on which the wet sheet is mounted. When the hot primary support plate is retracted from the dryer after the preheating period the thin, secondary support plate with wet sheet already taped on it is inserted quickly and easily into a receiving slot of the primary support plate and coating-drying experiment can be triggered as in air drying.

4.4.4 Coated sheet drying time selection

For drying the base sheet, drying time selection is reported in section 2.3.3. For drying the coated sheets the drying time selected for each combination of drying conditions was that required to dry below a dry basis moisture content of X = 0.053 kg/kg. A final moisture content-drying time empirical relation was generated when drying commercial base paper in air at 120°C and 200°C, and for laboratory made base paper dried in 120°C air. The type of base paper did not affect the drying curves, as seen in Figure 3.15. The selected drying times were 3 s for drying at 120°C, and 2 s for drying at 200°C. Because of the high support plate temperature it was very difficult to generate such a curve when drying in superheated steam. As the two differences, i.e. high support plate temperature but lower ΔT heat transfer driving force act in compensating directions, the same drying times as used for drying in air were therefore selected for drying in superheated steam. The same approach, using constant drying time for variable drying conditions, was used by Yamasaki et al. (1993) for investigating the drying of coated paper in the laboratory. In addition, the effect of drying time on paper properties was further investigated in Chapter 5. Like coating-to-drying delay time, drying time is not the same over the coating CD direction, with sheet insertion / retraction and nozzle oscillation at 90° to coating direction, because insertion time and retraction time differ somewhat between the two sides of the sheet. Figure 3.16 presents the drying time distribution over the sheet for a specific case of nominal drying time 3 s. The largest variation is between the two cross direction (CD) edges where drying time differs by only 3%. The new design, built as described in section 4.4.1, allowed successful use of this new strategy.

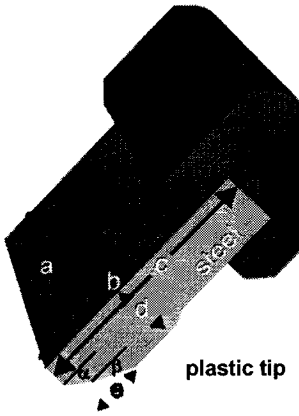

Figure 3.11 Blade geometry

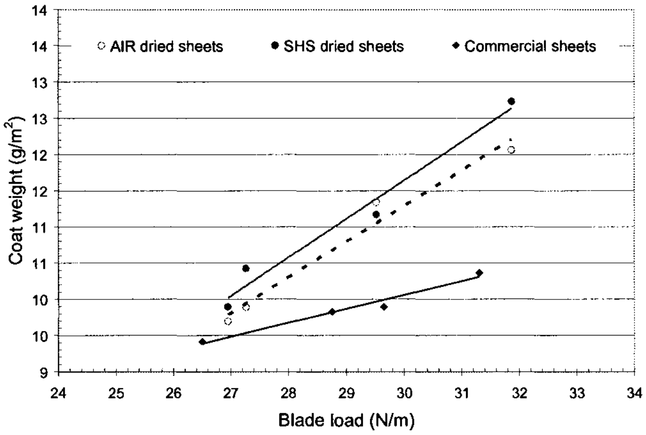

Figure 3.12 Blade load - coat weight calibration curve

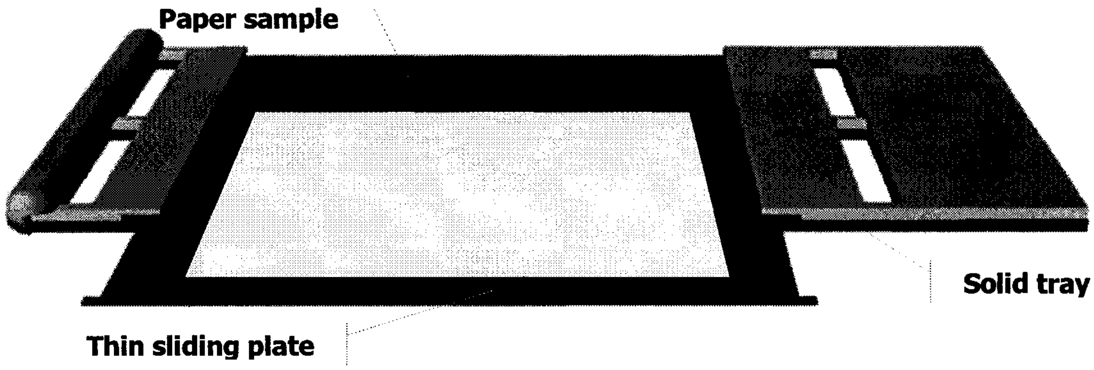

Figure 3.13 Sheet support tray assembly for coating-drying

4.4.5 Coated sheet drying procedure

The coated sheet drying procedure is recorded in Appendix A section 4.

4.5 Auxiliary equipment

The experimental set-up also comprises equipment to provide the high temperature drying fluid, to measure operating parameters and to control the drying fluid temperature. This equipment is described in Appendix A section 5.

5. Coated paper calendering

Almost all pigment-coated papers are calendered after coating to improve the surface smoothness and gloss. A common technique used for LWC papers is high temperature soft calendering in which a high roll temperature is used to selectively soften the coated surface and thereby achieve a higher degree of surface deformation with less compaction of the inner structure. In order to compare the final properties of the sheets produced in our laboratory unit relative to commercial paper, a similar calendering is therefore required. This operation was done on the 12 inch-wide laboratory calender (Beloit) available at Nexfor Technology Centre in Pointe-Claire. This calender comprises two heated metal rolls for hard nip calendering and one unheated polymer-covered roll for soft nip calendering. In soft nip calendering the sheet is fed into the nip with the coated side facing the hot metal surface while the soft roll serves as a backing roll. It was necessary to run calibration curves to select calendering operating parameters to reach the targeted gloss of 54° with a PPS roughness lower than 1.5 μm in the case of laboratory coated paper made from commercial base paper. Different combinations of three parameters - roll temperature, nip load and number of passes - can achieve this target.

Running one pass at a fixed roll temperature and varying the load is one possibility. This strategy was successful in reaching the gloss target with a low roughness as well. The selected calendering settings are given in Table 3.5.

Table 3.5 Calendering operating parameters

Roll temperature	**Nip Load**	**Speed**	**Calender Type**
100°C	121 kN/m	10 m/min	Soft Nip / one pass

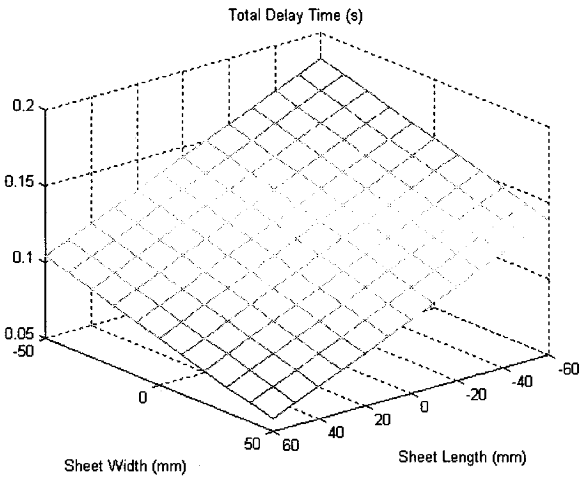

Figure 3.14 Coating-to-drying delay time distribution over a sheet of dimensions 120 mm (MD) X 100 mm (CD)

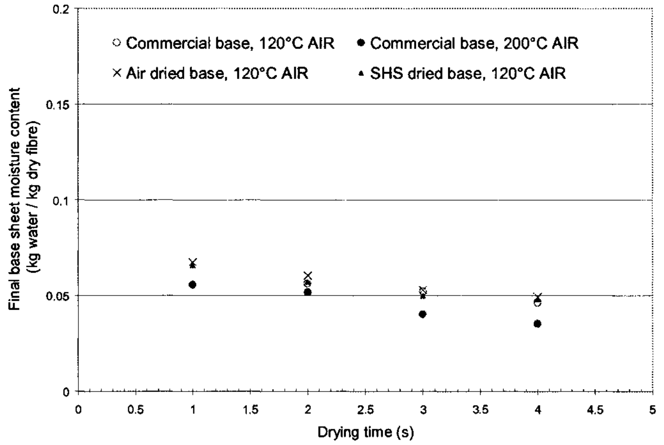

Figure 3.15 Coated sheet moisture content - drying time relations

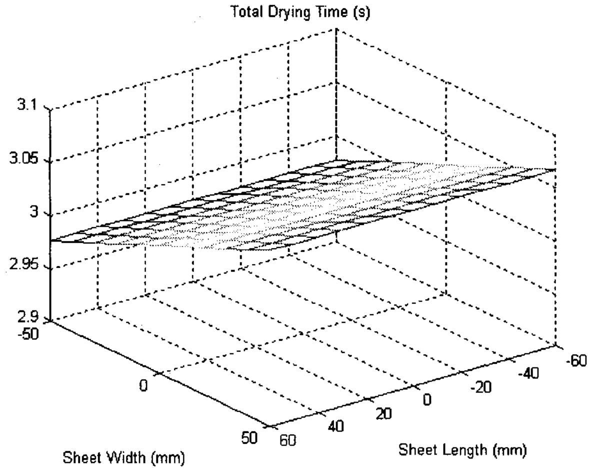

Figure 3.16 Drying time distribution over the sheet

6. Laboratory coated paper quality validation

6.1 Uncoated paper

The Dynamic Sheet Former (DSF) was the selected technique to produce wet base sheets for investigation of the effect on coated paper quality of changing the base sheet drying process. Good reproducibility in terms of basis weight, local grammage and good fines retention were obtained, as supported by the following documentation of these properties.

6.1.1 Basis weight

Base sheet grammage, the dry weight per unit area, must be controlled within a tight range because this factor influences the coating hold-out during blade application. Moreover basis weight is a major concern in the perspective of testing paper properties. In the Dynamic Sheet Former, the basis weight depends primarily on the stock consistency, jet velocity and number of jet passes and to a lesser extent on the nozzle angle and nozzle-to-forming wire distance and the forming wire speed. Therefore stock consistency was tightly controlled to 0.25% +/-0.005%, jet pressure (thereby jet velocity) to 22 psi +/-2 psi (152 kPa +/-14 kPa) and forming wire speed to 1000 m/min +/-3 m/min. The basis weight was checked every production day on a whole sheet and later on samples dried in the laboratory, as is reported in comparison to commercial paper in Table 3.6. The standard deviation of laboratory handsheets is larger than that of paper produced on a paper machine but still small which confirms the good control achieved by the precautions noted above. For comparison standard handsheets used for testing pulp properties must be prepared to 60 g/m^2 +/-1 g/m^2 according to PAPTAC standard methods.

Table 3.6 Base paper basis weight control

Sheet former	Average basis weight (g/m^2)	Standard deviation	Number of sheets
Dynamic Sheet Former	40.0	1.05	250
Paper Machine	37.7	0.52	200

6.1.2 Paper formation

Another concern for the coating process is the local grammage variation at the smaller scale, referred as the "formation" of the sheet. The quality of the sheet formation is related to physical processes involved during sheet forming from the suspension of fibres. Formation is generally evaluated by obtaining an image of the sheet by light transmission and analysing the local nonuniformity of sheet opacity. Current commercial formation test instruments all use simple analysis procedures which reduce the two-dimensional nonuniformity to some single-number index of formation nonuniformity. The most standard such index is the coefficient of variation of local grammage, in which case this index is defined as the "formation number".

Bernié and Douglas at McGill University have developed a substantially more sophisticated method of formation determination, with their original approach of partitioning formation nonuniformity into its components as a function of scale of formation over a range in scale of formation from a few tenths of a millimetre to several centimetres. At each specific value of scale of formation the intensity of nonuniformity of formation is evaluated by a two dimensional fast fourier transform based method and constitutes a component of formation. The complete series of values of intensity of formation nonuniformity evaluated over this range of scale of formation defines what is termed the "paper formation line". In the commercial version, the PaperPerfect Formation analyser, the nonuniformiy is determined at 10 values of scale of formation over the 0.6-37 mm range of scale of formation, providing 10 components of formation. In order to compare the formation of the sheet made on the Dynamic Sheet Former to that made on the commercial paper machine, the relative components of formation nonuniformity are reported, with the reference sheet being the commercial paper made with exactly the same pulp and at the about the same mean grammage, 38 g/m^2 for the commercial paper and 40 g/m^2 for the laboratory paper, Table 3.6. The relative component of formation is the ratio of the component of formation of the sheet tested to that of the previously determined reference paper, here the commercial paper. The same technique will be analogously applied for evaluation of print nonuniformity in Chapters 5 and 7.

The procedure involved taking by light transmission 4 independent images on each of 8 Dynamic Sheet Former sheets produced over a period of four days and made using two different batches of pulp. A single average paper formation line was produced for each of the 8 sheets by averaging the results from 4 images for each sheet. The components of formation of the paper formation line for each of these 8 sheets are given in Figure 3.17. On this basis a formation component value of 1.2 means that at this value of scale of formation, the formation nonuniformity is 20% less than that of the reference sheet; a value of 0.9 that the nonuniformity is 10% greater. From Figure 3.17 it is seen that relative to commercial paper Dynamic Sheet Former sheets have better formation (lower nonuniformity) over nearly the whole range of scale of formation. This difference is however very sensitive to scale of formation, being small over the 0.6-2 mm and 22-37 mm ranges near the lower and upper limits of scale of formation. The variability of formation within a single laboratory sheet, calculated as the coefficient of variation of the 4 components of formation obtained from the 4 independent images tested for each sheet, is higher than that over an equivalent area of commercial base paper, as shown on Figure 3.18. However the values obtained for the commercial paper were from paper samples produced in a very short time (same reel). For machine-made papers produced on different days on the same machine, greater variation is experienced. Even for a given paper reel, variations in the cross machine direction may be large, up to 15% relative to the mean value, as reported by Bernié and Douglas (1998).

6.1.3 Paper fines content

Paper is a network of fibres of various size and shape. For mechanical pulp the fibres shorter than 80 μm, termed the fines, play an important role in the fibre network cohesion. The fines also contain more lignin than long and are therefore more affected by superheated steam drying, as explained in Chapter 2. Particular attention was thus given to making handsheets with a fines content close to commercial paper, and to maintain the fines content constant. The Bauer McNett method was used to separate pulp samples into a number of fractions from which the fines content was determined. The Bauer McNett Classifier consists in five tanks arranged in a cascade. Each tank has a screen with a different mesh size that retains fibres greater in length than the mesh. This segregation is very precise for the coarse, stiff fibres of mechanical pulp but less so for the flexible, conformable fibres of chemical pulp which may bend and pass through openings smaller than their length. The fraction retained on each screen is reported as a percentage of the oven dry weight. The pulp passing through the final screen is deduced by the difference between the weight of batch and the total weight of all fractions.

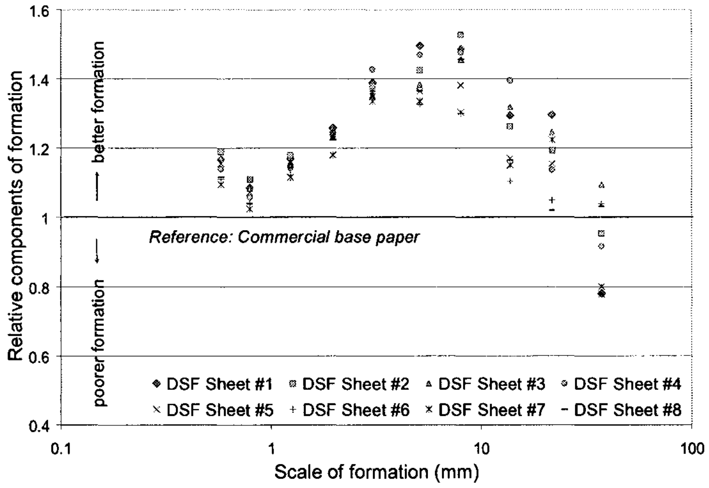

Figure 3.17 Formation lines for base paper

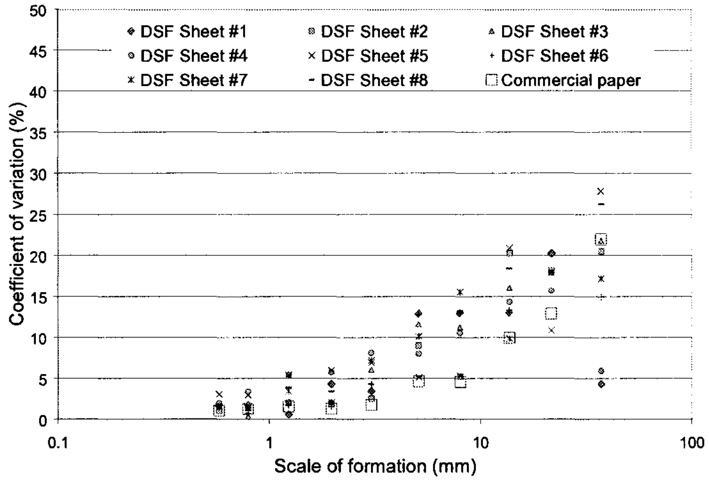

Figure 3.18 Variability of components of formation for base paper

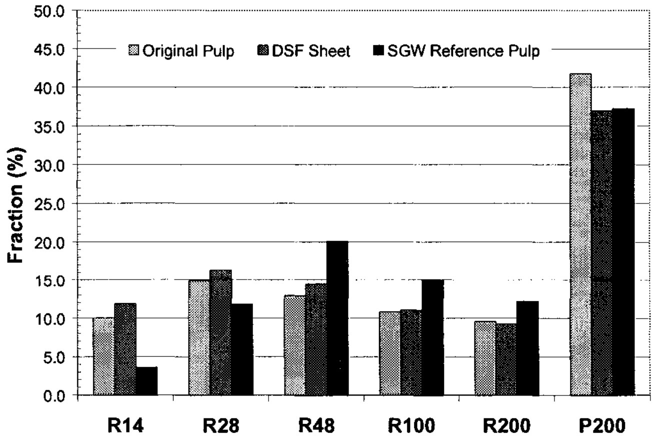

Figure 3.19 Fines content

This fraction is referred as the fines fraction. Both the original pulp and Dynamic Sheet Former paper have been tested in order to investigate as well the fibre retention in this handsheet forming process. For each pulp the average fines fraction value was calculated based on tests two 10 g (oven dry) batches, with using 4 successive screens of 14, 24, 48, 100 and 200 mesh.

The furnish, Table 3.1, is composed of stone ground wood (SGW) pulp and kraft pulp in 2:1 ratio. In the SGW process where pulp is produced by pressing the logs of against an abrasive rotating stone surface, a large fraction of fibre fines is produced, which is good for formation and high opacity of the sheet. Kraft pulp is obtained from wood chips cooked in an aqueous solution of chemicals at elevated temperature and pressure. This chemical conversion and extraction process converts lignin into soluble products, thereby freeing long cellulose fibres to separate easily. Such longer, softer and more flexible fibres strengthen the sheet for better runnability at the coating unit.

Figure 3.19 presents the results obtained from the Bauer McNett fractionation of original pulp, the paper made on the DSF and used in this study and a typical SGW pulp. The fraction of fibres retained on each screen, R14 to R200, is obtained by collecting and weighing the fibres on each screen, while the fraction of fibres that passed through the final screen, P200 also called fines, is deduced by difference with the total weight of pulp tested in the run. Figure 3.19 shows that the highest fines content is in the original pulp because of the greater proportion of SGW. However the presence of kraft pulp moves the length distribution peak to a longer average length, not as pronounced as for the SGW reference pulp. There is a 5 percentage point loss in the fines content in the Dynamic Sheet Former process with this particular furnish, which leaves 37% fines content in the sheet, a value close to that of the commercial base paper about 35%. Almost 100% retention of the longer fibres is obtained, which slightly increases this fraction in the pulp as some fines are lost.

6.2 Coated paper

6.2.1 Coat weight

The dry weight of coating applied to the paper, an important parameter, must be measured and controlled accurately. Coat weight influences greatly the mechanical, optical and surface properties of the coated paper not only in terms of the fraction of the sheet it represents, but also because during the coating consolidation process the drainage and binder migration depend on coating layer thickness.

In the present research the coat weight is measured gravimetrically by weighing the individual sheet before and after coating. Moisture content determination of the uncoated base sheet and the coated paper, both hygroscopic materials, is also required in order to calculate the bone dry coat weight. These moisture contents are determined when the paper reaches its pseudo-equilibrium moisture content after a standard time at conditions constant of air humidity and temperature. Thus uncoated and coated sheets are kept in a controlled environment room at 50% Relative Humidity (+/-2%) and 23°C (+/-1°C) for at least 12 h. Table 3.7 lists the terms used to designate weight, dimensions and moisture content, their nominal values and their measurement uncertainty.

The dry basis weight of the base sheet, *BWB*, the dry basis weight of the coated sheet, *BWC*, and coat weight, *CW*, were determined as follows:

Basis weight, base sheet (oven dry): $BWB = W_{uncoated} / (w_b l_b) \cdot 1/(1 + X_{beq})$

Basis weight, coated sheet (oven dry): $BWC = W_d / (w_c l_c)$

Coat weight (oven dry): $CW = BWC - BWB$

The uncertainty in coat weight calculated is determined as follows:

$$\delta CW = \sqrt{A_c + A_b} \text{ with } A = \left[\frac{X}{l \cdot w} \cdot \delta W\right]^2 + \left[\frac{W}{l \cdot w} \cdot \delta X\right]^2 + \left[\frac{-1}{l^2} \cdot \frac{W \cdot X}{w} \cdot \delta l\right]^2 + \left[\frac{-1}{w^2} \cdot \frac{W \cdot X}{l} \cdot \delta w\right]^2$$

applied to either the coated sheet, A_c, or the base sheet, A_b. From values in Table 3.7 the coat weight uncertainty is thereby determined to be +/-0.20 g/m^2. With the target coat weight of 10 g/m^2, the coat weight uncertainty is then 2 %. In addition, as the coating process is sensitive to the change in paper surface properties which accompanies any change in moisture content, the sheets are brought from the controlled environment room to the experimental laboratory in a well-sealed plastic bag, then bagged again immediately after the coating-drying experiment for return to the controlled conditions room. Table 3.8 shows the variability of coat weight could be maintained within +/-5%.

6.2.2 Coat weight MD and CD profiles

As detailed in section 4.2 the blade, supported from above by the mounting plate, applies the coating suspension to the base sheet mounted on a base plate.

Table 3.7 Definitions of abbreviations used for coat weight measurement uncertainty

Designation	**Definition**	**Value**	**Uncertainty**
l_b	Length, Base sheet	0.17 m	1 mm
l_c	Length, Coated sheet	0.12 m	1 mm
w_b	Width, Base sheet	0.14 m	1 mm
w_c	Width, Coated sheet	0.09 m	1 mm
W_c	Weight, Coated sheet after conditioning	0.8 g	0.0001 g
W_d	Weight, Coated sheet after oven drying at 105°C	0.5 g	0.0001 g
$W_{uncoated}$	Weight, Base sheet at equilibrium moisture content	1 g	0.0001 g
*X_{beq}	Equilibrium moisture content, Base sheet	0.076	0.002 %
X_{eq}	Equilibrium moisture content, Coated sheet	varies	0.002 %

**X: dry basis moisture content, kg/kg dry*

Table 3.8 Coat weight control

Sheet former	**Average coat weight (g/m^2)**	**Standard deviation**	**Number of sheets**
Dynamic Sheet Former	10.13	0.51	250
Paper Machine	10.25	0.52	200

In order to achieve an even distribution of the coating on the surface, the flatness of the sheet holder must be assured and the relative position of the support plate of the coating unit and the sheet holder tray must be adjusted.

The sheet support plate must provide a near perfect surface, level and smoother than the paper, so as not to be the source of any nonuniformity of the coating. As for the position of the coating unit support plate relative to the sheet holder tray, this is adjusted and optimised carefully using the three adjusting bolts which secure it. The adjustment of the mounting plate was documented in terms of the number of threads emerging from the bolt for each bolting point.

The coat weight distribution across the sheet was evaluated by the "burnout test". The burnout test designates the technique of chemical removal by dehydration of the lignocellulose base by reaction with strong acid-weak base salts, O'Neill and Jordan (2000). Burnout tests were carried out by immersion of the coated paper for several minutes in ammonium chloride solution followed by drying in ambient air, then in a muffle furnace at 225°C for 5 minutes. Images of the coating layers against the blackened base sheet were acquired digitally using a standard scanner at 150 dpi, Figure 3.20. The reflectance uniformity, i.e. coat weight uniformity, was evaluated across the sample in both directions at 10 different locations as illustrated in Figure 3.21 and Figure 3.22 The successive coating unit levelling steps allowed reaching even coat weight profiles in both machine (MD) and cross-machine (CD) directions.

6.2.3 Coated sheet average moisture content

a. Gravimetric measurement

The coated paper production procedure was adapted to enable measurement of the evolution with time of the sheet average moisture content, to be used in Chapter 5 for drying rate calculation, for the drying of coated paper, plus some supplementary measurements for base sheet drying. In a sequence of operations carried out very quickly after retraction from the drying chamber on completion of a preselected drying time, the sheet was transferred from the base plate to a cutting pad, covered with a recessed plate, a 120 mm x 90 mm section was cut using that cover as a template and this coated sheet was weighed (designated W_t) on an adjacent four-decimal point balance. These coated sheets were re-weighed (W_c) after conditioning in the controlled environment room at 23°C and 50% relative humidity, and again after overnight oven drying at 105°C (W_d). The dry basis weight of the base sheet, *BWB*, the dry basis weight of the coated sheet, *BWC*, and coat weight, *CW*, were thereby determined for each sample. Table 3.9 lists the terms used to designate weight, dimensions and moisture content, along with their nominal values.

Table 3.9 Definitions of abbreviations used for drying rate calculation

Designation	**Definition**	**Value**
W_t	Weight, Coated sheet immediately after experimental drying	varies
X_{cs}	Moisture content, Coating suspension	0.587
X_i	Initial moisture content, Coated sheet just after coating	0.182
X	Moisture content, Sheet after drying for time period t	varies

**X: dry basis moisture content, kg/kg dry*

The basic calculations associated with the terms defined in Table 3.9 are as follows:

Coated sheet moisture content (dry basis, kg/kg dry): $X_t = (W_t - W_d)/W_d$

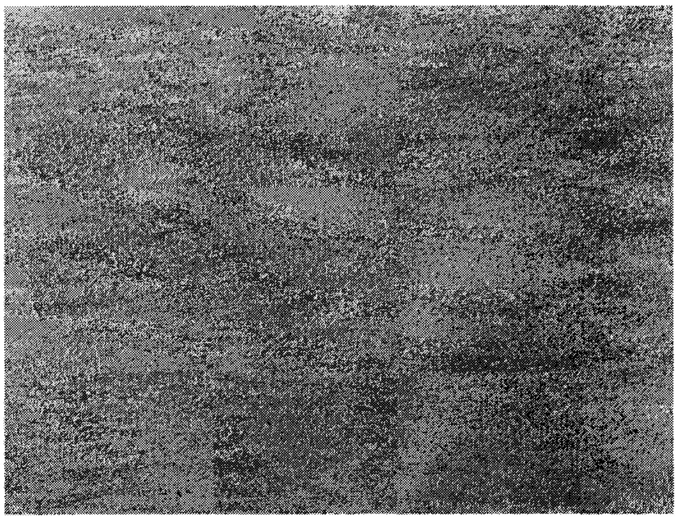

Figure 3.20 Coat weight distribution control: burnout image

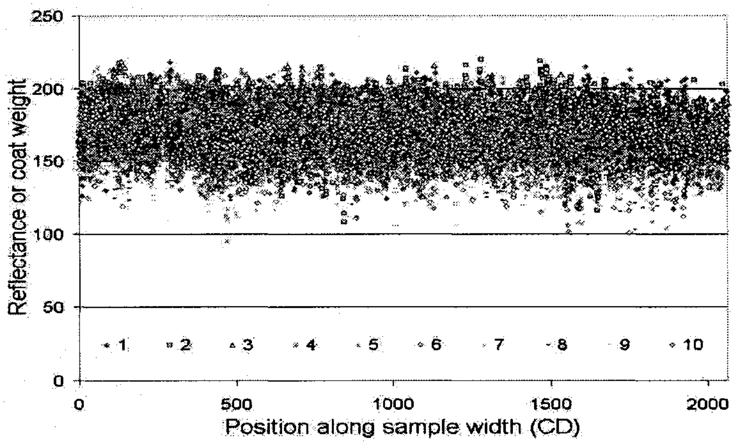

Figure 3.21 Coat weight distribution control: CD variation (reflectance value has no meaning)

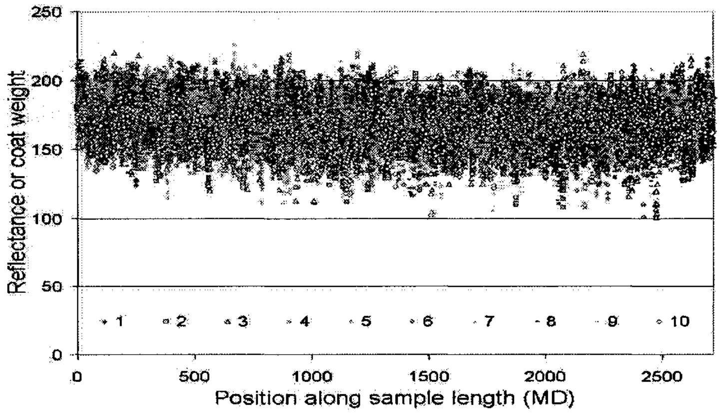

Figure 3.22 Coat weight distribution control: MD variation (reflectance value has no meaning)

Coated sheet equilibrium moisture content, kg/kg dry: $X_{eq} = (W_c - W_d)/W_d$

b. Measurement error of coated sheet moisture content

Measurement of coated sheet moisture content, X, was affected by the relative humidity of the room. This measurement error could be estimated by measuring the initial moisture content, X_i, just after coating but before drying, since this value can be determined precisely, from three values - the coating suspension moisture content, BWC and CW:

Coated paper initial moisture content: $X_i = \frac{BWB \cdot X_{beq} + CW \cdot X_c}{BWC} = 0.182$ kg/kg

Table 3.10 presents the successive attempts for improving the procedure in order to obtain a more accurate measurement of X_i. The designation "humidity control" in Table 3.10 indicates the use of a humidifier in an enclosure made of clear plastic sheeting around coating-drying facility, including later the balance as well. With this degree of humidity control the procedure finally selected enabled determination of sheet moisture with an underestimation of only 2 % when the dryer was off and of about 6 % when the dryer was running. Heat conduction from the hot dryer was minimized by insulating material but could not be completely removed, hence the lower value of X_i found and higher error with the dryer operating than the dryer is off.

Table 3.10 Measurement error for coated sheet moisture content

	X_i measured	**% error**
No humidity control	0.122	-33.3
No humidity control + timing optimized	0.133	-27.1
No humidity control + folding the sheet	0.130	-28.7
No humidity control + folding the sheet improved	0.139	-23.7
Humidity control around facility	0.158	-13.8
Humidity control around facility + balance; dryer off	0.181	-1.3
Humidity control around facility + balance; dryer on	0.173	-5.5

$* \% error = (X_i^{measured} - X_i^{calculated}) / X_i^{calculated} \cdot 100$

7. Paper properties definition and testing

For measurement of paper properties, uncoated and coated sheets were conditioned for hours at 23°C and 50% relative humidity before being tested. Testing was performed according to PAPTAC Standard Test Methods given in Table 3.11 when available, or custom procedures which are described here. The equilibrium moisture content of paper was measured by weighing after conditioning and after overnight oven drying at 105°C. The dry basis weight of paper, mass per unit area, was measured on conditioned sheets accounting for the moisture content as previously determined. For each property, 10 replicate sheets were tested except for Talyscan profilometry, mercury porosimetry and ESCA, for which a single sheet was tested. The definitions of properties and procedures for testing properties are given in Appendix A section 6.

8. Experimental conditions and results

8.1 Combination of paper type and drying conditions

Tables 3.12, 3.13 and 3.14 give the various conditions used in this study. Two types of base paper were used, laboratory made and paper machine made. The properties of uncoated base paper are reported in Chapter 4. The laboratory base paper was formed on a Dynamic Sheet Former, and dried under impinging jets of air or superheated steam at 140°C, while the commercial base paper was machine-formed and dried by conduction on conventional cylinder dryers. In the case of sheets coated on commercial base paper both coating-to-drying delay time and drying time were varied as well as the drying fluid and drying fluid temperature. As for sheets coated on laboratory base paper, the drying fluid was air or superheated steam, drying fluid temperature 120 or 200°C. The coating-to-drying delay time was fixed at 0.2 s and the drying time was that selected in section 4.4.4. The results with sheets coated on commercial base paper are given in Chapter 5 while that of sheets coated on laboratory made base paper in Chapters 6 and 7.

8.2 Statistical treatment of data

For each property determined and each sample tested, i, the mean value, $\bar{y}_i$, and the standard deviation, s_i, were calculated. A pooled standard deviation was calculated among the 3 samples tested in Chapter 4 and given in Table 3.12, the 33 samples of Chapter 5 given in Table 3.13 and the 8 samples of Chapters 6 and 7 given in Table 3.14. The equation used for the pooled sample standard deviation, s_p, is as follows when the number of observations, n, is the same for all the samples:

$$s_p = \sqrt{\frac{\sum_{i=1}^{r} s_i^2}{r}} \tag{3.1}$$

with r the number of samples, that is the number of production conditions used. To determine the significance of the differences between the means of the samples, the Ott's analysis of means (ANOM) test was used as described in Vardeman (1993). This method defines the decision limit, DL, in a similar manner as a confidence interval:

$$DL = h \cdot s_p \cdot \sqrt{\frac{r-1}{n \cdot r}} \tag{3.2}$$

with h a value taken from the table of "95% quantiles of the distribution of the ANOM statistic when all means are equal" with number of means is r and the degree of freedom is $v = r \cdot (n-1)$. The plots of the properties for the various conditions tested are then represented in with the line of the mean of all samples, the line of the upper decision limit and the line of the lower decision limit. It is thereby possible to visualize which drying condition leads to a significantly different level of a given property: the means that plot outside the decision limits are significantly different from those that do not, all of which are judged not significantly different.

Table 3.11 Testing procedures for paper properties

Property	**PAPTAC Standard**	**Related TAPPI Standard**	**Instrument**	**Sensing area**
Thickness	D4	T411om97	Micrometer	2.5 cm^2
Mercury porosimetry	-	-	Porosimetrics Pore Sizer 9320	9 cm^2
Permeability	-	TIS 460 om-96	ParkerPrintSurf *PPS-10*	5 cm^2
Brightness	E1	T452os77	Technibryte Micro TB1C	707 mm^2
Opacity	E2	T425om60	Technibryte Micro TB1C	707 mm^2
Tensile	D34	T220	Instron	15 cm^2
Burst	D8	T403om91	L&W	10 cm^2
Tear	D9	T414om88	Elmendorf	130 cm^2
Roughness	D31P	T555om94	ParkerPrintSurf *PPS-10*	2.5 mm^2
	-	-	Talyscan Profilometer	1 mm^2
Gloss	E3P	T480	Technibryte T480A	140 mm^2
Water absorption	-	T42om87	Custom set-up	5 cm^2
ESCA	-	-	-	100 mm^2
SEM	-	-	JEOL-840	varies

Table 3.12 Uncoated paper production: Laboratory and commercial base papers, Chapter 4

Condition designation	**Forming**	**Drying method**	**Drying fluid**
AIR	Laboratory Dynamic Sheet Former	Impingement	Air
SHS	Laboratory Dynamic Sheet Former	Impingement	Superheated steam (SHS)
COM	Commercial Machine Former	Cylinder	Air

Table 3.13 Coated paper drying conditions combinations: Commercial base paper, Chapter 5

Designation	**Drying fluid**	**Drying fluid temperature, T_j**	**Drying time, t**	**Coating-to-drying delay time, *CDD***
[1]CA120	Air – Impingement	120°C	0.4 to 40 s	0.2 and 1 s
CA200	Air – Impingement	200°C	0.4 to 20 s	0.2 to 1 s
CS200	SHS - Impingement	200°C	0.4 to 4 s	0.2 s
[2]CA(c)23	Air – Natural convection	23°C	24 h	-
[3]CA(h)23	Air – Natural convection	23°C	24 h	-

[1]The first letter C for commercial base paper, the second letter A or S for air or superheated steam (SHS), the coated sheet drying fluid, the 3-digit number 120 or 200 for 120 or 200°C, the coated sheet drying fluid temperature T_j, [2]c: Cold support tray, [3]h: Hot support tray

Table 3.14 Coated paper drying conditions combinations: Laboratory made base paper, Chapters 6 and 7

Drying condition designation	**Base sheet drying fluid**	**Coated sheet drying fluid**	**Coated sheet drying fluid temperature**
[1]AA120	Air	Air	120°C
AA200	Air	Air	200°C
AS120	Air	Superheated steam	120°C
AS200	Air	Superheated steam	200°C
SA120	Superheated steam	Air	120°C
SA200	Superheated steam	Air	200°C
SS120	Superheated steam	Superheated steam	120°C
SS200	Superheated steam	Superheated steam	200°C

[1]The first letter is A or S for air or superheated steam (SHS), the base sheet drying fluid, the second letter is A or S for air or superheated steam, the coated sheet drying fluid, the 3-digit number 120 or 200 for 120 or 200°C, the coated sheet drying fluid temperature.

Chapter 4 Effects of superheated steam drying on base paper properties

1. Introduction

1.1 Objective

One of the goals of the present study is to investigate the effects on coated paper properties from drying the base paper in superheated steam. Characterization of key properties of uncoated base paper dried variously is necessary to understand the impact from base paper drying on final coated paper quality. The effects on paper properties from drying some kinds of paper in superheated steam have been documented in previous studies from this laboratory. A comprehensive listing of these effects is provided in Chapter 2 section 4 and summarized in Tables 2.7 and 2.8 for comparison with those obtained in the present study. The effects of superheated steam drying on paper properties were determined for the specific uncoated paper used for the present study because the pulp furnish and experimental procedures differ significantly from those of previous work.

1.2 Summary of experimental conditions

The experimental details described in Chapter 3 section 2 are reviewed briefly. Two kinds of uncoated base sheets were used. DSF formed sheets were made from a pulp obtained from a mill producing LWC base stock and dried in air or superheated steam in the laboratory. Also used were dry machine-produced base stock for LWC, made from the same pulp, same mill. This pulp contained a mixture of SGW (Stone Ground Wood, mechanical) and kraft (chemical) pulps in 2:1 ratio. Wet sheets were produced from this pulp in a laboratory Dynamic Sheet Former (DSF). During DSF sheet making, particular attention was paid to retaining the fines in the sheet as previous work showed that this fraction of the pulp plays an important role in superheated steam drying. As demonstrated in Chapter 3 section 6.1.3, in contrast to standard handsheets the fines were successfully retained: 37% in the DSF sheet versus 42% originally in the pulp. These wet sheets were then dried in the laboratory impingement dryer using as the drying fluid air or superheated steam at 140°C and 40 m/s. For drying at atmospheric pressure the effect of temperature of the drying fluid when using superheated steam is secondary, Bond et al. (1992) because the wet sheet temperature reaches 100°C immediately and remains at that temperature for much of the drying regardless of the steam temperature. Thus a single drying fluid temperature, 140°C, was selected for both air and superheated steam drying for the experimental work reported here.

Paper properties were measured in a room maintained at 23°C and 50% relative humidity after conditioning at these conditions for at least 24 h. Properties were determined using PAPTAC standard methods unless otherwise specified, using 10 replicate sheets for each type of base paper. The details regarding the testing procedures are available in Chapter 3 section 7 and Appendix A section 6.

1.3 Differences in experimental procedures from previous work

Several important changes in experimental procedures from those of previous studies are identified as potential sources of differences in results. First, the furnish used here was a mixture of Stone Ground Wood pulp (SGW) and kraft pulp. The previous work of Poirier et al. (1994) included RMP pulp, the closest to SGW, to only a limited extent and never in a mixture with kraft pulp. The pulp blend the closest to that used here is TMP/Kraft used by Li (1993). As documented in McCall and Douglas (2001, 2004), the effects on strength enhancement with superheated steam drying depend very much on the type of paper, especially the composition of the pulp furnish. Also, properties of pulp blends are usually not linearly additive, Smook (1979). Therefore the properties of paper made in the present study cannot be predicted reliably from previous studies. A second change in procedure is that an impingement flow dryer was used here while a parallel flow dryer was used for most of the previous studies focusing on the effects of superheated steam drying on paper properties, except for some of the results of McCall and Douglas (2001, 2004). In a third major difference, Dynamic Sheet Formed (DSF) sheets rather than standard handsheets were used: relative to handsheets, DSF paper is anisotropic, as is machine-formed paper, and has formation much more similar to that of commercial paper, as shown in Chapter 3 section 6.1.2.

1.4 Summary of results

The properties and property changes are summarized in Tables 4.1 and 4.2. Figures 4.1 to 4.5, 4.7 and 4.9 plot the normalized percent change when switching from air to superheated steam drying. The normalized change is defined in Table 4.2 as the ratio of the change from air to superheated steam over the unique 95% decision limit calculated for the 3 types of base paper as described in Chapter 3 section 8.2. Changes larger than two decision limits are statistically significant.

The differences in paper properties between laboratory base paper dried in air and commercial base paper are also given in Tables 4.1 and 4.2. Commercial paper is compared to air-dried sheets because laboratory air drying is closer to conventional cylinder drying than steam drying. It is not the purpose of this chapter to analyse the differences in properties between the laboratory and the commercial base paper since production parameters other than drying conditions were varied. These differences are recorded in Appendix B.

2. Bulk properties

2.1 Sheet thickness and specific volume

From Table 4.2 and Figure 4.1, the thickness of DSF sheets dried in superheated steam is only about 3% lower than when dried in air. This small thickness decrease for steam-dried sheets corresponds to the 4% lower specific volume. The differences reported here, although minor, are significant at the 95% confidence level, corresponding to changes of 4 to 5 times the decision limit.

Results from previous studies show different effects of superheated steam drying on specific volume depending on the paper grade. Poirier et al. (1994, 1995), with either 100% TMP or 100% kraft pulps, showed respectively either no effect on thickness and specific volume, or a slight increase when drying in superheated steam. In the case of mechanical pulp, they believed that superheated steam drying primarily affects the fines fraction while leaving the long fibre network relatively unchanged. They used this selective effect to explain specific volume remaining unchanged. In the case of pure virgin or recycled kraft pulps, Poirier explained the increase in specific volume by a decrease in drying stress deriving from drying at higher sheet temperature.

Table 4.1 Properties of uncoated paper

Property		***Unit***	**AIR**	**SHS**	**COM**	***DL***	***COV***
Grammage		g/m^2	40.0	40.0	37.9	0.16	0.4
Thickness		µm	92	89	79	0.76	0.9
Specific volume		cm^3/g	2.3	2.2	2.1	0.019	0.9
Permeability factor		10^{-15} m^2	4.3	3.0	4.6	0.22	5.6
Moisture content		%	8.1	7.9	7.1	-	-
Tensile	Breaking length MD	km	5.92	7.19	8.68	0.238	3.3
	Stretch MD	%	3.6	3.5	1.7	0.13	4.3
	Breaking length CD	km	2.28	2.45	2.38	0.111	4.7
	Stretch CD	%	3.40	2.77	2.93	0.26	8.5
Burst Index		kPam^2/g	2.32	2.31	2.69	0.09	3.7
Tear	Index MD	mNm^2/g	6.02	5.45	-	0.50	9.1
	Index CD	mNm^2/g	11.9	10.3	8.6	1.4	14.1
Optical	Light scattering	m^2/kg	77.1	65.7	60.1	0.94	1.4
	Light absorption	m^2/kg	3.6	3.9	2.9	0.065	1.9
	Brightness	°	66.9	63.0	67.4	0.17	0.3
	Opacity	°	92.8	91.5	87.7	0.22	0.2
Roughness	PPS	µm	5.64	6.37	5.96	0.08	1.4
	Talyscan Sq	µm	3.67	3.63	3.65	0.24	6.6
	Talyscan Sfd	–	2.46	2.42	2.43	0.017	0.7
	Talyscan Sdq	–	0.65	0.51	0.63	0.089	15
	Talyscan Ssc	µm^{-1}	0.28	0.17	0.25	0.049	21
	Talyscan Sdr	–	0.18	0.11	0.15	0.032	22
Water penetration time		s	237	510	-	49	13

AIR: Laboratory DSF formed sheets dried under air impingement at $T_j = 140°C$ */* $V_j = 40$ *m/s*

SHS (superheated steam): Laboratory DSF formed sheets dried under superheated steam impingement, same jet temperature and velocity as for AIR

COM: Commercial paper made from the same pulp stock

DL: 95% decision limit calculated for the three sets of data as described in Chapter 3 section 8.2

COV: coefficient of variation, DL/mean value among the 3 conditions

See Chapter 3 section 7 and Appendix A section 6 for detailed definition of properties

Table 4.2 Changes in uncoated paper properties from using superheated steam

			Change **AIR -> SHS**		**Change** **AIR -> COM**	
Property		*unit*	Absolute	Norm.	Absolute	Norm.
Thickness		μm	-3.1	-4	-13	-17
Bulk		cm^3/g	-0.10	-5	-0.20	-11
Permeability		$10^{-15}\ m^2$	-1.3	-6	0.30	1
Moisture content		%	-0.2	-	-1.00	-
Tensile	Breaking length MD	km	1.27	5	2.76	12
	Stretch MD	%	-0.18	-1	-1.89	-15
	Breaking length CD	km	0.17	2	0.10	1
	Stretch CD	%	-0.63	-2	-0.47	-2
Burst index		$kPam^2/g$	-0.01	0	0.37	4
Tear	Index MD	mNm^2/g	-0.57	-1	-	-
	Index CD	mNm^2/g	-1.6	-1	-3.30	-2
Optical	Light scattering	m^2/kg	-11	-12	-17	-18
	Light absorption	m^2/kg	0.30	5	-0.70	-11
	Opacity	°	-1.3	-6	-5.1	-24
	Brightness	°	-3.9	-23	0.5	3
Roughness	PPS	μm	0.73	9	0.32	4
	Talyscan Sq	μm	-0.05	0	-0.02	0
	Talyscan Sfd	–	-0.04	-2	-0.03	-2
	Talyscan Sdq	–	-0.14	-2	-0.02	0
	Talyscan Ssc	μm^{-1}	-0.11	-2	-0.03	-1
	Talyscan Sdr	–	-0.07	-2	-0.03	-1
Water penetration time		s	270	6	-	-

$$Absolute\ change = SHSvalue - AIRvalue \text{ or } AIRvalue - COMvalue$$

$$Normalized\ change = \frac{SHSvalue - AIRvalue}{DL} \text{ or } \frac{COMvalue - AIRvalue}{DL}$$

Definitions as for Table 4.1

For the effect of superheated steam drying on specific volume, McCall and Douglas reported no effect for CTMP (1994, 1995), a slight increase for OCC, TMP/DIP or TMP/filler mixtures (2001, 2004), or a large increase for BCTMP (hardwood) (2001, 2004). With use in the present study of a mixture of SGW (softwood) and kraft pulp (softwood), the slight decrease in specific volume is therefore unexpected. However a decrease in thickness and bulk is in agreement with an increase in bonded area, as supported by the changes in tensile strength and light scattering coefficient reported in sections 3.1 and 4.1. Normally an increase in strength properties is accompanied by a decrease in specific volume in paper. This combination of the two effects was observed when increasing the sulfonation level of a pulp, as reported by McCall et al. (1995). In this paper they establish the mechanism of strength enhancement from superheated steam drying by comparison with the effect of increasing the sulfonation level of the pulp, i.e. a reduction of the glass transition temperature of lignin. However they observed that the decrease in thickness when increasing the sulfonation level did not occur when drying in superheated steam. The larger amount of fines present in SGW pulp, as used here, compared to that of TMP pulp, used in earlier study, may lead to the greater effect of superheated steam drying on paper structure found here.

2.2 Sheet permeability

A lower permeability is obtained for sheets dried in superheated steam, Table 4.2, Figure 4.1. In previous studies, when TMP was used, Poirier et al. (1994) found no difference, but with high yield kraft pulps McCall and Douglas (2001, 2004) found a large decrease in permeability from drying in steam. The effect of superheated steam drying leading to increased bonded area is also consistent with a lower permeability, as found here. Thus the lower specific volume and lower permeability support the hypothesis of some densification of the sheet due to the increase in bonded area when drying LWC base paper in superheated steam.

Pore diameter may be calculated from the measured permeability by identification of the two forms of the Lucas-Washburn relation: the permeability form derived from Darcy's law, and the cylindrical form derived from the Hagen-Poiseuille equation. This exercise, done in Chapter 2 section 2.2.2a, leads to the following relationship between pore diameter, R, and permeability, K:

$$R = 4\tau\sqrt{\frac{K}{\varepsilon}} \tag{2.12}$$

In the case of paper, the tortuosity τ in the direction normal to the surface ranges from 3 to 7 depending on the porosity. With $\tau = 3$ and $\varepsilon = 0.5$ the estimated pore radius is 1 µm. This is in very good agreement with the mean pore diameter of 2 µm obtained in Chapter 6 section 2.3 by mercury porosimetry for uncalendered base paper.

2.3 Equilibrium moisture content

The equilibrium moisture content of paper is measured gravimetrically after conditioning followed by oven drying at 105°C until the weight is stable. For paper made from a specific type of fibre, the equilibrium moisture content determined after consistent conditioning depends on the drying history, such as the final moisture content at the end of impingement drying, the drying rate and the temperature history during drying. During the present study an optimal drying procedure for DSF sheets was developed to fulfill the quality requirements of sheet flatness, as detailed in Chapter 3 section 2.3. Sheets were dried to 0.43 kg/kg dry moisture content in either air or superheated steam in the impingement dryer, then taken to 0.05 kg/kg dry basis moisture content by room temperature drying. Also, the sheets were lightly calendered (room temperature, 5 kN/m) after drying. With this procedure the equilibrium moisture content of DSF sheets is not affected by superheated steam drying, Table 4.2. However when in earlier experiments the sheets were dried to 0.05 kg/kg in the impingement dryer, the equilibrium moisture content of sheets dried in superheated steam is found significantly lower, by about 1 percentage point compared to sheets dried in air. This finding replicated the work of Poirier (1991) for which sheets were also dried to final dryness in the drying chamber.

3. Optical properties

Brightness and opacity are important properties of paper characterizing its visual appearance. Brightness is the reflectance of an opaque pad of sheets measured at 457 nm light wave length, while opacity is the ratio of a single sheet of paper to that of an opaque pad of paper but measured at 555 nm. These two properties depend on the light absorption and scattering ability of paper which are calculated from the opacity measurement, hence at 555 nm only. The effects of drying are first presented for each optical property, and then in an integrated manner in section 3.4 as these properties are all interrelated.

3.1 Light scattering and light absorption coefficients

As expected, the predominantly mechanical pulp furnish sheets of this study, when dried in superheated steam, show a much lower scattering coefficient, by 15% which is 12 times the decision limit, Table 4.2 and Figure 4.2 Previous studies showed that superheated steam drying leads to a decrease in light scattering, 17% in Poirier et al. (1994) and 14 to 17% in McCall and Douglas (1994, 2004) for paper made of mechanical pulps, but a slight increase for paper made of chemical pulps. For paper light scattering occurs at the interfaces between fibre and pores: the larger the surface of pores the higher the light scattering efficiency. The increase in interfibre bonding which is believed to occur when drying in superheated steam directly produces a loss in light scattering efficiency. The simultaneous increase in tensile strength reported in section 4.1 and decrease in light scattering coefficient therefore supports the hypothesis of an increase in inter-fibre bonding when drying in superheated steam as proposed by McCall et al. (1995).

Also observed is a small but statistically significant increase in light absorption coefficient by 8% which is 5 times the decision limit. Light absorption depends on the type and amount of chromophore groups present in the fibre constituents, principally in the lignin. Light absorption therefore depends mostly on the types of fibres, which are affected by the chemical processes occuring during pulping and papermaking that may affect these chromophore groups. The work by McCall and Douglas with CTMP and TMP (1994) showed an increase in light absorption coefficient by 14 to 30%. By contrast, Poirier et al. (1994) concluded that drying in superheated steam had no effect on light absorption or opacity except with the drying fluid at high temperature, in which case the effect was the same for air and steam. This difference is discussed further in section 3.4.

3.2 Opacity

Superheated steam drying slightly decreases opacity, by 1.3 percentage points. Previous studies (Poirier et al. 1994, 1995; McCall and Douglas 1994, 2001, 2004) found no effect from superheated steam drying on opacity. This finding may be attributed to the observed decrease in light scattering and, to a lesser extent, to the small decrease in thickness.

3.3 Brightness

As expected from previous studies brightness decreases significantly, by 4 percentage points, Table 4.2, Figure 4.2, when superheated steam drying is used. Brightness decreases because the resultant increase in fibre bonding decreases the fibre-air interfaces area, thereby decreasing the light scattering ability. This result for brightness is in agreement with previous work on steam drying by Poirier et al. (1994), McCall and Douglas (1994, 2001) with mechanical pulps. The increase in light absorption found in the present study for drying in steam may make an additional contribution in this effect as discussed in section 4.4.

3.4 Discussion

The relationships between the various optical properties derived from Kubelka-Munk theory are given in Appendix A section 6.2 and Figure A.2. This theory enables separating the contributions from light scattering and light absorption on visual appearance of paper, brightness and opacity. Figure A.2 shows that brightness increases with light scattering and decreases with light absorption coefficient, while opacity increases with both coefficients. The observations made in the present study of the concomitant decrease in light scattering, increase in light absorption and decrease in brightness and opacity are therefore consistent with the Kubelka-Munk theory.

McCall and Douglas (1994) did not discuss the change in light absorption noticeable with steam drying in their experiments. Poirier et al. (1994, 1995) reported neither change in light absorption nor opacity and therefore concluded that steam drying only changes light scattering. Figure A.2 shows that a decrease in brightness and in light scattering coefficient at constant opacity implies an increase in light absorption coefficient. In Poirier et al. (1994, 1995) studies along with the reported decrease in light scattering coefficient, an increase in opacity or in light absorption or both should therefore have been detected. In these studies the optical properties reported had a large variability, so a change in light absorption may have been hidden. In the present study there was very little variability in measurements of all four optical properties with the coefficient of variation for these four sets of measurements being below 2%, Table 4.1. The increase in light absorption is therefore consistent with the other changes in optical properties but is not fully understood. Some changes occurring in the chromophore groups upon exposure of the sheet to higher temperature may explain the increase in light absorption, Back (1982). Although the change in light scattering contributes the most to the change in brightness, responsible for 2/3 of the decrease, the effect from the change in light absorption is not negligible. It also reduces the loss in opacity, by 1/2 a point, which should have occurred with the large decrease in light scattering.

4. Strength properties

4.1 Tensile strength

The MD breaking length of DSF paper increases substantially, by about 20%, when switching from air to superheated steam, Table 4.2, Figure 4.3. Previous work done in this laboratory reported as well a large positive effect of superheated steam drying on tensile strength for paper from mechanical pulps: TMP (Poirier et al., 1994), CTMP (McCall and Douglas, 1994, 2004), TMP with a small amount of DIP or filler (McCall and Douglas, 2001). Different results were obtained in the case of paper from kraft pulps depending on their yield: for low yield kraft pulp, low lignin content, a decrease in strength properties was observed (Poirier et al., 1995), but an increase was seen for higher yield kraft pulps, higher lignin content, such as in linerboard made from recycled pulps (McCall and Douglas, 2001). The increase found in the present study is somewhat lower than that found by Poirier et al. (1994) with 100% TMP pulp, probably because of the presence of kraft pulp.

For other strength properties, stretch is not affected in the machine direction but decreases in the cross-machine direction. Paper made on a commercial machine and on the Dynamic Sheet Former shows preferential orientation of wood fibres in the machine direction, which makes the sheet stronger in this direction. Paper strength properties in the plane of paper are therefore strongly anisotropic and are measured in both directions: machine direction (MD) and cross-machine direction (CD). The cross-machine direction stretch decreases when drying in steam. This effect may be due to the kraft pulp fraction because such a decrease was also observed by Poirier et al. (1995) with 100% kraft pulp.

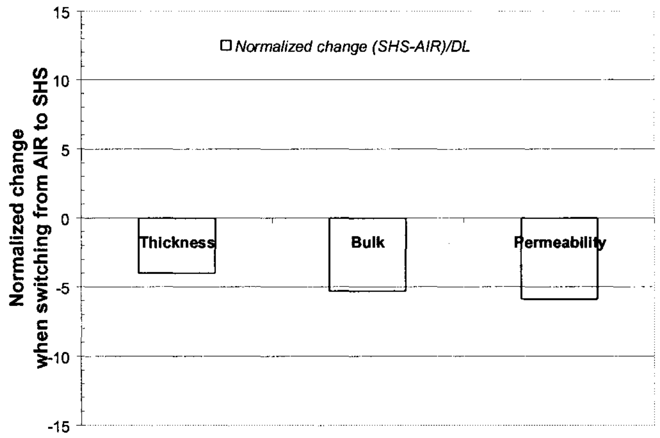

Figure 4.1 Change in bulk properties for switching from air to superheated steam drying

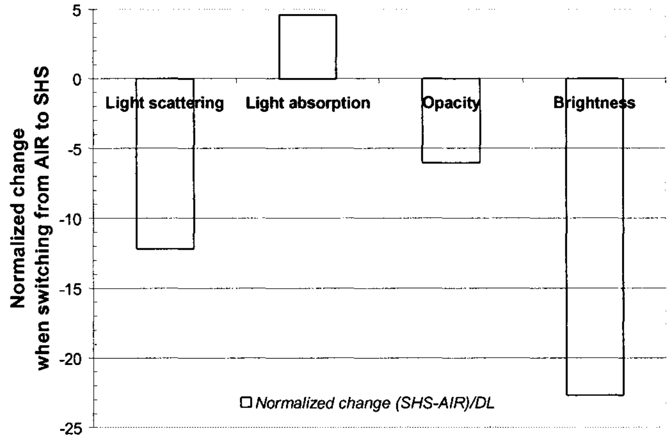

Figure 4.2 Change in optical properties for switching from air to superheated steam drying

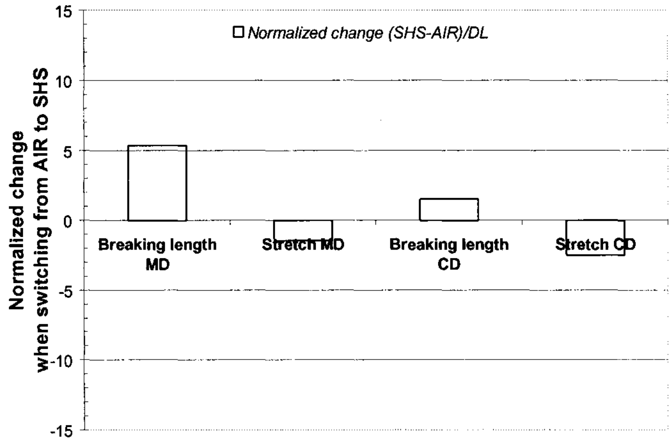

Figure 4.3 Change in tensile properties for switching from air to superheated steam drying

4.2 Bursting strength

No effect on bursting strength is observed from drying DSF paper in superheated steam, Table 4.2, Figure 4.4. Poirier et al. (1994, 1995) found that with superheated steam drying the bursting strength increases for paper made from mechanical pulp and decreases for kraft pulp. A similar effect was seen for CTMP (McCall and Douglas, 1994, 2004), TMP and small amount of DIP or filler (McCall and Douglas, 2001), while almost no effect was seen for paper made from recycled OCC made of blends of kraft pulps. Like tensile strength, bursting strength of paper from mechanical pulp dried in superheated steam increases due to increased bonded area, as established by McCall et al. (1995), while for paper made from chemical pulp the decrease in bursting strength was attributed to a decrease in sheet density. In the present study the two opposite effects may therefore cancel, leading to no change in burst when using superheated steam drying.

The bursting strength depends on tensile and stretch in both directions of the plane as modeled in the following equation from Böhmer (1962):

$$B = k\left[T_M + T_C\sqrt{\frac{E_M}{E_C}}\right]\frac{\sqrt{E_M}}{\left(1+E_M\right)^{3/2}} \tag{4.6}$$

with B the bursting strength, k a constant, T_M and T_C the tensile strength in the machine and cross-machine directions, E_M and E_C the elongation (stretch) in the machine and cross-machine directions. Sheet rupture occurs in the direction in which the stretch is lower, and the pressure at rupture depends on the tensile properties in both directions. On a commercial machine, paper is not restrained at the edges. During drying, paper can therefore shrink in the cross-machine direction, resulting in larger stretch in this direction relative to the machine direction. In the laboratory, sheets were fully restrained when drying, i.e. in both machine and cross-machine directions. Lower stretch values were found in the cross-machine direction, slightly lower for air-dried sheets but much lower for superheated steam-dried sheets. During the bursting test, paper failure was observed to occur in the cross-machine direction, i.e. the fracture line was along the machine direction. Superheated steam-dried paper has both higher tensile strength and lower stretch in the cross-machine direction compared to air-dried sheets, which may explain the identical bursting strength found for the two types of sheet.

4.3 Tear strength

As in the previous studies of Poirier et al. (1994) and McCall and Douglas (1994), no significant effect on tear strength is observed here from drying paper in superheated steam, the normalized changes being about 1 decision limit, Table 4.2 and Figure 4.4. The absence of a significant effect is probably because of the complex relationship between tear resistance and fibre bonded area. Resistance to tear depends on the force required to rupture an individual fibre and on the force required to pull a fibre out from the fibre network. Tear strength therefore depends strongly on fibre length, unchanged by drying, and interfibre bonding area. However an increase in fibre bonded area increases tear resistance only to the critical point where it reaches a maximum corresponding to fibres being ruptured rather than being pulled out. For sheets in the present study, tear strength may have already been optimized with respect to bonded area, in which case it would not be affected by superheated steam drying.

5. Surface properties

5.1 Roughness by air-leak method

With the Parker Print Surf apparatus the air flow rate parallel to paper is measured, from which roughness is calculated. The paper dried in superheated steam is rougher, by about 0.7 μm, as found in previous work, Poirier (1991) and Li (1993) for both mechanical and chemical pulps. Here the increase is again by about 0.7 μm, an increase 9 times greater than the decision limit, Figure 4.5. This effect may be attributed for mechanical pulp papers to the collapse of fines present at the surface, and for chemical pulp papers to the greater extent of stress relaxation at the paper surface because of the higher temperature of the wet sheet that is a basic characteristic of drying in superheated steam, Poirier (1991). The results from section 5.2 provide support for the hypothesis that the collapse of lignin-rich fines at the surface of long fibres is the cause for the difference in roughness between steam and air-dried mechanical furnish paper, a result seen for both methods of roughness determination. The Parker Print Surf apparatus measures roughness between paper and the annulus of the circular sensing head which is only 51 μm wide. Typical fibres are about 30 μm diameter by 1 to 4 mm long. This measurement is therefore more sensitive to the morphology of individual fibres than to the structure of the network of fibres.

5.2 Roughness by stylus profilometry

The average roughness, S_q, obtained by scanning 10 regions of 1 mm^2 of the paper surface with a stylus are identical for both the experimental DSF and commercial paper. Contrary to the PPS measurement, the average roughness, S_q, is measured on a wider area including many fibres. The S_q measurement would therefore be expected to be affected more by the long fibres network than by the individual fibre wall. The difference between the two roughness measurements is illustrated in Figure 4.6.

However the Talyscan hybrid parameters describing the complexity of the surface show significant differences between the types of paper used, Figure 4.7. S_{fd}, the fractal direction of a curve, is a number that characterizes the way in which the measured length between given points increases as scale decreases. S_{dq} is the mean quadratic slope of the surface. S_{sc} is the arithmetic mean summit curvature of the Surface. This parameter relates to the mean form of the peaks: pointed vs. rounded. S_{dr} is the developed interfacial area ratio and indicates the complexity of the surface relative to the support surface. The fractal direction, S_{fd}, and the hybrid parameters, S_{dq}, S_{sc} and S_{dr}, are found higher for laboratory air dried and commercial sheets. The S_{dr} value increases with increasing complexity of the surface, with a completely flat surface having a S_{dr} value approaching 0%. The combination of the results for the four parameters, S_{fd}, S_{dq}, S_{sc} and S_{dr}, therefore indicates a more complex surface is obtained when drying in air.

Surface photosimulation for 1 mm x 1 mm sections using the Talyscan image processing software, Figure 4.8, shows that for paper dried in superheated steam, the fines content collapses on the long fibres. In Figure 4.8 the edges of the long fibres appear clearer and sharper for superheated steam dried paper as compared to the air-dried for which the images of fibres appear somewhat fuzzy. When drying in superheated steam, the roughness at large scale remains unchanged because it is controlled by the unchanged network of long fibres, while the roughness at small scale, below the fibre width scale, 30 μm, is decreased because of the collapse of fines on to long fibres.

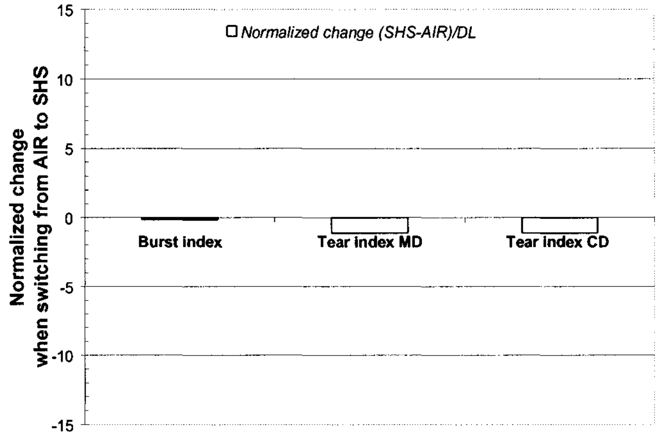

Figure 4.4 Change in burst and tear properties for switching from air to superheated steam drying

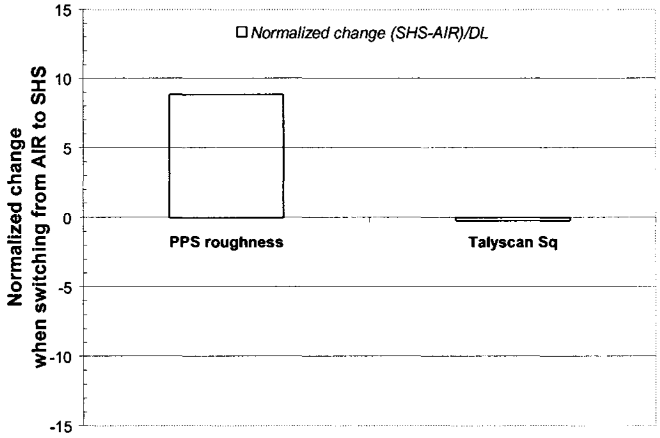

Figure 4.5 Change in roughness properties for switching from air to superheated steam drying

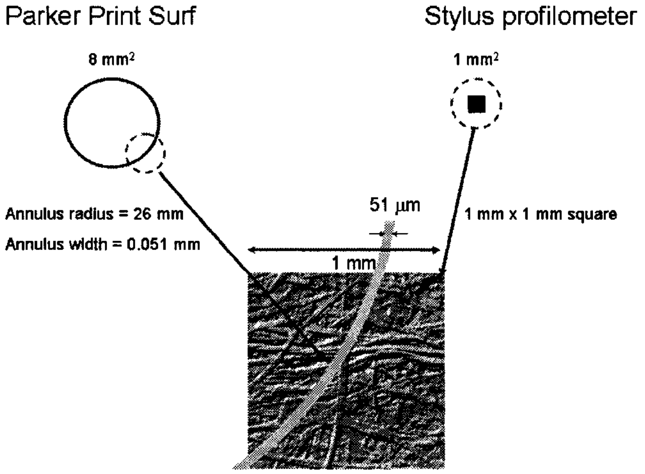

Figure 4.6 Difference between the two roughness measurement methods

5.3 Water penetration

For DSF sheets, the penetration time of 50 μL of water for steam dried sheets is about twice that with air drying, Table 4.1, which represents 6 times the decision limit, Figure 4.9. Water penetration occurs by capillarity and by diffusion. As both the porous structure and the surface chemistry affect penetration rate, it is not possible to separate quantitatively the effects on penetration time which derive from differences in porous structure or contact angle. However two reasons support the hypothesis that penetration time varied because of a different surface chemistry. First, penetration of a high surface tension liquid such as water is primarily affected by surface chemistry. Second, the present result is in agreement with contact angle measurements by Li (1993), which showed a more hydrophobic sheet for drying in superheated steam. The thermal softening of lignin is believed to allow redistribution of this hydrophobic polymer over the long fibres, thereby increasing paper hydrophobicity.

6. Conclusions

Drying in superheated steam significantly affects uncoated paper properties as expected from previous studies. The main effects are an increase in tensile strength and hydrophobicity, a decrease in light scattering efficiency and a decrease in surface roughness at small scale, but an increase at large scale. These results may be attributed to thermal softening of the lignin present to a substantial extent in mechanical pulp fibres, especially in the fines, resulting thereby in an increase in fibre bonded area and the collapse or micro-flow of fines over the long fibre as proved by McCall et al. (1995).

The increase in interfibre bonded area has a small but noticeable densification effect resulting in lower sheet thickness, specific volume and permeability. These effects had not been found in previous work, which reported either no effect or an increase in specific volume from superheated steam drying. The effects found here are however consistent with the increase in fibre bonded area previously reported. Also an increase in light absorption and a decrease in opacity are observed in the present study. In previous work no effect was noticed on opacity, and depending on the type of pulp, no effect or only a slight increase in light absorption was reported. The larger light absorption found here may be due to thermally induced changes in chromophore groups under exposure to high temperature.

The differences observed here for the first time may be due to the complex blend of pulps of the actual paper furnish used. SGW has a higher fines content than the mechanical pulps used in previous work, and it was mixed with kraft pulp. As observed by McCall and Douglas (2001), the effect of superheated steam drying on paper properties is very specific to the grade of paper and its furnish.

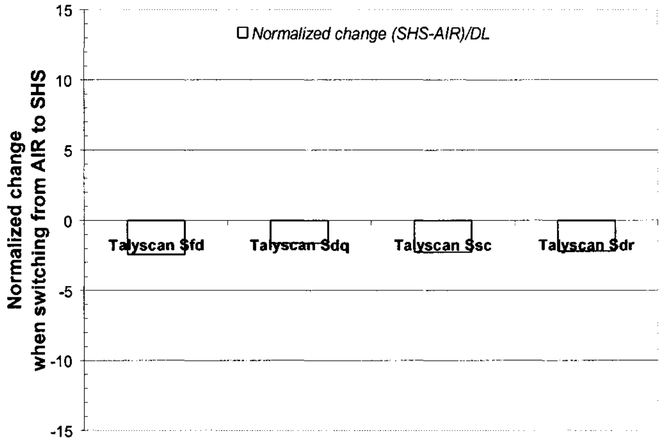

Figure 4.7 Change in hybrid roughness parameters for switching from air to superheated steam drying

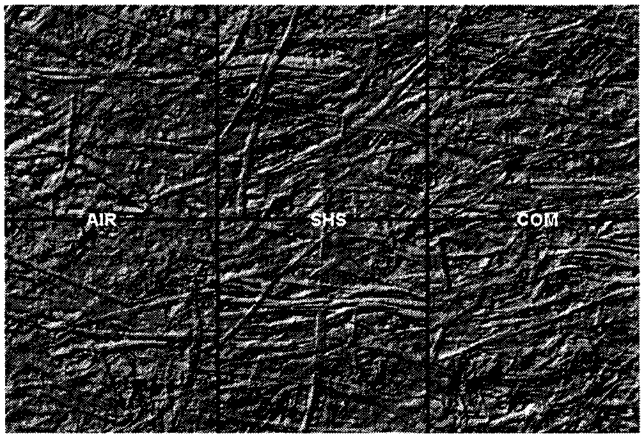

Figure 4.8 Images of surfaces of uncoated paper obtained from profilometry

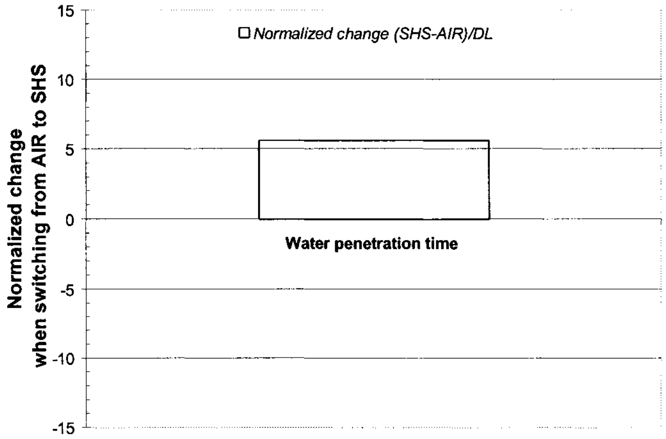

Figure 4.9 Change in water penetration time for switching from air to superheated steam drying

Chapter 5 Development of coated paper properties during drying: Commercial base paper

1. Introduction

In addition to the main focus with laboratory-made Dynamic Sheet Former (DSF) base sheets, reported subsequently, the present chapter describes work carried out using commercial base paper. The drying condition combinations used in this chapter are listed in Table 3.15. The parameters investigated were drying time, coating-to-drying delay time, drying medium temperature and the drying medium, air or superheated steam. The investigation of drying kinetics with machine-formed base paper, documented using gravimetric determination of sheet average moisture content, enabled estimation of drying rates. The experimental procedure is described in Chapter 3 section 6.2.3. Most coated paper properties were determined on uncalendered paper but a few sheets were calendered and printed.

The objective of determining the effect of coating-drying parameters on the properties of coated paper made from commercial base paper is to provide a reference and an aid in understanding for the more complex study using DSF base sheets dried variously. As the prime focus of the present study concerned coated paper produced from DSF base sheets, only a brief discussion of paper properties results is provided in Chapter 5, with the more detailed treatment later when the more extensive results are reported in Chapters 6 and 7.

2. Drying kinetics

2.1 Drying rate calculation

The drying of a wet coating in a single-zone impingement dryer with fixed operating parameters as used here would proceed in three phases: warm-up period, constant rate period and falling rate period, as represented in Figure 5.1. In the first period, the sheet temperature and drying rate increase. In the second drying period, as long as sufficient water is supplied to the coating surface the sheet temperature remains constant and consequently there is a period of constant drying rate. When the coated paper characteristics no longer permit water to be supplied at a sufficient rate to the surface, the surface temperature starts to rise and correspondingly the drying rate begins to drop: the falling rate drying period.

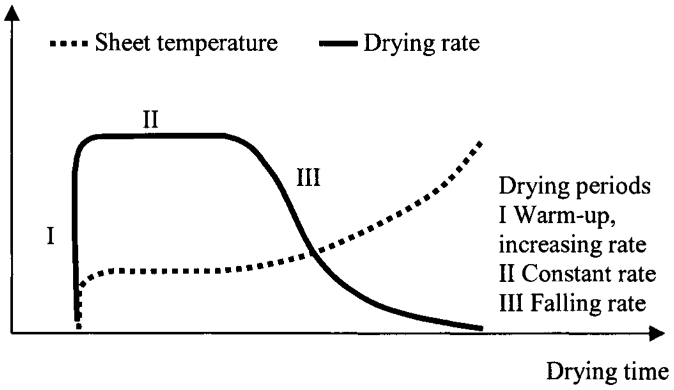

Figure 5.1 Drying periods

The present study permitted determination of sheet average moisture content gravimetrically as a function of drying time for sets of tests starting with the same initial moisture content and variable drying conditions. Drying rates are calculated by integrating the differential equations relating drying rate to sheet moisture content. Finally fitting these integral equations to the integral sheet moisture content-drying time data, then calculating drying rate from the differential form of these equations. The drying rate, constant initially and then decreasing with moisture content decay during the falling rate period, may be described as follows:

$$\text{Constant rate period:} \quad R = -BWC\frac{dX}{dt} = \text{Constant} = R_c \qquad (5.1)$$

$$\text{Falling rate period:} \quad R = -BWC\frac{dX}{dt} = aX + b \qquad (5.2)$$

with BWC, the coated paper basis weight, R_c the constant drying rate, a the slope and b the intercept of the drying rate curve. The assumption for eq. (5.2), i.e. a linear relationship between drying rate and sheet moisture content, is approximate but is commonly used over a limited range of X for drying uncoated paper. Integration provides what was determined experimentally, the evolution of sheet moisture content with time, as follows:

$$\text{Constant rate period:} \quad X(t) = X_i - \frac{R_c}{BWC}t \qquad (5.3)$$

Falling rate period: $$X(t) = k\exp(-\frac{a}{BWC}t) - \frac{b}{a} \qquad (5.4)$$

with k an integration constant.

The case of slow natural convection drying is treated separately later in this section. The first moisture content reading was obtained after 0.4 s of impingement drying, the shortest drying time that could be used. The average drying rate over the first 0.4 s of drying was found to be much greater than that by $t = 0.4$ s, which indicates that for $t \geq 0.4$ s the drying regime is already that of the falling rate period. Thus for $t \geq 0.4$ s the drying curves, $X = f$ (drying time), were fitted with the above function for X, eq. (5.4), with Excel Solver. For each measured value of X, drying rate was then calculated from eq. (5.2) with "a" and "b" as determined above.

No measurement is possible over the period $0 < t < 0.4$ s. During this short time both the heat-up and constant rate drying periods occur and the falling rate drying period starts. Warm-up of the very thin wet coating layer, expected to be very rapid, may be estimated from the following equation:

$$mc(T_{final} - T_{initial}) \approx h(T_j - T_{web})t \qquad (5.5)$$

with m the mass of the wet coating, c the heat capacity of the wet coating, $T_{initial}$ = room temperature and T_{final} = wet bulb temperature, ca. 50°C, h the heat transfer coefficient, and T_{web} the average web temperature during the warm-up period, ca. 35°C. The coating layer consists of 5.9 g/m^2 of water, of heat capacity 4200 J/kgK, and 10 g/m^2 of clay and latex particles, of heat capacity ~ 1000 J/kgK, Guérin and Morin (2003), a total thickness when wet of 10.5 μm. Using the value determined subsequently for h in section 2.2.4, 240 W/m^{2}K, the warm-up time is about 0.1 s. This period is therefore not negligible but too short to be measured from the present data obtained only for $t > 0.4$ s.

At the critical moisture content, X_c, and the corresponding drying time, t_c, the drying rates of the constant and falling rate periods are equal. Equating eq. (5.1) and (5.2) and eq. (5.3) and (5.4), the following equation for X_c, t_c, may be derived:

$$X_c + \frac{t_c}{BWC}[aX_c + b] = X_i \qquad (5.6)$$

with X_c as defined in eq. (5.4). From t_c thus determined the constant drying rate R_c would be:

$$R_c = aX_c + b \tag{5.7}$$

Using Excel Solver with results from the curve fitting obtained for $t \geq 0.4$ s, there was no solution to eq. (5.6). Even $t_c = 0$ gives values of the left-hand side of eq. (5.6) 20 to 40% lower than X_i. Modeling for $t \geq 0.4$ s adequately describes the portion of the R-X curve determined experimentally for $X < 0.12$ kg/kg but cannot be extrapolated to $0 < t < 0.4$ s. The source of this behavior is that the assumption of R as a linear function of X in the falling rate period is satisfactory during this latter part of the falling rate period but not back to the critical drying rate condition of X_c, t_c. With the constant rate period being considerably shorter than 0.4 s, time of the first measurement possible, the measurements do not allow modeling both the rate periods from only data late in the falling rate period. For drying paper after coating under high intensity drying from the relatively low initial moisture content of the coating, 0.587 kg/kg dry, one indeed expects most of the drying to occur in the falling rate period, as is observed experimentally here.

Although the X-t data available do not permit determining drying rate during the increasing or constant drying rate periods, the average initial drying rate for $0 < t < 0.4$ s may be calculated reliably using the following expression:

$$\text{Average drying rate to 0.4 s: } \overline{R_{0.4s}} = -BWC\frac{X_{0.4s} - X_i}{t_{0.4s}} \tag{5.8}$$

where $X_{0.4s}$ is the moisture content measured at shortest drying time, $t_{0.4s} = 0.4$ s and X_i the measured initial moisture content.

In the case of natural convection drying in room air, a very good correlation ($R^2 > 0.99$) is found between moisture content and time up to ~ 60 s after coating application, indicating a constant rate drying. The curve was therefore fitted with eq. (5.3) for $0 < t < 60$ s, and then with eq. (5.4). The corresponding drying rates for the constant rate period can be calculated from eq. (5.3) and for the falling rate period from eq. (5.4).

Eq. (5.4) was used for dry uncoated base sheet drying using the base sheet basis weight, BWB, 38 g/m^2, instead of BWC, and including the moisture content measured at $t = 0$. As a hygroscopic material, paper stored in ambient air conditions always contains some partially or entirely chemisorbed water, typically between 3 to 10% in standard conditions 23°C and 50% relative humidity. Removing this small fraction of water well sorbed to fibres occurs with falling rate drying.

2.2 Coated paper drying

2.2.1 Fitting moisture content decay curves

Table 5.1 presents the results from the $X = f(t)$ curve fitting. The maximum drying rate listed is the initial value at the start of the period covered by curve fitting, that is at $t = 0.4$ s for freshly coated sheets and at $t = 0$ for dry base sheet drying. The other rate listed is the average drying rate for coated paper from the start of drying until $t = 0.4$ s, determined from eq. (5.8). Table 5.1 also provides values of $X_{0.4s}$ for the different conditions of impingement drying. For drying coated paper under impingement, the sheet average moisture contents at $t = 0.4$ s were all in the narrow range 0.09 to 0.12 kg/kg dry.

2.2.2 Moisture content decay with drying time

Figures 5.2 to 5.4 present the experimental and fitted drying curves. The drying of coated paper is presented, first for air impingement drying, Figures 5.2 and 5.3, then for natural convection drying in room air, Figure 5.4. Air impingement drying of the dry base paper is given in Figure 5.6. For each drying condition two replicate sheets were coated, dried and weighed for moisture content determination. As the shortest drying time possible with coated paper was 0.4 s, the coated sheet impingement drying curves, Figure 5.2 and 5.3 start at $t = 0.4$ s with the drying curves shown deriving from the eq. (5.2) and (5.4) fitting described above.

Figures 5.2 and 5.3 show that by the time of the first measurement possible, at 0.4 s, from 1/3 to 1/2 of the initial moisture content is removed, which represents 40 to 60% of the moisture removed at longest drying time, $t = 12$ s. The rate of moisture content decay drops significantly as moisture becomes difficult to remove because of chemisorption at the surface of clay particles and fibres. In the case of paper drying the last water becomes increasingly difficult to remove as it goes from being physically absorbed, then multilayer chemisorption with progressively fewer sorbed layers, until the final water removed from paper of about 1% moisture content is chemisorbed in a monolayer to the fibres. Figure 5.4 shows the very slow moisture decay for natural convection drying of coated paper in ambient air while Figure 5.6 illustrates the evolution for drying in the impingement dryer of base paper from the condition of normal dryness in ambient air.

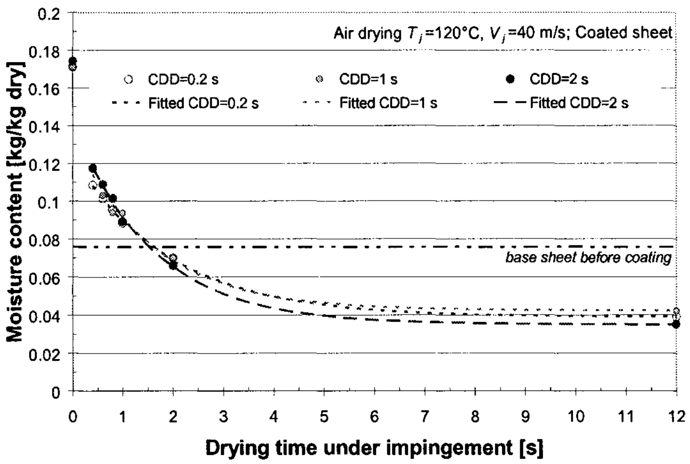

Figure 5.2 Coated paper drying: Drying in 120°C air

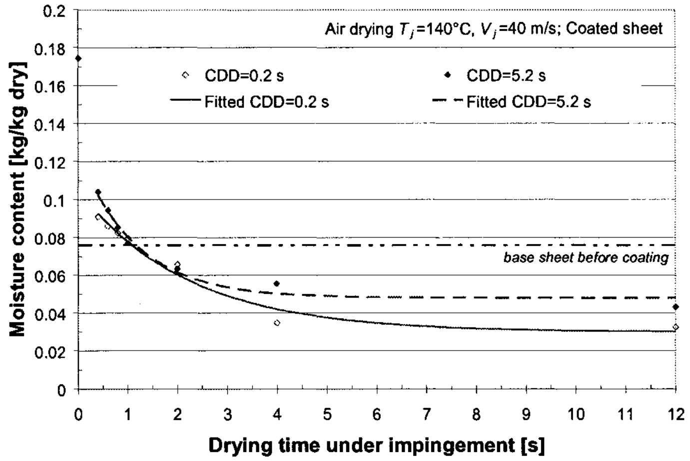

Figure 5.3 Coated paper drying: Drying in 140°C air

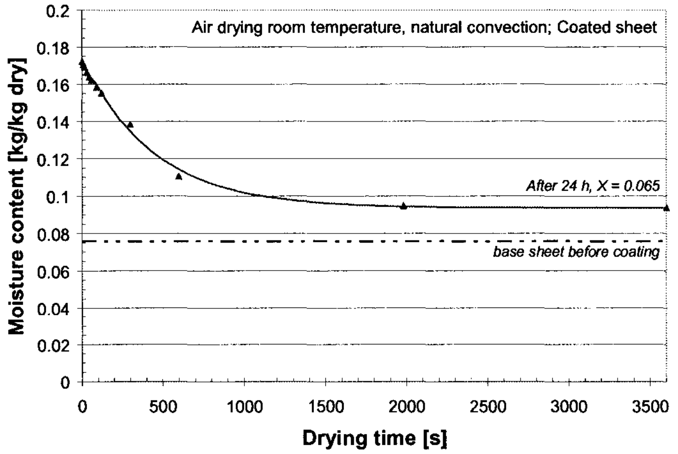

Figure 5.4 Coated paper drying: Natural convection drying at room temperature

Table 5.1 Drying curve fitting

Drying condition	**$X_{0.4s}$, kg/kg dry**	**Ave. drying rate eq. (5.8) kg/m²h**	**Max. drying rate eq. (5.2) kg/m²h**
CA120, CDD = 0.2 s	0.109	28	6.2
CA120, CDD = 1 s	0.118	24	8.2
CA120, CDD = 2 s	0.118	24	9.0
CA140, CDD = 0.2 s	0.091	35	4.8
CA140, CDD = 5.2 s	0.10	30	8.4
Natural convection 23°C	-	-	0.02
BA120	0.064	-	1.4
BA200	0.050	-	4.1

CA120: C for coated paper from commercial base sheet, A for drying in air, 120 for air at 120°C

CDD: coating-to-drying delay time

Natural convection: constant rate period with $R_c = 0.02$ kg/m²h followed by falling rate period

BA120: B for commercial base sheet, A and 120 as defined above

$X_{0.5s}$ in the case of base sheet

The sheet equilibrium moisture content, about 0.065 kg/kg, shown in Appendix C, was not much affected by the drying history. The uncoated paper equilibrium moisture content at 23°C and 50% relative humidity was 0.076 kg/kg before coating while after drying in the laboratory dryer but without coating, the base sheet equilibrium moisture content decreased to 0.064 and 0.060 kg/kg after being dried in, respectively, 120°C and 200°C air.

Figure 5.5 illustrates profiles in the thickness direction for moisture content through the coating and base sheet layers which are projected for various values of time. Figure 5.5a shows the thickness direction profile immediately after application of the coating suspension at X_{cs}. As discussed in Chapter 2 section 2.1.2, immediately after coating application there is water transport into the base sheet which continues until the coating reaches its immobilisation point, FCC. This dewatering causes build-up of a filter-cake of coating particles at the coating/base paper interface, Figure 5.5b. Although actual profiles through the filter cake of coating and through the rewetted base sheet would show a continuous change in local moisture content, as these profiles are unknown they are approximated in Figure 5.5 as constant values at X_{FCC} and X_{FSP}, respectively, which are limiting values. Figure 5.5c shows the case for a coating-to-drying delay time significantly long that the entire coating layer has been dewatered to the immobilization moisture content, X_{FCC}, and the rewetting has proceeded further into the base sheet.

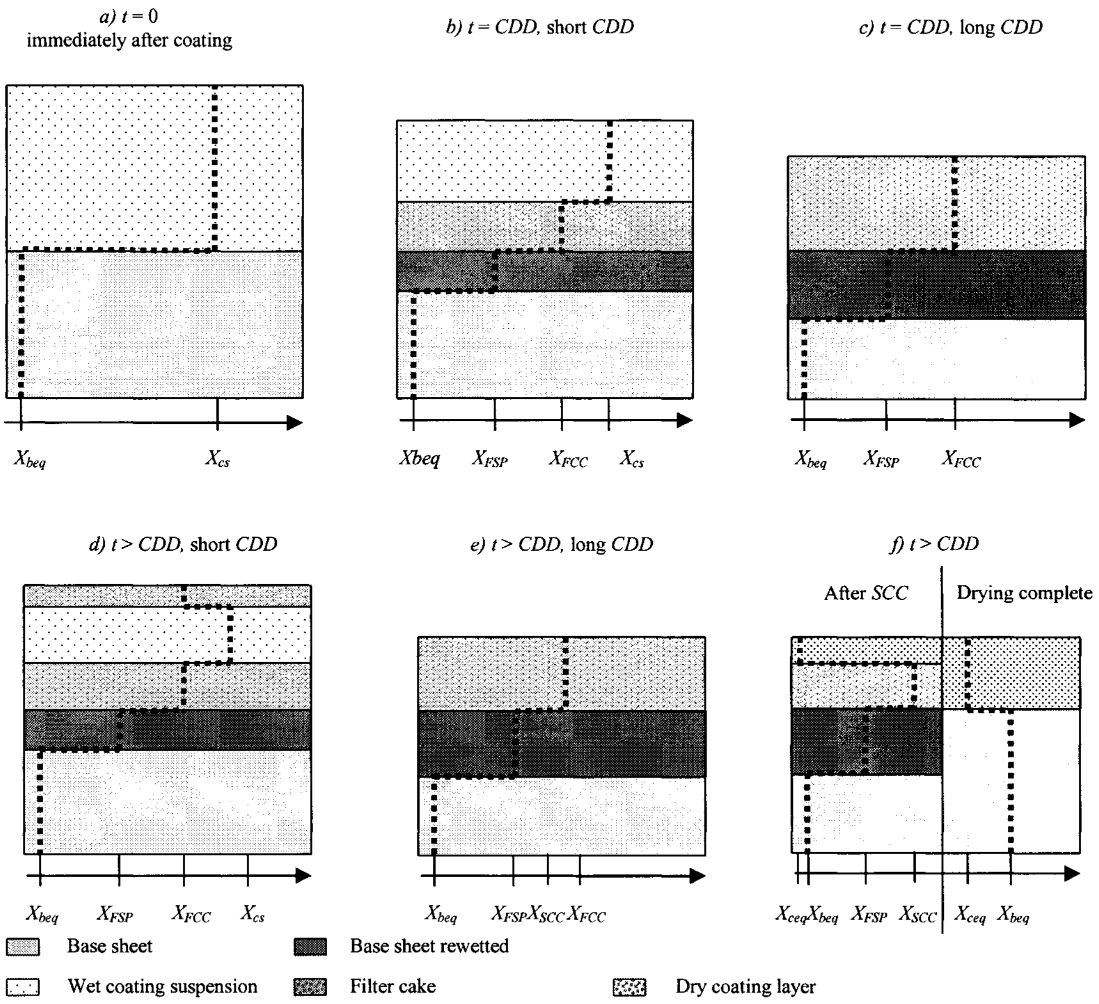

X: local moisture content
X_{beq}, base sheet equilibrium moisture content; X_{FSP} base sheetfibre saturation moisture content
X_{cs} coating suspension initial moisture content; X_{FCC} coating first critical moisture content; X_{SCC} coating second critical moisture content; X_{ceq} coating equilibrium moisture content
CDD: coating-to-drying delay time
For simplicity the moisture content profiles at boundaries are represented with step changes

Figure 5.5 Coated paper moisture distribution after coating

Figure 5.5d to f shows a schematic of these thickness profiles of local moisture content after drying has started, i.e. for $t > CDD$. Figure 5.5d shows profile for drying starting after a short *CDD* with the coating layer incompletely dewatered, Figure 5.5e projects profiles for the start of drying after a longer *CDD* has permitted complete dewatering of the coating layer to X_{FCC}. With the onset of drying at $t = CDD$, there is decreasing moisture content near the coating exterior surface from which water vapour leaves, which thereby creates a moisture gradient in the opposite direction from that created earlier from water transport from the coating into the base sheet. Figure 5.5f shows a schematic of the moisture profile after SCC has been reached, on the left, and after completion of drying, on the right. It is impossible to distinguish from the drying curves when the water movement into the base sheet is reversed by water transport towards the coating surface where it leaves as water vapour.

2.2.3 Drying rate curves

Figure 5.7 presents the average drying rate for the first 0.4 s of drying, obtained from eq. (5.8). The highest value found for $\overline{R_{0.4s}}$ is 35 kg/m^{2}h at the highest drying fluid temperature, shortest delay time tested in these experiments. The industrial drying rates reported for coated paper drying are in the same order of magnitude: 5 to 50 kg/m^{2}h. Up to 100 kg/m^{2}h dryer capacity are quoted in Hagen (1993) but lower drying rates are usually used to ensure good paper quality. In the initial drying period, $0 < t < 0.4$ s, Figure 5.7 shows that faster drying is observed for higher temperature and shorter delay time. As discussed in section 2.1.3, this initial period covers the increasing and constant rate periods and the beginning of the falling rate period but it is not possible to calculate critical moisture content based on the experimental data of the present study. During the constant rate period, the drying rate is fixed by the conditions prevailing in the impingement dryer: geometry, temperature and velocity of the jets. With higher jet temperature higher drying rates are therefore obtained. During the falling rate period the drying rate is limited by the material characteristics. Sheet heat and/or mass transfer limitations reduce water supply to the surface and hence drying rate. It follows that the state of consolidation of the coating at the beginning of drying affects the drying rate. When increasing coating-to-drying delay time the coating consolidation increases, hence decreasing the amount of water available at the surface and shortening the constant rate period. The average drying rate until 0.4 s which averages over the increasing, constant and falling rates, therefore decreases with increasing delay time. A 5 kg/m^{2}h decrease in drying rate, from 35 to 30 kg/m^{2}h, is observed when increasing the delay time from 0.2 to 5.2 s at 140°C. The effect is measurable but not large, which indicates that after 0.2 s the coating is probably already close to immobilisation. In the case of natural convection drying, the very small drying rate imposed by ambient air, 0.02 kg/m^{2}h in Table 5.1, allows the constant drying rate period to occur for an extended period of time, up to 60 s, before the falling drying rate period starts. The coated sheet can provide water to the top surface by capillarity and diffusion fast enough to match the evaporation rate.

Figure 5.8 gives the drying rate – moisture content relationships, calculated from eq. (5.8) and from the drying curve fitting of eq. (5.2). As the increasing and constant rate drying periods are very short, drying occurs mostly in the falling rate period, hence coated paper characteristics dominate drying rate. Therefore after 0.4 s, Figure 5.8 shows little change with increasing drying temperature since drying rate is controlled by the material transport characteristics not the dryer conditions. There is not much difference seen in drying rates with delay time, which indicates that resistance to heat and mass transfer is through the coating that has consolidated by dewatering only (long delay time) or by both dewatering and drying (short delay time). This is another indication that at 0.2 s the coating is already close to immobilization.

2.2.4 Heat and mass transfer

Assuming all the heat is used for vaporization, that is neglecting heat loss by conduction to the sheet, the heat transfer coefficient, h, may be calculated from the following expression:

$$h = \frac{\overline{R_{0.4s}} L_v}{T_j - T_{wb}} \tag{5.9}$$

with $\overline{R_{0.4s}}$ the initial drying rate obtained from eq. (5.8), ca. 30 kg/m^{2}h for drying in air at 120 or 140°C, L_v the heat of vaporization of water, 2200 kJ/kg, T_{air} is the drying fluid temperature and T_{wb} the sheet wet bulb temperature, ca. 50°C. For drying in air at 120°C or 140°C, $h \approx 240$ W/m^{2}K. The value may be compared with the heat transfer coefficient calculated from the average Nusselt number, $\overline{Nu}$:

$$\bar{h} = \frac{\overline{Nu} k}{D} \tag{5.10}$$

with k the thermal conductivity of air and D the nozzle diameter of the impingement dryer.

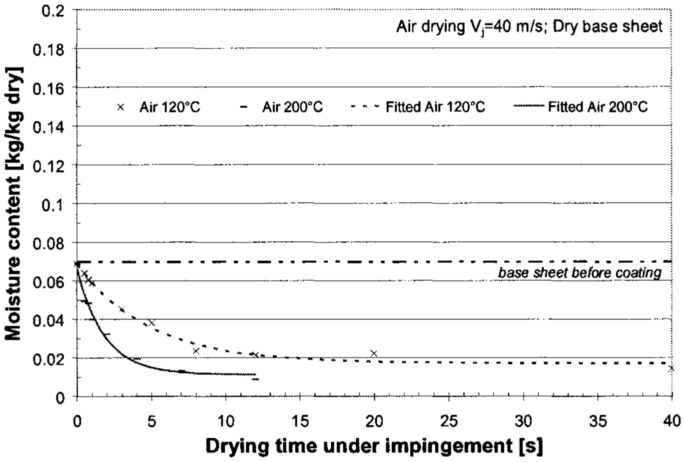

Figure 5.6 Base paper drying: No coating

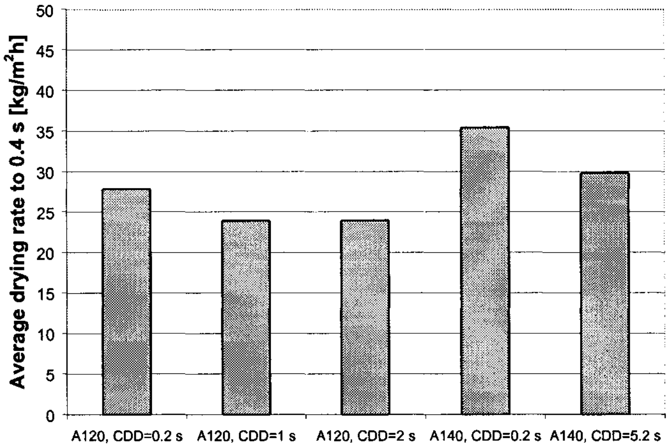

Figure 5.7 Average drying rates for the initial 0.4 s drying

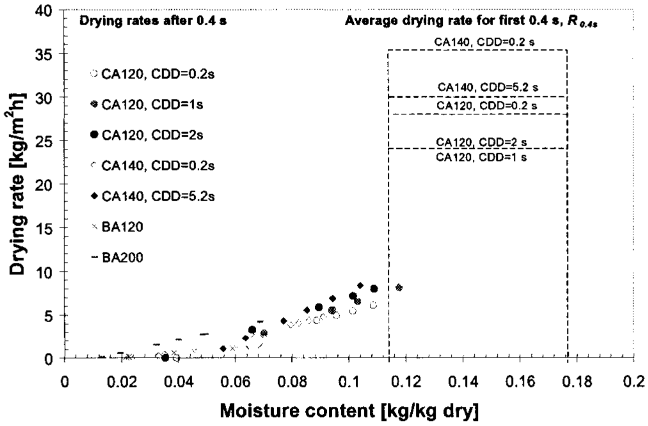

Figure 5.8 Drying rates curves

A relationship between $\overline{Nu}$ and the geometry of the impingement dryer and the drying fluid characteristics is given in Martin (1976):

$$\overline{Nu} = K\sqrt{f}\frac{1-2.2\sqrt{f}}{1+0.2(H/D-6)\sqrt{f}}\mathrm{Re}^{2/3}\,\mathrm{Pr}^{0.42} \tag{5.11}$$

with K the array correction factor, f the open area ratio (%), H the distance from the nozzle exit to the paper and D the nozzle diameter. For an array of round nozzles:

$$K = \left[1+\left(\frac{H/D}{0.6/\sqrt{f}}\right)^6\right]^{-0.05} \tag{5.12}$$

with f = *3.33%*, H = 26 mm, D = 3 mm, V_j = 40 m/s, K = 0.75. For air at 1 atm and temperature T_j between 120°C and 140°C, $\bar{h} \approx 200$ W/m^{2}K. This value is very close to that calculated from measured drying rates, eq. (5.9). In theory the value computed from the measured drying rate is expected to be lower than the correlation value because first, eq (5.10) does not account for vapour flow generated from the drying material, second, eq. (5.9) neglects heat loss as mentioned earlier, and finally, $\overline{R_{0.4s}}$ is used in place of constant drying rate R_c, which is unknown, $\overline{R_{0.4s}}$ being an average over a period covering both constant and falling drying rate so is smaller than R_c.

The residual moisture content after the longest time under impingement drying, t = 12 s, is larger for the coated sheet, Figures 5.2 and 5.3, than the uncoated dry base sheet, Figure 5.6, i.e. about 0.04 vs 0.02 kg/kg dry. It follows that either the residual moisture content in the coating layer is higher than that of the base sheet or that the moisture content in the base sheet is larger in the coated sheet than in the uncoated sheet dried under similar conditions. Since drying occurs from the exterior of the coating surface to the interior of the base sheet it seems illogical to have the base sheet more dry than the coating layer. It is however possible that some water remains trapped in small pores of the coating layer after such pores have been closed by the coating compaction and latex film forming which occur during drying. The second possibility case, i.e. higher moisture content in the base sheet, implies that removal of moisture from the base sheet under the coating is restricted compared to that from an uncoated base sheet. For this effect there could be two possible causes: heat or mass transfer restrictions from the dry coating.

The possibility that the dry coating might act as a thermal insulation layer, reducing the rate of heat conduction to the base sheet, thereby reducing the drying rate is considered first. Measuring the thermal conductivity of paper is very difficult, Sadeghi (2003). Guérin et al. (2001) measured the thermal conductivity of clay-latex coating layers in the range 0.5 to 0.7 W/mK depending on the latex content. Typical values for uncoated paper are in the range 0.10 to 0.18 W/mK. The heat transfer Biot number, Bi_h, that is the ratio of the internal resistance to heat transfer (by conduction) over the external resistance to heat transfer (by convection), can be calculated as follows to test the hypothesis that the coating layer acts as a thermal barrier:

$$Bi_h = \frac{\delta_c}{k_c} \Big/ \frac{1}{h} \tag{5.13}$$

with h the heat transfer coefficient, δ_c the dry coating thickness - about 5 μm and k_c the dry coating thermal conductivity: about 0.6 W/mK from Guérin et al. (2001). For drying in air at 120°C or 140°C, $h \approx 240$ W/m^{2}K and the coating thermal conduction resistance is found to be much lower than that from convection on the air side: 8x10^{-6} m^{2}K/W for the coating, vs 5x10^{-3} m^{2}K/W for air convection. It follows that Bi_h is much smaller than 1 and that the coating does not limit heat transfer.

The mass transfer limitation by the dry coating layer does not seem probable, judging by the high drying rates observed in the first stages of coated paper drying, Figure 5.8. However when the coating dries, it forms a complex network of very small pores, in the range 0.01 to 0.1 μm, that might limit mass transfer. Therefore water vapor transport from the base sheet through the dry coating might be slower. When more water is transported into the base sheet, this water is then harder to remove through the dry coating layer, so slower drying of the base sheet through the coating could be expected. For longer coating-to-drying delay time, 5.2 s vs 0.2 s, favouring coating dewatering, higher residual moisture contents at 12 s drying time, 0.05 vs 0.03 kg/kg dry, were also observed corresponding to slower drying.

3. Paper properties development during coating-drying

3.1 Experimental

Sheets coated on commercial base paper were dried in air at 120 and 200°C and in superheated steam at 200°C with drying time ranging from 0.4 to 40 s, coating-to-drying delay time varied when drying in air from 0.2 to 1 s. Table 3.13 in Chapter 3 lists the conditions tested. The two cases in Table 3.13 of natural convection drying at room temperature differ as to the conditions of coating application, i.e. with the base sheet mounted on a cold support tray, condition CA(c)23, or on a hot support, condition CA(h)23. The sheets from conditions CA(c)23 and CA(h)23 were coated under same conditions as the other sheets but were not dried under impingement drying. When drying in superheated steam the sheet support tray must be preheated, as detailed in Chapter 3 section 4.4.3, that is, coating with a hot sheet support. The last coating drying condition, CA(h)23, helps to identify changes in coated paper properties which may derive from coating on a hot support from just the effects from drying under superheated steam impinging jets. CA(h)23 is not a perfect blank because more than 0.2 s is required to remove the just coated sheet from the support tray, 0.2 s being the time a sheet dried in superheated steam spends on the hot support.

After drying experiments, the coated sheets were left in the controlled condition a sufficient amount of time for reaching their equilibrium moisture content. Testing was therefore performed on "dry" coated sheets, i.e. at equilibrium moisture content (about 0.065 kg/kg. Testing for non-destructive properties was performed on 5 uncalendered sheets for each drying condition while for gloss and printing testing was performed on 2 calendered sheets. For each property tested 10 measurements were taken for each condition except for the case of print mottle, determined twice on each print. For each property a unique decision limit was calculated from the pooled standard deviations of the 33 sets of sheets tested here, as described in Chapter 3 section 8.2. The mean value for sheets produced with variable drying time and for the sets of sheets produced with variable coating-to-drying delay time were calculated separately. Plotted on each graph are the mean value along with the upper and lower decision limits. This procedure provides the quantitative basis for identifying when there is a statistically significant difference between the values of a property for sets produced under different coating-drying conditions. The description of properties and testing procedures is provided in Chapter 3 section 7 and for print mottle evaluation in Chapter 7 section 4.3.

3.2 Effects of coating-drying parameters on paper properties

3.2.1 Introduction

In section 2 it was shown that under the impingement drying conditions of this study, about 50% of the moisture has already been removed in 1 s, and that normal moisture content of dry paper is reached in less than 5 s. In section 3 the effect of drying time is investigated in this range but also for $t > 5$ s to provide a thorough documentation the effects on coated paper properties of the moisture and temperature history during drying.

Table 5.2 presents the extreme values and changes observed for each property measured. Also given are the values for drying conditions as used in Chapters 6 and 7: coating-to-drying delay time of 0.2 s, drying time of 3 s for drying in 120°C air, and drying time of 2 s for drying in 200°C air or 200°C superheated steam. The drying variables that had the most effect are drying time and drying medium, then drying temperature, while coating-to-drying delay time had almost no effect. A very significant finding is that the confidence intervals for the experimental results are always much smaller than the changes which are of industrial significance, thereby confirming that coated paper was produced with good reproducibility and that properties were measured with sufficient accuracy. Moreover, as many of the changes in paper properties observed when varying drying conditions are statistically significant and some of those changes are as well industrially significant, the experimental design of this study has produced results of practical importance.

3.2.2 Effect of drying time

Drying time, t, has a significant effect on most of the properties tested. Moreover the effect of drying time is consistent for the 3 drying conditions tested: 120°C air, 200°C air and 200°C superheated steam. The two classes of coated paper properties measured, bulk and surface properties, follow consistent trends with drying time.

In the first class of properties, brightness, Figure 5.9, shows the most consistent trend: first increasing sharply, reaching a maximum, then decreasing slightly to a plateau value. Opacity, the light scattering coefficient and permeability, Figure 5.10, Figure 5.11, and Figure 5.12, follow the same trend but the changes are smaller.

Table 5.2 Limiting values of coated paper properties

Property tested		**Thickness**	**Permeability**	**Brightness**	**Opacity**	**Light scattering**	**Light absorption**	**Gloss, uncalendered**	**Gloss, calendered**	**Print mottle, calendered**
Unit		µm	10^{-16} m^2	o	o	m^2/kg	m^2/kg	o	o	
[1]Significant change		2	n/a	1	0.5	2	0.05	n/a	2	n/a
[2]Decision limit		0.77	0.19	0.13	0.26	1.32	0.04	0.25	0.90	n/a
Nat. Conv. Air 23°C	CA(c)23	80.1	2.5	70.7	91.9	66.6	2.31	15.4	57.8	1.1
	CA(h)23	78.3	3.9	71.1	92.0	67.7	2.26	13.5	45.6	1.0
	Change	-1.8	1.4	0.4	0.1	1.1	-0.04	-1.9	-12.1	-0.1
Impingement Air 120°C (CA120)	Min	78.0	2.5	71.3	92.0	69.1	2.28	14.0	50.9	1.1
	Max	80.2	3.2	72.1	92.7	73.4	2.36	16.2	55.8	1.2
	Change	2.3	0.8	0.8	0.7	4.4	0.08	2.2	5.0	0.1
	t =3 s	80.2	3.1	71.6	92.6	72.6	2.36	14.4	52.6	1.22
Impingement Air 200°C (CA200)	Min	77.9	2.5	71.4	92.1	69.4	2.31	13.9	49.5	1.1
	Max	80.2	3.3	71.8	92.8	74.1	2.36	15.6	54.0	1.3
	Change	2.2	0.8	0.5	0.8	4.7	0.05	1.7	4.6	0.1
	t = 2 s	80.2	3.0	71.6	92.8	73.8	2.36	14.1	50.9	1.15
Impingement SHS 200°C (CS200)	Min	79.3	3.9	71.3	92.0	69.6	2.28	12.7	44.5	1.0
	Max	82.0	4.2	71.6	92.4	71.4	2.35	13.4	45.1	1.0
	Change	2.7	0.4	0.2	0.4	1.8	0.07	0.8	0.7	0.1
	t = 2 s	80.2	3.9	71.4	92.4	71.4	2.35	13.4	44.7	0.97
Change CA120->CA200		0.0	-0.3	0.0	0.2	1.2	0.0	0.0	0.0	-0.07
Change CA200->CS200		0.0	-0.7	-0.2	-0.4	-2.4	-0.01	0.0	-0.01	-0.18

[1] *"Significant change" is the change significant to a papermaker for LWC paper quality*

[2] *The decision limit is calculated as described in Chapter 3 section 8.2 for all 33 sets of samples tested in this chapter*

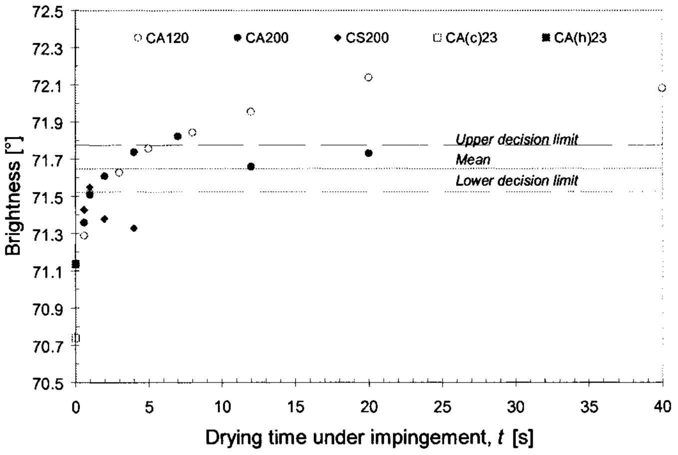

Figure 5.9 Effect of drying time on coated paper brightness: Uncalendered

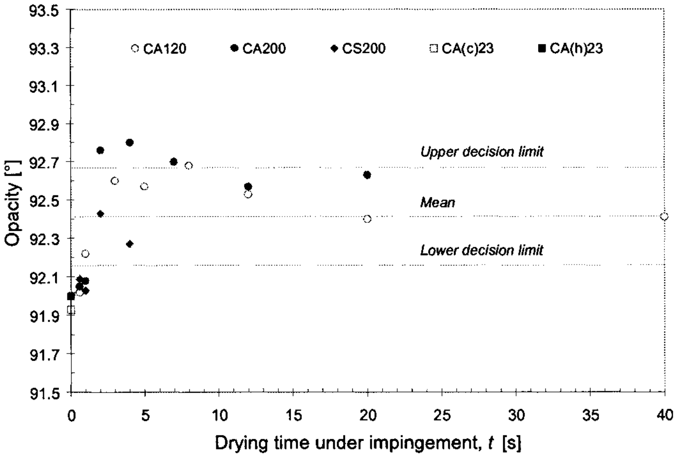

Figure 5.10 Effect of drying time on coated paper opacity: Uncalendered

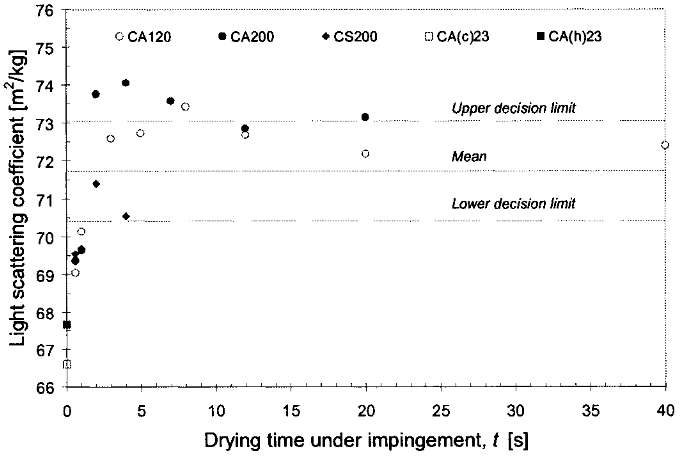

Figure 5.11 Effect of drying time on coated paper light scattering coefficient: Uncalendered

The light absorption coefficient and thickness, Figures 5.13 and 5.14, also follow this trend but the changes are within the precision of the measurements. Since the trends are consistent and repeatable, the changes, although small, are judged important and illustrate changes in the coating structure during drying. The locations of the maxima vary with the drying medium, the drying fluid temperature and the property tested, as discussed in sections 3.2.3 and 3.2.4.

A similar trend was observed for gloss measured on calendered sheets, Figure 5.15: rapid change in the first 4-5 s and then a plateau. The decrease was not as sharp when drying in superheated steam, the gloss values being always much lower for drying in steam as will be discussed in section 3.2.3. The trends are less clear when gloss is measured on uncalendered sheets, Figure 5.16. With uncalendered sheets the same decrease and plateau for gloss as on calendered sheets are observed in air drying. However at long drying times (> 10 s) for drying in air at 200°C the gloss on uncalendered sheets increases to the gloss after short drying time while gloss on calendered sheets remains unchanged. Also in the case of superheated steam drying, gloss on uncalendered sheets increases with drying time conversely to gloss on calendered sheets. Gloss, a measure of surface shininess, is directly related to surface microscale roughness. As for print mottle, Figure 5.17, gives the components of print mottle as a function of scale of print mottle. A detailed treatment of the meaning and significance of these print mottle components is provided in Chapter 7 section 4.3. The higher the value in Figure 5.17 the more mottle. Since the trend of mottle with the scale of print mottle on Figure 5.17 is very consistent at all scales, mottle at a single value of scale of mottle is retained for representation in Figure 5.18 as a function of drying time. Increasing drying time tends to decrease print mottle, but the effect is small. However, as will be seen from results presented in Chapter 7 where the instrumental measurement of mottle is supported by results from subjective ranking, the preliminary conclusions above from Figures 5.18 and 5.19 are consistent with subjective evaluation of print mottle to be presented subsequently.

Compared to air impingement drying, natural convection drying, condition CA(c)23, gives lower brightness for, opacity and light scattering coefficient and permeability, but higher gloss and print mottle of similar intensity.

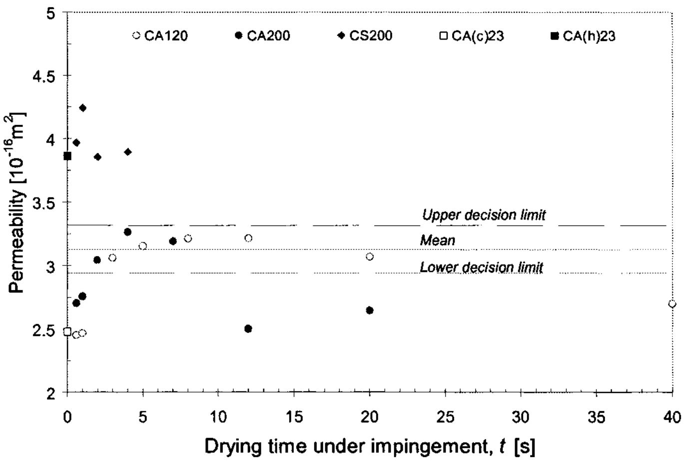

Figure 5.12 Effect of drying time on coated paper permeability: Uncalendered

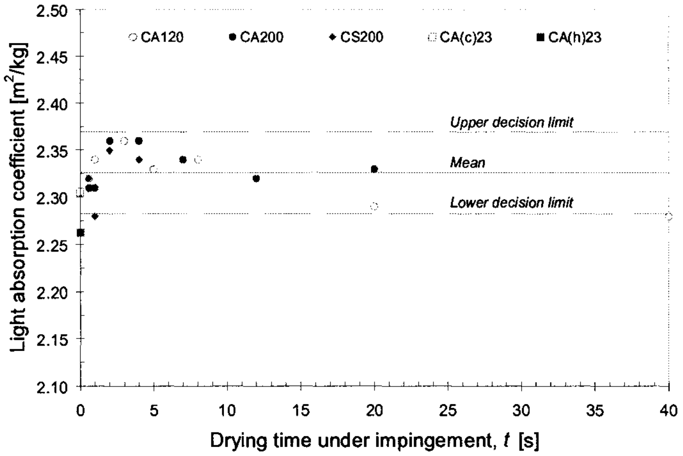

Figure 5.13 Effect of drying time on coated paper light absorption coefficient: Uncalendered

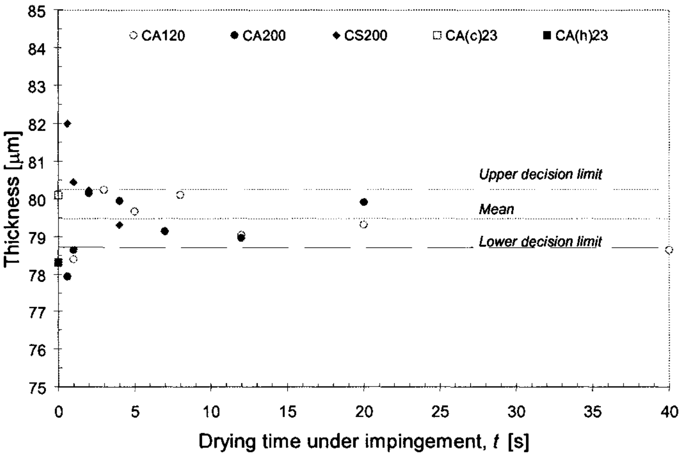

Figure 5.14 Effect of drying time on coated paper thickness: Uncalendered

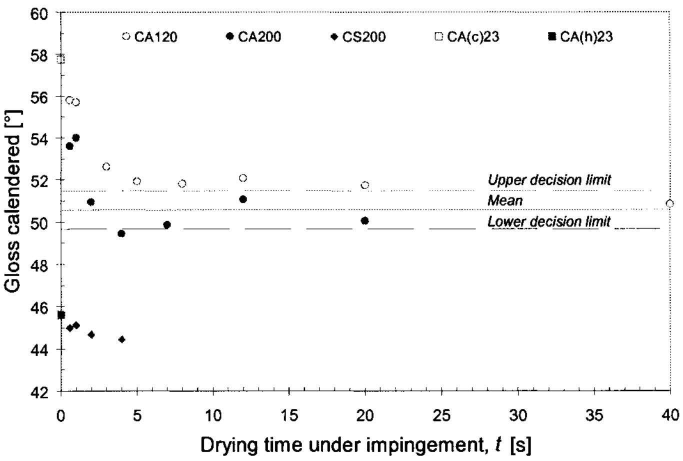

Figure 5.15 Effect of drying time on coated paper gloss: Calendered

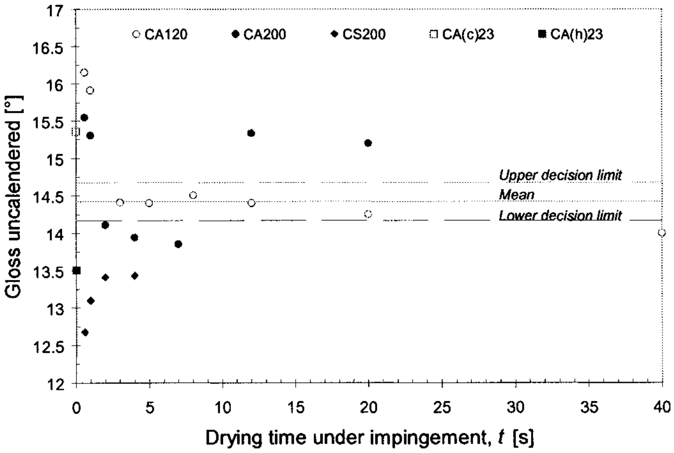

Figure 5.16 Effect of drying time on coated paper gloss: Uncalendered

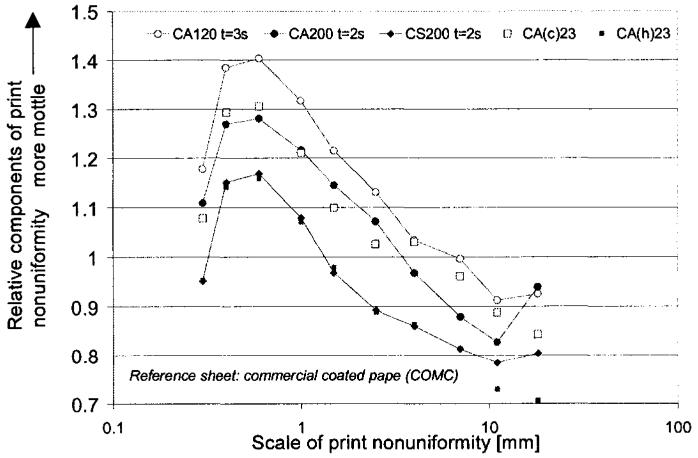

Figure 5.17 Effect of drying time on coated paper components of print mottle as a function of scale of mottle: Calendered

The effect of drying time is related to the sheet temperature and moisture history. The variable drying time is replaced by sheet moisture content, *X*, in Figure 5.19 and 5.20 for the case of 120°C air drying. Only brightness and gloss are reported here, the evolution of the other properties with moisture content being recorded in Appendix C. As sheet moisture content is reduced by impingement drying in 120°C air, there is an increase in brightness, light scattering coefficient, opacity and permeability of the coated paper but a decrease in both uncalendered and calendered gloss. When drying slows down significantly, $t > 5$ s, the properties still continue to change. The changes are not large but they seem to occur consistently: a decrease in all the properties is observed except for brightness which increases because of the decrease in light absorption.

3.2.3 Effect of drying medium

With superheated steam drying for most of the properties the same trends as described in section 3.2.2 are observed with increasing drying time. The limits are however reached much faster in superheated steam: earlier by 2-3 s (opacity, light scattering, and permeability, Figures 5.10 to 5.12) to 7 s (brightness, Figure 5.9). The effect that drying in steam has on gloss, permeability and print mottle is more pronunced. The gloss and permeability of coated paper in steam are much different than with air drying at all drying times, permeability higher by about 30%, Figure 5.12, and gloss lower by about 6 percentage points, Figure 5.15. The effect of drying time on those properties is similar to that observed for air drying, but the changes are smaller. The difference may derive from the much higher sheet temperature experienced in superheated steam from the onset of drying, 100°C as opposed to about 50°C in air drying, when the particles of coating pigment and binder may move the most easily.

3.2.4 Effect of drying fluid temperature – case of air drying

When the drying temperature is increased, the limits reported in section 3.2.2 are reached about 4 s earlier in 200°C than in 120°C air drying for light scattering coefficient, opacity and gloss, and up to 13 s earlier for brightness, Figures 5.9 to 5.15. Also opacity and light scattering coefficient are higher by respectively 0.25 and 1 point, Figures 5.10 and 5.11, and gloss is lower by more than 2 points, Figure 5.15, at the location of the maximum at the higher drying fluid temperature.

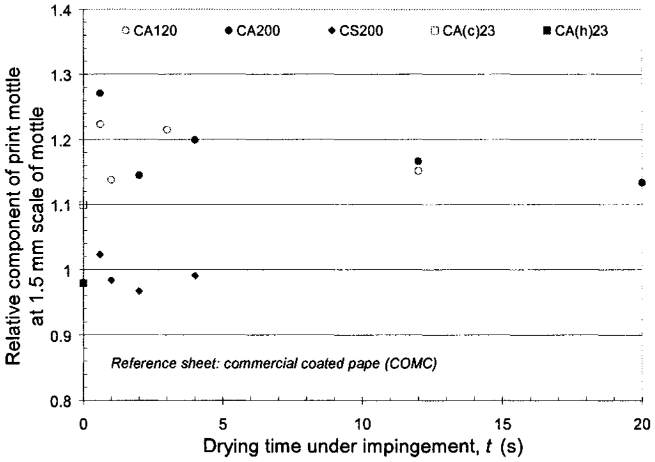

Figure 5.18 Effect of drying time on coated paper print mottle at 1.5 mm scale of mottle: Calendered

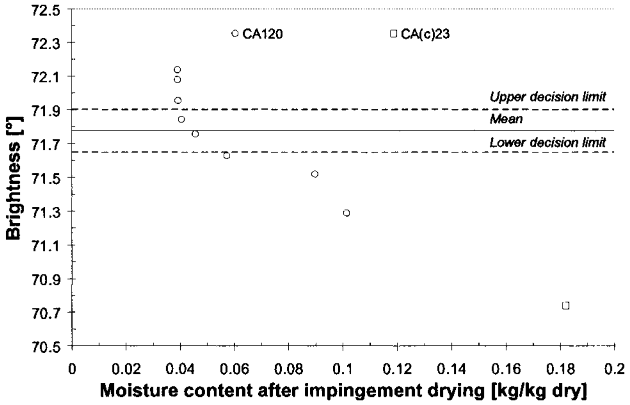

Figure 5.19 Effect of moisture content removed by 120°C air impingement drying on coated paper brightness: Uncalendered

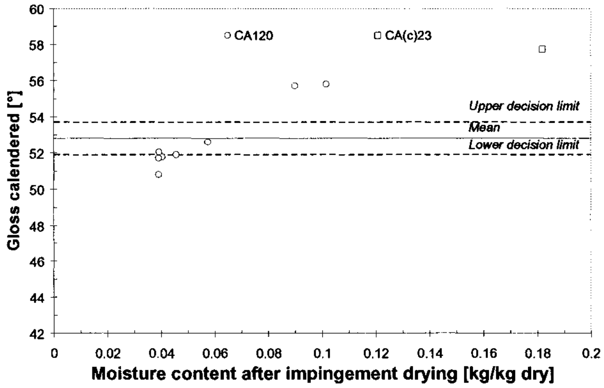

Figure 5.20 Effect of moisture content removed by 120°C air impingement drying on coated paper gloss: Calendered, 120°C air drying

3.2.5 Effect of delay time – case of air drying

Coating-to-drying delay time has almost no effect on coated paper properties with the level of precision available, Figures 5.21 to 5.23. Not much effect of this delay time on drying rate is observed either in the 0.2 - 1 s delay time range, as discussed in section 2.2. Only brightness, gloss and print mottle are shown here, while the effect of delay time on other properties are recorded in Appendix C.

3.2.6 Discussion

In section 2 it was shown that for drying under air impingement, the falling rate period has already been established by 0.4 s drying time, by which time the sheet average moisture content has been reduced to about 0.11-0.12 kg/kg dry, Figures 5.2 and 5.3. The end of the constant rate period should occur at the SCC, when the evaporation front recedes inside the coating layer. It follows that for all impingement drying conditions tested in section 3, $t > 0.6$ s, the SCC has already been reached. Typical moisture content values for the SCC of clay-latex coatings are in the range 82-85% wet basis, Makinen (1998), Kim et al. (1998), e.g. 0.18 – 0.22 kg/kg dry coating. Under the limiting assumption of no dewatering of the coating into the base sheet, Figure 5.24 shows that the coating moisture content would decrease from its initial value of $X_{cs} = 0.58$ kg/kg dry, to reach 0.18 kg/kg dry coating in only 0.7 s in 120°C air drying. In reality dewatering occurs, so the SCC would be reached even faster. Therefore the SCC has already been reached for $t = 0.6$ s, the shortest drying time for which properties have been tested. It is interesting to note in Figures 5.13 to 5.16 that in most cases coated paper properties change for $t > 0.6$ s, even though the SCC was reached earlier. For experiments involving slow drying at room temperature, Watanabe and Lepoutre (1982) concluded that shrinkage and latex film forming, so changes in coating structure, were completed by the time the coating reached the SCC. The present experiments under high intensity impingement drying, as used for industrial production of coated paper, show that properties continue to develop beyond SCC.

The effects of drying conditions on coating bulk and surface structure were discussed in Chapter 2 section 3.3.1. Drying rate and drying temperature may affect: (a) coating dewatering rate, (b) coating shrinkage and latex film forming and (c) coating disruption from water or water vapor flow, as are now discussed.

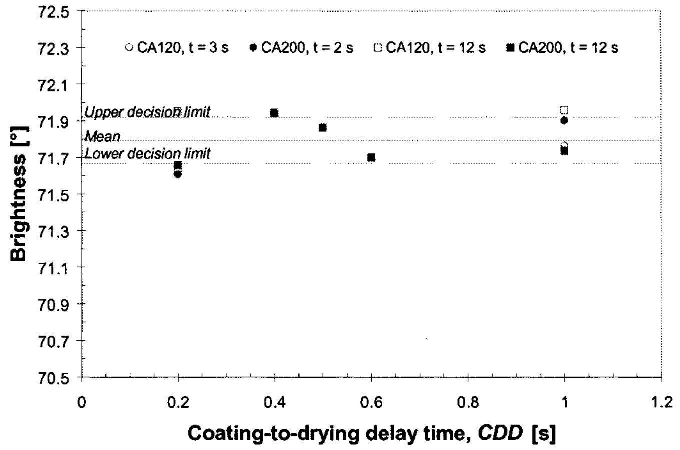

Figure 5.21 Effect of delay time on coated paper brightness: Uncalendered

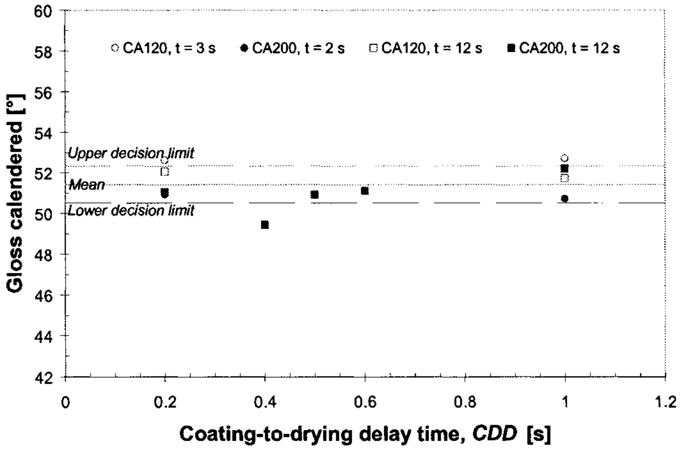

Figure 5.22 Effect of delay time on coated paper gloss: Calendered

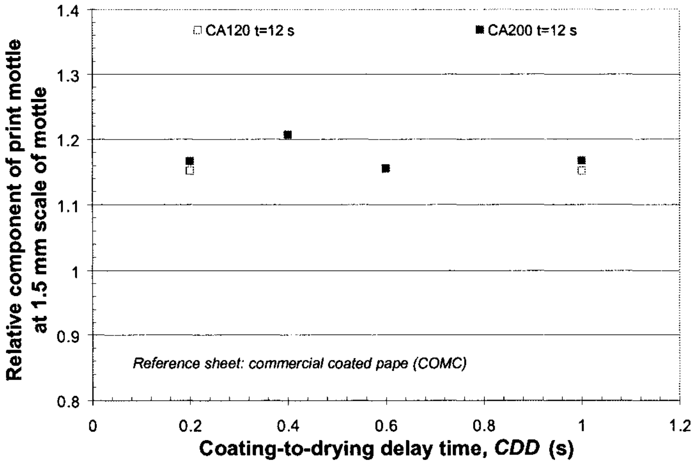

Figure 5.23 Effect of delay time on coated paper print mottle at 1.5 mm scale of mottle: Calendered

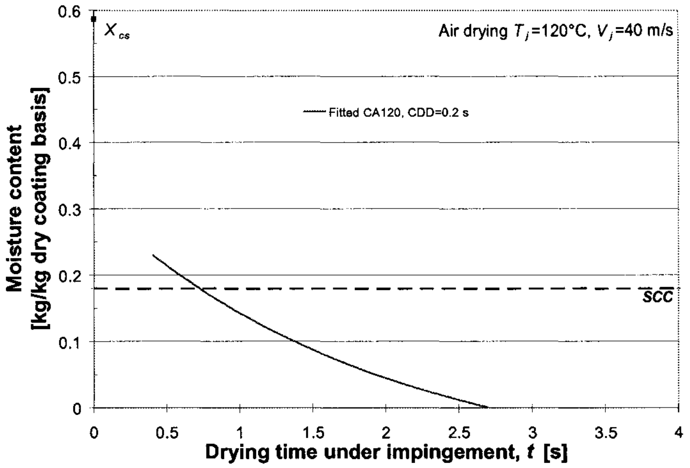

Figure 5.24 Drying time to SCC for the limiting case of no coating dewatering

a. Effect on dewatering rate

As discussed in Chapter 2 section 3, dewatering produces base sheet swelling. Since dewatering stops with the coating at the FCC, the effect from dewatering should already be visible at $t = 0.6$ s. At this drying time differences are observed between air and steam drying for permeability, thickness, and gloss, Figures 5.12, 5.14 and 5.15. Drying in steam sets the sheet temperature almost instantaneously at 100°C, which may lead to faster dewatering. The other properties are not statistically different for air or steam drying. For drying in air no difference is observed between 120 and 200°C at 0.6 s drying time, probably because the sheet temperature history, increasing from room temperature to the wet bulb temperature, which is not very different in 120 or 200°C air drying.

b. Effect on coating shrinkage and latex film forming

Coating shrinkage occurs when capillary forces act and latex film forming occurs, that is theoretically until reaching the SCC. In the present study with impingement drying the higher sheet temperature, and a latex of T_g= 12°C, the duration of latex film forming process may be extended and may occur by dry coalescence rather than wet coalescence. Coating porosity decreases with shrinkage, while Stanislwaska and Lepoutre (1996) showed that coating pore size increases with latex film forming. The consistent trends obtained for all bulk properties with drying time, described in section 3.2.2 may, be explained by these two opposite effects. Both light scattering and permeability vary with porosity and pore size. For light scattering there is an optimum pore size range specific to the pigment material and wavelength, as explained in Appendix A section 6.2.4. Permeability is expected to increase with increasing porosity and pore size. Bulk properties may therefore first increase with drying time as latex film forming increases pore size. This increase is rapid at first but slows and reaches a plateau because of the simultaneous decrease in porosity. Gloss in turn can only decrease with shrinkage. A higher sheet temperature enhances latex film forming which in turn would promote coating shrinkage. When increasing the drying fluid temperature from 120 to 200°C, the changes in properties occur faster. When switching from air to steam drying, the sheet temperature from the onset of drying is increased by about 50°C, which promotes both wet and dry coalescence and results in greater shrinkage. Extended coating shrinkage with steam drying may therefore explain the large drop in gloss already detected at 0.6 s drying time.

c. Effect on water vapour flow

Until the coating has not set into a fixed matrix, i.e. prior to the second coating consolidation (SCC), the clay particles may move individually under the flow of water or water vapour toward the coating surface. Under the action of such flow the plate-like clay particles may lose alignment and become oriented at an angle to the sheet surface. Any such movement of clay particles would result in a more open structure with larger pore size and lower gloss. However this process is complicated by the action of capillary forces causing coating shrinkage. Such movement of particles would act in opposition to the effect of coating compaction by the moisture removal and latex film forming which, in theory, occur simultaneously between the FCC and the SCC. Once a fixed solid matrix is formed, i.e. after the SCC, the pigment particles no longer move under the flow of water vapour. This effect should therefore be apparent at 0.6 s drying time, and may explain the large drop in gloss seen with steam drying already at $t = 0.6$ s.

4. Conclusions

Drying in the laboratory impingement dryer occurs mostly in the falling rate period, even for the shortest drying time possible, 0.4 s. Drying rates over the initial 0.4 s of impingement drying, calculated from experimental drying curves, are in the range 24 to 35 kg/m^{2}h, which are in the same order of magnitude as industrial drying rates for coated paper. A decrease of 5 kg/m^{2}h was observed when increasing the coating-to-drying delay time from 0.2 to 5.2 s.

Even though most of the moisture is removed in the first second, the coated paper properties continue to develop with increasing impingement drying time. Drying medium and drying time have the most effect on paper properties while drying temperature in air has less effect. Coating-to-drying delay time over the range 0.2-1 s has no effect on paper quality and only a slight effect on drying rate. Latex film forming beyond the SCC probably explains the changes of properties with drying time. The sharp and near instantaneous increase in sheet temperature to 100°C at the start of drying which results from switching from air to superheated steam as the impingement drying fluid probably strongly affects phenomena occurring at short drying times, such as dewatering, water vapour flow, and wet latex coalescence. Coated paper properties were determined here to be already affected at the shortest drying time, 0.6 s, when switching from air to superheated steam as the drying fluid.

Chapter 6 Effects of drying on coated paper properties: Laboratory base paper

1. Introduction

This chapter presents the effects of drying conditions on coated paper properties other than print quality. Coated sheets were produced from laboratory base paper and drying conditions used were those designated AA120, AA200, AS120, AS200, SA120, SA200, SS120 and SS200 in Table 3.14. The definition of the properties tested and the description of the procedures are available in Chapter 3 section 7 and Appendix A section 6.

For each property 10 replicate sheets were tested except for Talyscan profilometry, mercury porosimetry and ESCA, for which a single sheet was tested. The statistical treatment of data is detailed in Chapter 3 section 8.2. For each property a unique decision limit was calculated from the pooled standard deviation of the 8 sets of samples tested. The mean value among the samples produced with variable drying conditions was calculated. For each graph the mean value, the upper and the lower decision limits are also plotted. The upper and lower decision limits, corresponding to the mean value plus and minus the decision limit, enable deciding whether there is a statistically significant difference (at 95%) between the values of a property tested for coated paper produced under different drying conditions. All figures report properties for calendered paper except for Figure 6.6.

Table 6.1 gives the limiting values of properties found for the 8 drying conditions tested. An overall indication of the importance of drying conditions tested is that all values of the range of properties measured ("Change" column) substantially exceed the corresponding value for the change that would be of practical importance ("Significant" column). Thus the results summarized in Table 6.1 serve the valuable function of confirming that the experimental plan of this thesis involved a choice and range of variables which made significant changes in essential properties of the LWC grade of coated paper. Tables 6.2 and 6.3 provide the changes in properties found for changing between the two drying fluids used and the drying fluid temperature between the limits of 120 and 200°C.

Table 6.1 Limiting values of calendered coated paper properties

Property	**Unit**	**[1]Significant change**	**[2]Decision limit**	**Min**	**Max**	**[3]Absolute change**
Thickness	µm	2	1.1	50.9	55.2	4.3
Permeability	10^{-17} m^2	n/a	0.3	1.8	3.1	1.3
Paper pore diameter	µm	n/a	-	1.06	1.24	0.18
Paper porosity	%	n/a	-	30.6	34.8	4.2
Coating pore diameter	µm	n/a	-	0.042	0.043	0.001
Coating porosity	%	n/a	-	24.5	27.6	3.1
Light scattering	m^2/kg	2	1.00	61.5	69	7.5
Light absorption	m^2/kg	n/a	0.06	2.9	3.4	0.5
Opacity	°	0.5	0.20	93	94.3	1.3
Brightness	°	1	0.23	64.9	67.3	2.4
PPS roughness	µm	0.1	0.025	0.74	1.15	0.40
Talyscan roughness (S_q)	µm	-	0.045	0.31	0.45	0.14
Gloss	°	2	0.6	60.6	71.3	10.7
ESCA	%	n/a	-	23.2	27.2	4.0

[1] *"Significant change" is the change significant to a papermaker for LWC paper quality*

[2] *The "decision limit" is calculated as described in Chapter 3 section 7 from the pooled standard deviation among all 8 sets of samples tested in this chapter*

[3] *"Absoute change" is the difference between the maximum and minimum values*

Table 6.2 Absolute changes in coated paper properties with drying conditions

[1]Property	Base paper drying medium				Coated paper drying medium				Coated paper drying temperature			
	AA120->SA120	AA200->SA200	AS120->SS120	[2]AS200->SS200	AA120->AS120	[2]AA200->AS200	SA120->SS120	SA200->SS200	AA120->AA200	[2]AS120->AS200	SA120->SA200	SS120->SS200
Thickness	-0.55	2.45	0.60	3.17	0.88	1.10	2.03	1.82	-1.52	-1.30	1.48	1.27
Permeability	0.16	0.22	0.21	0.95	0.27	0.27	0.32	0.99	0.12	0.12	0.18	0.86
Porosity (base)	2.3	-	-	-1.6	-	-	-	-	-	-	-	-
Pore size (base)	0.2	-	-	0.1	-	-	-	-	-	-	-	-
Porosity (coating)	0.2	-	-	-2.3	-	-	-	-	-	-	-	-
Pore size(coating)	0.0	-	-	0.0	-	-	-	-	-	-	-	-
Light scattering	-5.45	-4.45	-6.43	-	2.07	-	1.09	3.03	-0.78	-	0.21	2.15
Light absorption	0.05	0.22	0.13	-	0.19	-	0.26	0.25	-0.17	-	0.00	-0.01
Opacity	-0.69	-0.28	-0.67	-	0.55	-	0.58	0.84	-0.39	-	0.02	0.29
Brightness	-1.35	-1.83	-1.75	-1.56	-0.32	-0.54	-0.72	-0.26	0.30	0.08	-0.18	0.27
PPS Roughness	0.22	0.23	0.25	0.26	0.15	0.11	0.18	0.13	0.03	-0.01	0.05	-0.01
Talyscan roughness (S_q)	0.07	0.09	0.05	0.05	0.09	0.05	0.07	0.00	0.01	-0.03	0.03	-0.03
Gloss	-3.71	-4.91	-3.44	-4.60	-6.67	-3.76	-6.40	-3.45	-2.32	0.59	-3.52	-0.57
Surface carbon concentration	1.50	-	-	1.70	-	-	-	-	-	-	-	-

[1] *Units of properties are as given in Table 6.1*

[2] *The values for light scattering, light absorption and opacity are not given for the AS200 drying condition as Figure 6.6 and section 3.1 establish that these anomalous results are not reliable.*

Table 6.3 Normalized changes in coated paper properties with drying conditions

Property	**Base paper drying medium**				**Coated paper drying medium**				**Coated paper drying temperature**			
	AA120->SA120	AA200->SA200	AS120->SS120	AS200->SS200	AA120->AS120	AA200->AS200	SA120->SS120	SA200->SS200	AA120->AA200	AS120->AS200	SA120->SA200	SS120->SS200
Thickness	-0.5	2	1	3	1	1	2	2	-1	-1	1	1
Permeability	1	1	1	3	1	1	1	3	0	0	1	3
Porosity (base)	n/a	-	-	n/a	-	-	-	-	-	-	-	-
Pore size (base)	n/a	-	-	n/a	-	-	-	-	-	-	-	-
Porosity (coating)	n/a	-	-	n/a	-	-	-	-	-	-	-	-
Pore size(coating)	n/a	-	-	n/a	-	-	-	-	-	-	-	-
Light scattering	-5	-4	-6	*0*	2	*-1*	1	3	-1	*-4*	0	2
Light absorption	1	3	2	*6*	3	*1*	4	4	-3	*-5*	0	0
Opacity	-3	-1	-3	*3*	3	*0*	3	4	-2	*-5*	0	1
Brightness	-6	-8	-8	-7	-1	-2	-3	-1	1	0	-1	1
PPS Roughness	9	9	10	10	6	4	7	5	1	-1	2	0
Talyscan roughness (S_q)	2	2	1	1	2	1	1	0	0	-1	1	-1
Gloss	-5	-7	-5	-6	-9	-5	-9	-5	-3	1	-5	-1
Surface carbon conc.	n/a	-	-	n/a	-	-	-	-	-	-	-	-

[1] *Units of properties are as given in Table 6.1*

[2] *Normalized change is the ratio of the absolute change (Table 6.2) to the decision limit for that property (Table 6.1)*

2. Bulk paper properties

2.1 Thickness

Thickness, measured on single coated sheets, is found to be around 53 μm. For the 8 cases tested, Figure 6.1, drying conditions had little effect on thickness, as expected. Thickness is mostly controlled by sheet basis weight, coating weight and calendering conditions, all of which were kept constant. Steam dried base sheets tend to give higher coated sheet thickness, although in Chapter 4 the thickness of uncoated steam-dried base sheets was found slightly lower than for air-dried sheets. Coating drying temperature has opposite effects depending on the base sheet drying strategy: increasing the coating drying temperature decreases coated sheet thickness for sheets coated on air-dried base sheets, but has the opposite effect for sheets coated on steam-dried base sheets. In addition to the main controlling factors noted above, base sheet expansion due to rewetting during coating, and coating consolidation during drying may affect thickness. Also if water vapour flow is promoted, opening up the coating, sheet thickness should increase; if coating shrinkage is promoted then thickness should decrease. These multiple simultaneous effects thus complicate the net effect. Figure 6.1 indicate that conditions AA200 and SS200 produce slightly different thickness. However these conclusions are weak because the effects are small.

2.2 Permeability

The permeability of coated paper was obtained, as for uncoated paper with the PPS apparatus used with permeance heads. For the 8 drying conditions tested, Figure 6.2, the differences were small but show consistent trends in all four comparative cases of base sheet drying medium and coated sheet drying medium, Table 6.3. Steam-dried base paper produces more permeable coated paper compared to air-dried base paper. Steam drying of the coated sheet increases permeability as compared to air drying. Increasing the coating drying temperature affects coated paper permeability only for steam drying, for which it increases.

The permeability, *K*, of a laminate composite material such as coated paper, may be calculated from the permeability and thickness of each constituent layer, the base sheet and coating layer for the case of single sided coated paper as follows:

$$\frac{1}{K}=\frac{l_c}{l_c+l_b}\frac{1}{K_c}+\frac{l_b}{l_c+l_b}\frac{1}{K_b} \quad \text{(resistances in series)} \tag{6.2}$$

with l_c and l_b the thickness and K_c and K_b the permeability of the coating layer and base paper. For each layer the permeability may be estimated from pore radius, porosity and tortuosity from equation (2.12). The permeability of uncoated sheets, K_b, and uncalendered sheets, K, coated on commercial base paper were measured in Chapter 4 and 5 respectively. Comparing these values to that of calendered coated paper obtained here show that coating and calendering reduce the permeability by two orders of magnitude: the permeability values obtained for calendered coated paper are 2-3 10^{-17} m^2, Figure 6.2, for uncalendered coated paper 2-5 10^{-16} m^2, Chapter 5 section 3, and for uncoated base paper 3-4 10^{-15} m^2, Chapter 4 section 2.2. The values found for uncalendered coated paper are comparable to that from Schoelkopf et al. (2003), ~10^{-17} m^2, and Asensio (2000) for uncoated base paper, 2-10 10^{-15} m^2. This reduction reflects the difference in pore structure between the fibre matrix and the coating layer: clay platelet particles, much smaller than fibres, arrange in a much denser porous structure, as indicated in the pore structure results in Table 6.5. The application of temperature and load during calendering further reduces porosity. Using eq. (6.2) with these values and the values of pore radius and porosity determined for uncalendered paper in section 2.3 from mercury porosimetry, the permeability of the uncalendered coating layer is found to be ~ 2 10^{-17}, i.e. two orders of magnitude smaller than that of the base paper. Assuming calendering does not change the relative values of coating and base paper permeabilities, it follows that the coating layer characteristics control coated paper permeability and the permeability measurement characterizes the coating layer. The following approximation may thus be used:

$$\frac{1}{K}\cong\frac{l_c}{l_c+l_b}\frac{1}{K_c} \tag{6.3}$$

With values of coating porosity and mean pore size from Table 6.5, the tortuosity of the coating layer may thus be calculated from measured values of coated paper permeability according to eq.(2.12):

$$R=4\tau\sqrt{\frac{K}{\varepsilon}} \tag{2.12}$$

The results are tabulated below.

Table 6.4 Calculated values of coating tortuosity

	Coated calendered				**Coated uncalendered**	
	AA120	**AS200**	**SA120**	**SS200**	**AA23**	**SA120**
Coating tortuosity	2.0	2.0	2.0	1.6	0.7	0.7

2.3 Pore structure

Mercury porosimetry is widely used to determine paper porosity and pore size distribution. In the case of coated paper the porosities and pore size distributions of the coating can be separated from that of the base paper because the pore dimensions are almost two orders of magnitude lower for the coating. The mercury pressure range used corresponded to pore size ranging from 0.02 μm to 0.1 μm for the coating layer, and to pore size above 0.3 μm for the base paper.

The results for pore size, porosity and pore density are summarized in Table 6.5. Besides the calendered sheets from the four extreme conditions, AA120, AS200, SA120 and SS200, two uncalendered sheets were tested: SA120 and air-dried base sheet coated and dried outside the impingement dryer at room temperature, identified as AA23. The pore density, the number of pores per μm^2, is calculated as follows:

$$N = \frac{\varepsilon}{\tau \cdot \Pi \cdot R^2} \tag{6.1}$$

with ε the porosity, R the average pore radius. For tortuosity, τ, the values used were 2 for the calendered coating and 0.8 for the uncalendered coating (see section 2.2), 10 for the calendered base paper and 3.7 for the uncalendered base paper, see Chapter 4 section 2.2.

Figure 6.3 and Figure 6.4 represent the pore size distribution of base paper and coating separately. It is important to note that because all determinations were made on coated paper the pore structure results for the base paper apply for the sheet under the coating, not the sheet prior to coating. Mercury porosimetry being time consuming experiment, no replicate sheet were tested. Mercury porosimetry results are believed to be very reproducible in terms of pore size, to the 0.001 μm for the same sample. The porosity is however determined based on measured mass and moisture content prior to intrusion.

Table 6.5 Pore structure from mercury porosimetry

	Calendered				**Uncalendered**	
	AA120	**AS200**	**SA120**	**SS200**	**AA23**	**SA120**
Base paper						
Average pore diameter (μm)	1.06	1.16	1.22	1.24	2.13	2.28
Porosity (%)	30.6	34.8	32.9	33.2	56.2	51.7
Pore density (μm^2)	0.03	0.03	0.03	0.03	0.04	0.03
Coating						
Average pore diameter (μm)	0.042	0.042	0.043	0.043	0.045	0.044
Porosity (%)	24.5	27.6	24.7	25.3	30.9	32.9
Pore density (μm^2)	87	102	85	109	270	300

The confidence on porosity is therefore believed to be around 2 percentage points only. Therefore the differences observed are not very large.

It is striking to see from Table 6.5 and the two figures that larger effects from drying conditions occur for the base paper than the coating layer. Moreover both drying stages, i.e. of the base sheet and of the coated sheet, affect pore size distribution of the base paper under the coating, whereas the coating porous structure remains essentially unchanged. For the coated base paper, using superheated steam for base sheet and coating drying leads to larger pores and a more porous sheet. For the coating, use of superheated steam does not affect porosity and mean pore size not much. There is however a trend toward wider pore size distribution when superheated steam is used for drying the coating, Figure 6.4. Changes in base sheet pore size distribution after coating is often associated to "coating penetration", Xiang et al. (2001), which closes the large pores at the surface of paper. Rather that penetration of the whole coating, fibre expansion due to coating liquid penetration into the base sheet may change the base sheet porous structure. According to this approach results in this chapter would indicate more penetration for base sheet dried in air and coating dried in air.

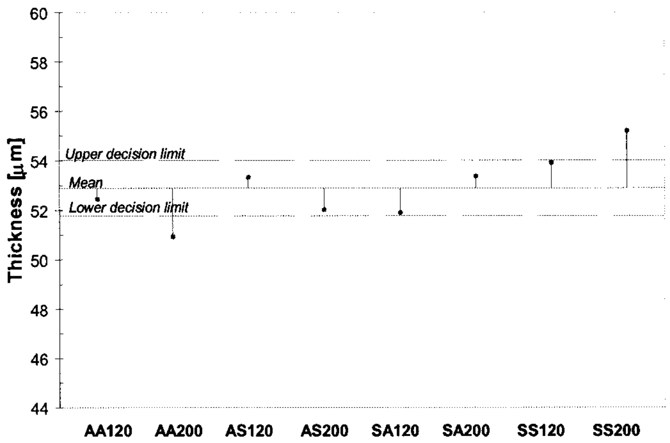

Figure 6.1 Thickness of coated paper

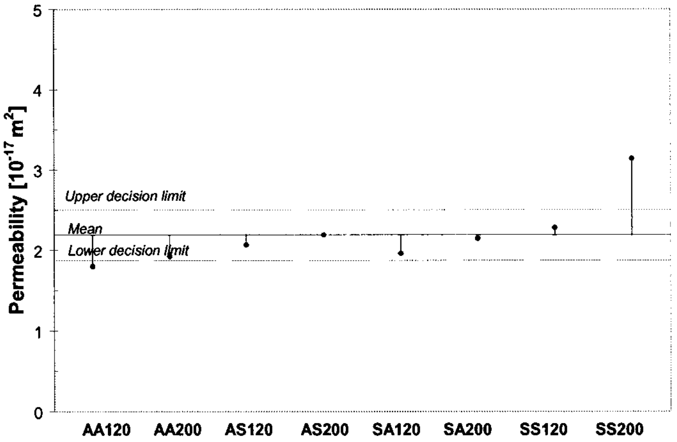

Figure 6.2 Permeability of coated paper

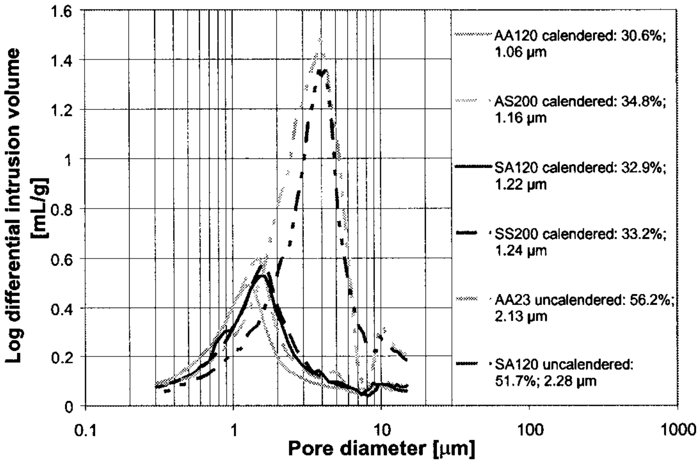

Figure 6.3 Base paper pore size distribution

Information on the effects of calendering on the porous structure is provided by the 2 uncalendered samples. For the drying condition SA120, a major reduction in porosity is observed for both the base paper, by about 1/3, and the coating layer, by about 1/4. As for mean pore size, the reduction with calendering is again very large for the base sheet, from 2.2 to 1.2 μm, but almost negligible for the coating from 0.045 to 0.043 μm.

In an extensive study on coated paper porosity, Preston (2001), reported values for clay-latex coatings in the same range as that found in this study: around 20% for porosity, 40 to 90 nm for pore diameter and 15 to 200 μm^{-2} for pore density calculated without accounting for tortuosity.

2.4 Scanning electron microscopy images of coated paper cross sections

SEM images of calendered coated sheets were taken in the cross-section direction. Samples were prepared according to a procedure, described in Appendix B, based on Paprican practice. The images were obtained in the BEI mode based on chemical composition. Typical images from AA120 and AS200 are shown in Figure 6.5. Images of the commercial coated paper and a laboratory coated paper from commercial base paper are also provided. The darker areas are the pores filled with the resin in which samples were embedded. The brighter areas are at the top layer, the coating, while the fibres appear in the grey tones.

The great difference in pore size between the coating and the base stock is apparent. The coating seems to fill in the large scale roughness of the base paper and presents a smoother surface than the base paper line. As a consequence a large local variation in coat weight is created. The difference in pore structure between drying conditions is seen more clearly from the quantitative results in Table 6.5 than in the visual representation of Figure 6.5.

2.5 Discussion

The effects of drying conditions on bulk properties reported above are not large. When superheated steam drying is used for drying the base sheet, an increase in permeability and base paper pore size is observed. However no effect of this change in base sheet drying is seen on the coating porosity, pore size or tortuosity which control permeability.

The bulk properties measured here are characteristic of the entire coated sheet while significant changes with drying conditions may be created just at the exterior surface of the coating layer only, as is suggested by results presented in section 4.

3. Optical properties

3.1 Introduction

Brightness and opacity are important properties of paper characterizing its visual appearance and performance as a printed product. Brightness and opacity are two distinct measurements. Brightness is the reflectance of an opaque pad of sheets measured with light at 457 nm wave length, while opacity is the ratio of the reflectance of a single sheet of paper to that of an opaque pad of paper but measured at 555 nm. These two properties depend on the light absorption and scattering coefficients of paper, which are calculated from the opacity measurement according to relationships developed by Kubelka-Munk and given in Chapter 3 section 7.3.

The values obtained for opacity, light scattering and light absorption coefficients (based on opacity measurements) for drying condition AS200 are suspicious. The relation between optical properties measured on uncalendered and calendered sheets, Figure 6.6, is clear and logical except for condition AS200 for opacity, light scattering and light absorption coefficients. Without the data for condition AS200 the correlation coefficients between uncalendered and calendered properties are between 0.91 and 0.99. The results for condition AS200 are therefore not be considered reliable and not included in the analysis of opacity, light scattering and light absorption coefficients. For brightness, a measurement separate from the opacity measurement, Figure 6.6 shows that this anomaly is not present so brightness results for AS200 are used.

3.2 Light Scattering Coefficient

As evidence in Table 6.1, over the 8 drying conditions tested the light scattering coefficient varied between the limits of 61.5 and 69 m^2/kg, a change of 7.5 m^2/kg where a difference of 2 m^2/kg is considered significant. The light scattering coefficient decreases by 5.4 m^2/kg when air is replaced by superheated steam for base sheet drying but increases by 2.1 m^2/kg when the same switch is made for drying the coating, Figure 6.7.

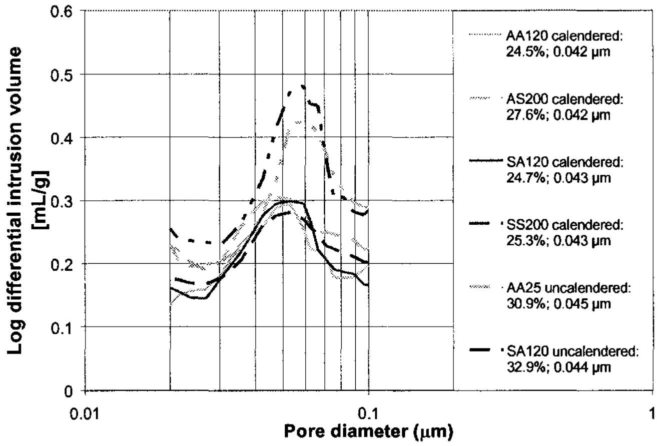

Figure 6.4 Coating pore size distribution

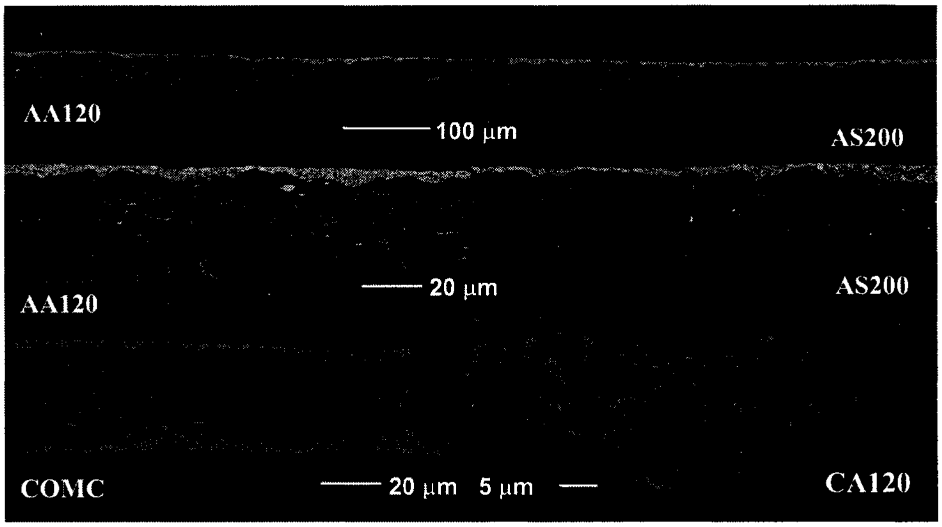

Figure 6.5 Coated paper cross sections by SEM

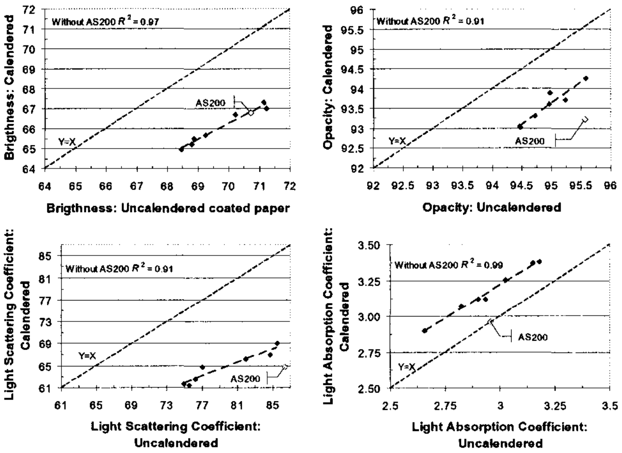

Figure 6.6 Relationships between uncalendered and calendered coated paper optical properties

The higher the value of the light scattering coefficient, the better the optical properties of coated paper. In terms of changes normalized to the decision limit, Table 6.3 shows that the use of steam instead of air as the drying fluid for base sheet drying reduces the light scattering coefficient by about 5*DL* while doing so for the coated sheet drying increases the light scattering coefficient by about 2*DL*. With respect to choice of drying fluid, these results show that the combination of air drying the base sheet and steam drying the coated sheet gives the highest light scattering coefficient. As it is clear that with respect to light scattering coefficient the base sheet should not be dried in steam the only relevant comparison for the effect of drying fluid temperature is the AA120-AA200 comparison for which Table 6.3 shows that the higher temperature is somewhat deleterious, decreasing the light scattering coefficient by about one decision limit.

In paper coating layers light is scattered by the microvoids present in the coating layer, Lepoutre (1989). The light scattering coefficient depends on the number and size of pores in the coating. The changes in light scattering coefficient therefore reveal changes in the coating structure. For clay coatings the optimum pore size for light scattering around is around 0.4-0.5 μm for light of 555 nm wavelength, Borch and Lepoutre (1978). A decrease in light scattering coefficient means fewer pores in this optimum size range but provides no information concerning pores bigger or smaller than this specific range.

For coated paper the light scattering coefficient is determined primarily by the coating layer porous structure. This was verified in the present work by examination of the light scattering coefficient-wavelength relation of Figure 6.8. This plot was obtained from a different set of reflectance measurements done with an Elrepho spectrophotometer apparatus with light wavelengths, every 20 nm, from 400 nm to 700 nm. The linear log-log relationship observed for scattering coefficient is typical of the coating layer only (coated on an impermeable transparent substrate) as shown by Gate (1972) and Lepoutre (1989). Thus the base sheet affected the light scattering coefficient measurement not directly but indirectly through affecting the consolidation when the sheet was coated. Then during drying of the coating the sheet temperature and moisture content history affected the extent of coating compaction, which in turn slightly affected the light scattering coefficient.

3.3 Light Absorption Coefficient

Table 6.1 records the range of 2.9 to 3.4 m^2/kg for the 8 drying conditions used, a range which is large relative to the decision limit of 0.06 m^2/kg. Light absorption coefficient increases by about 0.2 m^2/kg when superheated steam is used at either of the 2 drying stages, Figure 6.9. Increasing drying fluid temperature decreases light absorption coefficient for air dried base sheet and left it unchanged for superheated steam dried base sheet.

The Light Absorption Coefficient of coated paper is controlled by the base sheet as coating materials do not absorb much light. Light is absorbed by chromophore groups present in the fibres. The increase in light absorption coefficient for sheets coated on superheated steam-dried base sheet is explained by the higher light absorption coefficient of base sheets found in Chapter 4. It is less expected to see an increase in light absorption coefficient when superheated steam is used for drying the coating. Figure 6.6 also shows an increase in light absorption with calendering which is unexpected as only the porous structure changes.

3.4 Opacity

Figure 6.10 shows opacity decreases when superheated steam is used to dry the base sheet, but increases when superheated steam is used to dry the coated sheet. Increasing air temperature decreased opacity for AA200 condition but did not change opacity for the SA200 condition while increasing superheated steam temperature did not change opacity for the SS200 condition. Like brightness opacity is related to light scattering and absorption characteristics of paper, see again Figure 4.4. However opacity increases with both increasing values of light scattering coefficient and light absorption coefficient. When switching from air to superheated steam for drying the base sheet, light scattering coefficient decreases and light absorption coefficient is unaffected so opacity decreases. When switching from air to superheated steam for drying the coated sheet, both light scattering coefficient and light absorption coefficient increase so opacity increases.

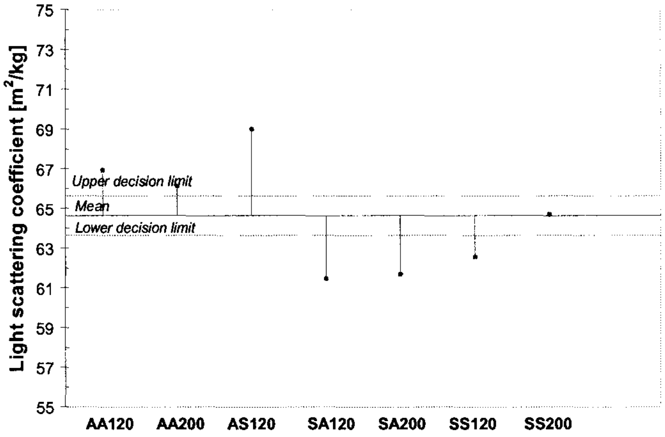

Figure 6.7 Light scattering coefficients of coated paper

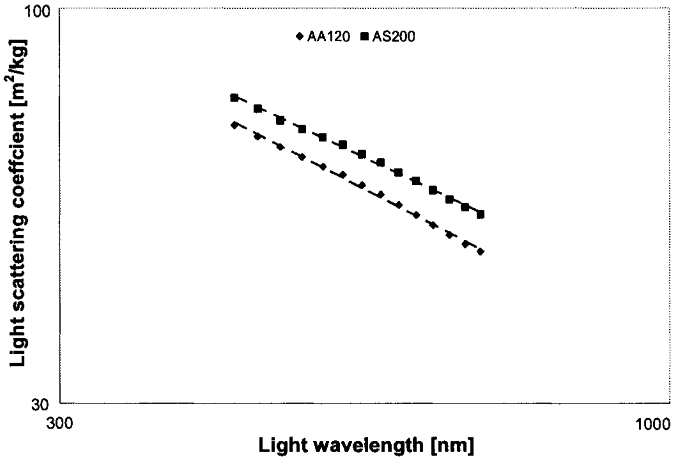

Figure 6.8 Light scattering coefficient of coated paper and light wavelength

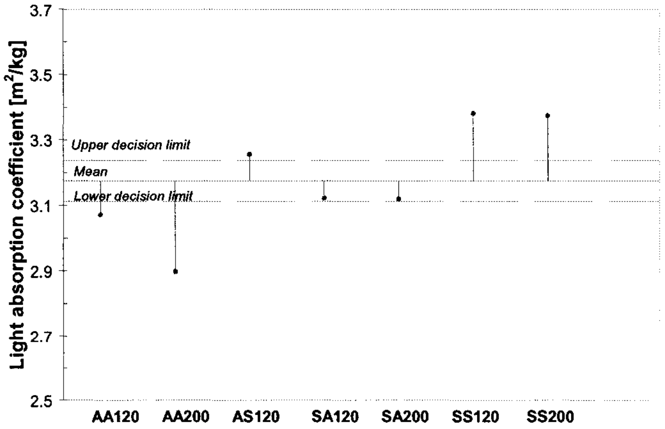

Figure 6.9 Light absorption coefficient of coated paper

3.5 Brightness

Brightness decreases when superheated steam is used for drying either the base sheet or the coated sheet, Figure 6.11. Brightness depends on the light absorption and scattering characteristics of the material as illustrated in Figure 4.4. The absorption ability mostly comes from the base sheet while the scattering efficiency comes from the coating layer. The coefficients defined in sections 3.1 and 3.2 were not evaluated at 457 nm. However when brightness is calculated based on these values of light scattering and absorption coefficients measured at 555 nm as in sections 3.1 and 3.2, an almost perfect correlation between the brightness measurements at 457 nm and the calculations is found ($R^2 = 0.98$), see Figure 6.12. The conclusion is that brightness variations can be predicted from the light scattering coefficient and light absorption coefficient variations described in the previous sections. The decrease in brightness is three times larger when superheated steam is used for drying the base sheet, 1.6 vs. 0.5 points, as both higher light absorption coefficient and lower light scattering coefficient are obtained, Figure 4.4. When superheated steam is used for drying the coating, a higher light scattering coefficient limited the decrease in brightness caused by the increase in light absorption coefficient. Drying fluid temperature either increases brightness, AA200 and SS200 conditions, or leaves it unchanged.

3.6 Discussion

Superheated steam has a larger effect on optical properties when used for drying the base sheet than the coated sheet. The effect of base sheet on light scattering coefficient is indirect through its effect on coating consolidation. The decrease in light scattering when coating on steam-dried base sheet may be due to the extent of coating dewatering varying with the sorption ability of the base sheet.

4. Surface properties

4.1 Roughness

4.1.1 Roughness by air-leak method (PPS)

With the Parker Print Surf apparatus the air flow rate parallel to paper is measured and roughness in μm is calculated. The roughness ranges from about 0.75 to 1.15 μm.

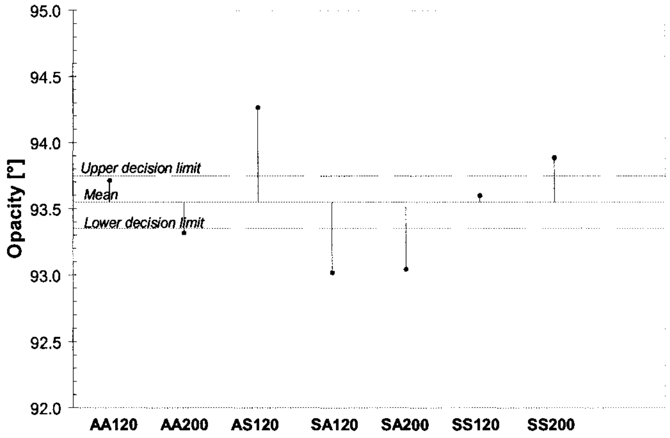

Figure 6.10 Opacity of coated paper

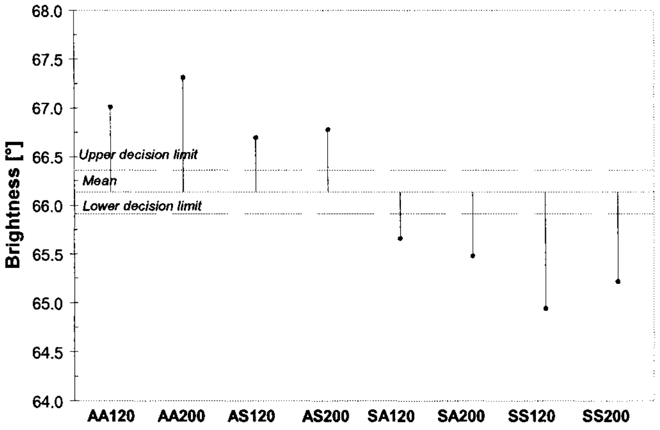

Figure 6.11 Brightness of coated paper

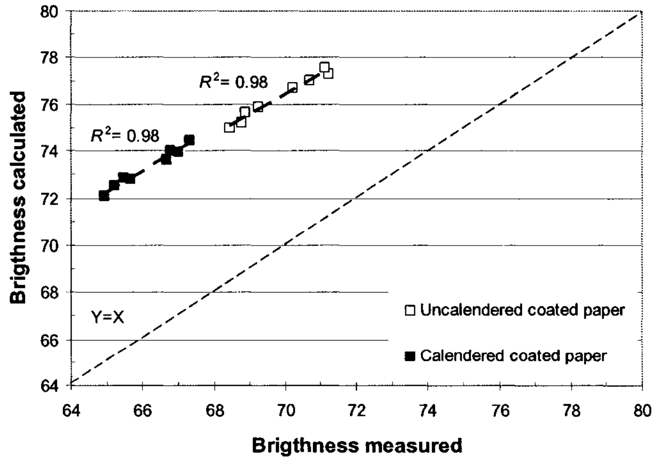

Figure 6.12 Relationships between brightness measured and calculated

Typical values for light weight coated papers are in the range 1 to 1.5 μm. Superheated steam drying increases coated paper roughness whether used for drying the base sheet or the coated sheet: Figure 6.13. Steam drying of the base sheet increases roughness almost twice as much as steam drying of the coated sheet: 0.25 vs. 0.15 μm increase. Drying fluid temperature when drying the coating affected roughness to a lesser extent, about 0.04 μm change, and only when air is the drying fluid.

4.1.2 Roughness by profilometry (Talyscan)

The coated paper surface was also characterized using the roughness profilometer described in Chapter 3, the Talyscan. A single sheet for each drying condition combination was scanned with the stylus in two directions at 8 random positions. The average roughness (root mean square), S_q, is plotted in Figure 6.14. It is to be noted that filtering the data with a Gaussian filter induces attenuation of the signal so the Sq values are much lower than values of roughness found with the PPS. However when calculated on unfiltered data, S_q is of the same order of magnitude as PPS values: around 1 μm.

PPS roughness and Talyscan S_q values are closely related in the case of coated paper in this study with $R^2 = 0.88$ between the values obtained for the 8 sets of samples tested, Figure 6.15. Here is a possible explanation why PPS and Talyscan measurements are in good agreement for coated paper but not for uncoated paper (Chapter 4 section 5.2). Roughness is a scale dependent property. With the PPS apparatus, roughness is measured over a 51 μm length and therefore evaluated at scales ≤ 50 μm, while with the Talyscan profilometer roughness is measured over a 1 mm length and therefore evaluated at scales ≤ 1000 μm with a lateral resolution of 2 μm. In the case of coated paper, roughness mostly occurs at micro scale as seen in the profiles of surface roughness of coated paper dried in conditions AA120 and AS200, Figure 6.17 and Figure 6.19. The two instruments therefore measure roughness at the same scale. In the case of uncoated paper, roughness originating from the fibre network is dominant over the fibre wall micro roughness and occurs at scales ≥ 30 μm (typical fibre width). Thus poor agreement was found between PPS roughness and roughness by profilometry for uncoated paper.

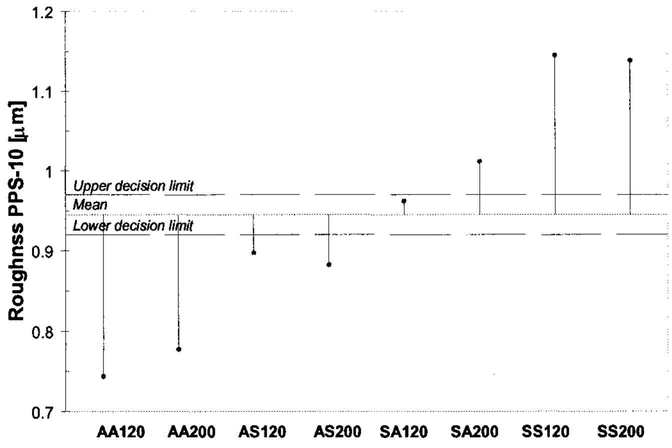

Figure 6.13 PPS-10 roughness of coated paper

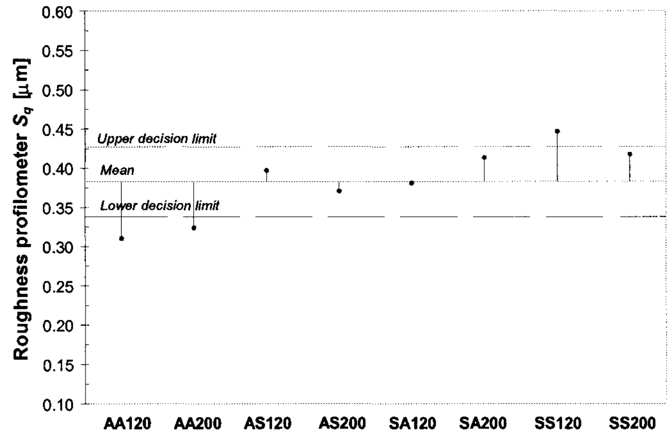

Figure 6.14 Talyscan S_q (RMS) roughness parameter of coated paper

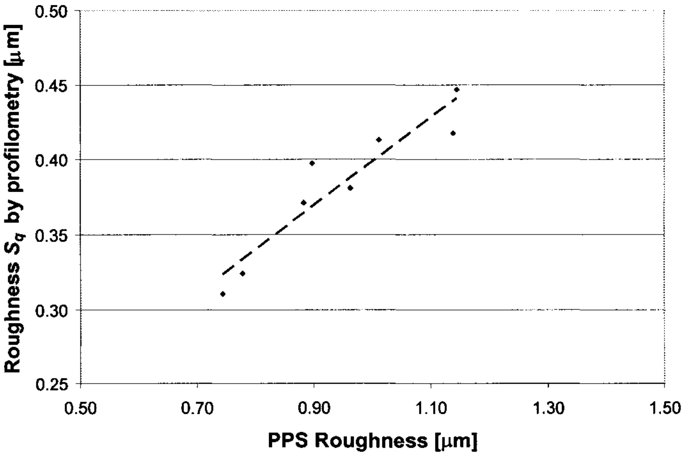

Figure 6.15 PPS and Talyscan S_q roughness measurements of coated paper

Because of the higher variability in the measurements with the Talsycan (related to the sensing area), above 10%, the differences between drying conditions are not as large as for PPS roughness but they are significant between AA120, AA200 and the other 6 conditions.

Images of the surface obtained with Talyscan provide a visual perception of the surface structure of coated paper, Figure 6.18. Figure 6.19 is obtained by slicing the surface in three ranges of elevation. The cutoff values were adjusted so that the two extreme slices each represent about 2.5% of the total elevation, and therefore the middle slice 95%. As seen in Figures 6.19 most surface deviations from mean value are between +/- 1.5 μm (unfiltered).

4.2 Gloss

Paper gloss is the degree to which the paper surface reflects light in the specular reflection direction. As shown in Figure 6.20 the use of superheated steam decreases gloss at both drying stages. Also increasing the drying temperature decreases gloss in the case of air drying but not for superheated steam drying. Gloss is the property that was the most affected by the drying conditions.

Gloss depends on surface roughness and specially roughness of the same order of magnitude as that of light wavelength. The work of Lee (1974) and Oittinen (1984) showed that for coated paper the substrate contributes a macroscopic roughness and thereby gloss. As coat weight increases, this contribution decreases and the optical or microscopic roughness contributes the most to the gloss value. The optical roughness has been related to orientation of facets at the surface but these facets did not appear to be clay platelets, Gate (1973). Lee (1974) further showed that gloss depends on the extent of coating shrinkage occurring during drying due to latex film forming. The extent of film forming depends on the drying temperature in relation to the latex glass transition temperature (T_g = 12°C for the styrene-butadiene latex used here).

In the present study the expected strong inverse relationship between gloss and roughness is observed. However there is not a unique relationship between gloss and roughness: gloss values as a function of roughness follow parallel trends depending on the fluid used for drying the base sheet, Figure 6.21.

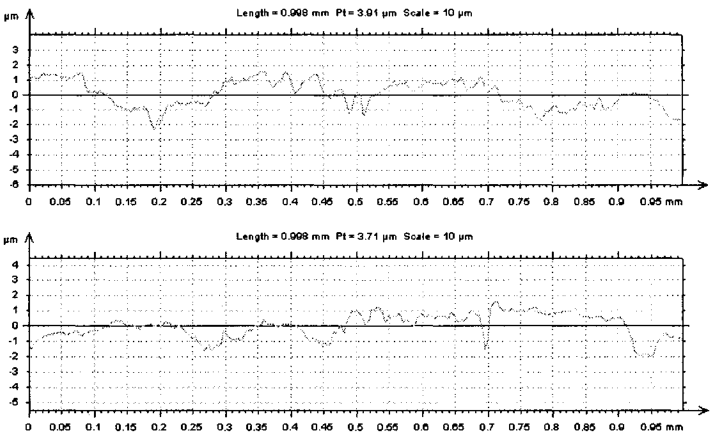

Figure 6.16 Talyscan unfiltered profiles AA120 (top) – AS200 (bottom)

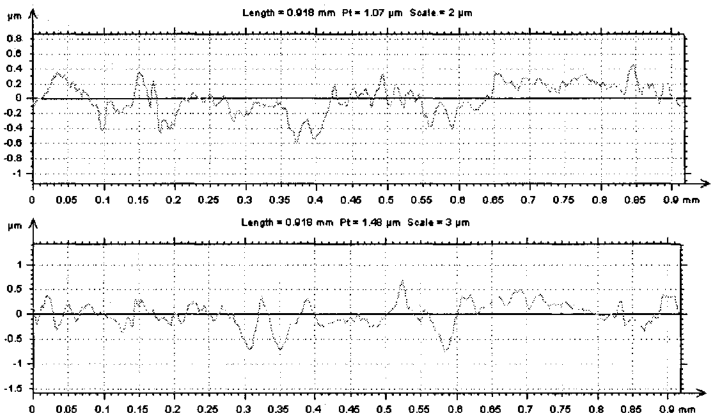

Figure 6.17 Talyscan filtered profiles AA120 (top) – AS200 (bottom)

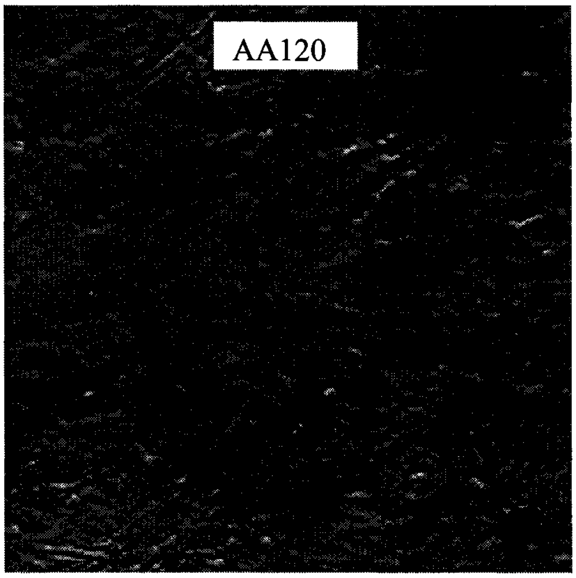

Figure 6.18 Talyscan pseudo-image of coated paper: AA120

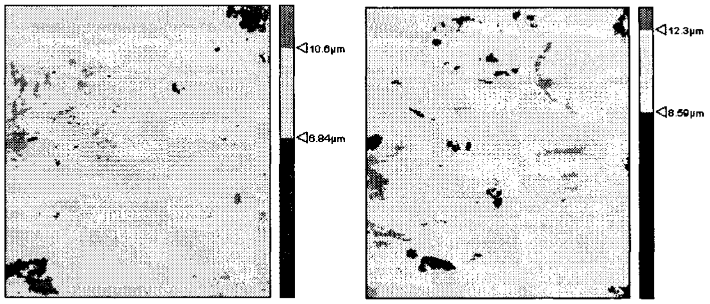

	■	□	▨
Area (%)	2.54	94.8	2.61
Volume of void (%)	0.213	37.6	99.7
Volume of material (%)	99.8	62.4	0.337
Volume of void (µmxmm2/mm)	0.0146	1.43	1.96
Volume of material (µmxmm2/mm2)	6.83	2.37	0.00629
Mean thickness of void (µm)	0.0146	1.43	1.86
Mean thickness of material (µm)	6.83	2.37	0.00629

	■	□	▨
Area (%)	2.48	94.8	2.73
Volume of void (%)	0.284	39.4	99.4
Volume of material (%)	99.7	60.6	0.624
Volume of void (µmxmm2/mm)	0.0244	1.48	1.06
Volume of material (µmxmm2/mm2)	8.56	2.27	0.00666
Mean thickness of void (µm)	0.0244	1.48	1.06
Mean thickness of material (µm)	8.56	2.27	0.00666

Figure 6.19 Talyscan unfiltered slices AA120 (left) – AS200 (right)

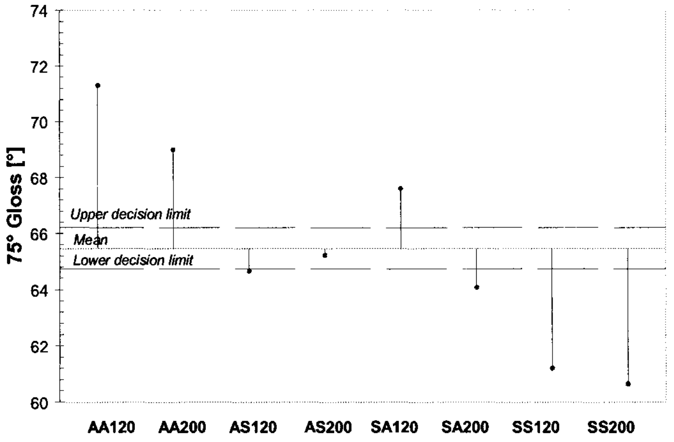

Figure 6.20 Gloss of coated paper

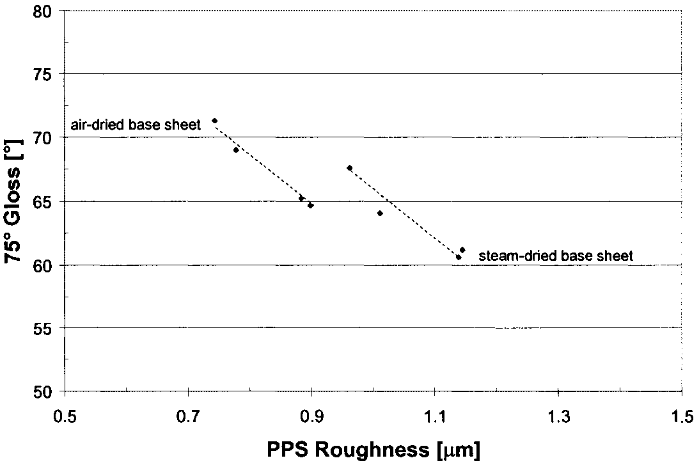

Figure 6.21 Relationship between gloss and PPS roughness

Superheated steam drying decreases gloss by 4 points when used for drying the base sheet and by 5 points when drying the coated sheet, relative to that for air drying. So the decrease is of the same order of magnitude when superheated steam is used for drying the base sheet or the coated sheet unlike for PPS.

4.3 Scanning Electron Microscopy images

Images of the surface of coated paper were taken by SEM to characterize qualitatively the coating surface. However the images from various conditions did not show major differences, perhaps because of the complexity of the coating surface with the wide size distribution of clay platelets. Typical images of coated sheets produced for the very different conditions designated AA120 and AS200 are shown in Figure 6.22 at magnification ranging from 150X to 2,000X. These images were taken in Secondary Electron Imaging mode (SEI) and Back-scattered Electron Imaging mode (BEI). The major characteristic of the coated paper surface seen on the SEI images is the presence of dark and bright areas. At very low magnification the dark areas seem to have the shape of fibres. At high magnification the dark areas are regions of low porosity while bright areas are more porous regions. The porosity affects the SEI image brightness by the presence on porous regions of the rough edges of clay platelets appearing brighter. It was not possible to detect any difference between the drying conditions regarding this feature. At high magnification, Figure 6.23, one can clearly see individual clay platelets and pores in between platelets. The pore size may be estimated from these pictures to be mostly below 0.2 μm as assumed in section 3.4 of this chapter concerning determination of pore size distribution. In SEI mode, the contour of platelets appear round as the latex cover them. The contour of the platelets is much sharper when seen in the BEI mode as the brightness depends on surface composition in this mode: the larger the element number the brighter the spot will appear. The latex is not visible in this type of image as it is made of the low element number of its constituents, carbon and hydrogen.

4.4 Surface chemical composition

Coated paper from 4 extreme conditions, AA120, AS200, SA120 and SS200, was analysed for surface chemical composition by ESCA - Electron Spectroscopy for Chemical Analysis (also called XPS - X-ray Photoelectron Spectroscopy).

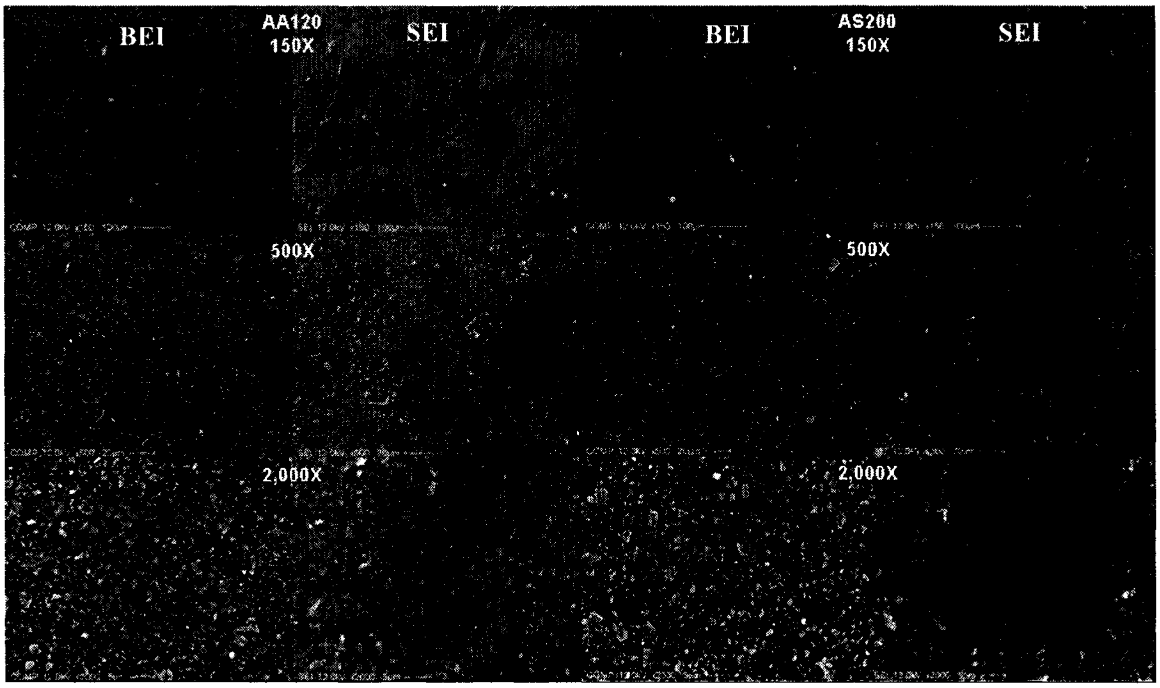

Figure 6.22 Coated paper surface by SEM: AA120 and AS200

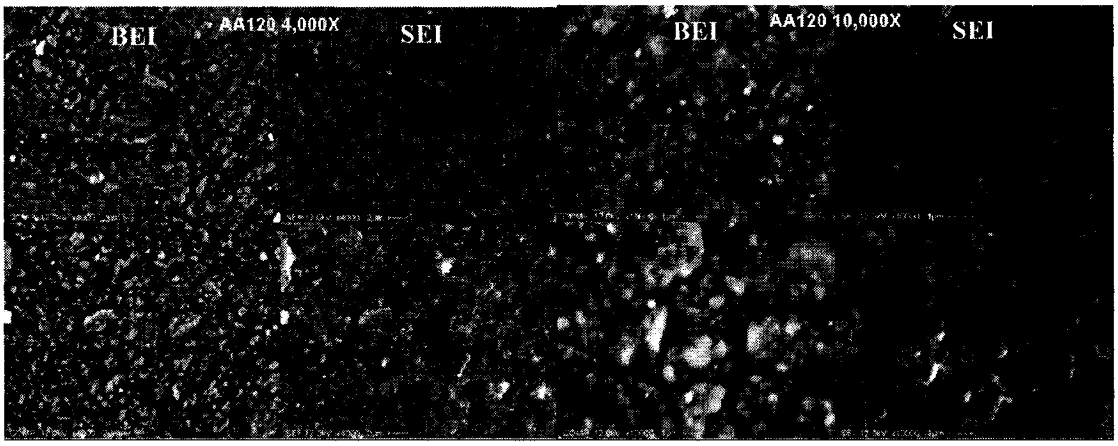

Figure 6.23 Coated paper surface by SEM: AA120 at high magnification

For coated paper, ESCA measurements are used principally to detect changes in latex concentration at the coated surface. The atomic and mass concentrations of each coating element are given in Table 6.6. The measurement error from the technique is considered to be +/-1 percentage point in concentration. A single sample was analysed for each drying condition and the sensing area was 100 mm^2. The main advantage of this technique is that the beam has a very small depth of penetration, typically between 2 and 5 nm, Al-Turaif et al. (1999), or at most 10 nm, Groves et al. (1991). Thus the results are considered representative of only the top coating surface because the X-ray beam does not reach the fibres of the base sheet.

It is customary to assume the C concentration to be a measure of the latex concentration at the surface. At fixed latex content in the coating suspension such as is the case in the present study, variable coated paper surface latex concentration may only be obtained because, during coating application and drying, latex particles are transported within the coating layer or even into the base sheet.

According to the ESCA specialist who made these determinations, there is no difference apparent between coated paper from the 4 drying conditions tested. It is however possible to see a trend toward lower C concentration for samples for which coating is dried in superheated steam. As only one ESCA determination was made for each of the Table 6.6 drying conditions, the trend is at the limit of significance assuming 1 percentage point resolution in concentration. With the limited ESCA data available, the conclusion is that there is no significant difference in chemical composition at the surface of coated papers produced using these 4 drying conditions.

Table 6.6 Chemical composition of coated paper by ESCA

Condition	**AA120**		**AS200**		**SA120**		**SS200**	
Element	Atomic Conc.* %	Mass Conc. %	Atomic Conc. %	Mass Conc. %	Atomic Conc. %	Mass Conc. %	Atomic Conc. %	Mass Conc. %
O	54.8	50.6	54.8	49.7	51.8	47.8	52.7	48.1
Si	11.2	18.2	12.3	19.6	11.6	18.8	12.2	19.6
Al	8.9	13.9	9.7	14.9	9.4	14.6	9.6	14.8
C	25	17.3	23.2	15.8	27.2	18.8	25.5	17.5

**Conc.: concentration*

The surface chemical composition obtained in the present study are very similar to those obtained by Eklund et al. (1995) with 12 pph binder (starch and latex, 1:1) and clay [Atomic concentration: 0, 55%; C, 25%; Si, 11%; Al: 9%] . The variations between the 4 drying conditions tested here are also of the same order of magnitude as those found by Eklund et al., who concluded there was no significant difference between the samples they tested. Other recent studies have found no effect of drying conditions on surface latex content: Groves et al. (2001), Xiang and Bousfield (2000), Kim et al. (1998) and Yamasaki et al. (1996). In the last study it is shown that unlike starch latex does not migrate much, and if it does it is only toward the base sheet during coating dewatering. As mentioned in Chapter 2 Groves (2001) also proved that for the the case of paper coatings of high solids latex particles are prevented from movement because of close packing of particles whereas soluble starch may migrate until its gel point.

4.5 Discussion

As discussed in Chapter 2, coated paper surface roughness and gloss are affected by (1) the roughness of the base sheet, (2) the base sheet sorption ability, (3) the base sheet compressibility and (4) the extent of coating disruption during drying. The first three effects relate to the base sheet properties while the fourth one to the drying conditions. Drying uncoated paper in superheated steam increased both roughness and hydrophobicity as shown in Chapter 4. Thus coated paper made from steam dried base paper may be rougher and less glossy either because the base sheet is rougher, is more hydrophobic, or both. Then the drying conditions favoring coating disruption by either vapor flow or coating shrinkage, that is higher drying rates and drying temperatures, lead to rougher and less glossy coated papers as expected. However there is not a unique relationship between gloss and roughness: gloss values as a function of roughness follow parallel trends depending on the fluid used for drying the base sheet. Probably the large roughness variation coming from the base sheet contributes less to variation in coated sheet gloss because gloss is affected primarily by smaller scale surface profile variation developed when drying the coating as explained above.

In this study there is no indication of changes in latex binder particles migration with drying conditions of the base sheet and the coated sheet.

5. Conclusions

The performance of a laminate product such as coated paper depends on the nature of its various constituent layers. For most of the material characteristics tested here the major contribution comes from the coating layer. However the structure of the base paper has a large effect on its coated sheet through influencing the coating consolidation during its application, drying and calendering, all of which influence the properties of the dry coated sheet. Properties are affected by drying conditions in various extents. The 8 drying conditions tested have more effect on surface properties than on bulk properties and no effect on chemical composition and coating average pore diameter. Base sheet drying medium may have more effect than coating drying conditions depending on the property tested. The temperature during coating drying has a marginal effect compared to drying fluid used.

The properties that are the most affected are surface properties, roughness and gloss, then optical properties. Superheated steam used for drying the base paper, the coated paper or both is detrimental to surface paper properties tested, increases roughness and decreases gloss, but has no visible effect on binder content at the surface. Paper roughness is not critical to the offset printing process for coated papers. This low sensitivity to roughness is because first they are already very smooth and second the printing image is not transferred directly from a hard printing plate but from the blanket which is a resilient material and can thus conform to the paper surface. Thus the detrimental effect of superheated steam drying on roughness is not a major concern for offset coated paper grades. On the contrary the large decrease in gloss observed when using superheated steam is a constraint for the extension of this experimental drying fluid to industrial production because gloss is one of the most important properties for the LWC paper grade. In this study the calendering conditions were kept constant but for industrial application calendering would be optimized in order to reach the target gloss. Chemical composition of the surface remains unaffected by the various coating drying conditions or changes in the base sheet characteristics.

As for bulk and optical properties they are affected to a lesser extent and in a more complex manner. The large decrease, 5 points, in base sheet brightness when drying the base sheet in superheated steam reported in Chapter 4 is reduced to only 1.6 points after coating, drying in air and calendering the coated sheet. There is still a decrease but it does not come from the base sheet being less bright. The effect of base sheet drying conditions on coated paper property is indirect as base sheet properties affect coating consolidation at the time of coating application.

Chapter 7 Effects of drying on coated paper printability

1. Introduction

Coating enhances paper surface properties to the level required for prints of higher quality. Printing performance is therefore the most important property to be tested for coated paper. Print quality and press runnability are equally important aspects of printing performance to the printers. However press runnability depends very much on specific press settings and cannot be tested easily in the laboratory. As for print quality it is on the contrary very extensively tested on proof presses which are recognized as reliable for accurate prediction of print quality of a paper-ink couple on commercial presses. In order to explain printing property trends and to identify the effect of drying conditions it is also important to understand mechanisms occurring during printing, e.g. ink transfer, ink splitting and ink setting. Therefore the present chapter documents standard printing properties determined on a proof press and reports additional printing trials carried out to help understand the results.

LWC paper is most often printed with offset lithography, commonly called the offset process. The printing plate is treated so that image areas are water repellent and non-image areas are hydrophilic. As water and oil-based ink are immiscible, the image and non-image areas can be in the same plane on the printing plate, i.e. there is no need for embossments or cavities as is the case for letterpress or rotogravure. For each printing station the plate goes through the dampening and inking systems where non-image areas receive fountain water solution while image areas receive the oil-based ink. Ink and water are first transferred to a roller covered with a resilient material, the blanket, and then from the blanket to the paper. Presses may be web offset, running a continuous reel of paper for larger runs, or sheet-fed offset running discrete sheets for shorter runs. Coldset (non-drying) ink is used for newsprint, heatset (drying) ink for magazines, the press being in this case followed by an oven and chilling rolls. Figure 7.1 presents a schematic layout of a four-colour offset press. In the present study all printing was of solids prints, so no fountain water was used.

2. Printing procedure

2.1 Printing conditions

Printing was performed with a two-nip Prüfbau Printability Tester at 23°C and 50% relative humidity on 110 x 40 mm sheets which had been conditioned to that temperature and relative humidity. Aluminium rollers, a sheet carrier covered with a soft resilient material and two types of ink were used: a conventional commercial black coldset offset ink and a cyan heatset offset ink from Sun Chemical (Boucherville, QC). Solid prints were made without using water fountain solution. Offset inks consist of a suspension of pigment particles (providing color and opacity) in an ink vehicle (for ink transfer and ink pigment binding to paper). Heatset offset ink vehicle contains, in addition to the solvent and oils, a resin which makes the ink very viscous or "tacky". The cyan heatset offset ink of composition given in Table 7.1 was a commercial ink used for LWC grade paper. The cyan ink suspension bulk density was measured to be 970 kg/m^3.

Table 7.1 Cyan heatset ink composition

Component	[1]Density g/cm^3	Mass fraction	Volume fraction
Ink pigment	1.5	0.10	0.065
Resin	1.1	0.40	0.353
Solvent	0.8	0.40	0.485
Oils	1	0.08	0.078
Additives	1	0.02	0.019

[1]values for component density are common values taken from literature (Zang & Aspler, 1991) except for the ink pigment. Ink pigment density was back-calculated from the measured ink suspension bulk density.

The investigation of printability consisted of two parts: first, printing performance testing, then variable printing condition trials in order to better understand processes involved during printing. In the first part sheets were printed with a fixed amount of ink on the printing plate, under a fixed nip load and at a fixed printing speed, while subsequently these parameters were varied. In both parts of the testing two printing configurations were used: single-nip (printing unit alone) and four-nip. The four-nip printing configuration consisted of a printing unit followed by three printing units without ink, thereby allowing for ink re-transfer, i.e. back-trap. With the two-nip Prüfbau press used, the four-nip configuration was obtained by a second pass on the same press, Figure 7.2, after replacing both printing units with clean uninked units. This custom printing method simulates conditions on a commercial four-color offset press where ink printed on any of the first three units may not be fully immobilized at the surface of paper and may therefore transfer back in the next unit (back-trap) onto the press. Waech (1998) and Xiang and Bousfield (2001) have used a similar technique with success in reproducing satisfactorily the multiple-nip offset process. The delay time between the two first units is short, 0.15 s, but that between the 2nd and the third units is larger, ~10 s, because of the manipulation required. Attention was paid to keep this latter delay time as constant as possible. For commercial offset presses, the delay time between two units vary: 1 to 3 s between all units for Heidelberg web offset presses, and 0.2-0.5 s between first and second and third and fourth units and 5 s between second and third for Roland sheetfed offset presses. Sheets printed with the single-nip configuration, without back-trap units, are designated below as 0BT, while those printed with the four-nip printing configuration are referred to as 3BT. Table 7.2 lists the printing conditions treated.

As the C-0BT and C-3BT standard condition printing trials of Table 7.2 with the typical cyan heatset ink used for LWC paper involved a greater number of replicate prints, those results provide the most significant information on printing performance of the paper tested. The other trials bring data to help understand the observed trends with the numerous combinations of test parameters.

2.2 Printing measurement procedures

2.2.1 Operating parameters

During the printing tests the amount of ink on the printing roller and the amount of ink transferred to the substrate were measured by weighing the printing roller before inking, after inking, i.e. before printing, and after printing. The printing rollers were cleaned thoroughly between printings.

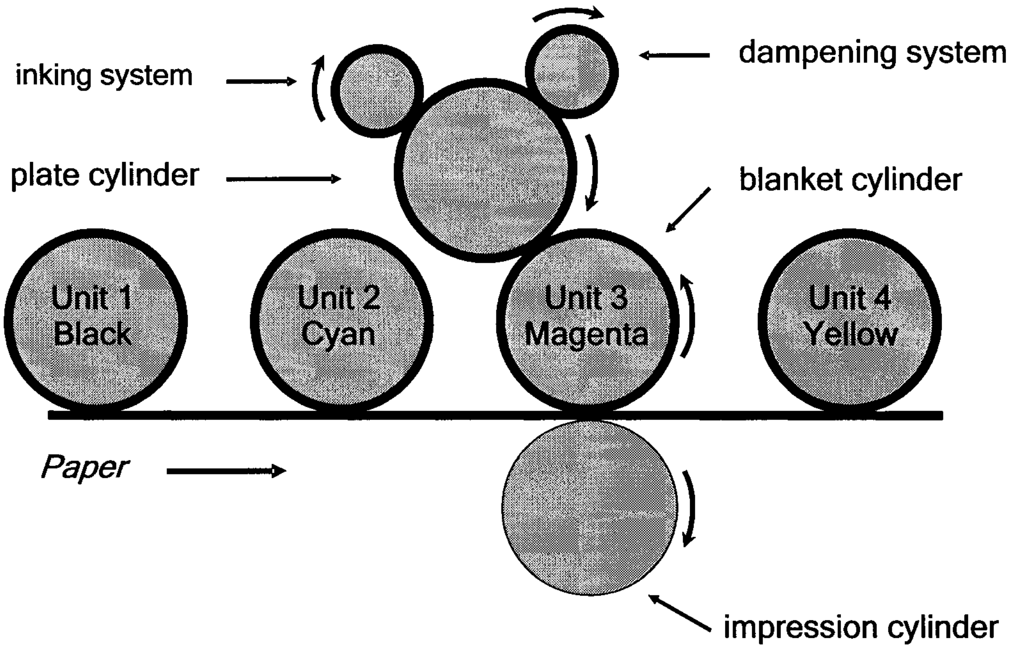

Figure 7.1 Schematic of commercial offset press layout (inking system and impression cylinder shown for the magenta unit applies to all printing units)

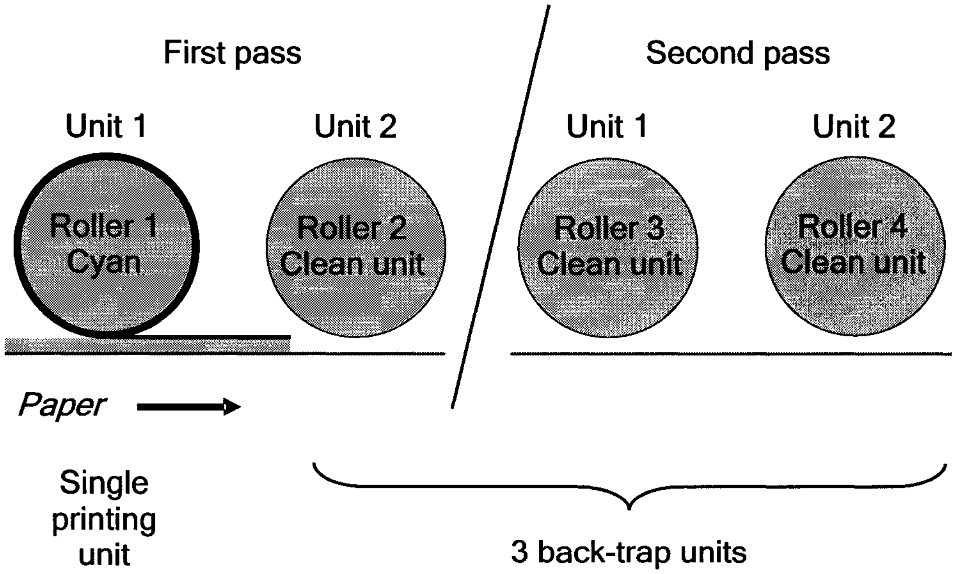

Figure 7.2 Laboratory multiple-nip sheet-fed printing configuration

Table 7.2 Printing conditions

[1]ID	**Configuration**	**[2]Substrate**	**Ink**	**[3]Variable**	***Section in this chapter***
STANDARD CONDITIONS					
B-ITC	0BT	DSF	BLACK	INK LOAD [3 m/s – 400 N]	3.2.2
C-ITC	0BT	COM	CYAN	INK LOAD [3 m/s – 600 N]	3.2.3
C-0BT	0BT	DSF&COM	CYAN	NONE	3.3/4.1.1/4.2.1
C-3BT	3BT	DSF&COM	CYAN	NONE	3.4/.24.1.2/4.2.2/4.3
ADDITIONAL TRIALS					
T-1	0BT	MYLAR	CYAN	INK & NIP LOADS, SPEED	3.3.3
T-2	BT	MYLAR	CYAN	NUMBER OF BT UNITS	3.3.3
T-3	0BT	MYLAR	CYAN	TIME BEFORE BT	3.3.3
T-4	BT	COMC, COMC1&2	BLACK	1 OR 3BT, INK LOAD	3.3.3
T-5	0BT	COMC	CYAN	INK & NIP LOADS, SPEED	3.3.3
T-6	BT	COMC	CYAN	NUMBER OF BT UNITS	3.4.3
T-7	BT	COMC	CYAN	TIME BEFORE BT	3.4.3
T-8	BT	DSF	BLACK	1 OR 3BT, INK LOAD	3.3.3
T-9	0BT	DSF	CYAN	INK LOAD, SPEED	3.3.3

[1] *In the four standard conditions, B identifies black ink, C cyan ink; ITC identifies determination of an ink transfer curve, i.e. with variable ink load; OBT and 3BT identify printing in a single-nip press with no back-trap possible, and in a four-nip configuration with back-trap possible from three printing units. Trial tests with the parameters of ink load, nip load and or printing speed varied are identified as T.*

[2] *Substrates used are laboratory produced coated paper made with laboratory formed DSF base paper, identified as DSF, and commercial coated sheets, COMC (from the mill providing the pulp for laboratory paper production), and COMC1 and COMC2 (from two other mills).*

[3] *The parameters varied are given, parameters kept constant are given in brackets: ink load,* g/m^2*; printing speed, m/s; nip load, N. Where not specified otherwise the printing conditions were: plate ink load, 3* g/m^2*; speed, 3 m/s; nip load, first unit 600 N, second unit 450 N.*

2.2.2 Definition of printing properties

Three important printing properties - optical density, print gloss and print mottle – have in common being dimensionless, relative values. Ink "island" coverage was also measured in the case of the 3BT printing configuration with cyan ink. Optical density designates the darkness of the print. Print gloss, i.e. print shininess, is the degree to which the surface simulates a perfect mirror in its capacity to reflect incident light. Ink coverage is normally the proportion of paper surface area covered with ink after printing. In the present work some sheets, printed in the 3BT configuration, had 100% coverage but showed quite nonuniform ink thickness with patches of much thicker ink film or ink "islands". In order to characterize this pattern, ink "island" coverage, defined as the surface area covered with a thicker ink film, was measured. Print mottle designates the local variation in print density. Mottle is conventionally and still widely evaluated qualitatively by visual assessment. However instrumental methods are also available to quantify mottle.

2.2.3 Property measurement instruments

Printing properties were evaluated 24 h after printing. For black prints, print density was measured with an Elrepho photometer, print gloss with a Technidyne T480A gloss meter. For cyan prints a single apparatus, the TMI SPECTRO/plus spectrophotometer, allowed measurement of print density and print gloss and the Paprican InkScanner for ink "island" coverage. The reflectance measurement is done with diffuse light and viewing at 0° for the Elrepho photometer and with 0° lighting and 45° viewing for the SPECTRO/plus instrument. The gloss measurement is done at 75° for the Technidyne and at 60° for the SPECTRO/plus instrument. The sensing areas are a 30 mm diameter circle for the Elrepho, a 20 mm x 10 mm rectangle for the Technidyne, a 10 mm diameter circle for the SPECTRO/plus instrument, and a 2.7 mm x 2.7 mm rectangle for the Paprican InkScanner. Print mottle was evaluated by a subjective evaluation method developed jointly by McGill University and Paprican, Donderi and Aspler (1994), as well as by a quantitative method developed at McGill University, Bernié and Douglas (2001). The two techniques are described in section 4.3.

2.2.4 Statistical treatment of data

For the C-0BT and C-3BT cyan prints, print density and print gloss were measured 5 times on each printed 100 mm x 36 mm Prüfbau strip. Two replicate sheets for the 0BT printing and 5 replicate sheets for the 3BT configuration were printed for each of the 8 sets of drying conditions for laboratory produced paper (DSF) and for the reference commercial paper (COMC). For each property a unique decision limit was calculated from the pooled standard deviations of the 8 sets of samples as described in Chapter 3 section 8.2. The mean value, the upper and the lower decision limits are plotted on the relevant graphs. The upper and lower decision limits enable deciding whether there is a statistically significant difference between the values of a property tested for two sets of sheets printed on coated paper produced under different drying conditions.

For the 9 sets of additional printing trials identified in Table 7.2 as T-1 to T-9, usually only a single sheet was printed for each set of printing conditions and 2 or 5 independent determinations were made on that single sheet for each of the ink, black and cyan. Therefore no decision limit can be computed.

3. Mechanisms involved during printing

3.1 Printing nip

Figure 7.3 is a schematic close-up view of the nip where paper is printed by contact with the inked roller in the Prüfbau press. The values shown are those applicable when printing with cyan ink in the standard conditions designated in Table 7.2 as C-0BT: plate ink load, 3 g/m^2; speed, 3 m/s; nip load, 600 N. The ink film thickness values indicated were calculated with the ink component densities in Table 7.1 and the average value of 46% measured for cyan ink transfer to paper for the C-0BT condition. The printing roller is thoroughly cleaned before inking for the next print; hence the residual ink film left after printing does not accumulate.

Part of the solvent fraction is maybe trapped within the resin network that forms by cross linking between resin molecules as the solvent leaves the ink film. The weight loss from an ink film on a MYLAR substrate which occurs for drying in the dryer attached to the proof press and then in ambient air for 24 h, was measured to be lower than 40%, the value (Table 7.1) corresponding to complete removal of the solvent.

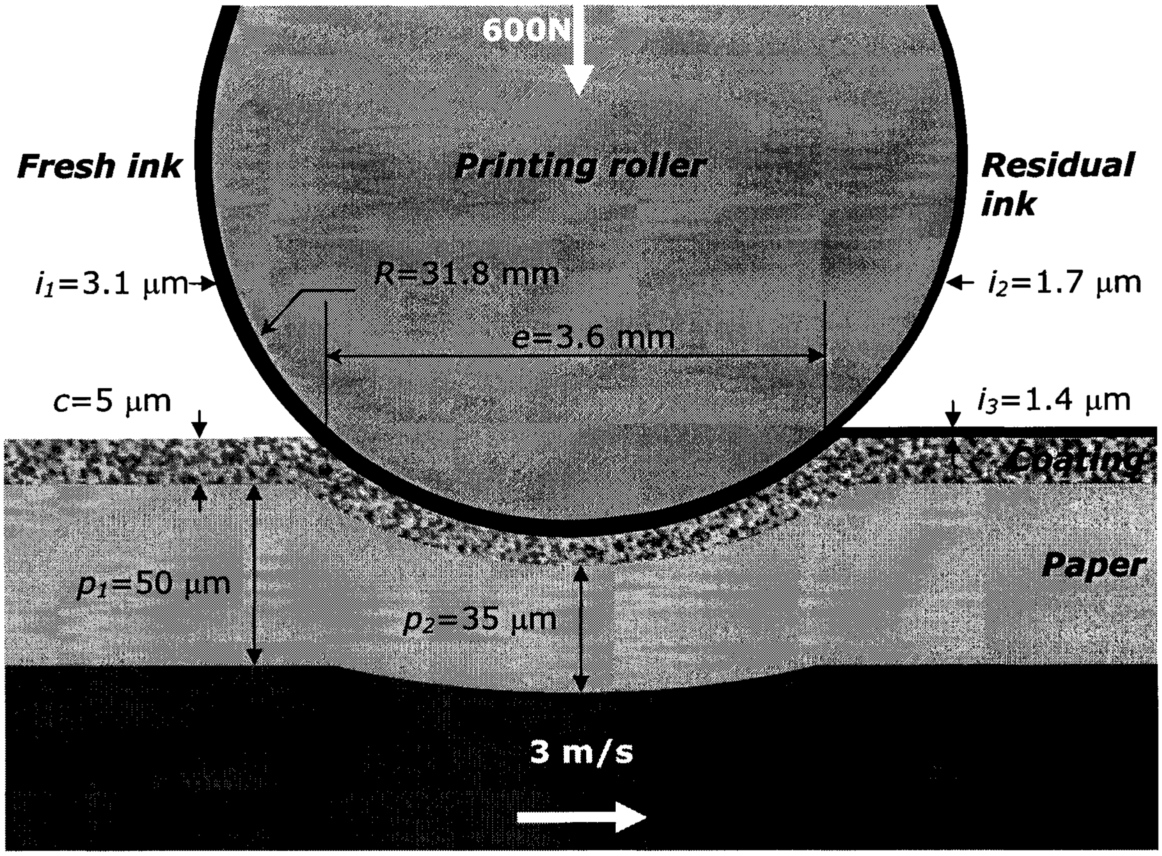

R: roller radius; *e*: nip width; *i*: ink film thickness (i_1: on roller before printing; i_2: on roller after printing; i_3: on paper); *c*: coating thickness, remains constant for nearly incompressible coating; *p*: base paper thickness (p_1: before the nip; p_2: minimum value in the nip); *b*: soft backing material thickness, ~ 5 mm

Figure 7.3 Schematic of printing nip (not to scale)

With the ink film on impermeable MYLAR, only the solvent fraction can leave while for an ink film on paper some oil may be transported with the solvent into the sheet. Therefore an ink film may lose between 75 and 100% of its solvent content (30 to 40% weight loss) if on MYLAR, or all its solvent + oil content if on a paper substrate (30 to 48% weight loss). Based on these assumptions a range of values for the ink film thickness, both initial and dry, are presented in Table 7.3. From the 3.1 μm film of the wet cyan ink suspension on the printing plate, 1.4 and 1.7 μm of this film are transferred to paper and MYLAR respectively. After the solvent (and the oil in the case of paper) leave the fresh ink, the thickness of the dry ink film left at the surface would be 0.6 to 0.9 μm, and 0.9 to 1.1 μm, for the case of paper or an impermeable substrate, respectively. As the Table 7.3 values for dry ink thickness are in good agreement with those for ink film thickness for an impermeable substrate obtained with roughness profilometry (section 3.3.2), the assumptions for ink constituent densities are acceptable.

Table 7.3 Cyan ink film thickness for standard printing conditions (C-0BT)

Thickness	**On printing plate**	**On paper**	**On MYLAR**
Fresh ink layer	3.14 μm	[1]1.45 μm	[1]1.73 μm
"Dry" ink layer	-	0.63-0.94 μm	0.89-1.1 μm

[1]Ink transfer to paper, 46%; ink transfer to MYLAR substrate: 55%

3.2 Ink transfer

3.2.1 Theory of ink transfer

During printing, the ink transfer is believed to occur in 3 steps: first, contact of the printing plate with paper; second, immobilization of part of the ink in paper pores by printing pressure and capillary penetration; and finally, splitting of the film of non-immobilized ink at the exit of the nip. Many researchers have derived empirical equations to fit their ink transfer data. The model of Walker and Fetsko (1955) is often used because it was shown to fit the experimental data best, Mangin et al. (1981), and it also describes physically the ink transfer phenomena. According to this model the ink transfer is a function of three parameters: *k*, a measure of the printing smoothness of the paper (*k* describes the rate at which ink coverage increases); *b*, the ink immobilized during the dwell time in the nip; and *f*, the free ink splitting factor. Zang (1995) improved this model by replacing the constant value of the splitting factor, *f*, in the original model, by an exponential function of ink load, decreasing from 0.5 at low ink load to a constant value at high ink load. Figure 7.4 presents three curves of ink transfer to coated paper fitted to two sets of experimental data from Walker (1981) and Zang (1995). Zang (1995) showed that the three parameters used to model ink transfer are not only paper properties because they also depend on printing conditions. However this description of the ink transfer process remains very useful in understanding ink – paper interaction.

Zang & Aspler (1995, 1998) studied ink transfer on coated paper. They found that for a smooth sheet such as the coated paper in the present study (roughness around 1 μm), *k* is not a determining parameter because ink coverage is complete at relatively low ink load. As the structure of coated paper consists of pores too fine to allow ink pigment passage, ink penetration is not significant and therefore the ink immobilisation term, *b*, does not affect ink transfer. The remaining parameter controlling ink transfer for coated papers of similar surface finish is therefore the splitting factor, *f*. Zang and Aspler related this factor to coating porosity and absorbency. They viewed the consolidation of offset ink on coated paper as occurring by transport of the ink liquid phase into the coating with concurrent formation of a filter cake or ink pigment layer at the paper surface, similar to the case for coating consolidation at the surface of paper as described in Chapter 2 section 2. With this assumption, if the coating absorbs ink liquid faster, then ink would consolidate more quickly at the paper surface and would move the splitting more towards the printing plate. Consequently more ink would be transferred to a more porous coated paper or to locally more porous regions of coated paper. Ink transfer and ink properties development with ink load curves therefore constitute valuable tools for the characterization of coated paper porous structure.

3.2.2 Ink transfer: Black ink [B-ITC]

Because of the very low weights involved the precision was poor for this measurement obtained by difference (section 2.2.1): an error of 0.5 mg when the weight to be measured is only about 5 mg, leads to a change of 10 percentage points in ink transfer for an ink load on the plate of 1 g/m^2. The ink transfer curves and printing properties development with ink load curves are therefore not presented here but are recorded in Appendix D. However the development of printing properties presented next, with the variable of ink load removed, may be regarded with greater confidence.

For coldset black ink, Figure 7.5 indicates that for all paper drying conditions print gloss increases linearly with print density (R^2 values ranging from 0.78 to 0.95). The slopes of the lines for all 8 drying conditions are approximately the same while the intercepts depend directly on the paper (unprinted) gloss. This effect is seen more clearly on the detailed results recorded in Appendix D. Figure 7.6 records the intercepts of the print gloss-print density curves of Figure 7.5, as a function of paper gloss. This linear trend shows that print gloss approaches the value of paper gloss when print density approaches 0. In other words, print gloss increases linearly with ink load, from the limiting value of paper gloss at zero ink load. Zang and Aspler (1995) showed that for coated paper the print density depends only on the ink load transferred to paper. As for print gloss, or shininess, they showed it increases with ink load on the paper but also depends on the coated paper absorbency and printing speed. Print gloss, a measure of the roughness of the print, is affected by both micro scale roughness of the ink film and macro roughness of the substrate, Oittinen (1980). At low ink loads, the print gloss depends on the unprinted paper roughness or gloss, which explains the results found here for black coldest ink. At high ink load the print gloss is expected to depend more on ink film micro roughness, which in turn depends on ink film splitting and levelling, two processes described in detail in the section 3.3.1. Both printing speed and coating absorbency affect ink film splitting while the extent of ink film levelling relates to coating absorbency. A different scenario will thus be reported for the case of heatset cyan ink at higher ink load in section 4.2.1.

3.2.3 Ink transfer: Cyan ink [C-ITC, C-0BT]

For heatset cyan ink, experiments for the effect of ink load on ink transfer, optical density and print gloss were done exclusively with the coated paper produced commercially from the same pulp and similar coating materials as used to produce the experimental coated paper, the substrate designated COMC in Table 7.2. The maximum ink transfer, around 60%, is reached with about 0.75 g/m^2 of ink on the plate, Figure 7.7.

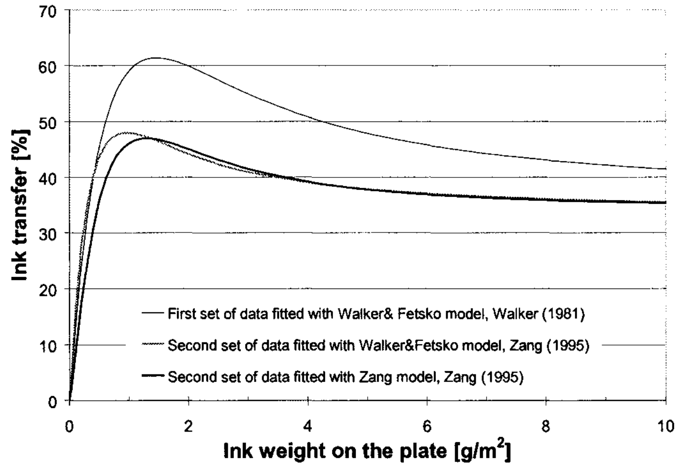

Figure 7.4 Ink transfer to coated paper: Theory

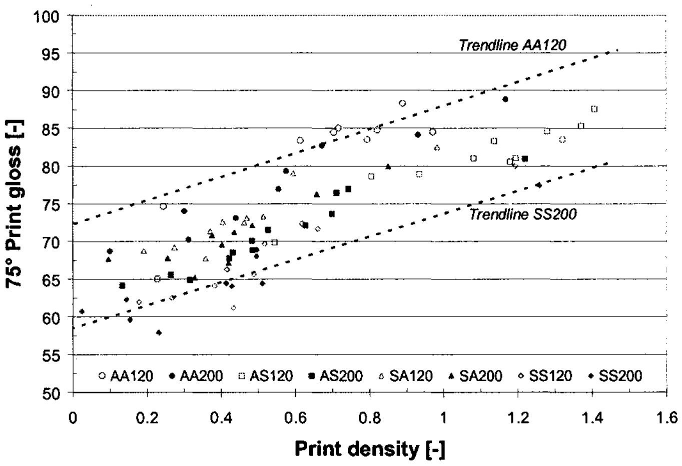

Figure 7.5 Print gloss and print density: Black coldset ink, B-ITC

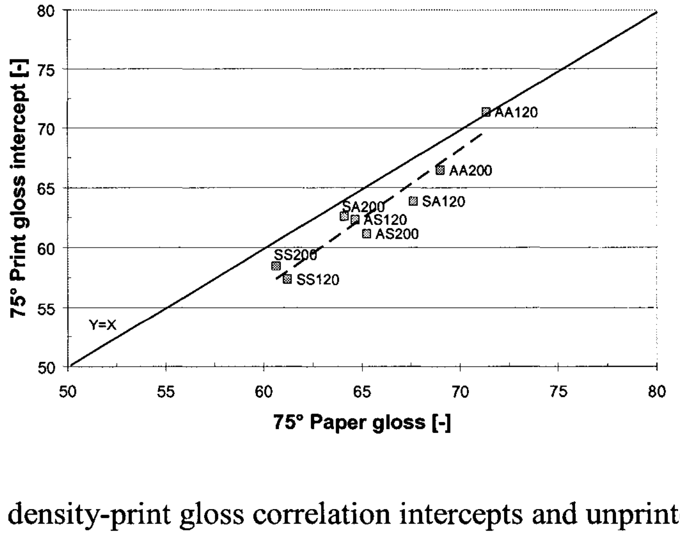

Figure 7.6 Print density-print gloss correlation intercepts and unprinted paper gloss: Black coldset ink, B-ITC

The print gloss-print density relationship for heatset cyan ink, Figure 7.8, follows the similar linear dependence shown by Figure 7.5 for coldset black ink. Unlike for black ink in section 3.2.2, both a higher plate ink load of 3.05 g/m^2 and a larger sample size allowed the measurement of a statistically representative ink transfer value at this ink weight. For the experimental and commercial coated paper, 7 prints were made at this ink load on the plate. Figure 7.9 shows that there is no difference in percentage ink transfer between papers dried under different drying conditions. Moreover at this ink load on the plate the percentage cyan ink transfer to commercial coated paper is identical to that to the experimental coated papers, about 45% in Figure 7.7.

3.2.4 Conclusion

For heatset cyan ink, ink transfer at 3.05 g/m^2 plate ink load remained unchanged by drying conditions tested in the present study and identical to that on commercial paper. For black coldset ink, any such conclusion is precluded by the lack of precision in the measurements. Zang and Aspler (1998) found that the changed coating porosity from changing latex binder content in the coating suspension does have an effect on percentage ink transfer but their results show that this effect becomes significant mostly above 5 g/m^2 of ink weight on the printing plate, a larger ink load than used in the present trials.

Another factor is the short timescale in the printing nip, ~1 ms at 3 m/s and 4.15 MPa (nip width ~ 4 mm). The transport of the ink vehicle may be sufficiently small during 1 ms that the ink transfer may not be affected by coating structure, as found in the present experiments, or only when larger differences in structure are tested, or when very rapid setting ink is used. Also print gloss increased linearly with print density, i.e. ink weight on paper, the intercept of the print gloss-print density curve being the unprinted paper gloss value.

3.3 Ink splitting

3.3.1 Theory of ink splitting

Depending on the printing roller speed, the ink film splitting may occur smoothly, or with a ribbing effect, or by cavitation, or with misting, MacPhee (1996). Under offset printing conditions experienced in practice, ink film splitting is believed to occur by cavitation, as illustrated in Figure 7.10 from De Grâce et al. (1992).

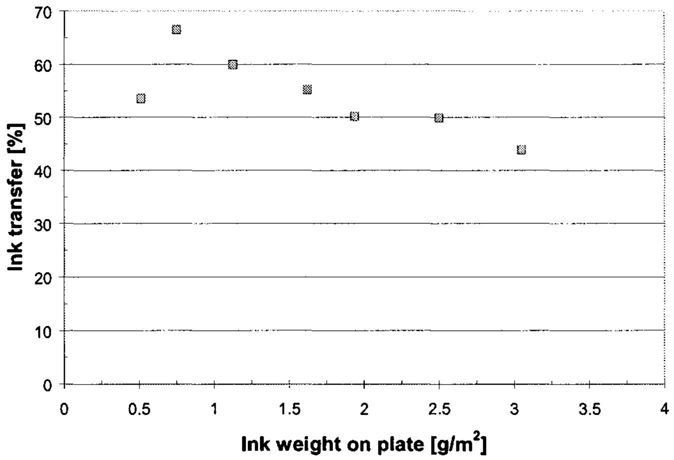

Figure 7.7 Ink transfer curve for commercial paper: Cyan heatset ink, C-ITC

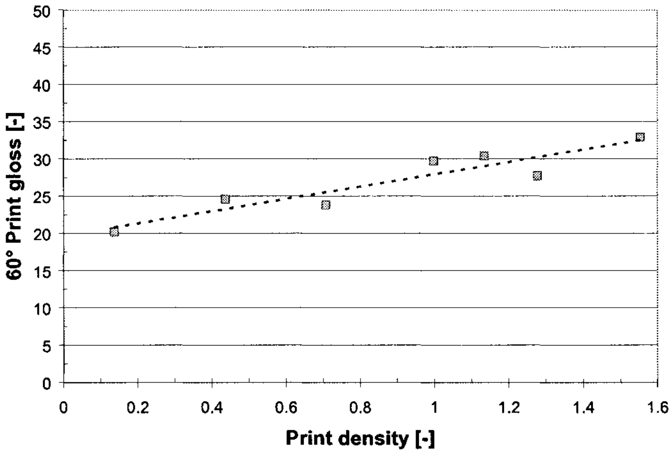

Figure 7.8 Print density and print gloss for commercial paper: Cyan heatset ink, C-ITC

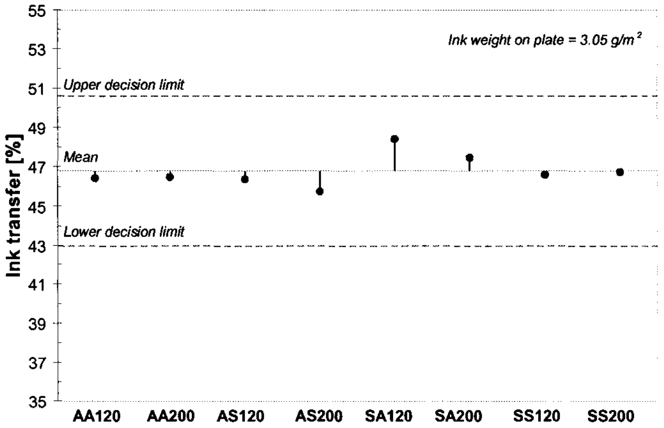

Figure 7.9 Ink transfer on experimental paper: Cyan heatset ink, C-0BT & C-3BT

Banks and Mills (1954) considered the ink film splitting to occur through a four-step sequential process consisting of cavitation, filamentation, elongation and rupture. Later, photographic evidence of filamentation was obtained for a non-porous smooth substrate by Thomson and Young (1975), De Grâce et al. (1992), Hayashi and Amari (1992), Ercan and Bousfield (2000). Pressure profiles supporting the occurrence of cavitation have been documented for both a non-porous smooth substrate, Zang and Aspler (1991), and a paper substrate, Aspler et al. (1993). These researchers have showed that for both non-porous and porous substrates the wet ink film experiences first a region of high pressure in the printing nip followed by a region of negative pressure at the exit of the nip. The negative pressure pulse may be as much as 0.5 MPa. This large negative pressure from the diverging surfaces subjects the wet ink film to tension, triggering cavitation. If printing speed and ink viscosity are low there is a smooth fluid film split. However at high printing speed and/or with high viscosity inks, such as in commercial presses and in the proof press in standard conditions with commercial ink, the wet ink cannot flow sufficiently fast to relieve this tension. In this case the tension leads to the formation of bubbles of solvent that grow, i.e. leads to cavitation, the first step in ink film splitting under these conditions. With cavitation, the second step in this process of ink splitting produces filaments which consist of ink liquid containing some bubbles. As the printing plate and substrate separate, ink filaments first elongate, which is the third step in such ink splitting and then break, thereby completing the four-step process of ink film splitting with ink filamentation.

However one may argue cavitation is the cause of the filamentation process. The process time in the nip being very short (< 5 ms), a viscoelastic response by the ink is expected, Zang and Aspler (1991) and Ercan and Bousfield (2000). Zang and Aspler (1991) found that ink "tack", defined as the limiting negative pressure reached at the exit of the nip, i.e. at the point of cavitation, increases with ink film thickness. As an increasing ink film thickness provides more fluid to respond to the expansion created by the diverging printed surfaces, it should reduce cavitation. Ink tack would therefore be expected to decrease with increasing ink film thickness. As the measurements of Zang and Aspler indicated just the opposite, they argue that the cavitation process, which they observed, is the controlling factor for ink splitting. They propose that the initiation of ink splitting derives from the viscoelastic nature of ink, while ink filament elongation and rupture may be more affected by flow properties.

After ink film splitting, filament formation and rupture, these filament elements recoil to both surfaces, to the print and to the printing roll surface. The splitting patterns on the printing plate and on the print are expected to be complementary, but the evolution of these is only analysed here for the print. The pattern resulting from ink splitting may not be recorded on the dry print depending on the extent of the redistribution of ink on the paper surface referred to as ink film levelling. Such levelling depends on the fluidity and state of consolidation of the ink film. Ink consolidation occurs through transport of ink vehicle by evaporation and by capillarity into a porous substrate. With the loss of ink vehicle the ink film becomes more viscous and its redistribution or levelling is reduced. Such levelling is believed to influence a key property of the print, print gloss, in a complex manner as noticed by many and illustrated in Figure 7.11 from Enomae et al. (2000). Print gloss depends on the micro roughness of the print and is therefore directly affected by the ink pattern left after printing and hence by the extent of decay of this pattern through ink film levelling. Direct observation of ink film splitting and filamentation on paper is difficult, while the much easier monitoring of the evolution of print gloss with time immediately after printing has brought a better understanding of ink film levelling and to some extent of ink film splitting. Glatter and Bousfield (1996) studied print gloss development on MYLAR and found that ink film thickness on the plate and printing speed affect the size and size distribution of filaments which level at different speed depending on their size: fast levelling for small filaments (< 100 μm), slow levelling for large ones (~500 μm). Desjumeaux and Bousfield (1996) studied the development of print gloss on paper coatings and found that the small sized pigment removes the ink vehicle faster, which slows or stops the levelling process. Preston et al. (2002) found that increasing ink load on the plate leads to a slower increase in print gloss and lower final gloss because of incomplete levelling of the larger ink filaments. They found that the redistribution of ink components (pigments and resin) also affected the final print gloss. Preston et al. (2003) found that coated paper leading to fast ink vehicle removal (larger pore density) reduced the extent of film levelling.

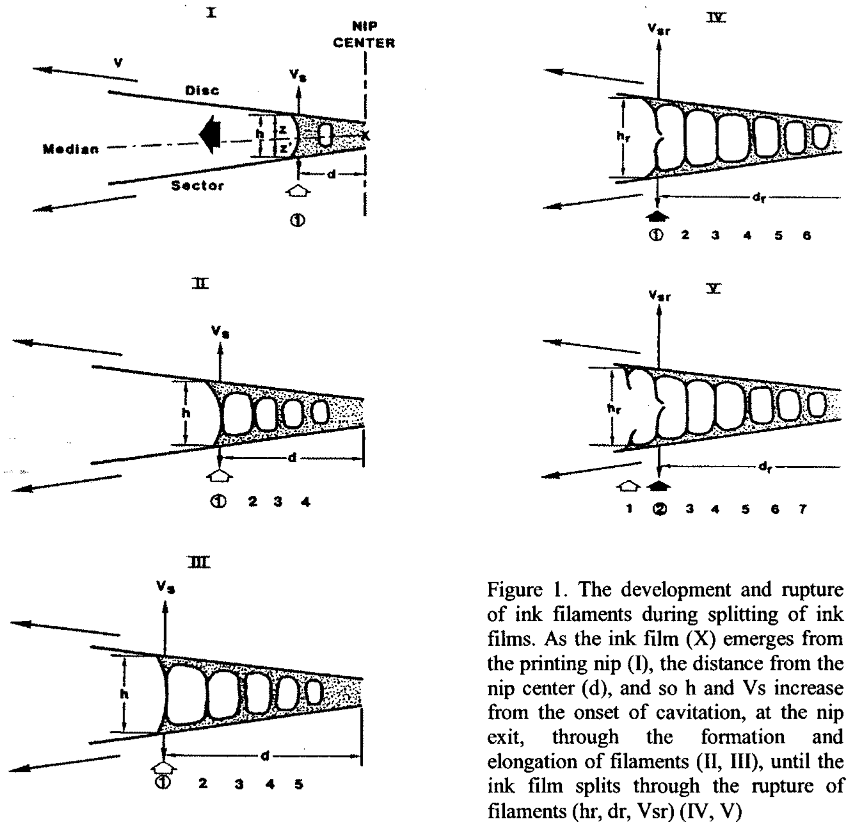

Figure 1. The development and rupture of ink filaments during splitting of ink films. As the ink film (X) emerges from the printing nip (I), the distance from the nip center (d), and so h and Vs increase from the onset of cavitation, at the nip exit, through the formation and elongation of filaments (II, III), until the ink film splits through the rupture of filaments (hr, dr, Vsr) (IV, V)

Figure 7.10 Schematic diagram of ink splitting process by homogeneous cavitation, from De Grâce et al. (1992)

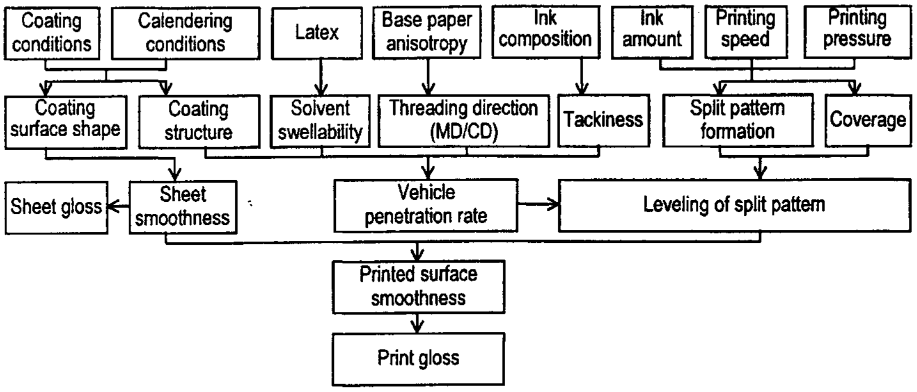

Figure 7.11 Interrelationship between factors affecting print gloss of coated paper, from Enomae et al. (2000)

3.3.2 Observations of ink splitting pattern

a. Observations by light microscopy: light and dark spots

Although the macro scale gravimetric measurements of ink transfer reported in section 3.2 remained unaffected by paper drying conditions, major differences at the micro scale were observed on examination of the prints by light and scanning electron microscopy. Prints were observed with a light microscope at magnification ranging from 50X to 300X. Such examination revealed the presence of light areas and dark areas, in both cases roughly circular and size ranging in diameter from 1 to 100 μm for the light spots and from 1 to 10 μm for the dark spots (1 μm is at the limit of resolution of the light microscope). These features were observed on experimental papers, on commercial coated paper and also on non-porous very smooth surfaces such as MYLAR and acetate transparency film, Figure 7.12 and Figure 7.13. These characteristic patterns of light and dark areas were observed under various printing conditions for both of the very different types of offset printing ink: black coldset and cyan heatset ink. For MYLAR substrates (printed with cyan ink only) these patterns were present on all the prints. For paper substrates, these areas appeared mostly after the back-trap unit with black ink, but after the printing unit for cyan ink. The size and density (number/mm^2) of light and dark spots varied depending on printing conditions and type of substrate, including variation with drying conditions. The light spots occurred with a density usually below 50/mm^2 but up to several hundred/mm^2 in a particular case (Black ink, 3BT, COMC1, 600/800N). The effects of substrate and printing conditions on these characteristic patterns detailed in section 3.3.3.

b. Observations by SEM microscopy: ink-free regions and ink hills

Under observation by SEM, in the secondary electron mode, of paper printed with cyan ink under the 0BT configuration, the entire printed surface appears black except for small light spots in variable quantity depending on paper drying conditions. When a light spot was observed under higher SEM magnification, Figure 7.14, bare clay platelets were visible, appearing as on the unprinted surface. The diameter of the light spot seen on Figure 7.14 is ca. 25 μm. This evidence establishes that these light spots did not result from coating picking, i.e. removal of coating material during printing, but were virtually ink-free regions of coating.

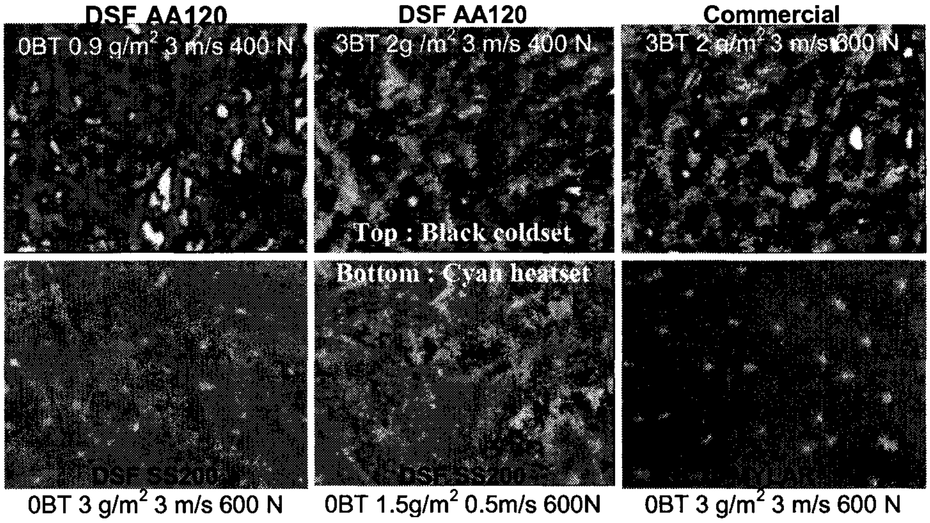

Figure 7.12 Light spots observed by light microscopy, magnification X150 (image width ~1 mm)

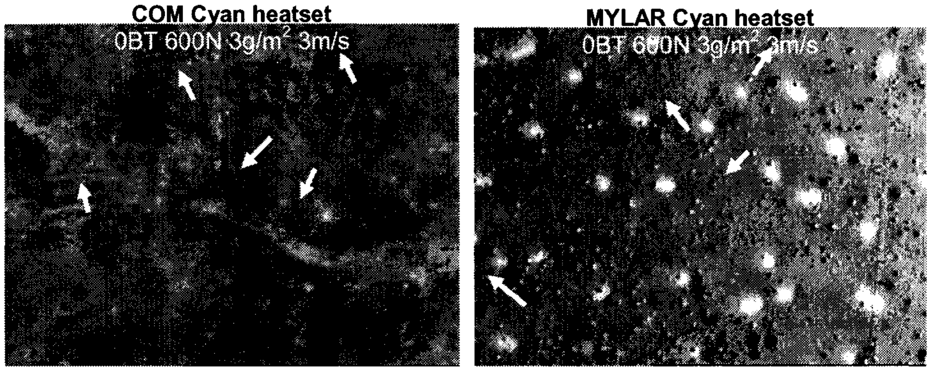

Figure 7.13 Dark spots observed light microscopy magnification X150 (contrast enhanced for clarity, image width ~1 mm))

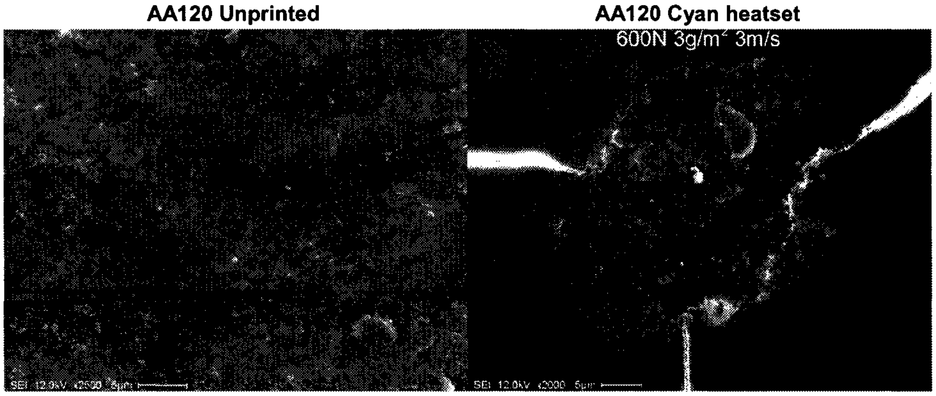

Figure 7.14 Light spots observed by SEM: DSF AA120 (picture width ~ 50 µm)

These light spots are therefore ink-free regions in the print film which terminate at the surface of undamaged coating, and their size corresponds to the light spots observed with light microscopy. Under observation by SEM, in the TOPO back-scattered electron mode, ink hills were also observed, Figure 7.14.

c. Observations by profilometry: Ink craters and ink hills

Dry ink film structure

The 3-D images, Figure 7.15, or profiles, Figure 7.16, of prints obtained on a MYLAR substrate by profilometry clearly show that the ink film consists of a layer of uniform thickness sprinkled with craters and conical peaks. The same profilometer used for characterization of uncoated and coated paper, Chapters 4 and 6, was used for the prints. As described in Chapter 3 section 7.5.1, a stylus head of 2 μm was used and the sample scanned over a 1 mm^2 area with 12 nm vertical resolution. In Figure 7.16 the central line is mean profile across the 1 mm^2 area of the surface, while the top and bottom lines are lines of maxima and minima respectively for the 1 mm width in the direction at 90° to that of the profile. The same profile is shown on two different scales, 5 and 20 μm to compare with the case of paper in Figure 7.17. These lines of minima and maxima serve to identify that both holes and peaks exist in the ink film.

The number and size of these ink craters and conical peaks correspond respectively to the light and dark spots found by microscopy. For the MYLAR substrate printed with cyan ink under base-case printing conditions (0BT, 3 g/m^2, 3 m/s, 600N), Figure 7.15 shows 25 - 35 craters per mm^2, of diameter ca. 30 μm, as well as 40 - 60 peaks per mm^2, of diameter around 5 μm. These characteristics agree well with values obtained with SEM and with light microscopy as summarized in Table 7.4 of section 3.3.3. The diameter of ink-free craters measured with the light microscope must be compared to that measured at the bottom of the crater in the profilometry profile because of the tapered shape of a crater, apparent in Figure 7.16: the top of a crater may be as much as 50% larger in diameter than at the bottom. The ink peaks are seen to be as high as 2 μm. As the craters terminate at the coating surface, as shown by the SEM examination, they have the depth of the mean ink film thickness, somewhat less than 1 μm as documented in Table 7.3. Because the conical peaks are ink hills and the craters are ink craters, these correspond to the dark and light spots, respectively, seen with light microscopy. When examining printed paper by profilometry the ink peaks are clearly visible on profiles, Figure 7.17, but the craters are not apparent because the amplitude of unprinted paper roughness is often larger than the ink film thickness. The characterization of coated paper roughness by profilometry shows that for the coated paper surface, the distance from peak to valley is about 1 μm and may be up to 4 μm, Figure 6.15. It follows that the ink-free regions of a 0.9 μm thick ink film (Table 7.3) cannot be easily detected with profilometry roughness profiles of ink printed on a coated paper substrate.

Dry ink film thickness

Through the presence of ink craters, ink film thickness can be evaluated. With the complex structure of this film described above, its thickness may be defined either as the thickness of the main ink film layer or as the equivalent thickness the ink film would have if there were no craters or peaks. According to the first definition the ink film thickness may be equated to the depth of the craters as obtained from micro roughness profiles such as in Figure 7.16. From the bottom line, the line of minima, a straight line corresponding to the surface of the MYLAR substrate can easily be traced, the depth of this line therefore is the ink film thickness: 0.85 μm. The volume of material roughness in the profilometer used designated as the "S_{mmr} parameter" - the mean material volume ratio – per mm^2 gives an ink film thickness of 1 μm. The value of the "S_{mmr} parameter" corresponds to the total volume of material per mm^2 surface contained between the surface and an imaginary horizontal plane at the minimum altitude of the surface. With MYLAR sheets, the substrate roughness is small compared to the ink film thickness so it may be assumed it does not contribute to calculation of the S_{mmr} parameter. Thus for MYLAR sheets the S_{mmr} parameter corresponds to the volume of the ink film. This result, 1 μm, falls in the range given in Table 7.3, 0.89-1.1 μm estimated from ink density measurement. The excellent agreement between the two independent estimation methods, from ink density and from profilometry, in the case of printed MYLAR therefore validates the approximation for ink film thickness in the case of paper substrate based on ink density assumptions: in the range 0.63-0.94 μm, Table 7.3.

3.3.3 Effect of printing conditions and type of substrate on ink craters, ink hills

Ink hill characterization by light microscopy was more difficult than ink craters because of the lack of contrast of ink hills with the surrounding ink. As noted, the visible bottom of an ink crater is the coating surface, which provides a sharp contrast for both light and SEM microscopy. The effects of printing conditions and type of substrate on the ink hill pattern could therefore not be determined precisely. Thus Table 7.4 summarizes the effects of printing conditions on the size and density of only the ink craters.

a. Effect of printing parameters

Table 7.4 shows that the type of ink, cyan heatset versus black coldset offset ink, and the ink load had the most effect on the ink crater characteristics, then printing speed and pressure. Figure 7.18 illustrates the effects of printing conditions and substrates.

For cyan ink, ink craters were observed on all prints made on MYLAR and on most of the prints on paper in the 0BT printing configuration. For black ink no prints were made on MYLAR, but ink craters on paper were observed in the 0BT printing configuration at low ink load and more extensively in the back-trap configuration. For both MYLAR and paper substrates, increasing ink load on the printing roll decreased the density of ink craters but increased their diameter. With a MYLAR substrate, decreasing the ink load also leads to generation of ink craters which are not completely ink-free. For black ink in the 0BT configuration, above a critical plate ink load of about 1.5 g/m^2 the pattern of craters disappears. Also for black ink, more ink craters were observed in the back-trap configuration. The action of the back-trap unit is similar to printing with a lower ink load in the second unit. Similarly the results observed under the back-trap configuration with a MYLAR substrate lead to the same conclusion. The opposite effect was observed in the case of cyan ink on paper: with the back-trap configuration no additional ink craters were created but rather areas of a different type were observed described in section 3.4.2 as ink "islands". These differences between the two inks and between MYLAR and paper for cyan ink are certainly related to ink setting characteristics. Ink sets on impermeable substrate by solvent evaporation and on paper by solvent and oil transport into the coating and solvent evaporation. This difference affects the free-ink film thickness, hence the splitting behaviour with the back-trap printing configuration

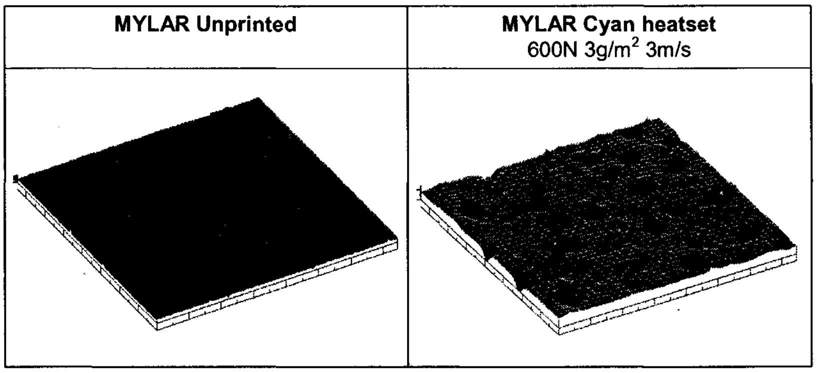

Figure 7.15 3-D axonometric representation of surface of 0BT cyan heatset print on MYLAR (1 mm^2)

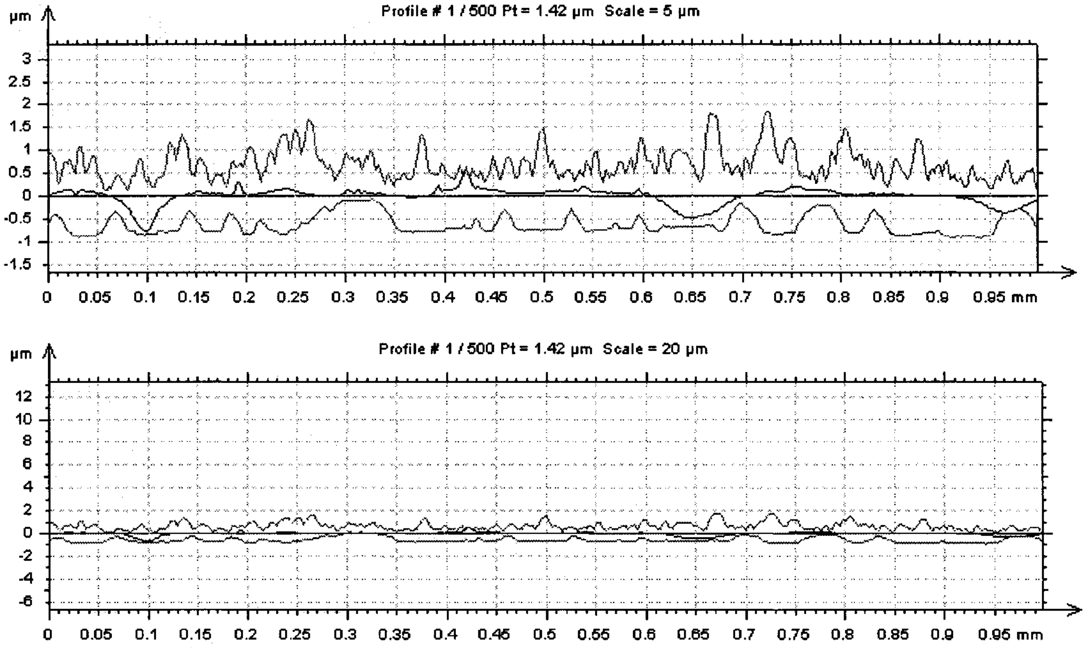

Figure 7.16 Profile across the surface of 0BT cyan heatset print on MYLAR; same profile with scale 5 µm (top) and 20 µm (bottom)

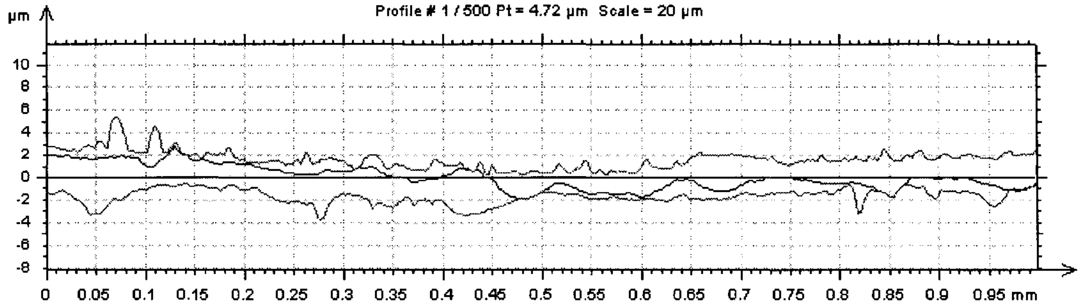

Figure 7.17 Profile across the surface of 0BT cyan heatset print on paper (AA120); scale 20 µm

Heatset inks are faster setting than coldset, which explains why no ink splitting pattern is seen on paper printed in cyan under the back-trap configuration as opposed to that printed in black. With MYLAR a non-porous material, ink setting occurs only by solvent evaporation, which was measured to be negligible within the time scale of the printing experiment (3% weight loss in 5 minutes). Therefore the back-trap printing configuration leaves a cyan ink splitting pattern on MYLAR but not on paper for which the ink is more consolidated (thinner free-ink film thickness).

Printing speed also had a smaller but discernable effect on the ink crater pattern. Increasing printing speed leads to fewer ink craters for both MYLAR and paper substrates in the case of cyan ink, the only ink tested for this effect. With a MYLAR substrate the diameter of ink craters also tended to increase with increasing speed. Increasing speed or decreasing ink load is accompanied by the appearance of a slightly different type of light spots, still circular but of a darker shade. These spots, believed to have the same origin as the light spots, are considered to be ink craters which are not totally ink-free and are the same as observed at low ink load as reported in the previous paragraph.

Printing pressure usually had less effect or contradictory effects. For black ink on paper in the back-trap configuration, increasing printing pressure increased ink crater density. For cyan ink on MYLAR, ink crater density remained unchanged but crater diameter was reduced. For cyan ink on paper there was no clear effect of printing pressure.

b. Effect of type of substrate

As noted above, increasing ink load and increasing printing speed had the same effects on MYLAR and paper substrates but on MYLAR there were generally more and larger ink craters. For cyan ink these craters were observed on all MYLAR prints and were generated in both the 0BT and back-trap configurations, while for paper, ink craters were generated in cyan print only in the OBT configuration. Significant differences in ink crater characteristics were also observed among the 3 commercial papers tested in the back-trap configuration with black ink, Figure 7.19. More important for the present study was the effect of drying conditions on the ink crater pattern.

Table 7.4 Effect of substrate and printing conditions on ink craters characteristics

ID	**Conf.**	**Substrate**	**Operating conditions**	**[1]Density**	**[2]Diameter μm**
B-ITC	0BT	DSF	BLACK	+/-	1-5
C-0BT	0BT	COMC	CYAN	+	1-5/10-60
C-0BT	0BT	AA120	CYAN	4	1-5/10-60
C-0BT	0BT	AA200	CYAN	5	1-5/10-60
C-0BT	0BT	AS120	CYAN	15	1-5/10-60
C-0BT	0BT	AS200	CYAN	17	1-5/10-60
C-0BT	0BT	SA120	CYAN	6	1-5/10-60
C-0BT	0BT	SA200	CYAN	7	1-5/10-60
C-0BT	0BT	SS120	CYAN	15	1-5/10-60
C-0BT	0BT	SS200	CYAN	14	1-5/10-60
T-1	0BT	MYLAR	CYAN–3 m/s	37	5-80
	0BT	MYLAR	CYAN-0.5 m/s	40	5-80
	0BT	MYLAR	CYAN–6 m/s	30	5-80
	0BT	MYLAR	CYAN-1.5 g/m^2-0.5 m/s	80	5-80
	0BT	MYLAR	CYAN–600 N	15	5-80
T-4	1BT	COMC, COMC1&2	BLACK–200 N	+	>10
	1BT	COMC, COMC1&2	BLACK–400 N	++	>10
	1BT	COMC, COMC1&2	BLACK–800 N	+++	>10
T-5	0BT	COMC	CYAN–0.5 m/s	++	1-5/10-60
T-9	0BT	AA120	CYAN–0.5 m/s	++	1-5/10-60
	0BT	AS200	CYAN–0.5 m/s	++++	1-5/10-60
	0BT	SS200	CYAN–0.5 m/s	++++	1-5/10-60
	0BT	SS200	CYAN-1.5 g/m^2-0.5 m/s	+++++	1-5/10-60

[1] *Density: Approximate number of craters per mm^2 (manual count by light microscopy. When no number is provided, the number of crosses is relative to the COMC in the C-0BT printing conditions.*

[2] *Diameter: For MYLAR one range of diameter is given. For most paper samples both small and large diameter craters were observed, hence two ranges of diameter are given. Where not specified, the ink load was 3 g/m^2.*

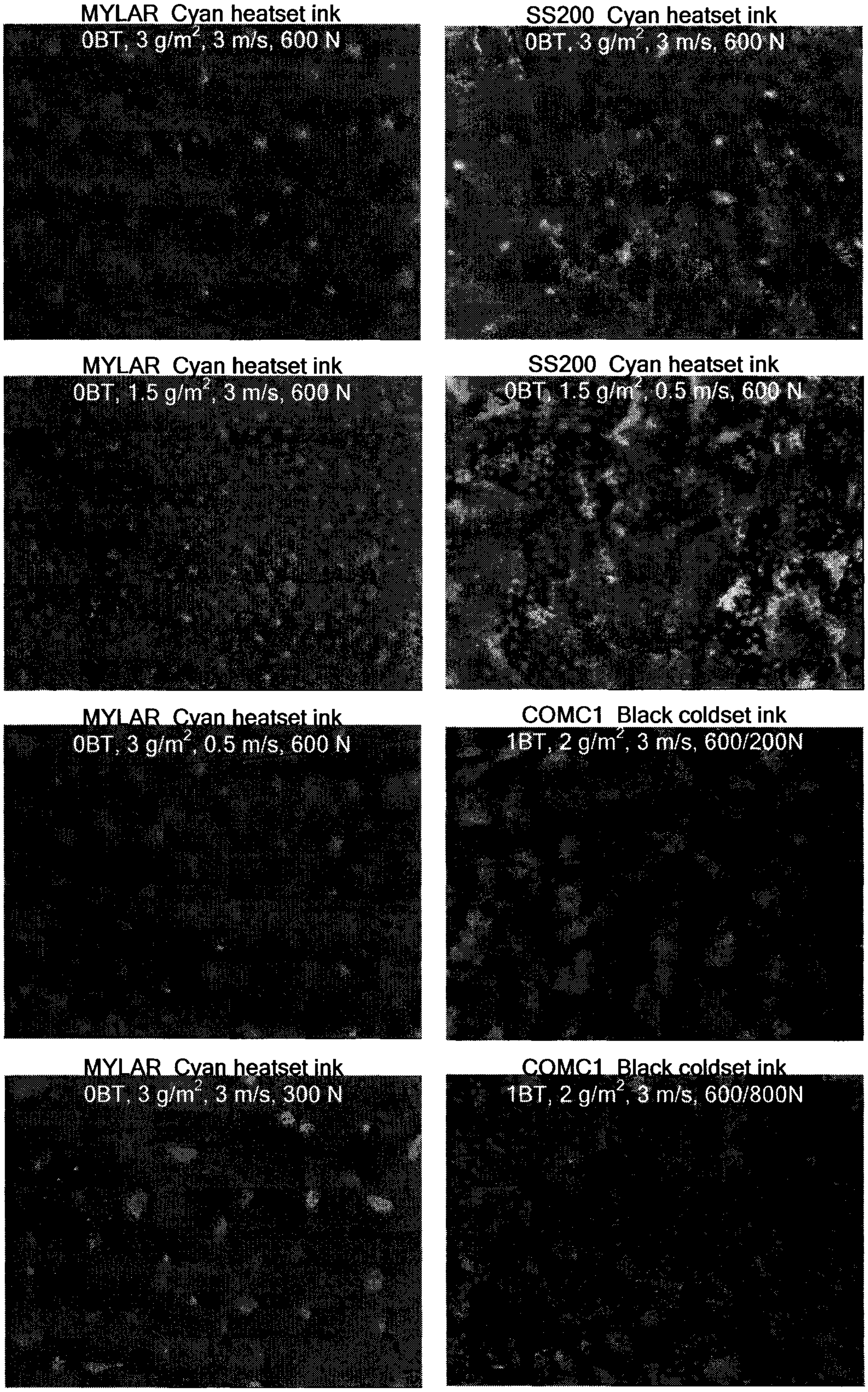

MYLAR Cyan heatset ink
0BT, 3 g/m^2, 3 m/s, 600 N

SS200 Cyan heatset ink
0BT, 3 g/m^2, 3 m/s, 600 N

MYLAR Cyan heatset ink
0BT, 1.5 g/m^2, 3 m/s, 600 N

SS200 Cyan heatset ink
0BT, 1.5 g/m^2, 0.5 m/s, 600 N

MYLAR Cyan heatset ink
0BT, 3 g/m^2, 0.5 m/s, 600 N

COMC1 Black coldset ink
1BT, 2 g/m^2, 3 m/s, 600/200N

MYLAR Cyan heatset ink
0BT, 3 g/m^2, 3 m/s, 300 N

COMC1 Black coldset ink
1BT, 2 g/m^2, 3 m/s, 600/800N

Figure 7.18 Effect of printing conditions on ink crater pattern (image width ~1 mm)

Experimental paper printed with cyan ink showed craters in variable number density depending on coated paper drying conditions, being favoured most strongly in the 0BT configuration, Figure 7.20. Drying the base sheet with superheated steam did not materially affect the ink crater pattern. By contrast, drying the coated sheet with steam increased the density of ink craters by a factor of 2 to 4. As the manual count of ink craters is difficult, hence not very precise. However visual examination by light microscopy in Figure 7.20 illustrates the effect clearly. The temperature of the coated sheet drying fluid did not have a strong effect, but a higher temperature tended to increase ink crater density. These differences in ink crater pattern will influence printing properties, as will be discussed in section 4.

3.3.4 Origin of ink craters and ink hills

The fact that these features were observed under standard proof press conditions (commercial ink, Prüfbau press, used under standard conditions for the printing unit) and varied with printing conditions, as well as the definitive SEM evidence presented in Figure 7.14, proves that these light and dark areas are not defects related to the experimental substrate. These ink craters and ink hills are the remains from and the evidence of ink film splitting during normal offset printing. Others have observed ink splitting remains, as is discussed next. Various patterns of filament remains have been observed: ridges of size similar to filaments (video recorded) by Hayashi et al. (1992) on fresh print (no scale in his pictures); ink hills in the range 5 to 200 μm diameter as reported by Nguyen et al. (1992) on dry print and by Ercan and Bousfield (2000) on fresh print; hills and holes seen by Glatter and Bousfield (1996) on dry print (MYLAR substrate); strips perpendicular to the printing direction observed by Enomae et al. (2000) on fresh print. Enomae did not report or discuss the white spots about 1 to 100 μm which appear in this publication.

It seems that in the present study the ink levelling process stops very rapidly as printing leaves a permanent pattern of ink craters and ink hills on the various substrates tested. The mechanism for formation of an ink hill is evident: when a filament which springs back to the printed substrate is sufficiently fluid that surface tension can act to reduce its surface:volume ratio to that of an approximately droplet form, an ink hill will be produced on the print. By contrast the mechanism for formation of an ink crater is less straight forward and will be discussed in section 3.3.5d.

3.3.5 Ink splitting and substrate structure

There is ample evidence in section 3.3.3 and from others that ink hills and ink craters come from ink film splitting at the exit of the printing nip, but it is not clear what is the mechanism which leads to the variable pattern of ink craters on the print with the various substrates. The splitting process must be quite different between porous, relatively rough coated paper and impermeable smooth MYLAR substrates. Three possible explanations are first presented, then examined, with the first mechanism related to surface roughness, the other two involving substrate surface porosity.

a. Surface roughness

One key surface property difference between paper and MYLAR and between the papers tested is roughness. As defined earlier, tack is the limiting negative pressure reached at the exit of the nip. Tack varies with the type of ink and consolidation of the ink at the surface of a porous substrate. Measurement of tack therefore provides information on the state of consolidation of the ink film, which affects its splitting behaviour. Gane et al. (1994) propose that ink tack relates both to the surface porous structure, to be discussed below in point c, and to substrate surface affinity for the ink, which they define as micro smoothness. De Grâce and Mangin (1984) proposed that asperities at the surface of paper would serves as nucleation sites and explain the asymmetric splitting of ink in favour of the printing plate with an ink splitting line closer to the paper substrate. They however reviewed their hypothesis after new experiments and concluded that micro protuberances may help cavitation, but are not sufficient explain asymmetric ink splitting, De Grâce and Mangin (1988). They propose another mechanism, namely air entrapment is playing a role as well, as discussed in the next paragraph.

b. Air entrapment in surface pores

Another important surface property that varies greatly from MYLAR to paper and among different papers is porosity. Cavitation is normally considered the evolution of a gas phase from a liquid phase, and may be triggered through two types of nucleation: homogeneous nucleation, which occurs in the bulk of the wet ink film, and heterogeneous nucleation, which is triggered by pre-existing gas trapped by surface inhomogeneities.

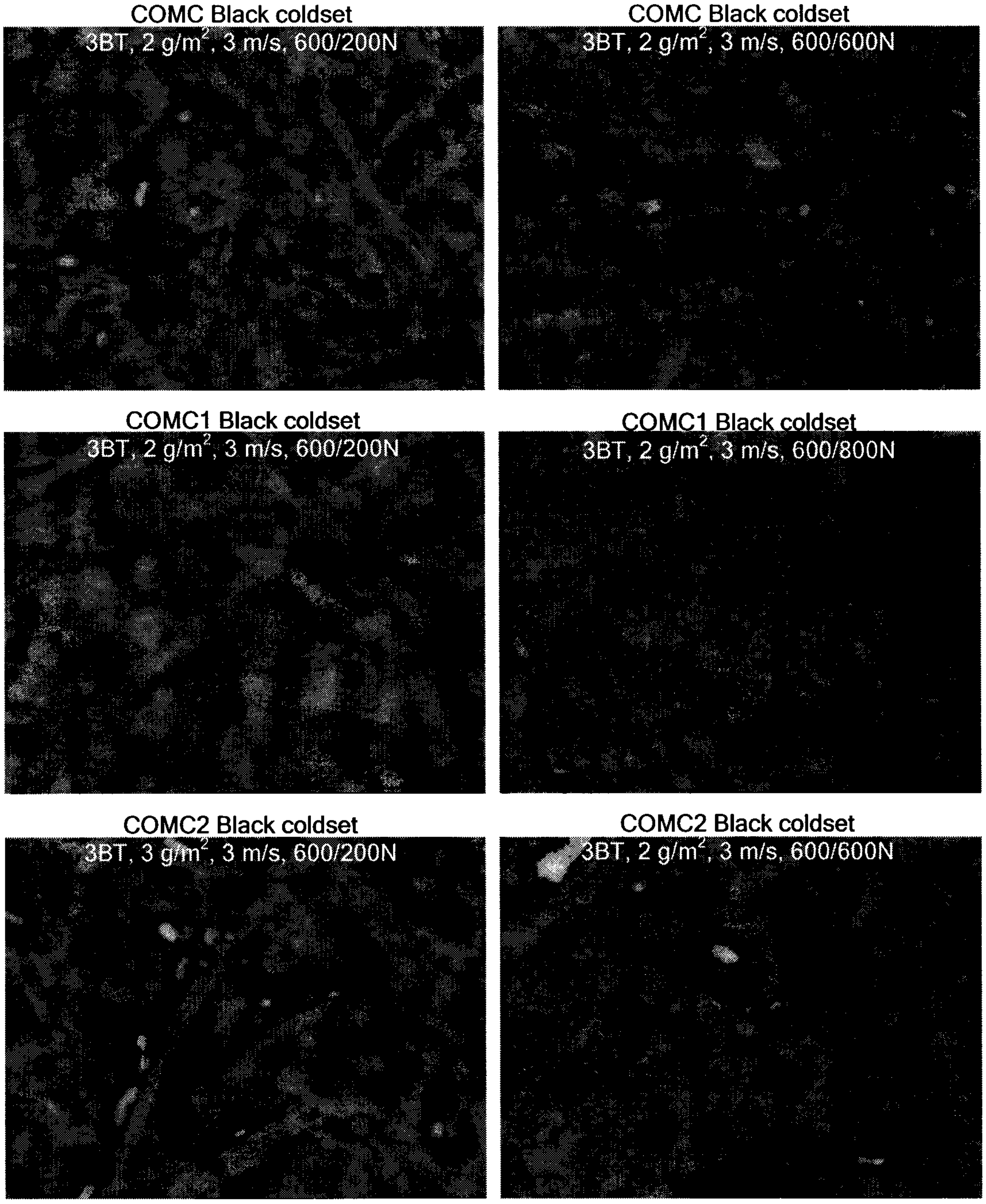

Figure 7.19 Ink crater pattern on three different commercial coated papers: Black coldset ink, BT configuration (image width ~1 mm)

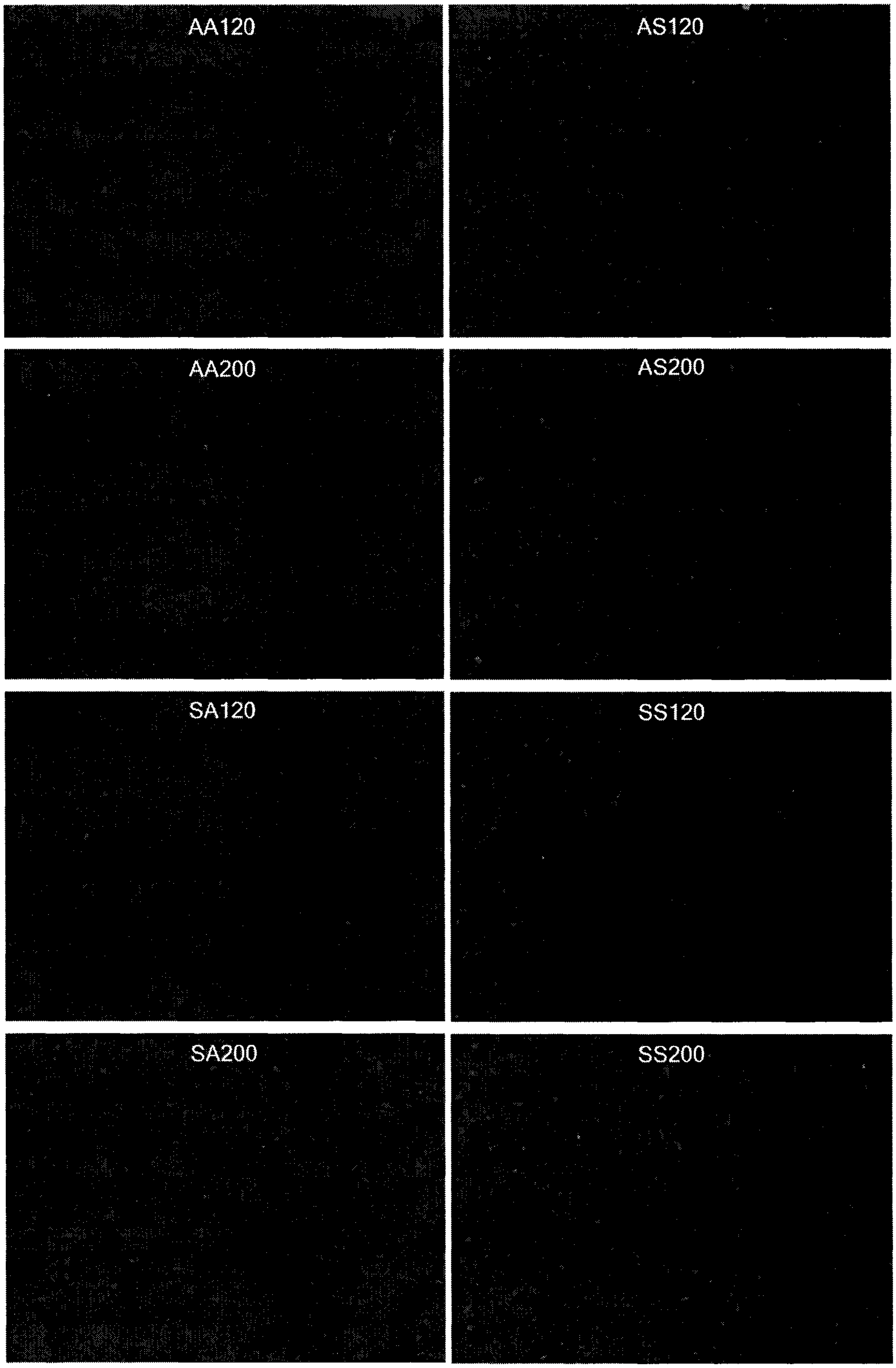

Figure 7.20 Ink crater pattern on experimental paper: Cyan heatset ink, 0BT configuration, standard conditions (image width ~ 3 mm)

Various investigators have proposed that the evolution of gas bubbles in the ink film at the exit of the printing nip can play an important role in the process of ink splitting. In the present study homogeneous nucleation is expected to be more likely for MYLAR substrates, since MYLAR is smoother than paper and impermeable. According to Ercan and Bousfield (2000), heterogeneous nucleation would occur at the paper surface at the location of micro roughness or micro voids. Fetsko (1958) and De Grâce and Mangin (1988) suggested that air entrainment in surface micro voids would provide nucleation sites for cavitation at the ink/substrate interface, which they propose explains asymmetric splitting of the ink film (closer to the paper surface). These investigators propose that air entrained in surface pores before the printing nip would help cavitation and filament formation at the exit of the nip. At the point of substrate-printing roll separation, they believe that such entrained air would be sucked into the region of filament formation, thereby easing the cavitation process. Thus from this point of view the porous structure at the paper surface would determine the ink filament crater pattern. Aspler et al. (1993) measured ink "tack" under a vacuum of 0.1 atm investigate whether cavitation is facilitated by air dissolved or entrained in the nip. Their finding that ink tack is the same under vacuum as at atmospheric pressure suggests that propagation of ink film splitting is not controlled by entrained air. However they made no definitive conclusion because a small amount of air, still present at 0.1 atm, might be sufficient to affect the splitting.

c. Effect of surface porosity on ink fluid properties

Surface porosity significantly affects ink setting, with faster setting being observed on a more porous substrate, Preston (2001). Aspler et al. (1993) and Preston et al. (2002) report that ink setting or immobilization at the surface of the substrate decreases the measured of tack because of the thinner free ink film available for splitting and moves the ink film splitting location closer to the nip centre. The ink film thickness being different the location of the ink film split and the tack pressure at the split are changed leading to a different ink film splitting pattern. As surface porosity affects ink setting rate, it would therefore affect as well the ink splitting process.

d. Conclusion

The process of ink splitting is not fully understood. The formation of filaments has been evidenced by photography but the mechanism for formation of a filament is not yet demonstrated. Filamentation is believed to occur after cavitation, evidenced by the recorded drop in pressure at the nip exit. Cavitation is the generation of bubbles growing from gas or vapour nuclei from the bulk of the fluid, homogeneous nucleation, or at an interface, heterogeneous nucleation. In the case of smooth impermeable substrate such as MYLAR, homogeneous nucleation may occur preferentially and lead to filamentation. In the case of rougher and porous materials such as coated paper, heterogeneous nucleation should be favoured. Homogeneous nucleation requires a larger negative pressure than heterogeneous nucleation. Bubbles of air trapped at the ink/coating surface pores or roughness crevices at the printing nip entrance may become nuclei generated heterogeneously. At the nip exit these bubbles expand as pressure falls below 1 atm. For homogeneous nucleation the pressure must be below the vapour pressure of the solvent so homogeneous nucleation is expected to occur later, if at all. The locations of nuclei would leave ink-free regions on the dry print, identified previously as ink craters. If this mechanism applied, the results found of the present study would thereby derive from the local variability of the surface roughness or micro porous structure associated with varying drying conditions. A simple mechanism may be that the filament forming process can continue until, over some region of diameter in the range 1-100 μm, all of the wet ink down to the printed substrate or the printing roller surface is drawn out into the filament, leaving an ink-free area or "ink crater". Ink-paper adhesion failure at the location of ink craters would explain the ink splitting pattern observed. Again both roughness and porosity may be responsible for adhesion failure.

As reported in section 3.3.3 b, experimental paper printed with cyan ink showed ink craters in variable number density depending on coated paper drying conditions. Drying the base sheet with superheated steam did not affect the ink crater pattern. By contrast, drying the coated sheet with steam increased significantly the density of ink craters. Large differences in micro roughness were recorded in Chapter 6 Figures 6.13 and 6.14 between different drying conditions, AA120 and SA120 for example. However it is seen from Table 7.4 that the ink crater characteristics of these two types of sheets are little different. The differences in micro roughness leading to variable ink film splitting pattern through the mechanisms presented above would probably not be related to sheet average roughness but rather to the occurrence of local crevices. The diameter of ink craters is in the range of only 1-60 μm. Very little difference in coating porosity and pore size distribution were recorded by mercury porosimetry in Chapter 6 for sheets for which coating was dried in steam, but again they are sheet average values and it is not possible to determine the local nonuniformity of pore structure. For printing, only the top surface porosity is important, while mercury porosimetry determines the porous structure of the entire coating layer. Therefore the mercury porosimetry results cannot be used either to support or reject the hypothesis of surface porosity triggering various ink film splitting patterns.

The conclusion is that very local differences in surface structure, roughness or porosity, probably explain differences observed in the ink crater pattern with variable drying conditions.

3.4 Ink back-trap

3.4.1 Theory of ink setting

The mechanisms of ink setting are those where a suspension of particulates is applied to a porous material, such as the consolidation or setting of a coating suspension on paper, described in Chapter 2 section 2. Consequently as soon as the ink suspension contacts paper, ink setting starts by transport of the ink liquid phase into the paper. The ink solids, ink pigments and resin, are filtered out at the coated paper surface as the liquid phase, ink solvent and oils, are transported into the porous coating. Thus Zang and Aspler (1995) proposed the consolidation of offset ink on coated paper occurs by capillary penetration with concurrent formation of a filter cake or ink pigment layer at the paper surface. Other mechanisms for water transport are diffusion into the latex binder of the coating, Xiang et al. (2003), evaporation at the exterior surface of the ink film, leading to the formation of a skin, Shoelkopf et al. (2000), resin cross-linking with the depletion of solvent, Preston et al. (2001), and curing, by oxidation or heating. Capillarity being the prevailing mechanism, the coating porous structure is the main parameter controlling ink setting. Preston et al. (2001) showed that at the same pore number density per surface area, larger pores give faster ink setting.

When an ink film freshly printed in one printing unit is fed into a printing nip, unconsolidated ink may transfer to that printing roller. The amount of ink thereby back-trapped would depend on the ink setting rate. Thus the back-trap experiments reported next provide information related to ink setting.

3.4.2 Ink island coverage in 3BT printing configuration

When prints from the 3BT printing condition are observed with light microscopy, Figure 7.21, the ink film appears to consist of a thin ink layer covering the entire print, plus some areas of higher ink film thickness distributed over the surface as discrete features or ink "islands". The explanation is believed to be that the islands of thicker ink film are where the ink was not back-trapped while the regions of thinner ink are where back-trapping occurred. This pattern indicates that the amount of ink back-trapped is locally nonuniform. On Figure 7.21 the ink islands show as the dark areas while the light areas are where ink where ink has been back-trapped. Since ink setting rate controls the amount of ink back-trapped in the clean uninked printing units, it controls the amount of ink remaining at the surface. The islands of thicker ink are therefore regions where the ink became sufficiently dry that it and could not be removed when the sheet passed through subsequent back-trap units. Higher ink island coverage means less ink re-transfer in the back-trap units, thus faster ink setting rate. Assuming the same ink film thickness within each region for all prints, the percent ink island coverage provides an indirect measurement of average ink setting rate.

The ink coverage as conventionally defined is 100%, but about half the area is covered by these ink islands. Moreover this ink island coverage can be measured precisely. The size of the light microscope images of Figure 7.21 is about the same as that of the image acquired by the Paprican InkScanner, which allows determination of what that instrument measures. Figure 7.22 is a schematic representation of the coverage measurement process with the Paprican InkScanner with ink islands of 50-200 μm diameter range. Since the threshold value is adjusted for each image to 50% of its specific greyscale range the average optical density of the printed sheet, which varies among the papers tested, does not affect the measurement.

The ink island coverage values in Figure 7.23 along with the ink distribution pattern visible in Figure 7.21 are indications that ink setting rate and local nonuniformity in ink setting rate varied with drying conditions. These results of ink island coverage for the C-3BT configuration reveal that relative to drying coated paper in air, superheated steam drying increases cyan heatset ink coverage by 3 to 7 percentage points when used for drying the coated sheet. The ink island coverage is not significantly affected by the fluid used to dry the base sheet or by the temperature of the drying fluid used to dry the coated sheet. The relation between ink island coverage and print gloss is examined in section 4.1.1, since gloss depends on the surface microscale nonuniformity and therefore on the ink film thickness nonuniformity. In addition, the pattern of locally darker areas, Figure 7.21, was affected by drying conditions: it appeared finer for coated paper dried in steam, which indicates that variation in local ink setting rate was also shifted to a smaller scale, and may explain the better print mottle observed for this paper in section 4.3.

3.4.3 Development of printing properties with print back-trap

In order to better understand mechanisms controlling ink back-trap, and thereby ink setting, commercial paper and impermeable MYLAR were printed with an increasing number of back-trap units and with increasing delay time between printing on the two printing units. The amount of ink back-trapped from the print to the printing plate could be determined by weighing each printing roller before and after printing, as for the ink transfer measurement described earlier. However because of the low weights of ink transferred, this procedure did not provide very precise measurement, especially for the 3rd and 4th BT units. The alternate procedure adopted was to weigh the substrate before and after printing. For the MYLAR substrate, another method for obtaining the back-trapped ink was by measuring the ink film thickness by profilometry with back-trap, and in the 0BT printing configuration. As noted in section 3.3.2, ink thickness on paper cannot be determined by profilometry because the paper roughness exceeds the ink film thickness. The values of percentage ink back-trap reported in Table 7.5 and Table 7.6 should therefore be regarded as approximate especially for the 2 last back-trap units where some ink was visibly back-trapped. For these sheets the measured printing properties are more reliable than the measured back-trap, enabling more definitive conclusions. When varying the number of back-trap units, 5 sheets were printed for each configuration and the average properties are reported. For the case of ink transfer a test using both methods, i.e. paper weighing and printing roller weighing, gave values in excellent agreement, 44% and (from section 3.2.2) 46% respectively.

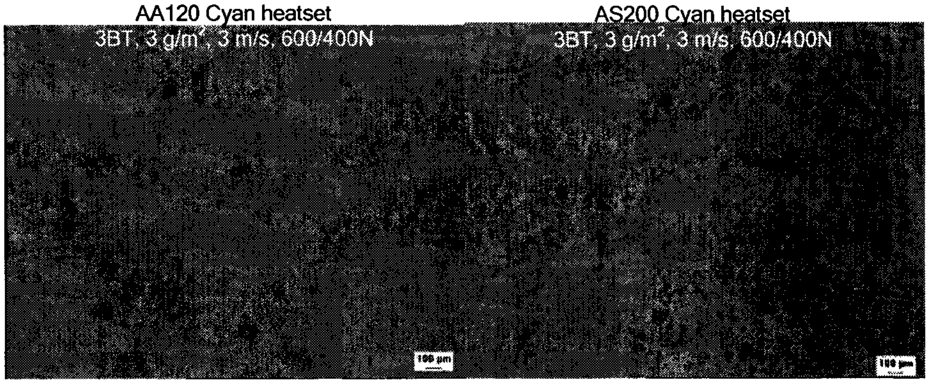

Figure 7.21 Ink island distribution by light microscopy: Cyan heatset ink, C-3BT (image width 3 mm)

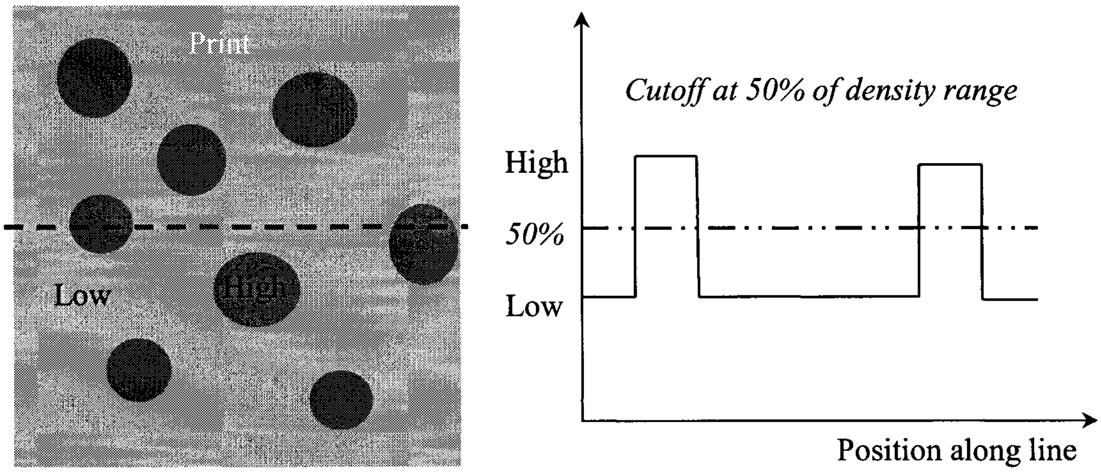

Figure 7.22 Interpretation of the ink coverage measurement by Paprican InkScanner

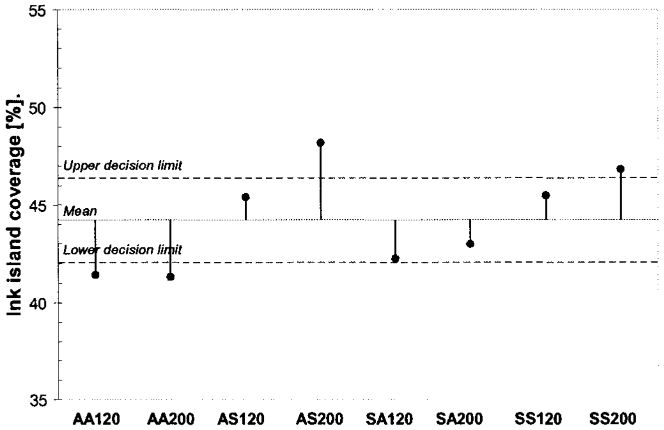

Figure 7.23 Ink island coverage on experimental papers: Cyan heatset heatset ink, C-3BT

The effect of delay time between the printing unit and the back-trap unit was also investigated: a single print was made for each delay time, the sheet weighing method being used for both paper and MYLAR substrates. The delay time was increased from 0.15 s, the value when the back-trap unit is loaded on the second nip of the two-nip Prüfbau press, up to 1 min, 5 min and hours, simulated by two passes on the press, a first pass with only the printing unit and no drying, followed by a second pass after the selected delay time with only the back-trap unit.

a. Effect of number of back-trap units

Table 7.5 shows the effect of number of back-trap units on the amount of ink back-trapped for commercial paper and for MYLAR sheets.

Table 7.5 Amount of ink [1]back-trapped with successive back-trap units

Number of back-trap units	**Paper**	**MYLAR**
1	43%	50%
2	15%	41%
3	negligible	40%
[2]*INK TRANSFER*	*46%*	*55%*

[1] *Ink back-trapped = ink on plate after printing/ink on substrate before back-trap*

[2] *Ink transfer for OBT printing configuration as determined in section 3.2 = ink on substrate after printing/ink on printing plate before printing*

The ink back-trapped on the 2nd and 3rd units is expressed relative to the amount of ink arriving at each unit. Thus for back-trapping from the MYLAR substrate the values of 50, 41 and 40% of Table 7.5indicate that after the 3 back-trap unit only 8% of the ink printed by the printing roll remains on the substrate. With paper as the substrate, Table 7.5 shows that the extent of back-trap decreases sharply with the number of back-trap units, from > 40% of the ink transferred to paper in the first unit, then only 15%, and then no measurable amount in the last unit. With only 0.15 s between the printing in the 1st and the 2nd nips it is not surprising that the ink back-trapped (43% for paper, 50% for MYLAR) is almost as much as the ink transfer from the first print roll (46% for paper, 55% for MYLAR). There is still some ink removed in the 3rd back-trap unit, as observed visually, but the amount could not be measured. By contrast for MYLAR there is only a slight decrease in back-trap from the 1st to the 2nd and 3rd back-trap units. On paper, ink consolidates by rapid transport of solvent and oil into the sheet while for impermeable

MYLAR, consolidation occurs only through solvent evaporation. Experiments to determine the ink solvent volatility from a thin ink film freshly printed showed that solvent evaporation is slow: less than 5% evaporation in 5 minutes, only about 18% after several hours. Thus the large fraction of ink back-trapped from MYLAR print in the successive back-trap units is as expected. On the contrary ink consolidation on paper proceeds by rapid ink vehicle transport into paper, leaving sharply reduced fluidity in the ink at the surface to be back-trapped by subsequent printing units. With only 0.15 s between printing in the 1st and 2nd nips, then about 10 s delay to replace the inked rolls with the pair of clean rolls, the sharp decrease from 43% to 15% back-trapping after the one and two back-trap units, Table 7.5, is consistent.

For printing on commercial paper, Figure 7.24 and Figure 7.25 show that with a single back-trap unit the effect from ink removal on optical density by back-trapping– a 33% drop – is much greater than for print gloss – 9% drop. Print gloss is in turn more decreased by the 2nd and 3rd back-trap unit than optical density. Optical density relates directly to the amount of ink, so for paper the effect of number of back-trap units on optical density, Figure 7.24, closely parallels that for ink back-trapped, Table 7.5. However print gloss, being a measure of ink film roughness depends not only on ink film thickness but also on its uniformity as seen in section 3.2.3. Thus where the loss of optical density becomes much less pronounced after successive back-trap units, the degradation of print gloss, Figure 7.25, remains substantial after passing through the 2nd, 3rd, and 4th nips. Figure 7.25 shows that the change in print gloss of paper drops by 3, 2, and 1 point after 1, 2 and 3 back-trap units, while the change in ink amount occurs mostly in the 1st unit. The change in ink film uniformity requires first investigation. While the 1st back-trap unit seems to remove quite a uniform ink layer over the entire print, the succeeding two units appear to remove ink selectively and leave patches or islands of darker or thicker ink areas as reported in section 3.4.2 and seen in Figure 7.26. This behaviour is related to nonuniform ink setting into the coating layer as discussed earlier. Thus although less ink is removed from the 2nd and 3rd back-trap units, print gloss continues to drop as there is more nonuniformity in removal of the back-trapped ink, so that ink film microroughness is increased.

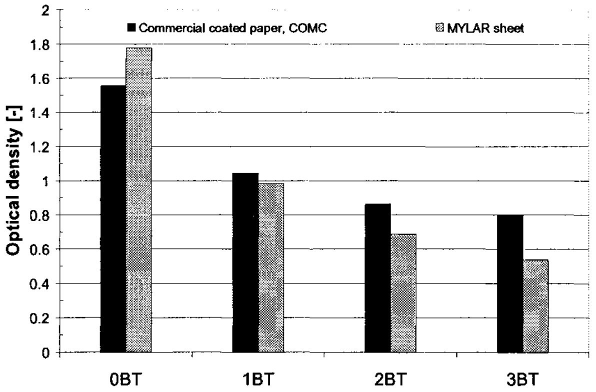

Figure 7.24 Effect on optical density of number of back-trap units: Cyan heatset ink, T-2 & T-6

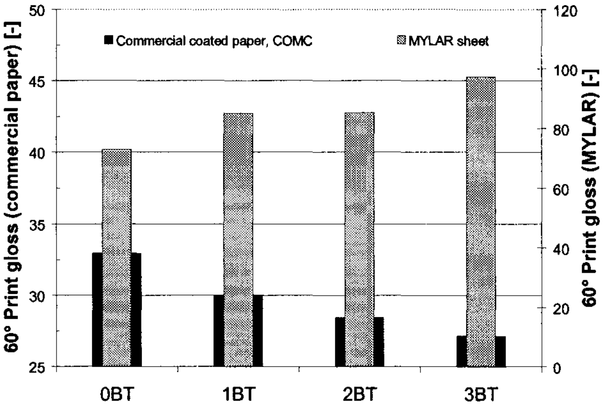

Figure 7.25 Effect on print gloss of number of back-trap units: Cyan heatset ink, T-2 & T-6

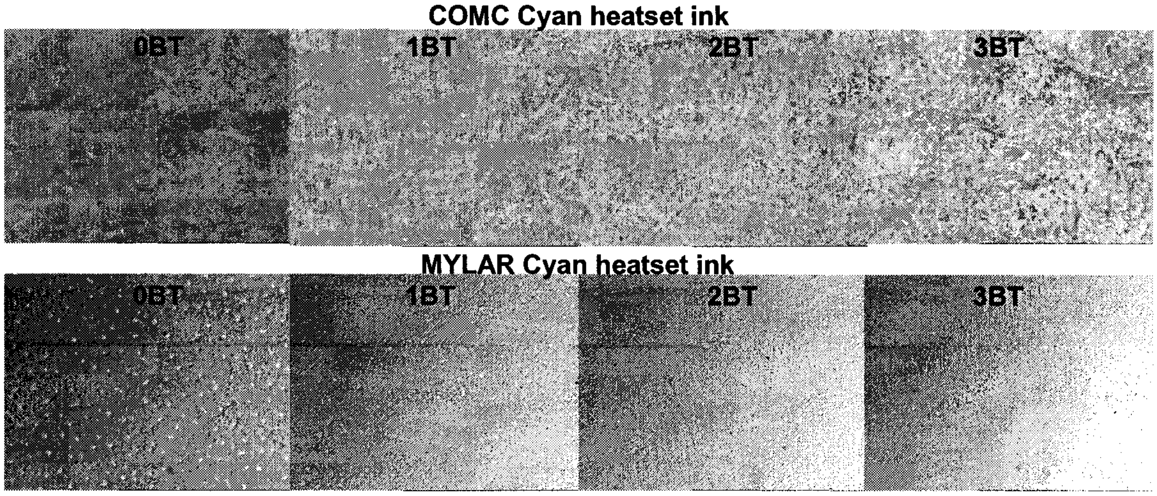

Figure 7.26 Effect on ink distribution of number of back-trap units: Cyan heatset ink, T-2 & T-6 (individual image width 3 mm)

For printing on MYLAR substrate, again optical density evolution with number of back-trap units, Figure 7.24, closely parallels that for ink back-trapped, Table 7.5. As for gloss on the MYLAR substrate, the behaviour is strikingly different than for paper. For MYLAR, the unprinted surface is smoother, thus shinier than the printed surface. Thus for MYLAR substrate, with increasing number of back-trap units the optical density decreases even more than for paper, Figure 7.24, but now print gloss increases, Figure 7.25, because of the mechanism above noted.

b. Effect of delay-time before back-trap units

The effect of increasing delay time before the back-trap unit, recorded in Table 7.6, indicates the extent to which the ink sets by both ink vehicle penetration into the substrate and evaporation in the case of paper but by evaporation only in the case of the MYLAR substrate.

Table 7.6 Effect of delay time before back-trapping on amount of ink back-trapped

Delay time before back-trap	**Paper**	**MYLAR**
0.15 s	43%	50%
60 s	34%	40%
5 min	14%	45%
hours	negligible	negligible

The less ink removed, the higher the optical density for both paper and MYLAR substrates, Figure 7.27. In the case of paper, Figure 7.28 shows that delay time before back-trap unit does not significantly affect print gloss, which is 32+/-2 points for all conditions measured. As discussed above, for paper s the substrate, print gloss depends on both the amount of ink, so is expected to increase with delay time, but also on the micro roughness of the ink film. Figure 7.29 shows that increasing delay time before back-trapping leads to more selective removal of ink, as for increasing the number of back-trap units. The print gloss after 5 min and hours of delay time before back-trapping may be lower because of this nonuniform distribution of ink at the surface of paper. A single print was made for this test which limits the extent of analysis possible. Print gloss on the MYLAR substrate decreases with increasing delay time, Figure 7.28, as more ink is left at the surface of a substrate for which, as noted above, the unprinted surface is shinier than the print.

3.4.4 Conclusion

For the cyan heatset ink used in this study, ink setting by evaporation was slow, as observed from back-trap experiments with time delays on MYLAR. By contrast, ink setting on paper by transport of ink vehicle into the coating occurred within the time scale of the printing experiment in the back-trap configuration. Most of the ink sets in less than 1 minute. With fast ink setting on paper, local nonuniformity becomes apparent. Thus indirect measurement of ink setting was allowed through the ink island coverage determination. Drying conditions affected the average ink setting rate: coated sheets for which the coating was dried in superheated steam showed faster ink setting rate. In addition, the pattern of locally darker areas appeared finer for coated paper dried in steam which may explain the better print mottle observed for this paper in section 4.3. Local nonuniformity in ink setting leads to local nonuniformity in ink back-trap which decreases print gloss and creates print mottle

Since ink setting rate is related to coated paper porous structure as discussed in section, the effect seen here would support the air entrapment mechanism proposed in section 3.3.4, to explain the increasing density of ink craters for coating dried in steam.

4. Printing properties of cyan prints

4.1 Measurements of printing properties changes

The results presented next concern the printing properties of the 8 sets of experimental paper with standard printing properties, e.g. heatset offset cyan ink printed from a plate at 3.05 g/m^2 ink load at 3 m/s printing speed with 600 N nip load. Table 7.7 presents the limiting values of printing properties. From Table 7.7 It is notable that the choice and range of experimental parameters used produced a change in print properties about an order of magnitude greater than the decision limit for the properties for which that is available. Also, relative to the change considered significant for the paper quality, the range of print density was slightly larger while the range for print gloss was larger by a factor of 10:1 or greater. Thus the limiting values shown in Table 7.7 establish that the printing properties were measured to a high reliability and that the experimental plan involved changing parameters that had very significant effects on these key printing properties.

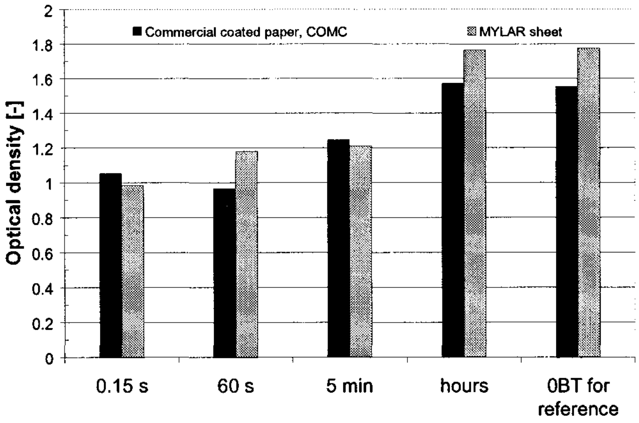

Figure 7.27 Effect on optical density of delay time before back-trap unit: Cyan heatset ink, T-3 & T-7

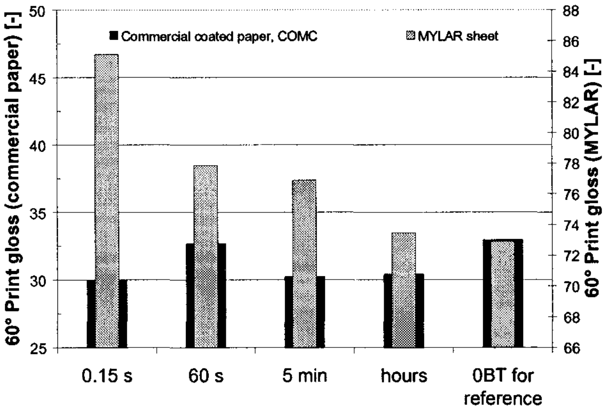

Figure 7.28 Effect on print gloss of delay time before back-trap unit: Cyan heatset ink, T-3 & T-7

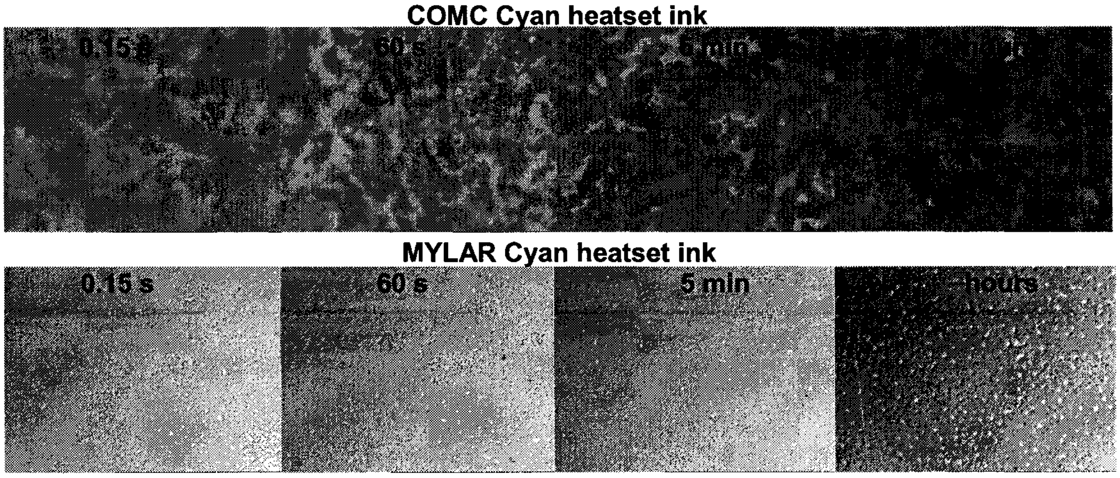

Figure 7.29 Effect on ink distribution of delay time before back-trap unit: Cyan heatset ink, T-3 & T-7 (individual image width 3 mm)

The changes in properties found for changing between the two drying fluids and the two drying fluid temperatures which are recorded in Table 7.8 are analysed in the next sections.

Table 7.7 Limiting values of calendered coated paper printing properties

Property	**[1]Significant change**	**[2]Decision limit**	**Min**	**Max**	**[3]Absolute change**
Print density, 0BT	0.1	0.011	1.53	1.64	0.11
Print density, 3BT	0.1	0.016	0.73	0.85	0.12
Print gloss, 0BT	2	0.9	33.6	48.1	14.5
Print gloss, 3BT	2	0.9	28.3	37.7	9.4
[4]Print mottle, subjective evaluation	n/a	0.12	3.17	7.72	4.6
[5]Print mottle, instrumental determination	n/a	0.057	0.95	1.16	0.21

[1] "Significant change" is the change significant to a papermaker for LWC paper quality

[2] The "decision limit" is calculated as described in Chapter 3 section 7 from the pooled standard deviation among all 8 sets of samples tested in this chapter

[3] "Absolute change" is the difference between the maximum and minimum values

[4] The values from Group 2 mottle evaluation are reported as explained in section 4.3.2

[5] The values for mottle at 1.5 mm of scale of mottle are reported as explained in section 4.3.3

4.2 Print density

4.2.1 The 0BT printing configuration

Figure 7.30 and Table 7.8 show that the print density varied with the drying conditions used to produce coated paper although Figure 7.9 demonstrated that there was no corresponding effect on the amount of ink transferred to the paper. The variations are not large but are statistically significant.

Table 7.8 Absolute and normalized changes in coated paper printing properties with drying conditions

Property	Base paper drying medium				Coated paper drying medium				Coated paper drying temperature			
	AA120->SA120	AA200->SA200	AS120->SS120	[2]AS200->SS200	AA120->AS120	[2]AA200->AS200	SA120->SS120	SA200->SS200	AA120->AA200	[2]AS120->AS200	SA120->SA200	SS120->SS200
[1]Absolute change												
Print density, 0BT	0.03	0.01	0.03	0.06	-0.04	-0.08	-0.04	-0.03	0.00	-0.04	-0.02	-0.01
Print density, 3BT	0.03	0.06	0.02	0.06	0.03	0.06	0.02	0.06	-0.02	0.01	0.01	0.05
Print gloss, 0BT	-1.5	-4.3	-1.1	-2.5	-9.9	-11.2	-9.5	-9.4	-0.8	-2.1	-3.5	-3.5
Print gloss, 3BT	-0.0	-3.7	-0.2	-2.4	-6.2	-6.9	-6.3	-5.6	-0.2	-0.9	-3.8	-3.1
Print mottle, subjective	-0.7	-3.4	0.6	0.0	1.2	1.1	2.6	4.6	1.1	0.9	-1.6	0.4
Print mottle, instrumental	0.11	0.19	0.097	0.10	-0.06	-0.02	-0.07	-0.11	-0.06	-0.02	0.02	-0.01
[2]Normalized change												
Print density, 0BT	4	1	3	6	-4	-8	-4	-4	0	-5	-2	-1
Print density, 3BT	2	5	2	4	2	5	2	5	-2	1	1	4
Print gloss, 0BT	-2	-6	-2	-3	-13	-15	-13	-13	-1	-3	-5	-5
Print gloss, 3BT	0	-5	0	-3	-8	-9	-9	-8	0	-1	-5	-4
Print mottle, subjective	-7	-35	6	1	13	11	27	47	11	10	-17	4
Print mottle, instrumental.	2	4	2	2	-1	0	-1	-2	-1	0	0	0

[1] *The absolute change is the difference between the two conditions tested*

[2] *The normalized change is the ratio of the absolute change to the decision limit for that property (Table 7.7)*

Zang and Aspler (1998) report that an average viewer is sensitive to a difference in print density of about 0.02 units, while differences of up to 0.11 density units are found in the present study. Coated paper for which the base sheet was dried in steam gave higher print density while that for which the coating was dried in steam gave lower print density. As noted previously, print density depends mostly on the ink amount transferred to paper, Zang and Aspler (1998). As the ink transfer remained constant for the set of sheets tested here, no change in print density is expected. However as noted in section 3.3.2, ink craters were observed and moreover, depending on the drying conditions used, the density of ink craters was variable: a higher number density of craters was seen on sheets for which the coating was dried in steam, Table 7.4 and Figure 7.20. The diameter size of these ink craters, areas containing virtually no ink, is at the low end of the range used for halftone dots generally. It is therefore probable that ink craters act like halftone light spots on a dark cyan tone, decreasing the apparent print density. However the effects on ink craters from base sheet drying strategy and coating drying fluid temperature were not clear and cannot explain the changes in print density observed here.

4.2.2 The 3BT printing configuration

Results obtained for the print density of cyan print with the 3BT configuration, Figure 7.31, are substantially different from those for the 0BT case, Figure 7.30, as is documented by the various bases of comparison presented in Table 7.8. Superheated steam drying of either the base sheet, the coated sheet, or at both stages leads to higher print density. Contrary to 0BT sheets, those from 3BT printing have a variable amount of ink as determined by the ink island coverage measurement, Figure 7.23. The variation of ink weight may therefore explain the variation in print density with drying conditions after 3 back-trap units compared to the no back-trap case. Figure 7.9 shows that the same ink amount was transferred to the paper in the printing unit for all 8 drying conditions tested. However a quite variable amount of ink remains on the sheet after the 3BT printing configuration. The amount of ink transferred to the back-trap units is believed to depend on ink setting rate, Piette et al. (1999) and Xiang et al. (2000): the faster the coating consolidates the ink, the less ink will be back-trapped.

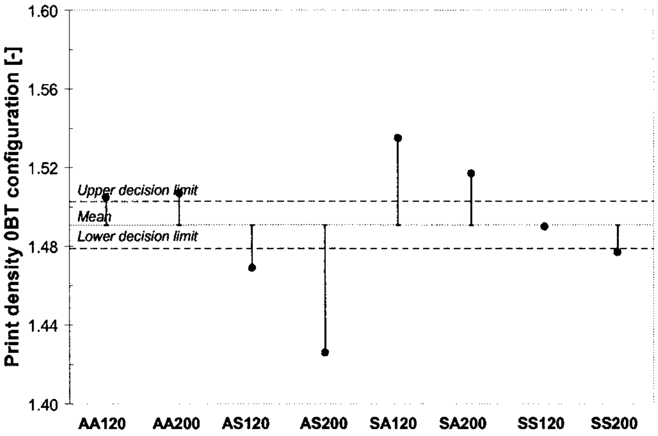

Figure 7.30 Effect of drying conditions on print density with no back-trap unit: Cyan heatset ink, C-0BT

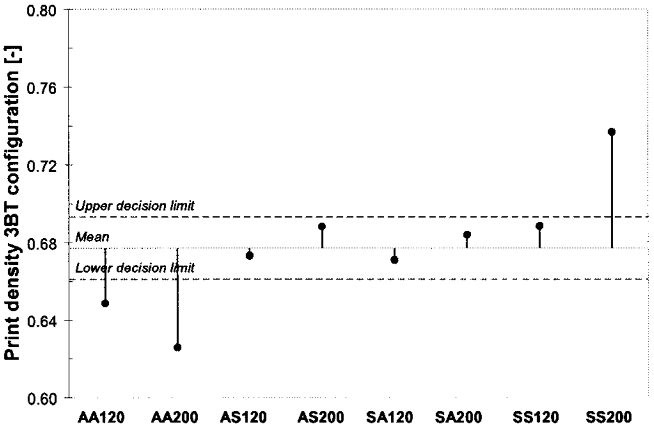

Figure 7.31 Effect of drying conditions on print density with three back-trap units: Cyan heatset ink, C-3BT

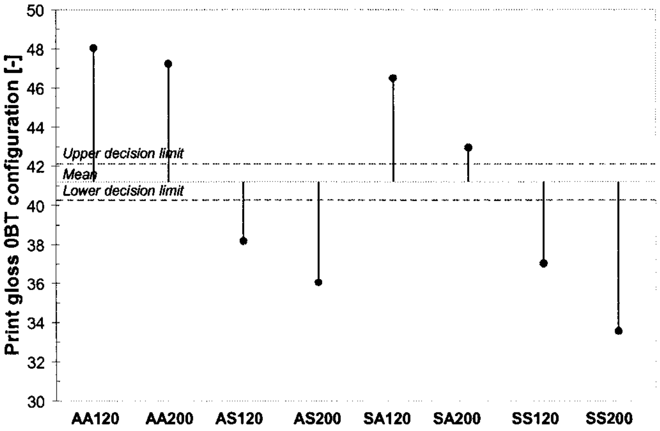

Figure 7.32 Effect of drying conditions on print gloss with no back-trap unit: Cyan heatset ink, C-0BT

The ink island coverage results of Figure 7.23 therefore indicate that drying conditions affect ink setting rate and, in particular, that ink sets faster on coated paper for which the coating was dried in superheated steam, which increases print density. Although paper made using drying condition AS200 retained more ink than paper from condition SA120, the corresponding print density was not much higher. Because the ink amount on the paper surface for the 3BT case is much less than for the 0BT configuration, the contrast between areas inked and not inked is much less. As a consequence ink craters would not appear due to the lack in contrast. However ink craters were still detected and showed the same trend, i.e. more ink-free craters on paper for which the coating was dried in steam because these were generated in the printing unit only and remained unaffected by the back-trap units. The ink crater characteristics may therefore again lead to lower print density for steam dried coating although overall more ink was kept at the paper surface.

4.3 Print gloss

4.3.1 The 0BT printing configuration

For drying the coating, Figure 7.32 and Table 7.8 show that large differences in print gloss with cyan ink were obtained between drying in air or in superheated steam. How the base sheet was dried had less effect, but in the same direction: lower gloss when drying in steam. Increasing drying fluid temperature also decreased gloss slightly. However the major effect is that a substantial reduction in print gloss results from switching the fluid from air to steam for drying the coated sheet. Like print density, print gloss depends to some extent on ink amount. However as mentioned in section 3.2.2, the most important effect is the inverse relation of print gloss to ink film nonuniformity at the micro scale, whether coming from either the coated paper surface roughness or the ink film nonuniformity. In section 3.2.2 it was suggested that paper roughness explained differences in print gloss obtained with black coldset ink.

Here for cyan heatset ink the paper roughness variation does not seem to be the major contributor to print gloss variation because the trend for paper gloss with drying strategy, in Chapter 6 Figure 6.21, is very different from that for print gloss. For example, sheets from drying strategies AS200 and SA120 have similar paper gloss but very different print gloss, while AA120 and SA120 drying conditions produce very different paper gloss but only slightly different print gloss. Therefore ink film nonuniformity is the likely the explanation for print gloss variation. The presence of the ink-free craters reported in section 3.3.1 has probably decreased print gloss. It is notable that print density and print gloss trends are similar except for the effect of base sheet drying strategy. So if ink craters explain the main print density trend, the same effect may also explain the main print gloss trend. The effect of using superheated steam when drying the base paper is not fully understood. The slight decrease in print gloss when drying the base paper in steam may come from paper roughness at a large scale, which was higher for such paper.

4.3.2 The 3BT printing configuration

There is a very good correlation between print gloss with cyan ink between the 0BT and 3BT configurations, Table 7.8 and Figure 7.32 and Figure 7.33. Absolute print gloss is of course lower for the 3BT case because of the smaller amount of ink remains after multiple back-trapping, less than half the original amount. As noted earlier, print gloss depends primarily on ink film roughness but to some extent also on ink film thickness. The ink island nonuniformity structure after the 3BT printing configuration, described in section 3.4.1, explains the lower gloss of paper for which the coating was dried in superheated steam because such paper showed more discrete ink islands. A greater local micro scale variation in ink film thickness, as is the case here, lowers print gloss considerably. Also the ink craters created in the printing unit, even if less visible after 3 back-trap units are still present, and would contribute to decreasing the print gloss.

4.4 Print mottle

4.4.1 Effect of printing configuration on print mottle

For paper printed with cyan ink from a plate at 3.05 g/m^2 ink load, at 3 m/s under a nip load of 600 N, the sheets printed with a single printing unit did not show much print mottle. Little difference was detectable by eye between the different drying conditions and even between experimental and commercial paper. Print local nonuniformity may be difficult to detect because of the high print density of these solids prints, it being well known that mottle of solid print is most visible at low print density, i.e. light prints such as skies. At the relatively high printed ink load of 1.4 g/m^2 the macro scale ink transfer remained unaffected by drying conditions, as reported in section 3.2.2. Although inspection by light microscopy showed the patterns identified earlier as ink craters and ink filament remains, by eye no local nonuniformity in print density could be detected.

By contrast with the 3BT printing configuration, there was visible mottle and clear differences in mottle between papers dried under different conditions as illustrated in Figure 7.34. Subjective evaluation of print mottle is complicated by the dependence on print density noted above. Therefore print quality was evaluated with both subjective ranking by a panel of judges and instrumentally.

There are no accepted standard methods for evaluating print mottle, either subjectively or instrumentally, therefore the methods used are first described.

4.4.2 Subjective evaluation of print mottle

a. Method

"Proscale" is a statistical protocol developed by Donderi (1997) for subjective evaluation of similarity. This multidimensional scaling program allows finding the linearly independent dimensions that describe the similarity judgements made by observers. The uniqueness of the method is to present that the observer views at one time as many examples as possible of the items to be ranked. Donderi and Aspler (1994, 2000) applied this method for ranking prints. The most common method for ranking prints has been the all-pairs ranking for which observers need to compare every pair of items. The time required for such an evaluation increases the cost and limits the number of sheets that can be submitted for ranking. The advantage of Proscale is that as many as 45 prints may be ranked simultaneously in about 30 minutes (Donderi and Aspler, 1994).

In the present study the Proscale method and associated program in the Preference mode, e.g. one-dimensional scaling, Donderi (2002), were used to evaluate the nonuniformity or mottle of solid prints made using the 3BT printing configuration. A panel of 15 judges examined 44 sheets; 5 replicate sheets for each of the 8 drying conditions used for the experimental paper and 4 replicate sheets for the commercial paper. The evaluation took place, as recommended, in a large room combining natural and artificial light leading to a light intensity well above the minimum 50 lux required. Each observer did the evaluation separately, being given written instructions and allowed to ask questions when necessary.

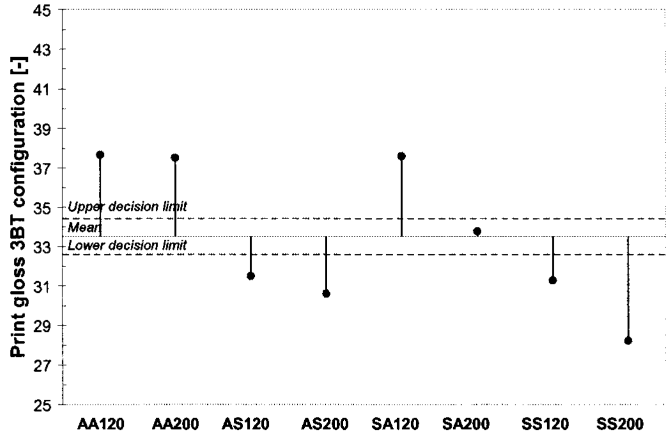

Figure 7.33 Effect of drying conditions on print gloss with three back-trap units: Cyan heatset ink, C-3BT

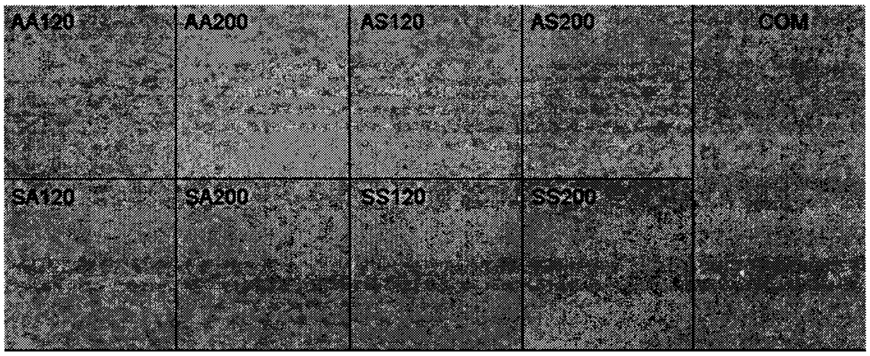

Figure 7.34 Print mottle pattern after three back-trap units: Cyan heatset ink, C-3BT (individual image width ~3 cm)

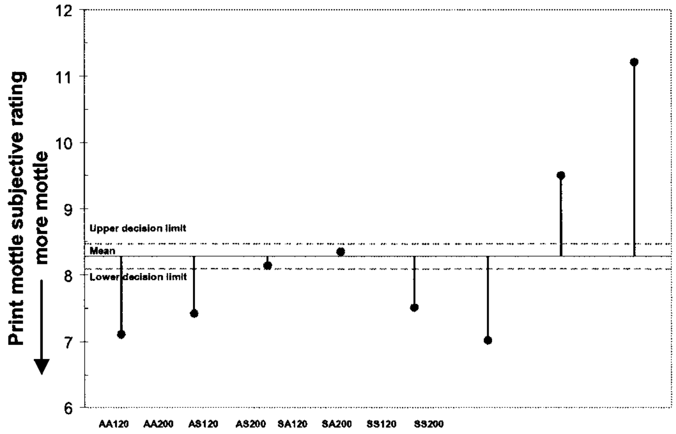

Figure 7.35 Subjective determination of print mottle after 3 back-trap units; 15 observers: Cyan ink, C-3BT

The observer was asked to rate prints according to how much nonuniformity they saw in them, using any scale they preferred provided a higher number means a better print, i.e. less nonuniformity. The instructions and rating sheet are given in Appendix D.

A feature of the Donderi method is that each judge is allowed to use a rating scale of their choice, i.e., 0-5, 1-10, etc. The program normalizes the scales used by each observer and allows calculation of average values for each sheet among all the observers, as well as the average for each set of replicate sheets from the same production condition. Another feature of the program is the identification of the number and the composition of distinct subgroups of observers whose judgements are found, by the principal components analysis method, to be similar. This method identifies the inter-correlations between ratings, the principal components and the associated variance percentages that indicate how much of the variance across observers can be accounted for by each subgroups.

b. Results

The results of the principal component analysis are presented in Table 7.9. There is a large increase in the percentage of variance which is explained when the number of subgroups is increased from 1 to 2, +0.15 points, with more than 50% of the variance then explained. Thus there are clearly two distinct subgroups of observers whose ratings may be analysed separately: Groups 1 & 2 of respectively, 11 and 4 individuals[1].

Table 7.9 Analysis of subgroups of observers

Number of groups	1	2	3	4	5	6	10	15
Cumulative fraction of variance explained	0.36	0.51	0.60	0.69	0.74	0.79	0.92	1.0

The ratings for the 44 sheets from the 15 observers gave the results presented in Figure 7.35 for all 15 observers together, Figure 7.36 for Group 1 only and Figure 7.37 for Group 2. The rating process, which most of the observers said was difficult, was completed in an average of 30 minutes (range of 15 to 80 minutes). For the 11 observers of Group 1, their rating was highly affected by the print density of the sample as indicated by a R^2 value of 0.86 between the two properties. As is well known, it is more difficult to see local print density nonuniformity on a darker print. However the 4 observers of Group

---

[1] *My ranking, not included in the analysis, would place me in Group 2*

2 did detect the print mottle differences between the samples independently from print density, R^2 value of only 0.09. The ratings from Group 2 are therefore considered as the subjective evaluation of the prints. Analysis of the effect of drying conditions based on subjective evaluation is deferred for consideration along with the comparable results determined from instrumental evaluation.

4.4.3 Instrumental determination of print mottle:

a. Method

The objective technique used to evaluate print mottle derives from the commercial "PaperPerFect" instrument developed for the determination of paper formation nonuniformity. The PrintPerFect adaptation of this paper formation analyzer using essentially the same algorithm for the measurement of solid print nonuniformity, but using reflected rather than transmitted light, Bernié and Douglas (2001). The technique partitions solid print nonuniformity into its components relative to the scale of the print nonuniformity for 9 values of scale of print mottle over the range of scale 0.4-18 mm. The specific values of scale of print mottle used here are 0.4, 0.6, 1.0, 1.5, 2.5, 4, 7, 11 and 18 mm. With this method, a determination leads not to a single-number index of print mottle, but to a Print Mottle Line which provides the components of print nonuniformity as a function of the scale of print mottle.

From each replicate sheet 2 independent images, 32.5 mm x 32.5 mm, were taken in reflected light for print mottle analysis. Since 5 replicate printed sheets were made, this procedure provided 10 independent determinations of print mottle for each of the 8 drying conditions with the experimental paper and 10 determinations for the commercial paper. For each paper the 10 determinations were averaged to give a single Print Mottle Line representative of that paper. The higher the print nonuniformity, the worse the mottle. These print mottle results are most easily interpreted when expressed relative to those for a standard sheet, leading thereby to values of intensity of print nonuniformity which are of the order of unity. Commercial coated paper made from the same pulp furnish and similar coating materials but produced in a paper mill, designated as COMC, was used as the reference sheet for the components of print nonuniformity of the experimental coated paper. With this method the print mottle is relative to the commercial paper, thus a value of 1.15 for a print mottle component means that, at this value of scale of print mottle, there is 15% more print nonuniformity than for the reference sheet. Similarly, a print mottle component of 0.9 means 10% less solid print nonuniformity than for the reference sheet.

b. Results

The results in the form of 8 Print Mottle Lines are given in Figure 7.38. One clear characteristic is that the mottle of experimental paper relative to that for commercial paper varies with scale of mottle. Another characteristic is that over the lower range of scale of print mottle the intensity of mottle of the experimental paper is greater than that for commercial paper, but over the upper range of scale the effect is the opposite, i.e. mottle on the experimental paper is less than that on commercial paper. Figure 7.38 shows that it is not possible to make a generalization as whether the experimental papers have better or worse mottle than commercial paper, the reality being that the experimental papers have both better and worse mottle, depending on the scale of mottle. This switchover from worse then to better than commercial paper occurs in the range of 1-4 mm scale of mottle, the exact value depending on the conditions used for drying the base sheet and the coated sheet.

As noted earlier the base paper for the experimental coated paper was made from essentially the same furnish, obtained from the same mill from which the comparative commercial base paper and commercial coated paper were obtained. The print mottle work reported here uses this commercial coated paper as the basis of comparison for the experimental coated papers. The laboratory produced coated paper tested in this chapter differs in two ways from the comparative commercial paper: the base sheet is made on a Dynamic Sheet Former and the coated sheet is produced in the laboratory coater-dryer facility. In Chapter 5 the print mottle of coated paper made in the laboratory using commercial base paper was evaluated relative to this same commercial coated paper. This experimental plan now enables examination of the effects from the base paper forming technique separate from the effects of the coating technique as sources of the trends apparent in Figure 7.38 and Figure 5.19 for the difference in print mottle between the laboratory and industrial coated paper.

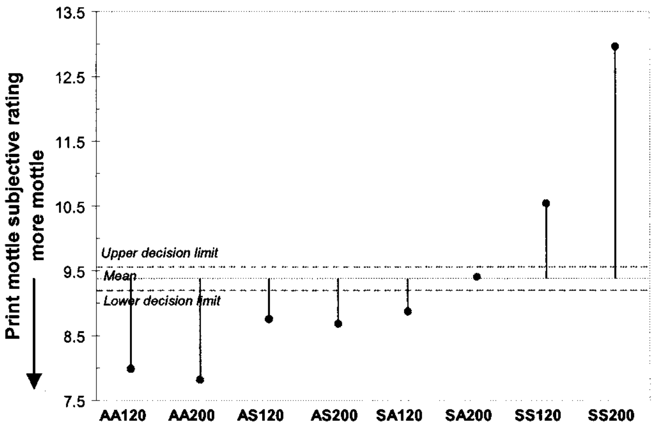

Figure 7.36 Subjective determination of print mottle after 3 back-trap units; Group 1, 11 observers: Cyan heatset ink, C-3BT

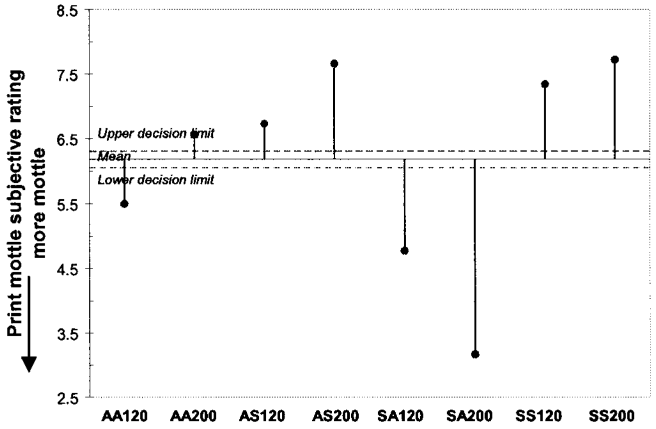

Figure 7.37 Subjective determination of print mottle after 3 back-trap units; Group 2, 4 observers: Cyan heatset ink, C-3BT

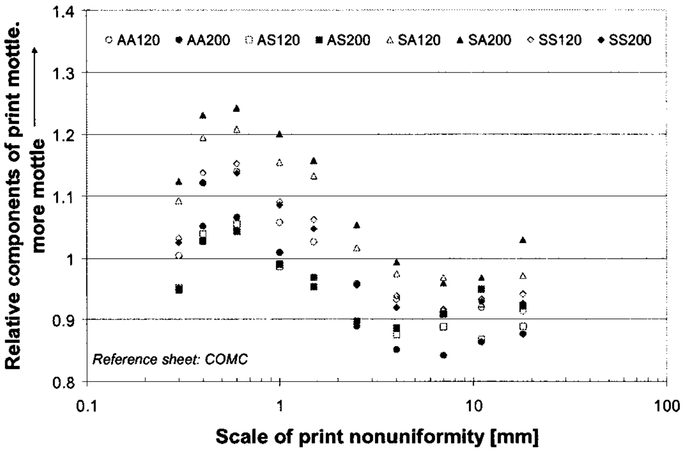

Figure 7.38 Instrumental determination of print mottle after 3 back-trap units: Cyan heatset ink, C-3BT

Figure 7.39 shows the Print Mottle Lines of laboratory coated papers made from commercial base paper (COM) and laboratory Dynamic Sheet Former (DSF) paper, the components of print mottle being relative to the commercial coated paper (COMC). The Print Mottle Lines of Figure 7.39 reveal that both the forming and the coating techniques affect print mottle. For laboratory formed paper, print mottle was reduced significantly over the range 0.4 to 1.5 mm scale of mottle as compared to commercial base paper which was then laboratory coated under the same conditions.

Local grammage nonuniformity, i.e. formation, is the paper property related to the forming technique. The components of formation nonuniformity were determined with transmitted light by the PaperPerFect method for the Dynamic Sheet Formed laboratory base paper using the commercial LWC base paper (COM) used for producing the commercial coated paper reference for the print mottle determination of Figure 7.39. The result from this procedure was reported in Figure 3.17: over the 0.4 to 18 mm scale of formation the laboratory base paper showed better formation than the comparable commercial base paper. With only two samples for each technique it is not possible to conclude definitively on the effect of formation on print mottle. However there is consistency between the difference in base sheet formation, laboratory DSF formed vs. commercial paper, Figure 3.17, the difference in the print mottle between those papers, Figure 7.39. Better formation over 0.4-18 mm scale of formation is associated with less print mottle over the 0.4-7 mm scale of mottle. Both the forming and coating techniques affect print mottle, especially at small scale 0.6 to 1.5 mm. The laboratory coating technique increased mottle while the better formation provided by the laboratory forming technique improved print mottle at small scale, these effects being more pronounced at small scales < 1.5 mm.

Another characteristic of the results on Figure 7.38 is that there is relatively little crossing of the Print Mottle Lines for the 8 drying conditions tested. In other words, between the various drying conditions the pattern of mottle intensity vs. scale of mottle of the experimental paper does not vary much with scale, but the level of the intensity of mottle varies considerably. Thus drying conditions change the intensity of print mottle substantially but these changes are similar in magnitude over the 0.4-18 mm range of scale of print mottle of this test method. Therefore the values of the print mottle components at the intermediate value of print mottle scale of 1.5 mm is used as indicative of the effect of drying conditions on intensity of mottle.

4.4.4 Effects of drying on print mottle: Subjective and instrumental determination

Both subjective and instrumental methods reveal a significant effect of drying fluid choice on print mottle. Figure 7.37 and 7.40 show that with both methods superheated steam drying of base paper increases mottle and superheated steam drying of coated paper decreases mottle. Also the effect of drying fluid temperature was minor according to both mottle determination techniques except for the AIR-AIR drying strategy: increasing the drying temperature decreased mottle in this case.

An integration of the results of print mottle evaluation by the two methods is presented through Figure 7.41. Figure 7.41 shows the relation between the instrumental and subjective determination of print mottle. The least squares line on Figure 7.41 shows that the relation between the instrumental and subjective determination is less close than would be desired, with an R^2 value of 0.56. The negative slope of the correlation line reflects the fact that more mottle means a higher number in the instrumental measurement of print nonuniformity but a lower number in the Proscale subjective evaluation. Both subjective and instrumental methods identify the case of worst print mottle as being SA200, and likewise agree on the second worst print mottle, that for drying with SA120. At the other extreme, AS200 gives the least print mottle by the instrumental determination and is effectively tied with SS200 for the least mottle by the subjective evaluation.

The results for the 8 drying conditions tested fall into two sets of four conditions, differentiated by whether the base sheet is dried in air or in steam. Within each of these sets there is consistency between the results for print mottle whether determined instrumentally and subjectively. For coated paper produced from steam-dried base paper, there is seen on Figure 7.41 shows that there is less print mottle if the coated sheet is dried in steam rather than in air. When air dried base paper is used, Figure 7.41 shows the same effect, i.e. there is less print mottle, whether determined instrumentally or subjectively, if the coated sheet is dried in steam rather than in air. For air-dried base paper, the extremes are the worst print mottle for drying the coated sheet in 120°C air (AA120) and the least print mottle for drying the coated sheet in 200°C steam (AS200).

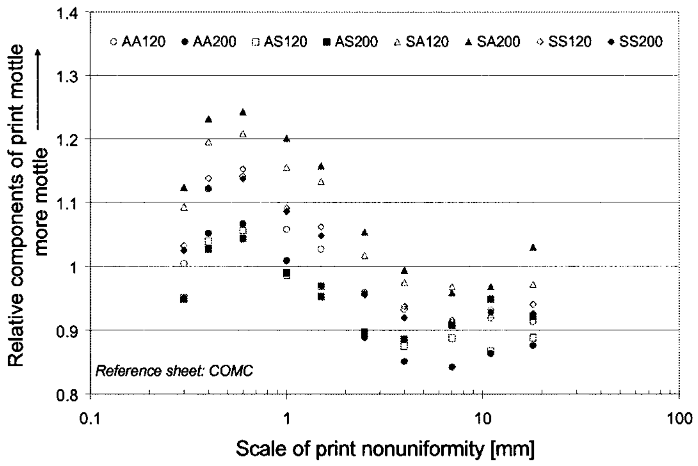

Figure 7.39 Comparison of Print Mottle Lines after 3 back-trap units: Laboratory coated on DSF and commercial base papers

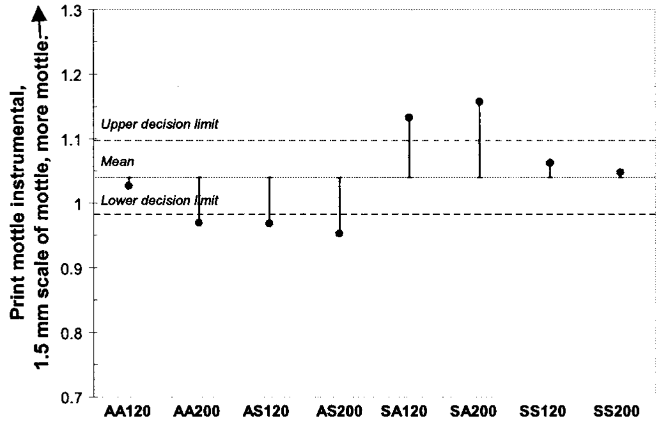

Figure 7.40 Instrumental determination of print mottle at 1.5 mm scale of mottle, after 3 back-trap units: Cyan heatset ink, C-3BT

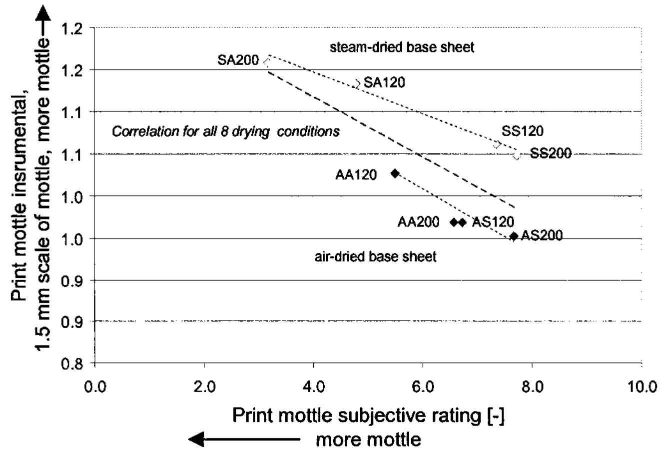

Figure 7.41 Print mottle by subjective and instrumental methods: Cyan ink heatset, C-3BT

Also for three out of the four pairs of conditions where temperature is the only difference, the use of the higher drying fluid temperature gives less mottle, by both instrumental and subjective evaluation. The only exception is the SA120 vs. SA200 condition, two conditions giving the worst mottle of the 8 cases, as noted above. Thus within each of the two subsets, according to the drying fluid used for the base paper, there is consistency and a high correlation between print mottle determined instrumentally and subjectively. However this good agreement between the two methods exists along with a relatively poor correlation for coated sheet print mottle when the results are not segregated according to the drying fluid used to produce the base paper. The reason for this limited correlation is not yet apparent.

5. Conclusions

Printing performance of paper dried in various conditions was tested with two inks on a laboratory proof press. For the printing parameters used, ink transfer is the only printing property that remained unchanged, while print density, print gloss and print mottle were all affected. With heatset cyan ink, the ink transfer was not affected by drying conditions probably because the coating structure does not affect ink transfer at low ink loads but also possibly because of the short time scale at which ink transfer occurs relative to ink vehicle transport into paper.

In spite of the little variation ink transfer measured at the macro scale, differences were observed at micro scale among the prints depending on their drying history. Observation of the prints with light and SEM microscopy and a micro roughness profilometer revealed the presence of remains, ink hills and ink craters, from the ink splitting process occurring at the exit of the printing nip. The microscopy images proved these features were neither defects nor the results of coating picking. The number density and size of both ink craters and inks were highly sensitive to the substrate and the printing conditions, especially type of ink, ink load on the printing plate and printing speed. The evidence from SEM observation is that the ink craters are ink-free regions. Two mechanisms may explain the formation of such craters. The first mechanism relates to the initiation of cavitation occurring during ink film splitting. Air bubbles entrapped in coated paper surface crevices or pores would trigger heterogeneous nucleation of cavitation. As the bubble expands it detaches from the cavity leaving a small gas bubble behind. The gas bubble becomes the ink crater. The second mechanism relates to the mechanism of rupture of the ink filaments: ink craters would occur when a filament grew, without rupture, until all the ink from the wet ink film surface down to the substrate had been consumed in producing that filament. In the case of paper the ink crater pattern variation is believed to illustrate coating surface structure variation, the presence of crevices or voids may be responsible for both mechanisms previously described. For printing without the possibility for back-trapping, the drying conditions used when drying the coating affected the number of ink craters, indicating development of a different surface structure.

The back-trap experiments showed that ink setting on paper by transport of ink vehicle into the substrate occurs rapidly, at a similar time scale as that involved in the four-nip configuration printing. The investigation thereby possible concerning the ink setting rate and local variation in setting rate showed variation with drying conditions used to produce the coated sheet. The heatset cyan ink sets faster on paper for which the coating was dried in superheated steam, and the local nonuniformity in ink setting rate occurs at a smaller scale than for a coating dried in air, resulting in higher ink island coverage, higher print density, less print mottle, and lower print gloss in the printing configuration allowing back-trapping.

The printing properties measured on sheets printed with cyan ink in standard single-nip and four-nip printing were affected by both base sheet and coated sheet drying conditions. Print density showed the opposite trend when evaluated for single nip and multiple nip printing configurations. In the case of steam drying of the coating, this decrease in print density appears to be the consequence of the presence of more ink craters. As for print gloss, there was consistency between results without back-trapping and with three back-trapping units. Superheated steam drying of the base sheet only slightly decreased print gloss. Superheated steam drying of the coating decreased print gloss greatly. This large decrease in print gloss was related to the difference in surface structure developed during drying the coating in steam. Specifically, for printing without the possibility of back-trapping, drying in steam led to a denser pattern of ink craters while in the 3BT configuration it led to a denser pattern of ink islands left after back-trapping. In both cases the higher level of print surface nonuniformity or micro-roughness of the ink film decreased print gloss.

Print mottle showed similar trends when evaluated by a recent subjective method and by a new instrumental method. Superheated steam drying of the base sheet increases mottle while steam drying of coated sheet decreases mottle. The mechanism related to the effect of base sheet drying strategy is not well understood. For the effect of drying the coating in superheated steam the effects found are believed to be related to a different surface structure developed for drying under higher sheet temperature.

For printing with three back-trap units the results for ink island coverage, print density and print gloss indicate that faster ink setting is obtained when drying the coating in superheated steam. This paper also shows a larger density of ink craters. Ink setting rate is related to the surface porous structure. Therefore it is hypothesized that differences in surface porous structure rather than in roughness are responsible for the ink craters.

Chapter 8 Conclusions

1. Summary

This work aimed at documenting the effects from drying conditions on coated paper quality. For drying the base sheet the variable was the impingement drying medium, air or superheated steam. For drying the coated sheet the variables were the impingement drying medium, drying medium temperature, drying time and coating-to-drying delay time. This work constitutes the first reported use of superheated steam for the production of coated paper.

A laboratory coating-drying facility was upgraded to enable investigation of the effects of drying conditions on coated paper quality. This facility allows impingement drying similar to industrial impingement air drying of coated paper, and a variable coating-to-drying delay time after coating application, down to only 0.2 s. This facility also enables drying with superheated steam, already used industrially for drying several materials, studied experimentally in this laboratory for uncoated paper but never applied to coated paper production.

The coated paper was typical of the Light Weight Coated (LWC) paper grade: a clay-latex-CMC coating was applied at 63% solids content to a base paper made from 60% ground wood pulp, 40% KRAFT chemical pulp. To investigate base paper drying, wet sheets were formed on a laboratory Dynamic Sheet Former using pulp from a mill producing coated paper. Those base sheets were dried, coated and then redried. For comparison, commercial base paper from the same mill was also coated and dried. Paper properties determined for both uncoated and coated sheets were thickness, permeability, optical properties and roughness. For uncoated paper, the strength properties and water sorption potential were documented as well. For coated paper, the gloss and printing properties were measured. Pore structure properties were also investigated using mercury porosimetry and SEM, and surface chemical composition using ESCA.

Compared to LWC base paper produced by air impingement drying, switching to impingement drying in superheated steam gives higher strength (breaking length increase of 20% in machine direction) but lower light scattering (brightness loss of 4 points) with a slight reduction in bulk and permeability. Steam drying of LWC base paper reduces roughness for scales below the fibre wall dimension (about 50 μm) but increases roughness at larger scales. The fines being rich in lignin, a hydrophobic material, its redistribution when drying in steam also increases water penetration time compared to air drying. Drying in superheated steam also increases the light absorption coefficient of LWC base paper.

Varying base sheet and coated sheet drying conditions has the largest effects on the following surface properties of the coated sheet: gloss, roughness and printing properties. The choice of drying fluid for the base sheet or the coating has the largest effect, followed by the drying fluid temperature for drying the coating. Unexpectedly, coating-to-drying delay time had only a small effect on the properties of coated paper.

Superheated steam drying of the base paper affects coated paper quality significantly, this effect being indirect, the different base paper structure obtained with steam drying affecting the coating consolidation. Relative to coated paper made from base paper dried in air, that produced from superheated steam dried base paper is rougher, with lower gloss and lower light scattering (brightness and opacity) than that from air dried base paper. The pores in steam dried base paper are larger, but there is no effect on the porosity of either the base paper or the coating.

Measurement of moisture decay under laboratory impingement drying indicates that the falling rate regime is already established by a drying time of 0.4 s for impingement air drying of the coating at jet temperature above 120°C. The drying rate for $t > 0.4$ s is only slightly affected by the coating-to-drying delay time. For impingement drying in air at 120°C or higher, the properties of coated paper continue to develop when drying is extended to bring the sheet moisture content below normal dryer exit moisture content. Coating shrinkage and dry coalescence of latex are proposed to explain this late development of paper properties.

The experimental evidence indicates that the significant changes in properties of coated paper which result from switching from air to superheated steam drying of the coated sheet are determined at drying time less than 0.6 s. The much higher sheet temperature reached almost instantaneously for drying in steam compared to that in air at the onset of drying is expected to affect the coating dewatering, the coating layer water vapour flow, the coating shrinkage and the coating wet latex coalescence.

Superheated steam drying of the coated sheet reduces its gloss and smoothness compared to air drying. Coating porosity is not affected. Coating mean pore size remains unchanged but the pore size distribution is wider. Increasing the drying fluid temperature from 120° to 200°C during coated sheet drying affects the coated paper properties less than the choice of drying medium used for drying either the base sheet or the coated sheet. The most consistent effects of increasing drying medium temperature are the reduction in gloss and smoothness.

The coating-drying conditions have no effect on the chemical composition of the coating surface as measured by ESCA.

Concerning printability characteristics determined with a single printing nip and with a four-nip printing configuration, the drying conditions have no effect on percent ink transfer at 3.05 g/m^2 of cyan heatset ink on the press, the only ink load tested. Ink craters and conical ink hills, produced by the ink film splitting process, were found by microscopy and profilometry on prints made on various paper and Mylar substrates. With commercial cyan heatset ink the density of ink craters was greater on coated sheets dried in steam. The presence of more roughness crevices or surface micro voids with steam drying of the coating may explain the different ink splitting remains pattern observed. The effects that changes in coated sheet drying have on ink back-trapping illustrate changes in the surface porous structure of the coating. Less ink back-trap was observed and local nonuniformity in back-trap at smaller scale was found for coated sheets dried in superheated steam than in air.

Compared to air drying, superheated steam drying of the base paper increases print density and decreases print gloss, with these effects found for both the single and the four-nip printing configurations. Steam drying of the coating decreases both print density and print gloss in the no back trap configuration of a single printing nip. The greater number of ink craters found on steam dried coated paper is proposed as the cause of these effects. In the four-nip printing configuration which provides three opportunities for ink back-trapping, superheated steam drying of the coating increases print density and decreases print gloss. With a steam-dried coated sheet, faster ink setting and smaller scale nonuniformity of ink setting are the likely causes of these effects.

The undesirable print quality characteristic of print mottle was usually found with the four-nip printing configuration which permits ink back-trapping. Print mottle increases if the base paper is dried in steam. Subjective and instrumental evaluation indicate that the intensity of mottle decreases if the coated sheet is dried in superheated steam rather than air, while for dying in air, increasing the air drying temperature also decreases print mottle.

2. Contributions to knowledge

1. This study constitutes the first reported use of superheated steam for drying coated paper. Novel experimental techniques were developed to determine the effects on coated paper quality of various aspects of drying strategy, including comparison of air and superheated steam as the drying fluid for impingement drying of both the base sheet and the coated sheet.

2. The light weight coated (LWC) paper made from base paper dried in superheated steam is rougher, with lower gloss and light scattering (brightness and opacity) than from air-dried base paper. With steam drying the pores in the base paper are larger, while the porosity of both the base paper and the coating is the same as for air drying.

3. Superheated steam drying of the coated sheet reduces its gloss and smoothness compared to air drying. Coating porosity is not affected.

4. The undesirable property of printed paper, print mottle, is decreased by drying the coated sheet in superheated steam instead of in air, but increased by drying the base sheet in superheated steam instead of in air.

5. The differences in surface and printing properties between coated paper dried in superheated steam and in air impingement are determined in the first 0.6 s of coating drying.

3. Suggestions for future work

1. Surface porosity and pore size of coatings dried in steam should be characterized. The porous structure at the surface affects ink setting properties, found to be different for air and steam-dried coated paper. With a less complex coating formulation, having a narrower particle size, measurements could be made by surface SEM.

2. The development of properties during drying, investigated to a limited extent in the present study, should be extended to a broader range of jet temperature, to variable impinging jet velocity and to variable coating composition, especially the type of pigment, the content and glass transition temperature of the latex binder. Such studies would bring knowledge more relevant to industrial drying than does the conventional use of room temperature natural convection drying.

3. In addition to brightness and gloss, roughness changes with drying should be characterized with the type of profilometer used in the present study, thereby providing local variation in roughness rather than average values. With roughness being highly affected by drying conditions, it would be an appropriate property to trace changes occurring during drying.

4. A calendering study to improve gloss of steam-dried coated sheets should be done.

References

Al-Turaif, H., Unertl, W.N., Lepoutre, P., J. Adhesion Sci. Technol., Vol. 9, No. 7, pp 801-811, 1999

Aspler, J.S, Maine, C., De Grâce, J.H., Zang, Y.H., Taylor, S., 22nd IARIGAI Conference 1993

Back, E.L., Salmen, N.L., Tappi J., Vol. 65, No. 7 (1982)

Banks, W.H., Mill, C.C., J.Coll.Sci., 8:137 (1954)

Bernada, P., Bruneau, D., September 1996, TAPPI J., Vol. 79, No. 9, pp 130-143

Bernié, J. P. and Douglas, W.J.M., January 1998, 84th Annual Meeting Technical Section CPPA, pp A329-A332

Bernié, J. P. and Douglas, W.J.M., May 2001, TAPPI Coating and Graphic Arts Conference, San Diego, CA

Bond, J.F., PhD Thesis 1991, McGill University

Borch, J., Lepoutre, P., Tappi J., 61 (2) 45 (1978)

Bosanquet, C. M., Phil. Mag. , S6 45(267), 1923, p525-531

Carman, P.C., 1937, Transactions of the Institution of Chemical Engineering (London), Vol. 15, pp.150-166

Cui, W.K., Douglas, W.J.M, and Mujumdar, A.S., Drying technology 3 (2) : 307-320 (1985)

Cui, W.K., Douglas, W.J.M, and Mujumdar, A.S., Drying '86' : 575-580, Hemisphere, NY (1986)

David, M., M. Eng. Thesis, 1987, McGill University

De Grâce, J. H., Mangin, P. J., Advances in Printing Science and Technology, .W.H. Banks Ed.17:312 (1984)

De Grâce, J. H., Mangin, P. J., Advances in Printing Science and Technology, vol. 19 (1988)

De Grâce, J.H., Dalphond J. E., Mangin, P. J., Advances in Printing Science and Technology, 21, 312, 1992

Desjumeaux, D.M., Bousfield, D.W., 1996 TAPPI Coating Conference

Desjumeaux, D.M., Bousfield, D.W., 1996 International Printing and Graphic Arts Conference

Donderi, D.C., Behaviour Research Methods Instruments and computer, 1997 29(4) 549-555

Donderi, D.C., Paprican Misc. Report, MR 382, July 1998

Donderi, D C; Aspler, J, Pulp and Paper Canada. 2000, v.101 , n5, p3,2

Douglas, W.J.M., Drying Technology, 12(6) : 1341-1355 (1994)

Drage G, Vaughan Craig, Henderson K. F., Parsons J, Hiorns T., TAPPI Coating Conf. may 99, Toronto ON Canada

Eklund, D., Nordahl, P. and Heikkinen, M-L., Drying Technology, 13(4), 919-944 (1995)

Eklund, D., Salminen, P., September 1986 TAPPI J., pp 116-119

Engström, G., Tappi J 77(4): 160 (1994)

Engström, G., Lafaye, J-F., 1992 Tappi Coating Conf., p61

Engström, G., Morin, V., Tappi Journal, Sept 1996, p120

Engström, G., Rigdahl, M., Tappi Journal, Jan 1986, p86

Engström, G., Rigdahl, M., Kline, J., and Ahlroos, J., Tappi J., May 1991

Engström, G., Ström, G., Norrdahl, P., December 1987, TAPPI J., pp 45-49
Engström, G., Nordic Pulp and Paper Research Journal, no. 2-1992 7 (1992)
Enomae, T., Teramoto, M., Onabe, F., Hayano, S., Naito, H., Takano, K., Kamada, K., 2000 TAPPI International Printing and Graphic Arts Conference
Ercan S. N., Bousfield, D.W., 2000 TAPPI International Printing & Graphic Arts Conference
Eriksson U., Rigdahl M., JPPS, Vol 20: No. 11, Nov 1994, p J333
Farkas, I., Lampinen, M. J., Ojala, K., Drying Technology, 9(4), 1019-1049 (1991)
Fetsko, J., TAPPI J. Feb 1958 Vol. 41 No. 2
Fisera, P., Vyse, B., 1999 TAPPI Coating Conference
Fujiwara, H., Fujisaki, N., Shimizu, I., and Kano, I., May 1989, J. TAPPI, pp 91-97
Fujiwara, H., Wakai, C. and Kozuka, O., 1993 Tappi Coating Conf., p10
Gane, P.A.C., Seyler, E.N., Swan, A., 1994 International Printing and Graphic Arts Conference
Gate, L. F., J. Phys. D: Appl. Phys., Vol. 5, 1972
Glatter, T.P., Bousfield, D.W., 1996International Printing and Graphic Arts Conference
Groves, R., Lanham, A., January 1991, J. Paper Technology, pp 28-34
Groves, R., Mattews, G.P., Heap, J., McInnes, M.D., Penson, J.E., Ridgway, C.J., 12th FRC, Sept 2001
Guérin, D., Morin, V., Chaussy, D., Auriault, J.-L., 12th FRC, Sept. 2001
Guérin, D., Morin, 2003 Advanced Coating Fundamentals Symposium
Hagen, K.G, TAPPI J. 69(1):93 (1986)
Hagen, K.G, Binder Migration in Paper and Paperboard Coating", Chapter 3, Tappi publication (1993)
Hashemi, S. J., Tawfik, R. P., Bernié, J-Ph., and Douglas, W.J.M, 1999 TAPPI Engineering/Process & Product Quality Conference, pp 665-683
Hashemi, S. J., Sidwall, S., Douglas, W.J.M., 2001 12th International Drying Symposium, August 2000
Hashemi, S.J., Forel, F., Bernié, J-Ph., Douglas, W.J.M, PIRA Coating Conference, Prague (2000)
Hayashi, T., Amari, T. International Printing and Graphic Arts Conference (1992)
Huang, T. and Lepoutre, P., Paperi Ja Puu – Paper and Timber Vol. 77: No 8, 1995, p484
Huang, T. and Lepoutre, P., 1996 Tappi Coating Conf., p167
Huang, T. and Lepoutre, P., TAPPI J. Vol. 81:NO8 (1998)
Johansson, P.-A., 22nd IARIGAI Conference, September 1993
Jordan, B.D. and Nguyen, N.G., (1986)
Kim-H., L., Pollock, M., Wittbrodt, E., Roper, J., et al. August 1998, J. TAPPI, pp 153-164
Kim-Habermehl, L., Pollock, M., Wittbrodt, E., Roper III., 1998 International Printing and Graphic Arts Conference
Kozeny, J., 1927, Akad. Wiss. Wien., Math-Nat. KL. 36 (Abt IIa), pp206-271
Lee, D. I., Whalen-Shaw, M., Binder Migration in Paper and Paperboard Coatings, Chapter 2, pp 19-38, TAPPI publication (1993)
Lepoutre P., de Silverira, G., September 1991, JPPS, Vol 17, No 5,
Lepoutre, P., Journal of Pulp and Paper Science, 15(5):183 (1989)
Lepoutre, P., Progress in Organic Coatings, 17:89 (1989)

Lepoutre, P., Skowronksi, J., Bichard, W., 1986 Coating Conference, TAPPI Proceedings, pp 113-120

Lezelter P., Eklund D., TAPPI J, May 1993, p63, 1993b

Lezelter, P., 1995 Advanced Fundamentals Coating Symposium

Li, R., M. Eng. Thesis (1993), McGill University

Lohmander S, Martinez M, Lason Lucyna, Rigdahl M, Li T. Q., TAPPI Coating Conf. may 99, Toronto ON Canada

MacPhee, J., American Ink Maker, 75, 1, 42-49, 1996

Mäkinen, J., Rajala, P., Nuyan, S., 98 Tappi Coating Conference, New Orleans

Mangin, P.J., Lyne, M.B., Page D.H., De Grâce, J.H., Adv. Print. Sci. Technol. 16:180 (1981)

Matsubayashi, H., Saito, Y., 1992 Tappi Coating Conf., preprints p161

McCall, J.M. and Douglas, W.J.M., Tappi J., 77 (2): 153-161 (1994)

McCall, J.M., Cacchione, E. and Douglas, W.J.M., Tappi J., 78 : 115-122 (1995)

McCall , J.M., Douglas, W.J.M., United States Patent US 6,322,667 B1 Nov. 27, 2001

McCall, J., Douglas W.J.M. IDS 2004, 14th International Drying Symposium, Sao Paulo, Brazil, Aug 22-25 2004

Miettinen, P. Tammi, A.-L., IPGAC Bordeaux 2002

Ming, 1995 Coating Fundamentals Symposium

Moreau-Tabiche, S., Morin, V., Lemaitre, A., Nguyen Minh, T., Revue ATIP May 1996

Morin, V., Piette, P., Maume, JP., June 1996, 3rd European Research Symposium of Image Analysis for Pulp and Paper Research and Production, Stockholm, Sweden, pp 20:1-20:16

Ness, C., and Göttsching, L., Advances in printing science and technology: proceedings of the 23rd Research Conf. IARIGAI, Paris, France

Nguyen N., Jordan B., De Grâce J., 1992 International Printing & Graphic Arts Conference

Nissan, A.H., Proc. Tech. Sect. P.M.A., XXX (1), 96-. Ref. Hoyland, R.W., Field, R., Paper Technology and Industry 17 (8):304-306 (1976)

Noboa, H.L., Seyed-Yagoobi, J., Proceedings of ASME/IMECE, 1999 ASME International Mechanical Engineering Congress and Exposition (1999)

Norrdahl, P., Tappi J., May 1991

O'Neill, M., Jordan, B., JPPS Vol.26 No. 4 April 2000

Oittinen, P., Saarelma,. H., Tuovinen, P., 1990 International Printing and Graphic Arts Conference

Oittinen, P. Adv. Print. Sci. Technol., 15, p344 (1980)

Oittinen, P., Papri ja Puu, 11:718 (1984)

Pan, S. X., Davis, H. T., Scriven, L. E., 1995 Coating Conference, TAPPI Proceedings, pp 37-52

Pan, S. X., Davis, H. T., Scriven, L. E., 1996 Coating Conference, TAPPI Proceedings, pp 115-133

Piette, P., Morin, V., Trehoult, C., Wiatr, C International Printing & Graphic Arts Conference 2002

Plowman, N., July 1994, J. TAPPI, Vol. 77, No 7, pp 173-184

Poirier, N.A., PhD Thesis (1991), McGill University

Poirier, N.A., Crotogino, R.H., Mujumdar, A.S and Douglas, W.J.M., J. Pulp & Paper Sci., 20, J97-J102, (1994)

Poirier, N.A., Crotogino, R.H., Mujumdar, A.S and Douglas, W.J.M., “The effect of Superheated Steam Drying on the Properties of Paper from Chemical Pulp”, J. Pulp & Paper Sci., 21, J374-378 (1995)
Preston, J.S., Elton, N.J., Legris, A., Nutbeem, C., 2001 Advanced Coating Fundamentals Symposium
Preston, J.S., Parsons, D.J., Gate, L.F., Husband, J.C., Legrix, A., Jones, M., 2002 International Printing and Graphic Arts Conference (2002)
Preston, J.S., Parsons, D.J., Nutbeem, C., 2003 Advanced Coating Fundamentals Symposium (2003)
Rajala, P., Karlsson, M., 1996,
Proceedings of the 10th International Drying Symposium, pp 1205-1211
Robinson, J.V., TAPPI 58(10):152 (1975)
Rosenberg, R.R., IPGAC Bordeaux 2002
Rousu, S., Eklund D.E., Gane, P.A.C, Spielmann, D.C., 2000 TAPPI International Printing and Graphic Arts Conference
Sadeghi, M., Ph.D. Thesis, McGill University (2003)
Salmén, L. J. Master Sci. 19:3090 (1984)
Salminen, P., 1988, Ph. D. Thesis, Abo Akademi, Finland,
Salminen, P.,1988 Coating Conference, pp 209-215
Salminen, P., Roper, J., Pollock, M., Chonde, Y., 1995 TAPPPI Coating Conference (1995)
Schoelkopf, J., Gane, P.A.C., Ridgway, C.J., Spielmann, D.C., Matthews, G.P., 2001 Advanced Coating Fundamentals Symposium
Schoelkopf, J., Gane, P.A.C., Fischer, S., 2002 Printing and Graphic Arts Conference
Schoelkopf, J., Gane, P.A.C., Ridgway, C., Advanced Coating Fundamentals Symposium (2003)
Semi, K. and Kohmoto, N., “1997 Pulp and Paper Research Conference Tokyo Japan
Smook, G.A., Handbook for pulp and paper technologists, Joint Textbook Committee of the Paper Industry (1979)
Stanislawska, A. and Lepoutre, P., Tappi Journal, Vol. 79: No. 5, May 1996, p117
Tomimasu, H., Suzuki, K., Toshimasa, O. and Luner, P., Tappi Journal, May 1990, p179
Thomson, I.G., Young, F.R., “High-speed photographic studies on ink filamentation”, Jour. Oil. Col. Chem. Assoc., 58, 389, 1975
Vardeman, S.B., PWS Foundation in Engineering Series (1993)
Waech, T.G. 1998 International Printing and Graphic Arts Conference
Walker, W. C. TAPPI J. May 1981 Vol. 64, No. 5
Walker, W.C., Fetsko, J. M., American Ink Maker 33 (12): 28, 42, 44, 69, 71 (1955)
Watanabe, Lepoutre, P. Journal of Applied Polymer Science 27 (11) 4202 – 4219 (1982)
Xiang, Y., Bousfield, D. W., 2000a TAPPI Coating conference and Trade Fair, pp 45-58
Xiang, Y., Bousfield, D. W., 2000b TAPPI Intenational Printing & Graphic Arts Conference, pp 299-308
Xiang, Y., Bousfield, D.W., 2001 Advances Coating Fundamentals Symposium
Xiang, Y., Bousfield, D.W., Hayes, P.C., Kettle, J., Hultgren, L., Journal of Graphic Technology 1:1 (2003)
Yamasaki, K., Nishioka, T., Hattori, Y., and Fujita, K., Tappi J., Vol. 76: No 5, May 1993, p79

Young, T.S., Pivonka, D.E., Weyer, L.G., Ching, R., Tappi J., Vol. 76: No. 10, Oct 1993, p71
Zang, Y. H., TAPPI J Vol. 76, No. 7 1995
Zang, Y. H., and Aspler, J.S., TAPPI J. Vol. 78, No. 1 1995
Zang, Y.H., Aspler, J.S, Boluk, M.Y., De Grâce, J.H., J. Rheol 35 (3), April 1991
Zang, Y-H. and Aspler, J.S., JPPS, Vol. 24:No. 5, May 1998, pp141-145

Appendix A Experimental details

1. Base sheet supply

1.1 Base sheet forming

Three main requirements governed the production of these wet handsheets:

- Size: Overall, base sheet must first be dried in that unit of our laboratory facility, then be processed in this coating-drying facility before being tested for coated paper properties. As the coating blade width is 120 mm, the minimum sheet dimension in the coater cross-machine (CD) direction is about 140 mm, allowing for taping during the successive drying and coating stages. In the other (MD) dimension it is necessary, for some paper property tests, to have a length of about 120 mm. Additionally, it is necessary to trim for the part of the sheet coated during the acceleration stage of blade travel (section 4.2.4). The minimum size specification for the initial sheet is then 140 mm (CD) x 170 mm (MD).
- Fines content: Good retention of the furnish fines content is vital for two reasons. First, fines are an important characteristic of base paper made from mechanical pulp, playing a role in the coating process and in coated paper property development during conventional drying in air. Secondly, the changes in properties of mechanical furnish paper produced by superheated steam drying have been reported to derive particularly from this fraction of the pulp. Thus if this fraction was not fully retained, some of the potential effects of superheated steam drying on paper properties would be lost.
- Reproducibility: A large number of handsheets are required for the study, hence selecting a technique allowing good reproducibility in base sheet composition and formation is essential.

The several methods available to produce wet handsheets and their main features are listed in Table A.1. The forming technique of the Dynamic Sheet Former consists of two concentric metal drums. The inner drum, rotating, is perforated to allow water to drain into the solid outer drum, fixed, by flow through a forming fabric laid along the inside wall of the inner drum. A jet of the pulp furnish sprayed through a vertically oscillating nozzle on to the inner drum forms the wet web.

Table A.1 Base sheet production techniques available

Technique	**Dimensions (mm)**	**Fines retention**	**Fibre orientation**
British Handsheet Maker	160 diameter	Poor*	Isotropic
Large British Handsheet Maker	203 diameter	Poor*	Isotropic
Williams Square Handsheet Maker	203 x 203	Poor*	Isotropic
M/K System *(unit idle)*	500 x 500	?	Isotropic
Pilot Machine *(expensive)*	500 x ∞	Good	Anisotropic
Dynamic Sheet Former	200 x 900	Good	Anisotropic

**If equipped with a white water recirculation loop these techniques allow good fines retention, but the procedure is tedious*

The drum rotation speed and jet pressure or velocity are variable, which allows for a range of fibre orientation at a given pulp furnish consistency. Both the distance and angle of the jet nozzle relative to the forming wire screen may also be varied. When fibre deposition is complete, the water build up is removed from the outer drum using a scoop, then the drum rotation is stopped. The wet web is compacted on the forming wire screen, then both the sheet and forming screen are removed from the drum for the next step of sheet pressing. The sheet size at this stage is 220 mm (CD) x 910 mm (MD), but some paper must be trimmed to remove edge effects, which reduces the usable dimensions to about 170 mm x 900 mm.

1.2 Base sheet making operating parameters

With the characteristics of Dynamic Sheet Former sheets being known in order to approximate commercial sheet properties the correct choices were known for the forming parameters noted earlier. The key requirement was for reproducibility, to keep these forming parameters constant and under tight control from sheet to sheet while one batch of pulp furnish was being used, and from batch to batch of the pulp furnish. In addition, with this pulp containing some long softwood kraft fibres it was recommended to use a lower pulp consistency (0.25% solids) in order to avoid blocking of the jet nozzles.

The pulp was taken at the mixing chest from the mill selected as described earlier. This furnish, Table 3.1 was a blend at 3% solids consistency of approximately 67% ground wood pulp (mechanical pulp) and 33% kraft pulp (chemical pulp). Each 210 L batch of pulp suspension was prepared at 2.5 g/L +/- 0.05 g/L, which allowed production of about 30 Dynamic Sheet Former sheets. The drainage parameters control the compaction of the fibres on the forming wire screen and therefore the formation. The Dynamic Sheet Former unit at Paprican is equipped with an automated drainage system which ensures better reproducibility of formation than does manual drainage.

The drainage sequence proceeds in three steps with the user entering, for each step, the desired angle that the scoop should travel and the time for this travel. The total angle travelled by the scoop must equal 90° for the wall of water on the outer drum to be completely removed and pauses between steps can be programmed. The Dynamic Sheet Former operating parameters are listed in Table A.2. The sheet was then pressed twice between two blotter papers, which were replaced for the second pressing. The press load was 1.4 bar. This pressing procedure produced a sheet moisture content to begin the drying step of $X = 1.22$ kg water/kg dry fibre (55% wet basis, or 45% solids content). In order to maintain this moisture content precisely, the pressed sheets were rolled between two polyethylene sheets and stored at 4°C in a refrigerator until the drying stage in the impingement drying unit of the laboratory coating-drying facility.

Table A.2 Dynamic Sheet Former operating parameters

Pulp consistency		0.25%
Forming Drum Peripheral Speed		1000 m/min
Jet-to-wire distance		25 mm
Jet-to-wire angle		15°
Pressure to jet		22 psig
Number of jet sweeps		150
Drainage Sequence (automated)	**First Period**	50 s / 25° angle
	Delay 1	10 s
	Second Period	55 s / 20° angle
	Delay 2	10 s
	Third Period	55 s / 45° angle

1.3 Dynamic Sheet Former

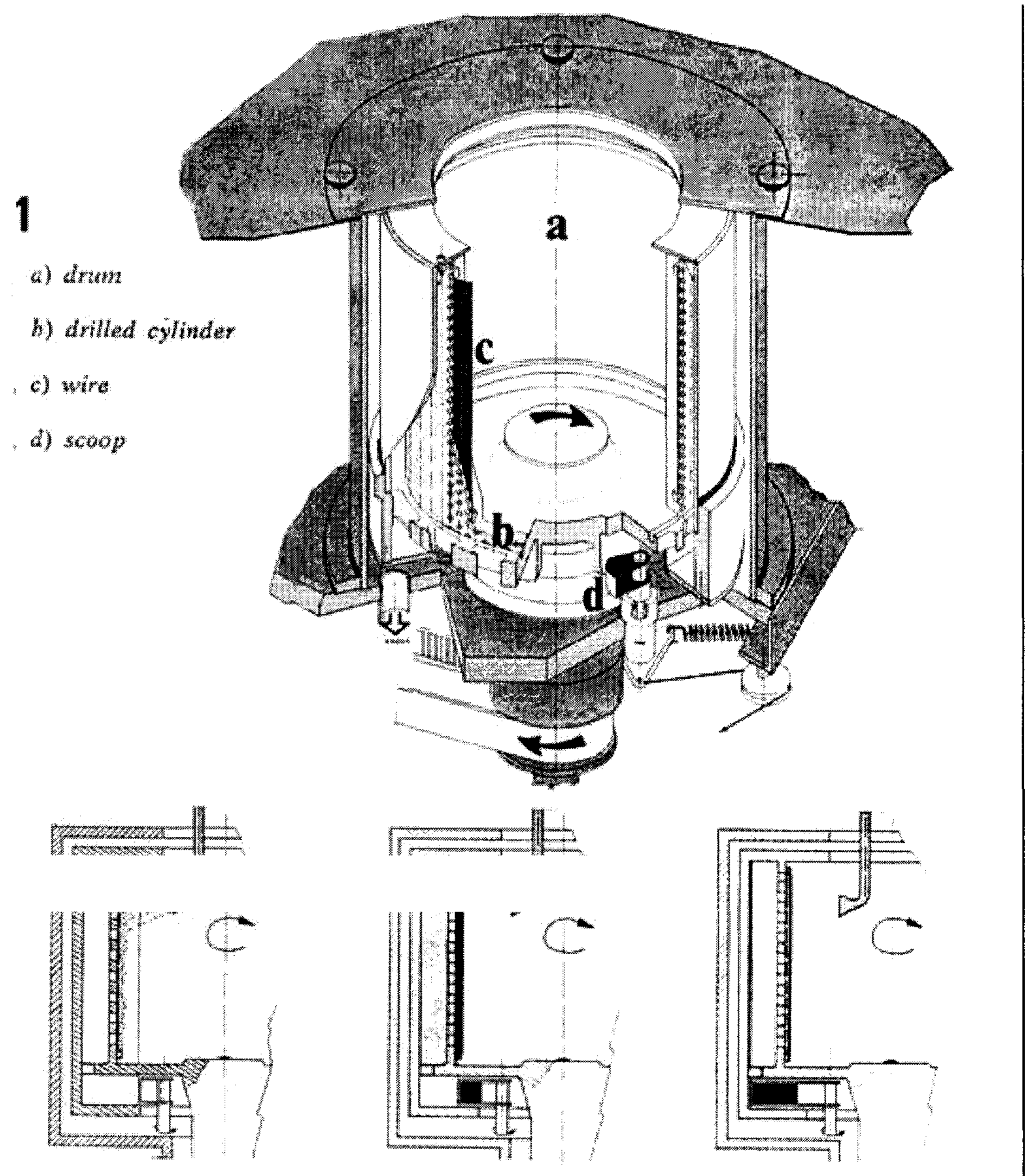

2 The water-wall has been built up
The stock is thrown on the water-wall

3 Stock projection is over
Water is progressively sucked away by the scoop device

4 Water-wall is now entirely sucked away
The sheet has been formed

Figure A.1 Dynamic Sheet Former

2. Base sheet drying procedure

The drying unit of the coating-drying facility is warmed with the sequence described in section 4.4.5 until the operating conditions are stabilised. The blade coater, not used in this case, is put in the back position during use of only the drying unit. Drying at T_j=140°C and V_j=40 m/s is carried out as follows:

1- Wet never-dried sheets as described in section 2.2.2 are taken from the refrigerator and brought to room temperature (while staying in the bags)

2- These sheets, 220 mm x 910 mm, are cut into four equal sheets and kept between plastic sheets until the time of experiment

3- A 220 mm x 230 mm sheet is mounted on the spring steel plate covered with a silicon rubber pad as noted earlier. The sheet is wrapped around the plate, well engaged in the teeth edges of the plate, taped fully from underneath and covered by a thick plastic pad to minimise loss of moisture to ambient air

4a- For drying in air, this thin secondary plate carrying the wet sheet + silicon cover are positioned on the main base plate, the cover removed and the computer controlled system for tray insertion is triggered. The selected drying time is 8 s

4b- For drying in superheated steam, the tray carrying the primary base plate is first inserted into the dryer for a 55 s preheating period, then the thin secondary base plate carrying the sheet + cover are mounted on the main base plate and left for 10 s, the time required to heat the secondary base plate. The cover is removed and the tray carrying the base plate and wet sheet is then inserted by the computer controlled actuator for 13 s drying time.

5- When the tray is retracted from the drying chamber, the thin secondary base plate and the sheet mounted on it are removed together very quickly from the primary base plate

6- The sheet and its thin support plate are placed on a room temperature steel plate for drying completion for 10 minutes at room temperature

7- The sheet is removed from its support with a knife, bagged to avoid moisture gain or loss, then stored in a controlled conditions room.

3. Coating suspension testing

The coating suspension viscosity was measured on a rotational viscometer (HAAKE Rotovisco) consisting of two coaxial cylinders with the inner cylinder being rotated at a controlled angular velocity. The viscosity-related torque, caused by resistance to shear of the suspension, acts on the inner cylinder, deflecting a measuring spring placed between the motor and inner cylinder. The apparent viscosity η is deduced from the following relationship:

$$\eta = f \cdot \frac{M}{n} \qquad [\text{Pa.s}]$$

with f the viscosimeter shape factor [m^{-3}], M the measured torque [N.m], and n the cylinder rotational speed [s^{-1}]. The suspension is subjected to a shear rate range by cycling the inner cylinder rotational speed from rest to 1,000 rpm and back to 0 rpm, over identical, periods of 300 s for the speed increase and speed decrease stages, with also a constant hold time of 1 s at each of the increments of the rotational speed.

The "coating retention value" was evaluated on an apparatus developed in Finland called the AA-GWR (Abo Akademi Gravimetric Water Retention). This static laboratory device allows the gravimetric measurement of dewatering under pressure through a filter. Although the absolute value provided by this test does not have physical meaning, it is an effective relative reference for comparison of coating suspensions which, in our case, were to be kept unchanged. Some coating suspension is spread uniformly over a 5 μm filter, which seals a rubber cylinder. The filter stands on two square blotter papers. A 15 psi pressure is applied for 60 s. The weights of the blotter papers before and after the test provide the amount of water lost from the coating suspension to the paper.

4. Coated sheet drying procedure

The base sheet drying procedure was reported in section 2.3.4. The experimental facility is first warmed with the following sequence:

1- Turn on the computer and control boxes

2- Balance the differential pressure transducer used to measure drying air flow rate

3- Open air and cold water supply

4- Select drying fluid temperature and temperature variation in the MONITOR program

5- Load the selected blade & tray motion program on the controller

6- Turn on the sheet insertion-retraction drive interface

7- Trigger a blank run to check for any problems

This is a basic procedure used for every drying experiment. When superheated steam is the drying fluid, the same procedure applies until the dryer has reached the targeted temperature while operating with air, not steam. At that time the air supply is replaced by superheated steam.

Different programs for blade motion and for insertion-retraction tray motion are stored in the computer for the different applications – i.e. coated sheet or base sheet drying, air or superheated steam drying fluid, variable delay-time, variable drying time…

When the operating conditions have equilibrated to their targeted values, the experiment proceeds with the following sequence:

1- Mount the base sheet on the secondary (thin) support plate with tape and keep it covered with a plastic pad

2- For drying in air, insert this plate carrying the sheet in the slot of the primary (thick) support plate and remove the covering plastic pad

2bis – For drying in superheated steam:

- initiate the preheating of the primary (thick) sheet support plate
- when the preheated tray carrying the primary support plate is retracted from the drying chamber, return the coating blade to the starting position

- insert the unheated, thin secondary sheet support plate carrying the sheet in the slot of the primary (hot) support plate and remove the covering plastic pad

3- Place the coating pool on the taped area of the wet sheet

4- Trigger the control computer to start the programmed sequence of coating blade motion and tray insertion/retraction operation

5- Read the insertion time display

6- Cover the retracted dried sheet immediately with a recessed plate and remove the secondary sheet support plate carrying the now dry sheet

7- Remove the tape from the sides of the sheet

8- Place the dried sheet in a moisture-proof plastic bag for storage in the controlled conditions room

5. Laboratory coating-drying facility auxiliary equipment

5.1 High temperature drying fluid supply

The drying fluid, air or superheated steam is provided at atmospheric pressure through a pressure regulator and is brought to the desired temperature by means of an electrical 35 kW heater. The drying fluid then passes through a turbine flow meter, a throttle valve and a venturi flow meter, before entering the drying chamber. The drying fluid temperature in the drying chamber is controlled to within +/-2°C by a computer program, written in QuickBasic. It was found that with the large thermal inertia of the heater on/off control of the power provided satisfactory drying chamber temperature control. The exhaust fluid is cooled by direct contact in a spray condenser.

5.2 Instrumentation and data monitoring

Fluid temperature and flow rate as well as blade nip load are monitored through an A/D board. Digital data are converted to physical quantities and displayed on the screen by means of a QuickBasic program named MONITOR. The screen is checked while running experiments to keep operating conditions constant from sheet to sheet, but no data acquisition is performed.

Thermocouples are used to measure temperatures at the superheater outlet (for superheater computer control), in the plenum chamber and in the exhaust line (for drying conditions control).

The fluid flow rate is measured by means of both a venturi flow meter (Preso model #V100-65) and a turbine flow meter (Sponsler model 11/4-MB-PH7-A-4HTX). The venturi flow meter is placed immediately before the drying chamber while the turbine flow meter is mounted before the throttle valve. The differential pressure transducer (Weed instruments model 90 DP), measuring the pressure drop in the venturi, is protected from the high temperatures by cold water. Its voltage signal, calibrated with a water column, is sent to the monitor where it is implemented in the venturi equation with specific constants given by the venturi flow meter supplier. The turbine flow meter reading (Hz) is transmitted to a voltmeter through a frequency-voltage interface (SP-471) and manually converted into flow rate along the calibration curve which had been plotted with an off-line gas flow meter. The two flow rates measured are within 5%, which gives confidence to using only one flow meter on-line while using superheated steam. The reason for this practice is that the blades of the expensive turbine flow meter are very fragile and can easily be damaged by entrained solid particles or water droplets. Thus when operating with superheated steam the turbine flow meter is only used occasionally to verify the results from the venturi flow meter.

The coating blade load, an extremely important and sensitive parameter of the coating process, is measured by means a pair of high sensitivity load cells (Tedea Huntleigh model 1030) one at each end of the blade. Through use of an aluminium fork, these load cells accurately measure the strain on the die springs. This reading is converted to blade load, N/m, the sum of the net force applied on each spring divided by blade length.

5.3 Process control

Separate computer programs with a high performance I/O board (National Instrument model AT-MIO-16) and a controller are used for the control of drying fluid temperature blade motion and sheet insertion.

Drying fluid temperature control is performed with a QuickBasic program (the same as used to monitor the data) which activates the superheater through the digital output of the I/O board. In automatic mode, the user enters the desired plenum temperature (drying temperature) and plenum temperature variation. With the large thermal inertia of the superheater, on/off control of power achieves satisfactory plenum temperature control within the specified limits. These lower and upper temperature limits are tuned for each drying temperature.

The blade motion and the tray insertion and retraction sequence is programmed with Superior Electric MS2000 software. Blade motion settings and the residence time in the dryer are selected, then the program is downloaded onto the controller (Model SS20001) that pulses the stepper motor (Model MH112-FJ8030) through a drive interface (Model SS2000-D12) and also activates the solenoid valves through the I/O board. The program comprises two inputs and two outputs. The first input is push button manually triggered to initiate the full sequence. Then the program automatically activates the following steps. The blade is made to travel over the sheet until the second input is triggered: this is a micro-switch pushed by the blade holder plate when the blade arrives at its end-of-coating position. This second input triggers the first output, which simultaneously opens the solenoid valve responsible for insertion of the sheet holder tray and activates the oscillation of the nozzle plate. The sheet is inserted into the drying chamber where it remains for the desired time. With passage of the selected residence time, the second output is triggered, which simultaneously opens the solenoid valve initiating retraction of the sheet holder tray, and stops the nozzle plate oscillation.

6. Paper properties definition and testing

6.1 Bulk properties

6.1.1 Specific volume

The sheet specific volume also called bulk, cm^3/g, is obtained by the ratio of sheet thickness (measured on single sheet in this study) in μm, over the sheet basis weight in g/m^2.

6.1.2 Permeability

Permeability was measured on the Parker Print Surf apparatus. This instrument has two pairs of heads, one for measuring permeability, one for roughness. The measurement is done with air for 4 s. The permeability, K, is derived from the permeance measured and expressed in μm/Pa.s as follows:

$$K = P\mu L \tag{3.1}$$

with K permeability in $[10^{-12}\ m^2]$, P the measured permeance to air $[\mu m.Pa^{-1}.s^{-1}]$, μ the viscosity of air at 23°C, $1.8\ 10^{-5}$ Pa.s, and L the sheet thickness [μm].

6.1.3 Mercury porosimetry

The mercury porosimetry technique is widely used to determine paper porosity and pore size distribution. The pore size calculation is based on the Laplace equation relating pore size to mercury pressure:

$$d = -\frac{4 \cdot \gamma \cdot \cos\theta}{P} \tag{3.2}$$

with γ the surface tension of mercury, 48 N/m, θ is the contact angle (140° at 23°C, corrected for temperature variation), P the pressure applied [MPa]. The pressure is increased by increments and the volume intruded is measured at each step. With the Micromeritics PoreSizer 9320 used here there were two pressure runs: a low pressure run, from 0 to 0.207 MPa, to fill pores ranging from 360 to 6 μm, and a high pressure run, from 0.207 to 207 MPa to fill pores ranging from 6 to 0.006 μm. From the specific cumulative intrusion volume (volume divided by the given sample weight), I_i, read at each step the program attached to the porosimeter calculates the incremental specific intrusion volume, $I_{i1} = I_i - I_{i-1}$, and the incremental specific pore area, $A_{i1} = 4\ I_{i1}/(D_i - D_{i-1})$. The log differential specific intrusion volume is then calculated and plotted as a function of pore size. This log-normal curve represents the pore size distribution. Three diameters representative of the porous structure may be defined. Median pore diameters are calculated from eq. (3.2) with the pressure interpolated from the data collected at either half the total intrusion cumulative volume, I_{tot}, median pore diameter based on volume, or half the total area, A_{tot}, median pore diameter based on area. The average pore diameter, D_{av}, based on both volume and area, is calculated as follows:

$$D_{av} = \frac{4I_{tot}}{A_{tot}} \tag{3.3}$$

The porosity, ε expressed in %, is derived from the total intrusion volume, V_{void}, and the sample volume, V_{bulk}, as follows:

$$\varepsilon = \frac{Vvoid}{Vbulk} \cdot 100 \tag{3.4}$$

In the case of coated paper the porosity and pore size distribution of the coating can be separated from that of the base paper because the pore dimensions are almost 2 orders of magnitude lower for the coating than the base paper. The pressure range used for the coating layer was that corresponding to pore size ranging from 0.01 μm to 0.2 μm and that for the base paper was that corresponding to pore size above 0.3 μm. The main limitations of this technique are the uncertainties in θ and the approximation of non-connecting cylindrical pores (maybe tortuous) for which the Laplace equation applies. In a complex porous structure, as in paper, a small pore may block access for mercury to a larger pore. This effect leads to a pore size distribution shifted toward smaller pore sizes, the porosimeter measuring the pore throat size rather than the actual pore size. It is however a well established technique particularly useful to compare samples with identical composition.

6.2 Optical properties

6.2.1 Light Scattering Coefficient and Light Absorption Coefficient

The theory developed by Kubelka (1948) allows separating light scattering and light absorption ability of a sheet of paper from 2 reflectance measurements: that of a single sheet over a black background, R_0, and that of an opaque pad of sheets, R_∞. The light scattering and light absorption coefficients, S and K, expressed in m^2/kg (scattering and absorption ability divided by basis weight) are calculated based on reflectance measurements used for opacity determination, that is, using diffuse light of mean wavelength 555 nm. The equations used here are taken from the review by Robinson (1975) of optical properties according to the Kubelka - Munk theory:

$$S = \frac{1000}{BW}\frac{1}{1/R_\infty - R_\infty}\ln\frac{(1-R_0R_\infty)}{(1-R_0/R_\infty)} \tag{3.5}$$

and

$$K = S\frac{(1-R_\infty)^2}{2R_\infty} \tag{3.6}$$

with BW the basis weight in g/m^2.

6.2.2 *Brightness*

The reflectance of an opaque pad of paper sheets, R_∞, measured with a blue light source peaking at 457 nm, is termed brightness. Brightness depends on the light absorption and scattering characteristics of the material as described by the following equation:

$$Brightness = R_\infty\big|_{457nm} = 1 + K/S - \left(2K/S + (K/S)^2\right)^{1/2} \tag{3.7}$$

with K the light absorption and S the light scattering coefficients at 457 nm in m^2/kg.

6.2.3 *Opacity*

Opacity, a measure of the ability of paper to block light, is the ratio of reflectance of a single sheet, R_0, to that of an opaque pad of sheets, R_∞. The light used for opacity is different from that used for brightness: peaking at 555 nm. Opacity is mainly related to basis weight, light scattering and absorption characteristics of paper according to the following equation:

$$Opacity = \frac{R_0}{R_\infty}\bigg|_{555nm} = \frac{1}{R^2{}_\infty}\frac{1-\exp[S(1/R_\infty - R_\infty)]}{R_\infty - \exp[S(1/R_\infty - R_\infty)]} \tag{3.8}$$

with R_∞ from eq. (3.7) and K and S the light absorption and scattering coefficients at 555 nm in m^2/kg.

6.2.4 Relationships between optical properties

The relationships between the optical properties derived according to the Kubelka-Munk theory are illustrated in Figure A.2. Brightness corresponds to R_∞ when K and S are obtained at 457 nm, and opacity to R_0/R_∞ when K and S are obtained at 555 nm. When a beam of light impinges at the surface of paper part of it is transmitted through the sheet, part of it is absorbed and the rest is reflected back because of multiple refractions and reflections inside paper or scattering. Paper absorbs light because of the presence of chromophore groups mostly in the lignin.

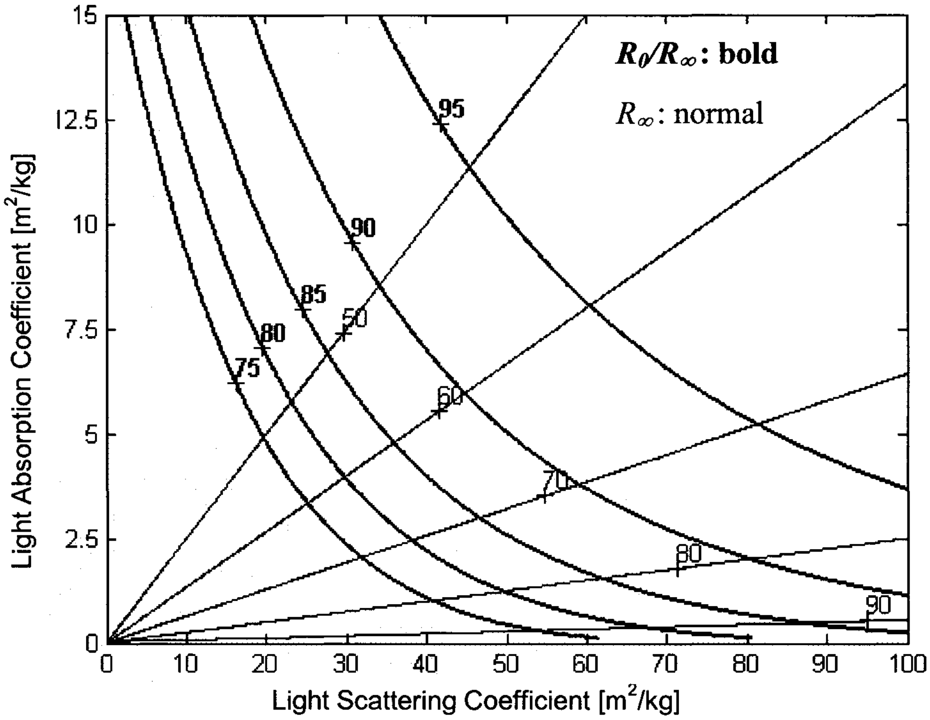

Figure A.2 Optical property relationships according to Kubelka-Munk theory

Light absorption therefore depends on the type and number of chromophore groups. Light scattering occurs at the interface of materials of different index of refraction, n. For uncoated paper, porous material made of cellulose fibres, $n = 1.55$, and air voids, $n = 1$, light scattering therefore occurs at fibre-air interface and increases linearly with the surface area of the pores, Scallan and Borch (1972, 1974). Light scattering is not sensitive to the wavelength of light. For coated paper scattering is sensitive to wavelength because pores of the coating layer are of the same order of magnitude as light wavelength, Lepoutre et al. (1989). Light scattering first increases then decreases with reduction in pore size. For coating made of low refractive index materials, such as clay and latex, the light scattering species are the pores themselves and light scattering depends on their size and volume. Light scattering coefficient, S, exhibits a strong dependence on the wavelength of light, λ: a linear relationship between $\log(S)$ and $\log(\lambda)$, Gate (1972) and Lepoutre et al. (1989). The slope and intercept of this curve depend on the porosity, the average pore size and pore size distribution of the coating layer. The optimum pore size for light scattering depends on the coating material refractive index, and on the light wavelength. Borch and Lepoutre (1978) found the optimal size is 0.3-0.4 μm and 0.5-0.6 μm for scattering light of wavelength 457 or 555 nm, respectively.

6.3 Strength properties

6.3.1 Tensile

The breaking length, km, is derived from the maximum stress recorded during the strain – stress curve test:

$$Breaking\ Length = \frac{Load\ at\ break}{Sample\ width \cdot Basis\ weight \cdot g} \tag{3.9}$$

with *sample width* = 15 mm and g = 9.81 m/s^2 the acceleration of the gravity. The breaking length is often used because it has a practical physical meaning: the length of a band of paper for which failure would occur under its own weight. The stretch is the strain at paper failure expressed in %.

6.3.2 Burst

Bursting strength is a paper strength property closely related to its paper tensile strength. A sheet is clamped over a membrane (33 mm diameter) that is then pressurized. The maximum pressure recorded divided by the sheet basis weight gives the burst index in kPa.m^2/g.

6.3.3 Tear

The tearing test measures the energy required to tear a sheet of paper from a defined cut. Four plies, 63 mm long, are clamped tightly between two jaws, the cut is initiated with a blade and a pendulum is released that continues the tearing action.

Knowing the weight of the pendulum and the length of the sheet the level reached by the pendulum represents the energy required to tear the paper. The tear index, $mN.m^2.g^{-1}$, is then obtained with the following formula:

$$Tear'Index = Scale\ reading \cdot \frac{8}{No\ of\ \ plies(4)} \cdot \frac{g}{Basis\ weight} \tag{3.10}$$

with 8 the number of plies for which the apparatus is calibrated and g the acceleration of the gravity.

6.4 Surface properties

6.4.1 Roughness

a. PPS roughness determination

Paper surface roughness has been conventionally measured by an air-leak method. The sheet is clamped under precisely defined conditions and the air flow leakage made between the clamping surface and the paper surface is measured: the rougher the paper surface, the larger the air flow rate. An equation relating air leakage flow rate and roughness allows expressing the results in μm of roughness. The Parker Print Surf (PPS-10) was used for this measurement with 1 MPa clamping pressure.

b. Profilometry rouhgness determination

A more recently developed measurement of roughness is with a stylus profilometer. The Talyscan profilometer developed at Paprican was used for extensive surface roughness characterization. The talyscan stylus head, of diameter 2 μm, scans the surface in 2 dimensions. Once the image of the surface is acquired it is leveled (so that any continuous linear trend in X or Y is removed) and the mean elevation measured. Roughness is defined as the deviation from this mean level. The image is then imported into a software where a number of roughness parameters or image processing steps may be performed. The image is usually filtered to separate roughness (small scale variation) from waviness (large scale deviation). Table A.3 presents the operating parameters used. The amplitude and hybrid parameters defined in Table A.4 were calculated for each of the 10 (uncoated paper) or 8 (coated paper) scans.

Table A.3 Roughness profilometer settings

	Setting	
Scanning area	$1\ mm^2$	
Scanning speed	5 mm/s	
X resolution	2 μm	
Y resolution	2 μm	
Z resolution	0.06 μm (uncoated)	0.012 μm (coated)
Filter size	250 μm	80 μm

Table A.4 Definition of roughness parameters

ID	Name	Description
S_q	root-mean-square deviation of the surface	$\sqrt{\frac{\sum x_i^2}{n}}$ x being the deviation
S_{dq}	root-mean-square slope of the surface	$\sqrt{\frac{\sum x_i^2}{n}}$ x being the slope
S_{sc}	arithmetic mean summit curvature of the surface	mean form of the peaks: pointed or rounded, higher for pointed peaks
S_{dr}	developed interfacial area ratio	complexity of the surface; comparison of the curvilinear surface and the support surface: flat surface ~ 0% / complex surface several %
S_{fd}	fractal dimension	characterize how same length increases with increasing scale

6.4.2 Gloss

Paper gloss is the degree to which the paper surface reflects light in the specular reflection direction. Specular reflection refers to the portion of the incident light which is reflected from the surface of an object, with the angle of reflection being equal to the angle of incidence. The light beam is directed at an angle of 75° to the paper and the reflection in the specular direction is measured and expressed in degree or % with respect to the gloss of a reference material.

6.4.3 Water penetration time

Another important surface property when applying coating is the sheet hydrophobicity level. In the present work a water drop test was performed according to TAPPI T42 om-87. The penetration time of a drop of controlled volume, 50 μL, was measured on an unsupported area of paper elsewhere supported, and covered with a recessed plastic frame. Deionized distilled water was used.

6.4.4 ESCA

Surface chemical composition was determined by the ESCA technique (Electron Spectroscopy for Chemical Analysis) also called XPS (X-ray Photoelectron Spectroscopy). When an X-ray beam is directed at a sample surface, X-ray photons collide with electrons leaving the surface. The latter are collected and characterized. The energy associated with the electron discharge allows identifying the element from which the electron comes, while the number of electrons with a specific energy allows counting the content of this specific element at the sample surface. For coated paper, ESCA measurements are principally made in order to determine latex binder concentration at the coating surface and, thereby to identify the extent and nonuniformity of binder migration to or from the final dry coated surface.

6.4.5 SEM

Scanning Electron Microscopy uses electrons to produce images. The sample is bombarded with an electron beam that collides with the atoms of the specimen. Two types of collision may occur, depending whether the electrons collide with an electron or a nucleus, creating two electron beam signals, of respectively low or high energy, collected separately. Electron-electron or inelastic collisions produce the Secondary Electron Imaging (SEI) signal, providing structural information about the surface. Electron-nucleus or elastic collisions produce the Backscattering Electron Imaging (BEI) signal, providing both topographical and elemental composition information.

SEM observation of paper requires sample preparation. In the case of a paper surface, the preparation is minimal: the sheet is taped on a stub with conducting tape and coated with carbon to make it conducting. In the case of a paper cross section (observation in the thickness dimension) the preparation is long and tedious as described in Appendix B, the paper samples is first embedded in a resin that is cured, carefully polished and finally carbon coated.

The JEOL-840 model of SEM was used with the following setting:

- 15 mm working distance
- 12 kV accelerating voltage

- $1e^{-9}$ A probe current
- magnification ranging from 70 X to 10,000 X

This SEM is equipped with a digital image acquisition system.

Appendix B Laboratory and commercial uncoated paper properties

The commercial and laboratory base papers differ in many ways: formation, fibre orientation, fines content and state of tension during production. A slightly lower grammage, by 2 g/m^2, for the commercial base paper explains its lower thickness, specific volume, and opacity. As it proceeds toward the end of the machine the commercial paper web is drawn which increases its strength and reduces its stretch, as observed in Table 4.1 with tensile and burst measurements. The roughness of the two base papers is found very similar. With the commercial base paper holding less fines, its scattering and light absorption coefficients and opacity are lower, while its brightness is slightly higher. The differences in tear are not evident to explain. Tear usually relates to fibre length, fibre orientation and fibre bonding. Fibre length is the same between the two base paper made from the same furnish, fibre orientation was not evaluated here and fibre bonding is measured from these properties.

Appendix C Development of paper properties during drying

1. Equilibrium moisture content

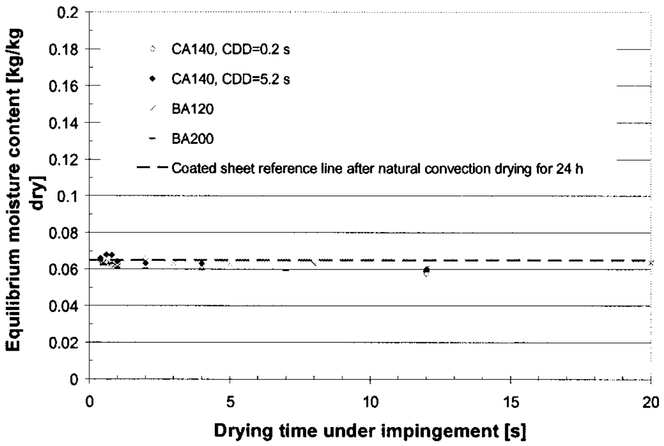

Figure C.1 Equilibrium moisture content

2. Coated paper properties vs final moisture content after impringement drying

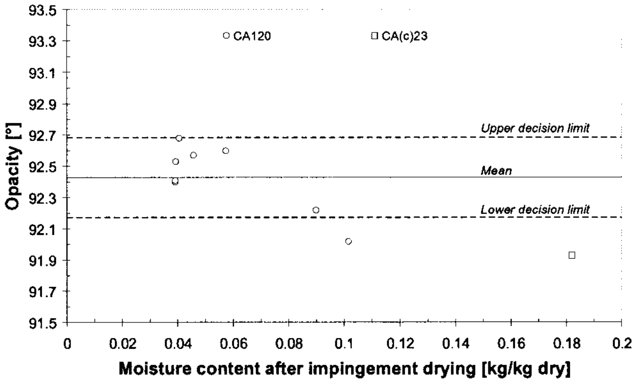

Figure C.2 Effect of moisture content on coated paper opacity: Uncalendered, 120°C air drying

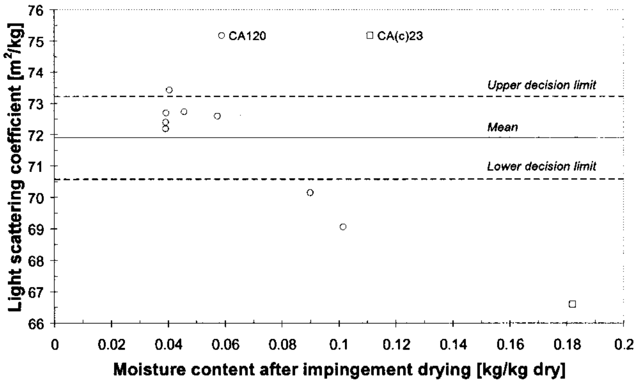

Figure C.3 Effect of moisture content on coated paper light scattering coefficient: Uncalendered, 120°C air drying

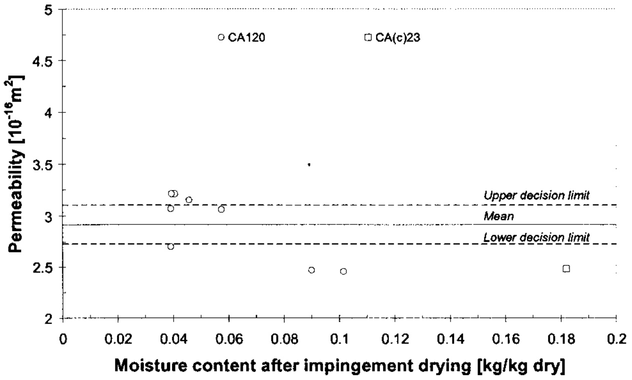

Figure C.4 Effect of moisture content on coated paper permeability: Uncalendered, 120°C air drying

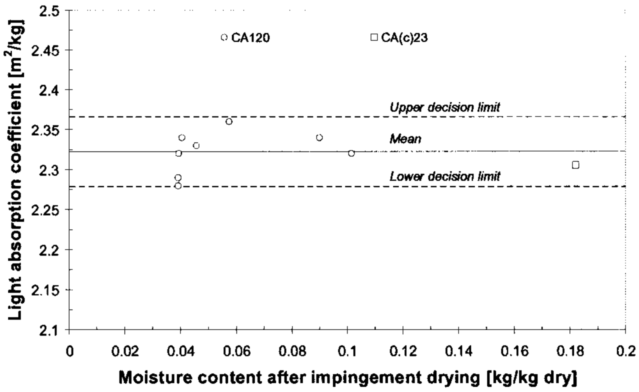

Figure C.5 Effect of moisture content on coated paper light absorption coefficient: Uncalendered, 120°C air drying

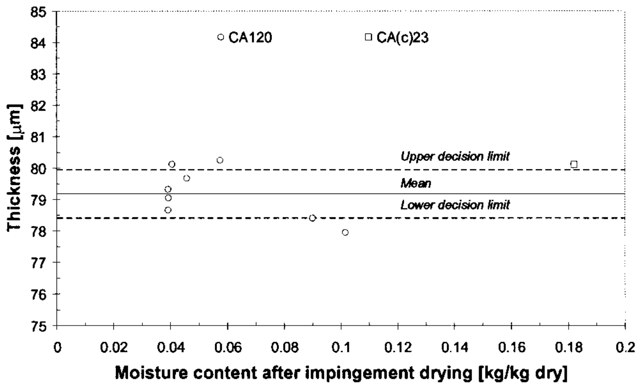

Figure C.6 Effect of moisture content on coated paper thickess: Uncalendered, 120°C air drying

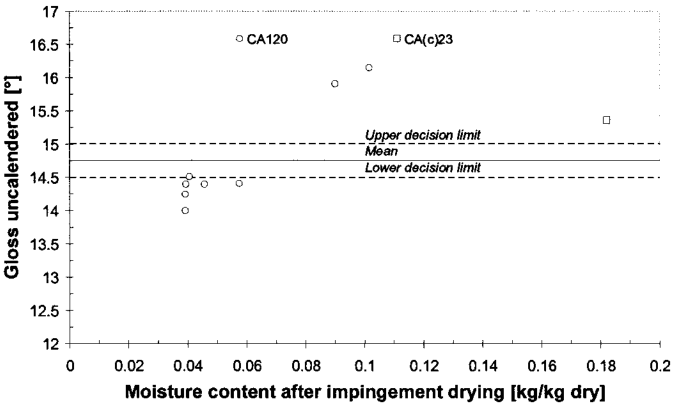

Figure C.7 Effect of moisture content on coated paper gloss: Uncalendered, 120°C air drying

3. Coated paper properties vs. coating-to-drying delay time

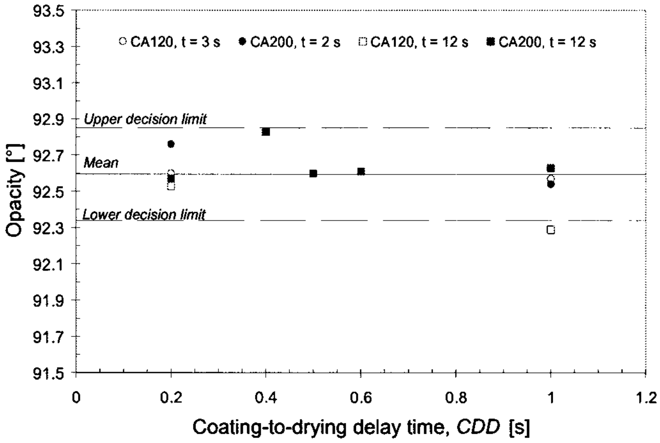

Figure C.8 Effect of delay time on coated paper opacity: Uncalendered

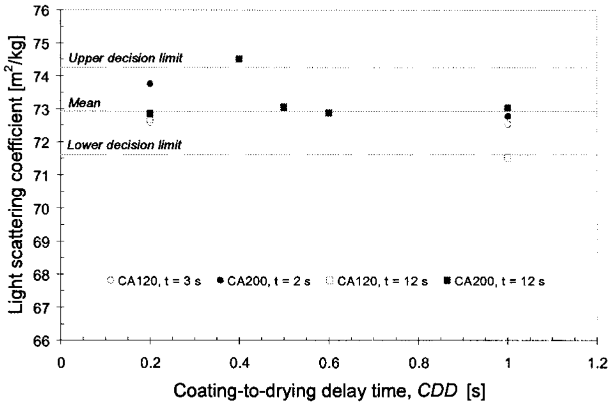

Figure C.9 Effect of delay time on coated paper light scattering coefficient: Uncalendered

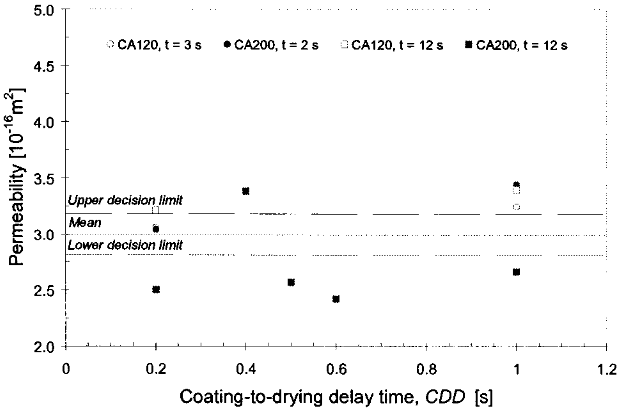

Figure C.10 Effect of delay time on coated paper permeability: Uncalendered

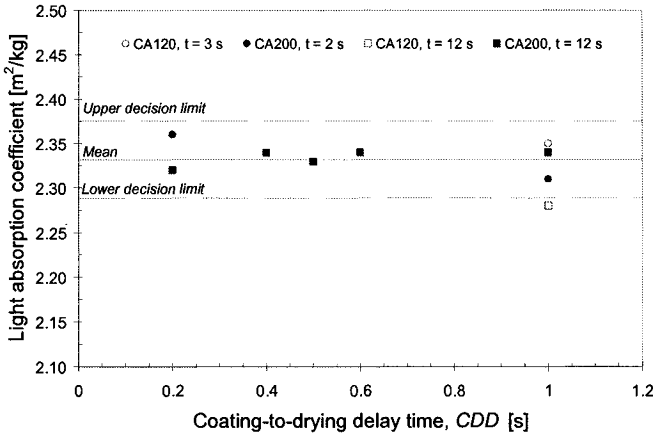

Figure C.11 Effect of delay time on coated paper light absorption coefficient: Uncalendered

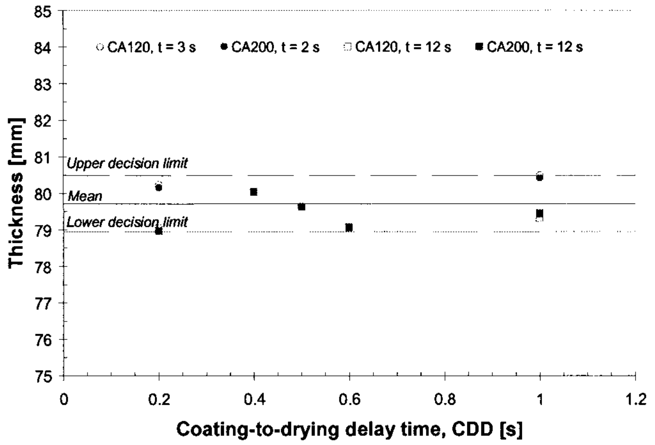

Figure C.12 Effect of delay time on coated paper thickness: Uncalendered

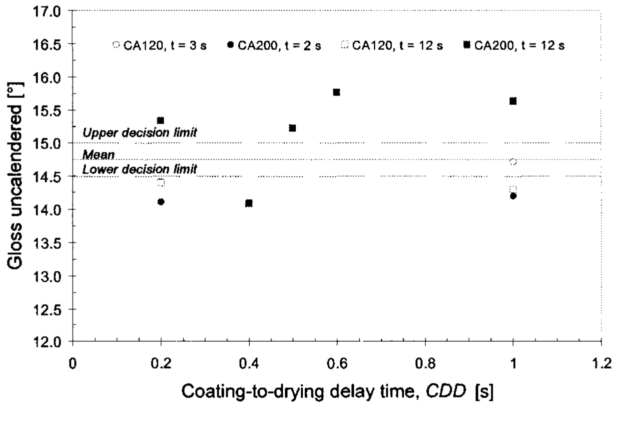

Figure C.13 Effect of delay time on coated paper gloss: Uncalendered

Appendix D Coated paper printing

1. Printing measurement procedures

1.1 Operating parameters

During the printing tests the amount of ink on the printing roller and the amount of ink transferred to the substrate were measured by weighing the printing roller before inking, after inking, i.e. before printing, and after printing. With the surface area of the print being that of the roller surface area (0.0080 m^2) the following data were calculated:

- $\text{Ink weight on roller}\,[\text{g/m}^2] = \dfrac{\text{weight of roller [after inking - before inking]}}{\text{surface area of roller}}$
- $\text{Ink weight on paper}\,[\text{g/m}^2] = \dfrac{\text{weight of roller [after printing - after inking]}}{\text{surface area of roller}}$
- $\text{Ink transfer}\,[\%] = \dfrac{\text{ink weight on paper}}{\text{ink weight on roller}} \cdot 100$

The printing rollers were cleaned thoroughly between printings.

1.2 Definition of printing properties

Three important printing properties - optical density, print gloss and print mottle – have in common being dimensionless, relative values. Ink "island" coverage was also measured in the case of the 3BT printing configuration with cyan ink. Optical density designates the darkness of the print. Because the human eye evaluates optical stimuli on a logarithmic scale, optical density is expressed on a logarithmically. It is defined as the base-10 logarithm of the inverse of light reflectance of the print, usually expressed with respect to the reflectance of a reference material. The contribution to the reflectance measurement from the paper may be removed by measuring unprinted reflectance and calculating the base-10 logarithm of unprinted paper reflectance relative to the printed paper reflectance. This latter measurement, with the effect of the substrate removed, is called the print density. For black prints the reflectance is measured using a FMY-C visual efficiency filter (545 nm); for cyan prints a red filter is used, the wavelength where cyan absorbs.

Print gloss is the degree to which the surface simulates a perfect mirror in its capacity to reflect incident light. Light is directed to the sheet at an angle of 60 or 75° and the measured specular reflection is expressed in ° or % with respect to the gloss of a reference material. Specular reflection refers to the portion of the incident light which is reflected from the surface of an object with an angle of reflection equal to the angle of incidence.

Ink coverage is normally the proportion of paper surface area covered with ink after printing. In the present work some sheets, printed in the 3BT configuration, had 100% coverage but showed quite nonuniform ink thickness with patches of much thicker ink film or ink “islands”. In order to characterize this pattern, ink “island” coverage, defined as the surface area covered with a thicker ink film, was measured with the Paprican InkScanner. This commercial instrument was designed to measure particles of residual ink in paper made from recycled furnish. Using high resolution and diffuse illumination in the far-red spectrum (680 nm), it was effective here for measuring the surface covered by thicker ink film (darker) areas. An image is acquired, converted to a greyscale image and binarized using a threshold value set at 50% of the greyscale range specific to each image.

Print mottle designates the local variation in print density. Mottle is conventionally and still widely evaluated qualitatively by visual assessment. With subjective evaluation the all-pairs ranking or range-finder methods are the most common statistical procedures, with these general methods being customized based on the experience and needs of the user. However instrumental methods are also available to quantify mottle. An image of the print is acquired, digitalized and then processed with a mathematical algorithm to calculate some measure of print local nonuniformity. Print mottle is variously determined through the use of first order statistics such as coefficient of variation, or more sophisticated mottle texture parameters by using techniques such as: band-pass filtering (Johansson 1993); 2-D Fourier Transform (Morin et al. 1996; Bernié & Douglas 2001); wavelet transform (Miettinen and Tammi 2002); co-occurrence matrix (Ness and Göttsching1998); specific perimeter of mottle features (Jordan and Nguyen, 1986); stochastic method (Waech 1998; Rosenberger 2002). The objective of sophisticated image processing is to obtain parameters for spatial distribution of density or texture of mottle that match visual perception of print mottle. Active development of new techniques continues but no method has yet been adopted as a print mottle standard.

2. Ink transfer: Black ink [B-ITC]

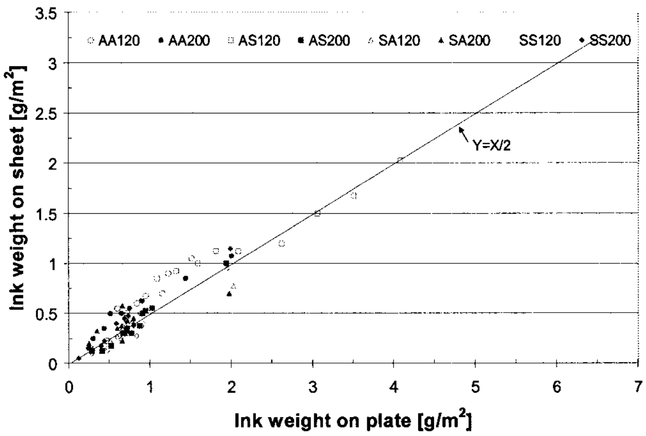

Figure D.1 Ink weight transferred: Black ink, B-ITC

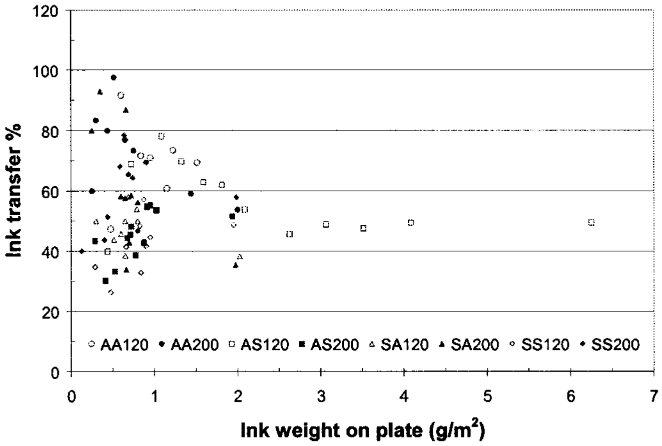

Figure D.2 Percent ink transfer: Black ink, B-ITC

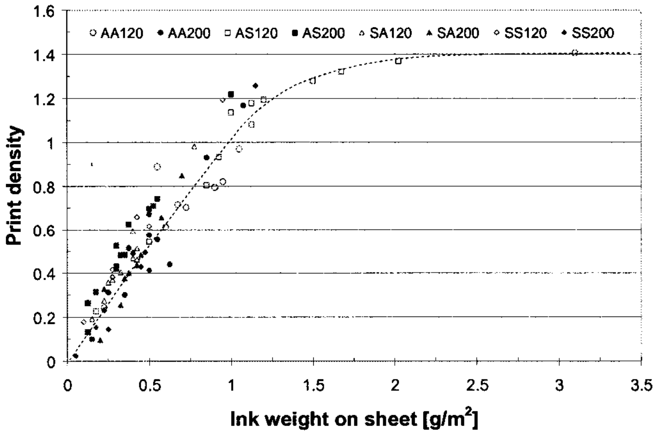

Figure D.3 Print density and ink weight on the sheet: Black ink, B-ITC

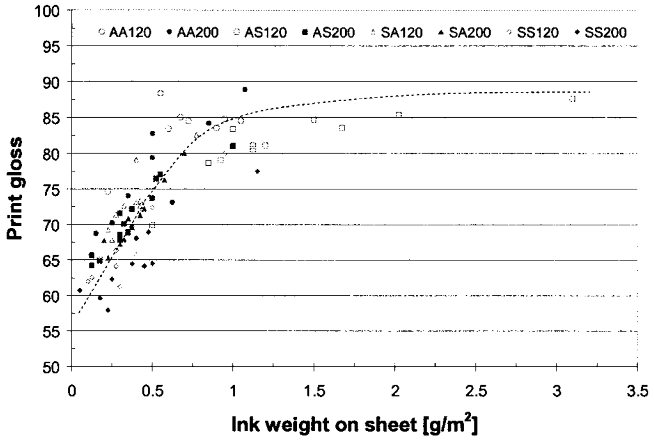

Figure D.4 Print gloss and ink weight on the sheet: Black ink, B-ITC

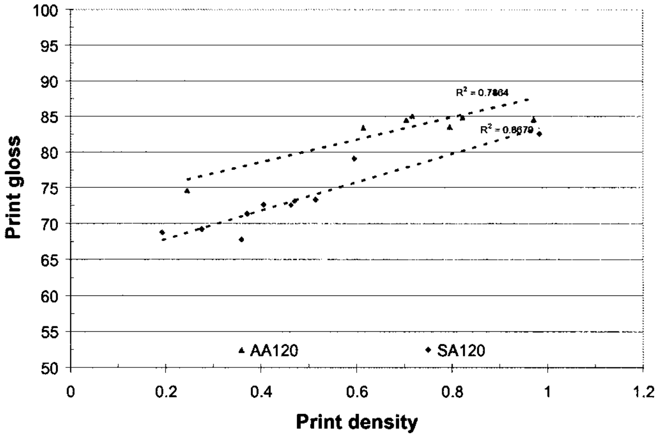

Figure D.5 Print gloss-print density, AA120-SA120: Black ink, B-ITC

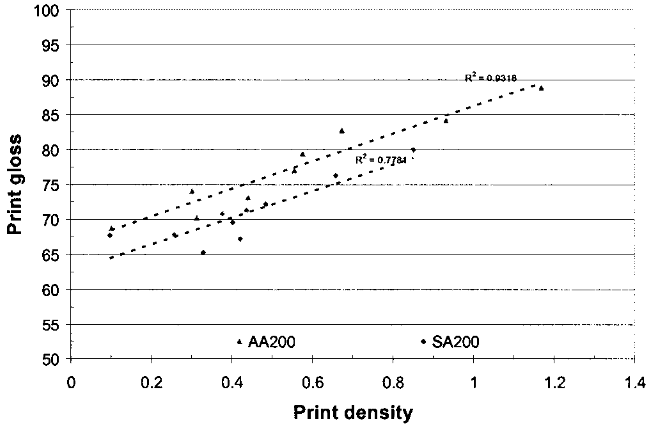

Figure D.6 Print gloss-print density, AA200-SA200: Black ink, B-ITC

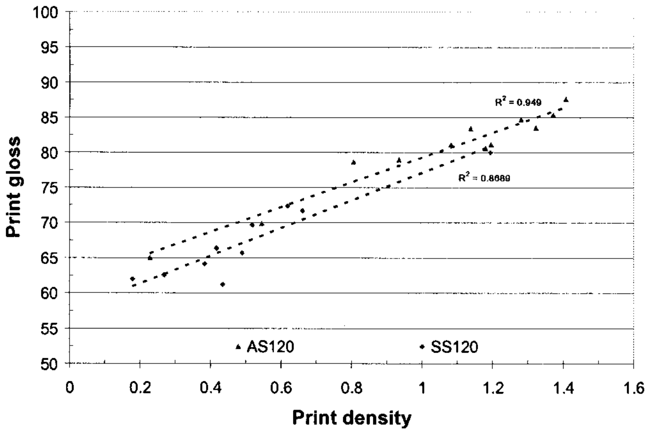

Figure D.7 Print gloss-print density, AS120-SS120: Black ink, B-ITC

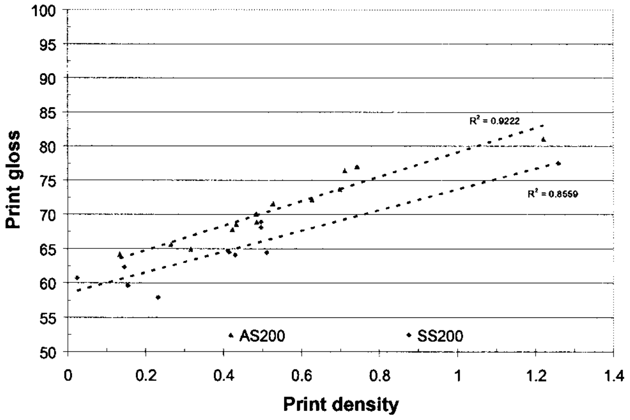

Figure D.8 Print gloss-print density, AS120-SS120: Black ink, B-ITC

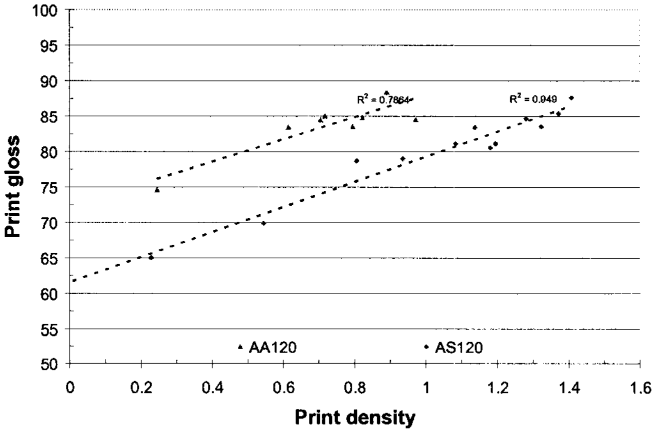

Figure D.9 Print gloss-print density, AA120-AS120: Black ink, B-ITC

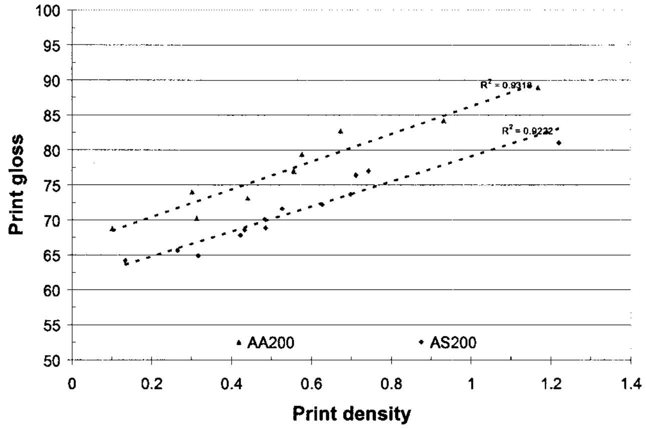

Figure D.10 Print gloss-print density, AA200-AS200: Black ink, B-ITC

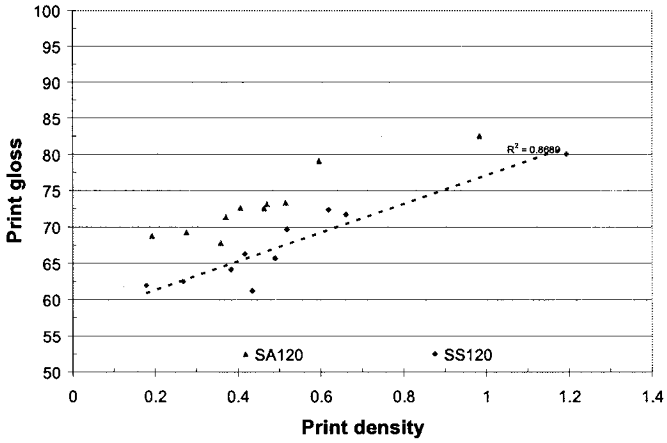

Figure D.11 Print gloss-print density, SA120-SS120: Black ink, B-ITC

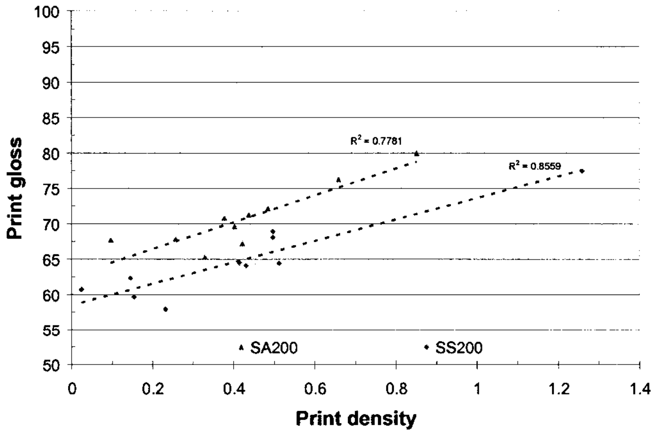

Figure D.12 Print gloss-print density, SA200-SS200: Black ink, B-ITC

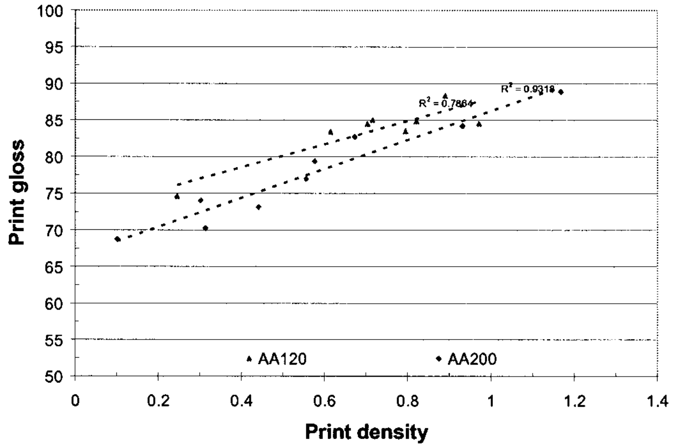

Figure D.13 Print gloss-print density, AA120-AA200: Black ink, B-ITC

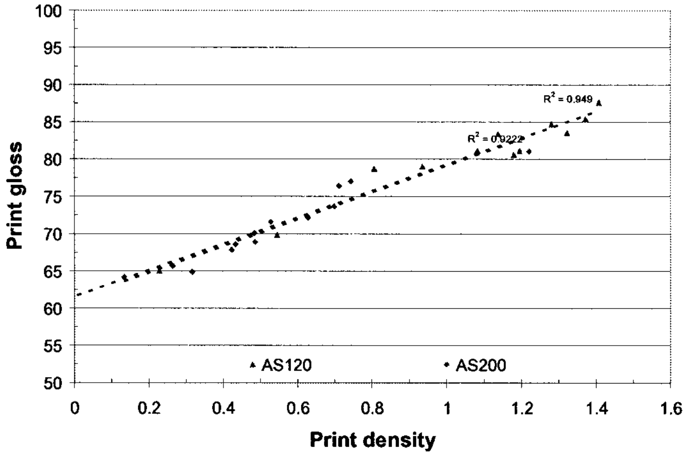

Figure D.14 Print gloss-print density, AS120-AS200: Black ink, B-ITC

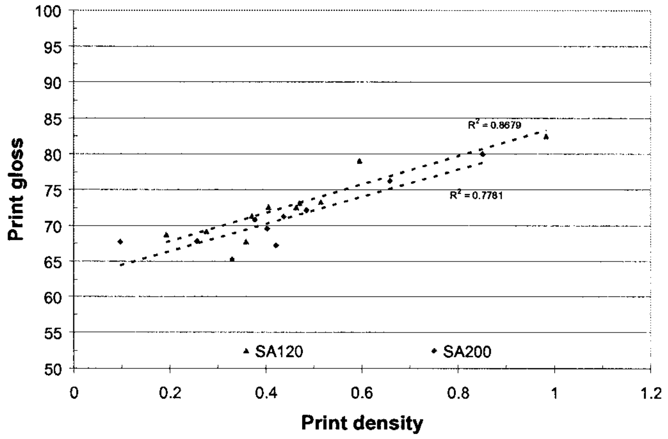

Figure D.15 Print gloss-print density, SA120-SA200: Black ink, B-ITC

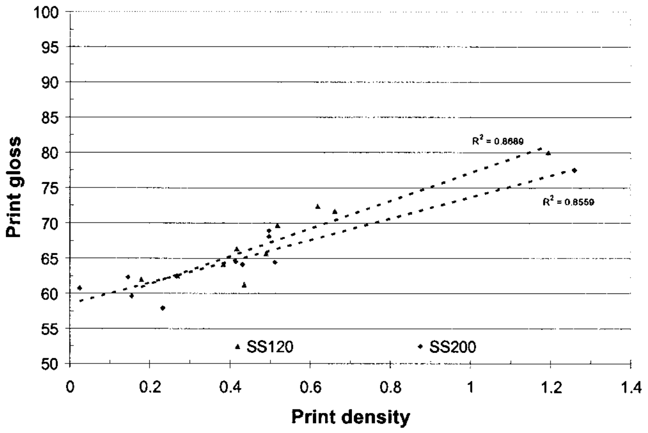

Figure D.16 Print gloss-print density, SS120-SS200: Black ink, B-ITC

3. Subjective determination of print mottle

3.1 Instructions

Here are 45 samples which carry solid printing. Please rate each sample according to how uniform the printing appears to you. Higher numbers mean that you see better print uniformity. You can use the same rating for more than one sample. Use any range of numbers that seems right to you, so long as all of them are greater than zero and higher numbers mean better print uniformity. If one sample is twice as uniform as another, give it a rating that is twice as big.

In your evaluation of print uniformity do not consider local defects such as small spots of high contrast, white or dark, but concentrate on the overall print uniformity.

Please start by spreading out all the samples and look at all of them before making any ratings. Then decide what range of numbers to use from the poorest to best print uniformity. If you change your mind before you're finished, just erase your previous rating and write down the new one. You should be able to finish the task without rushing in one-half hour.

Enter your print uniformity rating for each sample on the data sheet beside the identification number for that sample.

After you have rated all the samples, then decide which samples are acceptable to you. Decide the numerical rating of the lowest-quality acceptable sample that you would be willing to buy or to use. This means that you would buy or use that sample or any sample with a higher rating, but that you would not buy or use any sample with a lower rating. Write this lowest-quality acceptable rating in the "rating cutoff value" space on the ranking sheet.

3.2 Rating sheet

SUBJECTIVE PRINT UNIFORMITY RANKING DATA SHEET			
OBSERVER NAME			
DATE			
RATING CUTOFF VALUE			
ID	RATING	ID	RATING
1		24	
2		25	
3		26	
4		27	
5		28	
6		29	
7		30	
8		31	
9		32	
10		33	
11		34	
12		35	
13		36	
14		37	
15		38	
16		39	
17		40	
18		41	
19		42	
20		43	
21		44	
22		45	
23			